Design and Synthesis of Novel Actinide Selective Ligands for Future Spent Nuclear Fuel Reprocessing

Rachel Bulmer

Ph.D. 2019

Design and Synthesis of Novel Actinide Selective Ligands for Future Spent Nuclear Fuel Reprocessing

Rachel Bulmer

MChem. (Hons), AMRSC

A thesis in part-fulfilment of the requirements of the University of Northumbria at Newcastle for the degree of Doctor of Philosophy. Research undertaken in the Faculty of Health and Life Sciences

April 2019

Abstract

At the end of electricity generation through nuclear power, spent nuclear fuel remains highly radiotoxic due to the presence of the minor actinides, americium(III), curium(III) and neptunium(III). The separation of these requires highly selective ligands with soft *N*-donor atoms that are capable of distinguishing between the actinides and the much more abundant and chemically similar trivalent lanthanides.

This thesis discusses the development of novel classes of *N*-donor ligands, using an innovative ligand design approach, to improve on the current benchmark ligands developed. In particular the ligand design will take inspiration from the pharmaceutical industry, introducing hydrogen bond donor and/or acceptor groups and limiting the aromaticity introduced. This approach is hoped to improve the two drawbacks of currently available ligands, most notably poor solubility and slow rates of extraction.

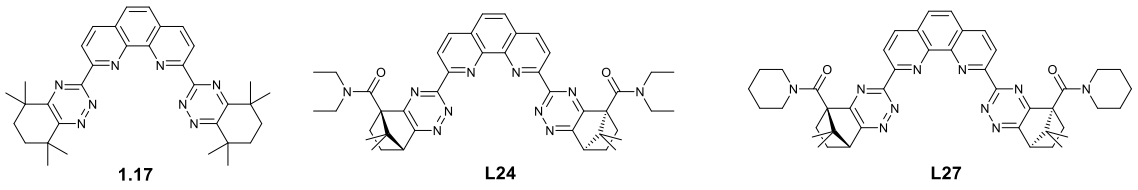

Figure 1: Molecular structure of the benchmark BTPhen ligand and the most promising novel ligands developed in this thesis.

Introduction of an amine bridge between the triazine and linker (e.g. phenanthroline) was found to have a drastically negative impact on the ability of the ligands to extract. The additional flexibility that was introduced into these ligands resulted in a ligand conformation incapable of forming a complex with the minor actinides. Efforts to introduce some rigidty into these molecules offered no improvements.

A further investigation considered two of the dominant diketones used to form the 1,2,4-triazine ring, notably tetramethyl-cyclohexyl-1,2-diketone and camphorquinone. These groups were functionalised further to validate the proposed design approach. The most promising novel

ligands developed were based upon the BTPhens, with additional hydrogen bond donor and acceptor groups present, Figure 1. These ligands showed improved rates of extraction as well as achieving a sufficiently high separation factor of the minor actinides from the trivalent lanthanides. Studies on the complexing properties of some of the ligands with trivalent lanthanides are also reported.

Further ligand designs and synthesis, and the subsequent extraction results, are discussed in this thesis. Analysis of the subsequent results supports the proposed design approach as a potentially effective method in which to streamline future ligand design.

Declaration

I declare that the work contained in this thesis has not been submitted for any other award and that it is all my own work.

I declare that the Word Count of this thesis is 64,138 words.

Name: Rachel Bulmer

Signature:

Date: 01.05.2019

Acknowledgements

Firstly, I would like to thank my supervisor Dr. Frank W. Lewis for giving me the opportunity to carry out this research project and also for his continued guidance, encouragement and support throughout my PhD. Additional thanks to Associate Professor Valery Kozhevnikov, for his enthusiasm in the subject and encouragement to take this opportunity. I would additionally like to thank Northumbria University for providing the financial support for this research.

I would like to extend my gratitude to Professor Giuseppe Modolo and Dr. Andreas Wilden at the Forschungszentrum Jülich, for welcoming me into their research lab and extending their wisdom in solvent extraction studies. In addition I would like to thank the Royal Society of Chemistry for giving me the funding to complete this research visit. I would like to thank Dr. Mike Drew for completing the X-ray crystallography studies and Dr. Mark Sims for completing the computational studies.

I am especially grateful to all members of staff at Northumbria University, with special thanks to Gordon Forrest and Dr. Karen Haggerty for their technical support.

To all my friends and colleagues at Northumbria University, both past and present, who offered much needed support, laughter and unusual discussions throughout my PhD. I would like to thank Dr. Andrey Zaytsev, for imparting a wealth of knowledge and wisdom. In particular special thanks go to Dr. Hannah Sykes, Dr. Ruth Daniels, Dr Ross Martinscroft and Dr Matthew Knight for their unwavering friendship and support and making these past three years extremely special.

I would like to thank all my family and friends for their love, encouragement and necessary distractions throughout my PhD. Thank you to my Mam and Dad for instilling in me a love of learning and to my friends Danielle, Jasmine, Haley and Rachel, for ensuring I always had shoulders to lean on.

Lastly I would like to impart a special thanks to my partner Andrew, who has shown nothing but unconditional love, support and at times patience, throughout my PhD. Without you, none of this would have been possible.

"Remember to look up at the stars and not down at your feet. Try to make sense of what you see and wonder about what makes the universe exist. Be curious. And however difficult life may seem, there is always something you can do and succeed at. It matters that you don't just give up."

Professor Stephen W. Hawking

1942 –2018

Contents

Abbreviations

Ac_2O	Acetic anhydride
AcOH	Acetic acid
ACSEPT	Actinide recycling by separation and transmutation
$AgNO_3$	Silver nitrate
Am(III)	Americium(III)
An(III)	Trivalent actinides
BODO	2,6-Bis(benzoazol-2-yl)-4-dodecyloxypyridine
BTBP	6,6-Bis-(1,2,4-triazin-3-yl)-2,2'-bipyridine
BTP	2,6-Bis-(1,2,4-triazin-3-yl)pyridines
BTPhen	2,9-Bis-(1,2,4-triazin-3-yl)-1,10-phenanthroline
$CDCl_3$	Deutrated chloroform
CD_3CN-d_3	Deutrated acetonitrile
CDTA	Trans-1,2-diaminocyclohexane-*N,N,N',N'*-tetraacetic acid
$CHCl_3$	Chloroform
Cm(III)	Curium(III)
Cs_2CO_3	Caesium carbonate
CuMeSal	Copper(I) 3-methylsalicylate
$CyMe_4$	Tetramethyl-cyclohexyl
D	Distribution ratio
DBU	1,8-Dizabicyclo(5.4.0)undec-7-ene
DCM	Dichloromethane
DEHBA	*N,N*-Di-2-ethylhexyl-butyramide
DIAMEX	Diamide extraction
DMDBTDMA	*N,N'*-Dimethyl-*N,N'*-dibutyltetradecylmalonamide
DMDOHEMA	*N,N'*-Dimethyl-*N,N'*-dioctyl[(hexyloxy)ethyl]malonamide
DMSO	Dimethyl sulfoxide
DTPA	Diethylenetriaminepentaacetic acid
ESI-MS	Electrospray ionisation mass spectrometry
EtOH	Ethanol
Eu(III)	Europium(III)
EXAFS	Extended X-ray absorption fine structure
FS-13	Phenyl trifluoromethyl sulfone
Fsp^3	Fraction of saturated carbon atoms
GANEX	Grouped actinide extraction
GENIORS	Generation IV integrated oxide fuels recycling strategies

HBD/HBA	Hydrogen bond donor/hydrogen bond acceptor
HDEHP	Di(2-ethylhexyl)phosphoric acid
HEDTA	*N*-(2-Hydroxyethyl)ethylenediamine-*N, N', N'*-triacetic acid
HLLW	High level liquid waste
HNO_3	Nitric acid
HRMS	High resolution mass spectrometry
H_2SO_4	Sulphuric acid
ICP-MS	Inductively coupled plasma mass spectrometry
$KMnO_4$	Potassium permanganate
$La(NO_3)_3$	Lanthanum nitrate
Ln(III)	Trivalent lanthanides
$Lu(NO_3)_3 . H_2O$	Lutetium(III) nitrate hydrate
LWR	Light water reactors
MeCN	Acetonitrile
MeOH	Methanol
MOX	Mixed oxide (fuel)
$NaBH_4$	Sodium borohydide
Na_2CO_3	Sodium bicarbonate
NaH	Sodium hydride
NH_4Cl	Ammonium chloride
NH_4OH	Ammonium hydroxide solution
NMR	Nuclear Magnetic Resonance
P & T	Partitioning and Transmutation
$Pd_2(dba)_3$	Tris(dibenzylideneacetone)dipalladium (0)
$Pd(OAc)_2$	Palladium acetate
PUREX	Plutonium and uranium extraction
SACSESS	Safety of actinide separation processes
SANEX	Selective actinide extraction
SeO_2	Selenium dioxide
SF	Separation factor
$SOCl_2$	Thionyl chloride
***t*-BuOK**	Potassium *tert*-butoxide
TALSPEAK	Trivalent actinide from lanthanide separation by phosphorus reagent extraction from aqueous komplexes
TBP	Tributyl phosphate
TEDGA	Tetraethyl diglycolamide
TERPY	2,6-Bis(2-pyridyl)pyridine
THF	Tetrahydrofuran
TODGA	*N,N,N',N'*-Tetraoctyl diglycolamide

TPTZ	2,4,6-Tri(2-pyridyl)-1,3,5-triazine
TRLFS	Time-Resolved laser fluorescence spectroscopy
TRLIL	Time resoled laser-induced luminescence
Xantphos	4,5-Bis(diphenylphosphino)-9,9-dimethylxanthene
XAS	X-Ray spectroscopy
XRD	X-Ray diffraction
$Y(NO_3)_3.6H_2O$	Yttrium(III) nitrate hexahydrate

Chapter 1

Introduction

1. Introduction

In the last decade a 'nuclear renaissance' has taken hold. As stricter rules regarding carbon dioxide (CO_2) emissions are enforced but global electricity demand continues to increase, especially in the developing world, many countries are turning to nuclear power as a low carbon energy source.[1],[2] With this increasing demand, preservation of natural resources, such as uranium supplies, waste minimisation and increasing the resistance to proliferation of spent nuclear fuel needs to be considered in order to increase the sustainability of civil nuclear energy. Currently nuclear power is the optimum choice for providing the required energy output, with renewable energy sources, including wind, solar, tidal and geothermal, suffering from issues in their scale up and their own environmental impact. When considering solar power, the farms themselves require mass land use, affecting the natural habitat and the use hazardous materials during their manufacturing. Nuclear power has advantages in the reduced carbon-emissions and continuous supply it offers once the reaction begins, although it isn't without its own drawbacks.

In this chapter, a review of the literature will give an overview of the nuclear fuel cycle, reprocessing considerations and the separation processes currently employed or in development for the reprocessing of spent nuclear fuel. A discussion on the key developments of relevant hydrophobic extractant molecules to this thesis will be given before the project aims and objectives are outlined.

1.1. The Nuclear Fuel Cycle

The Nuclear Fuel Cycle encompasses all processes that are involved in electricity production via nuclear power, Figure 2. It can be split into two distinct sections; the 'front end' of the cycle; considering everything from the mining of the uranium ore up until fuel fabrication and the back end of the cycle; which constitutes the reprocessing and storage of the spent nuclear fuel. The Earth's crust contains uranium deposits which, although abundant, are not an unlimited resource. Its natural isotope has low levels of radioactivity, with the radiotoxicity associated with uranium coming from its decay products. An outline of the Nuclear Fuel Cycle is discussed in the following section.[3]

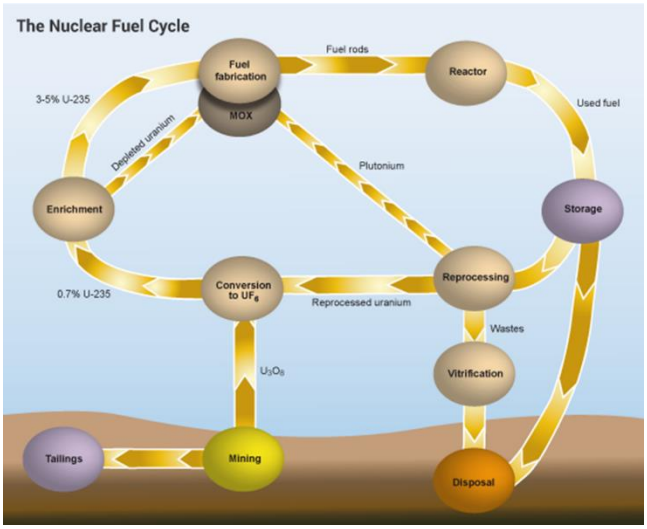

Figure 2: Diagram representing the Nuclear Fuel Cycle. Reference: world-nuclear.org [4]

The 'front end' of the cycle includes the steps required to prepare the uranium for use in a nuclear reactor. Uranium-235 (U-235) is the form required for fission within a nuclear reactor, but constitutes less than 1% of the natural uranium that is mined (the rest is composed of uranium-238). After mining the uranium ore, milling is a technique used to extract triuranium octoxide U_3O_8 (or 'yellow cake'). This product then needs to be refined in order to increase the concentration of the U-235 isotope.

Preparing this uranium concentrate for use in nuclear reactors requires enrichment, which include a number of chemical processes to increase the concentration of the fissile U-235 isotope to 3-5% for use in light water reactors (LWR). Firstly the uranium oxide is converted to uranium hexafluoride via uranium dioxide. For those reactors that don't require enriched uranium this uranium dioxide can be used directly as a fuel, although this is not the norm. The enriched uranium is produced by utilising the mass difference between the isotopes to ensure U-235 can be separated, typically using a centrifuge or gaseous diffusion. This produces two streams, a product stream which is reconverted to give enriched uranium oxide (UO_2) and the depleted uranium product.

The enriched UO_2, containing approximately 3 to 5% of the U-235 isotope, is encased into fuel rods for use within the nuclear reactor during fuel fabrication. Within the nuclear reactor these fuel rods undergo fission in a continuous chain reaction. The fission process involves the splitting

of the uranium nucleus when impacted by a neutron, producing more neutrons in the process. Plutonium-239 is a decay product formed when a U-235 atom collides with U-238, with further products formed when Pu-239 itself undergoes the fission process. This reaction produces considerable heat which is used to produce steam, which in turn drives a turbine and electric generator, providing the electricity.

A nuclear reactor typically produces electricity for over 20 years. However, radioactive impurities building up within the reactor affect the efficiency of the fission process. As a consequence this 'spent fuel', with the composition represented in Figure 3, needs to be removed and the reactor refuelled after a minimum period of 18 months. The spent fuel is stored in a body of water (a spent fuel pond), which acts as a radiation shield in addition to cooling the fuel through absorbing the heat. Once a decreased radiation level is reached, the spent fuel can be reprocessed to recover and recycle some of the components or be prepared for long-term storage in geological repositories. Further attempts to 'close' the nuclear fuel cycle will see the recycling of as many components of the waste as is feasible, to maximise the efficiency of the process, through enhancing the use of natural resources and reducing the hazards associated with the remaining spent fuel. At the end of 2015 there were over 350,000 tonnes of spent nuclear fuel produced by the civil nuclear energy sector, which will only continue to grow as nuclear energy programmes expand around the world.[5]

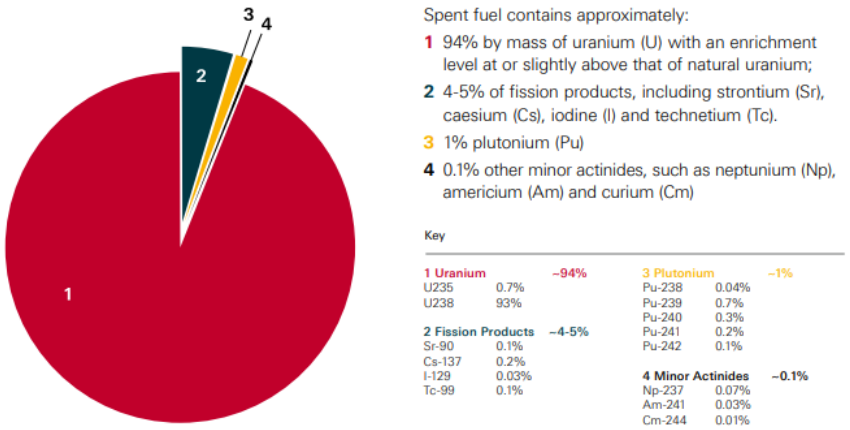

Figure 3: Representative composition of spent fuel from light water reactors (LWR), taken from reference [1].

Exploiting the energy released in nuclear fission has resulted in electricity generation through nuclear reactors. When comparing the energy from the complete combustion of 1 kg of coal and the complete fission of 1 kg of U-235, the uranium produces almost three million times more energy than the coal. The energy density of coal is 9.0 kWh/kg compared to the approximately 24,000,000 kWh/kg for 100% U-235.[6] The enriched uranium used in a typical LWR produces 960,000 kWh/kg, still one hundred thousand times more than that of an equal mass of coal. The appeal in nuclear power is clearly perceived for an increasing electricity demand.

1.2. Spent Nuclear Fuel Reprocessing

In order to make nuclear power more appealing to the wider public it is necessary to make electricity production through nuclear power as safe as possible, especially in the wake of well publicised nuclear incidents, such as the Fukushima incident of 2011. One of the factors found to cause concern to the general public is the disposal of the radioactive waste at the end of electricity production.[7] The reprocessing of spent nuclear fuel from nuclear reactors is essential in reducing the radiotoxicity of the subsequent waste as well as ensuring sustainable use of the uranium resource. A current method of reprocessing spent fuel that is employed worldwide is the PUREX process (Plutonium and Uranium Extraction),[8] which recycles the plutonium and uranium from the spent nuclear fuel rods as Mixed Oxide (MOX) fuel in advanced (generation IV) reactors.

The remaining waste stream, or high level liquid waste (HLLW), still contains the minor actinides (An(III)); americium (Am) and curium (Cm) and the trivalent lanthanides (Ln(III)). It is the minor An(III) that account for most of the remaining long-lived radiotoxicity and heat load, despite comprising only 0.1% by mass of the waste.[9] After the removal of uranium and plutonium the remaining waste, containing the minor actinides, remains radiotoxic for approximately 9,000 years before reaching the radiotoxicity level of the natural uranium found in the earth's crust, Figure 4. This is too long a timeframe for the safe management of the remaining waste if this material was to be disposed of in geological repositories at this stage. It has several implications for the long-term integrity and resistance to leaching of the waste in a geological site. The remaining waste is also comprised of other transition metals (corrosion products) as a result of radiolysis and corrosion of the steel cladding used to encase the fuel rods.

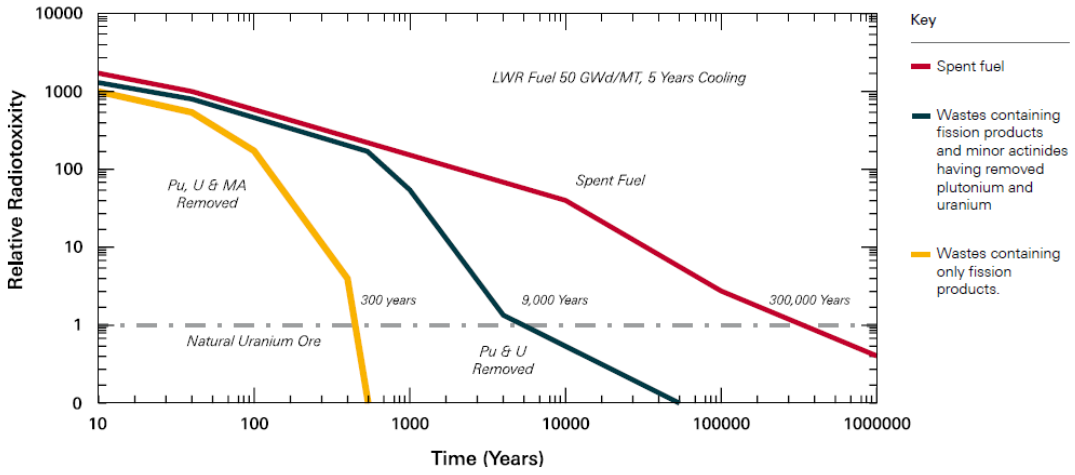

Figure 4: The relative radioactive decay of nuclear waste at various waste management stages, taken from reference [1].

1.2.1. Partitioning and Transmutation Strategy

Various European initiatives are and have been working towards realising a safer and more efficient industrial process for removing these minor actinides from spent nuclear fuel. Projects including ACSEPT (Actinide reCycling by SEParation and Transmutation),[10] part of the Euratom FP7 collaboration, and SACSESS (Safety of Actinide SEparation ProceSSes),[11] aimed to develop and improve minor actinide separation (partitioning) processes to remove the minor actinides and ultimately close the nuclear fuel cycle. The current European project, GENIORS Horizon 2020 (GEN IV Integrated Oxide fuels Recycling Strategies),[12] aims to continue improving current recycling processes and have recycling strategies implemented in anticipation of the 4th generation of reactors becoming operational by 2030.

One European proposal arising from these initiatives is the Partitioning and Transmutation (P&T) strategy. This uses a liquid-liquid solvent extraction process to remove or partition the minor actinides from the remaining waste, which includes the Ln(III), reducing the remaining radiotoxicity of the PUREX raffinate.[13] The partitioning of the An(III) is necessary to ensure transmutation efficiency as a result of the chemically similar, and much more abundant Ln(III), having a much higher neutron affinity.[14] This is followed by high-energy neutron-induced fission (transmutation) of the minor actinides to shorter-lived or stable, non-radioactive elements in

advanced reactors.[15] The removal of the minor actinides reduces the radiotoxicity of the remaining waste down to 300 years, Figure 4, which is a much more manageable timeframe for disposal in a geological repository. Due to the chemical similarities between the Ln(III) and An(III) this partitioning poses a complex chemical challenge. Once implemented, the strategy would substantially reduce the radiotoxicity and heat load of the remaining waste, allowing for a less complex future waste management programmes and reducing the strain on future geological repositories.

1.3. The Lanthanides and Actinides

The lanthanides (Ln) and actinides (An) are metallic elements found in the f-block of the periodic table and contain valence electrons in the 4*f* and 5*f* orbitals, respectively. They have similar chemical properties, especially in aqueous solution, such as oxidation states, ionic radii, charges and they tend to be both strongly hydrated.[16] As the An(III) and Ln(III) are both hard Lewis acids, as defined by Pearson,[17] their coordination chemistry with Lewis bases containing hard donor atoms, for example oxygen, is very similar. Due to these similarities, the separation of the minor actinides, Am(III) and Cm(III), from the Ln(III) fission products is a massive undertaking within nuclear reprocessing.

1.3.1. The Lanthanides

The Ln or "rare-earth" elements have chemistry which is defined by their *f*-orbital electrons. Across the series, the outer 5*d* and 6*s* electrons are more susceptible to the influence of the nuclear charge resulting in a higher than expected decrease in atomic radius, as the atomic number increases, known as the Lanthanide Contraction. The contraction is the result of the poor shielding of the nuclear charge by the inner 4*f* electrons, thus causing a greater attraction between the nucleus and the outer 5*d* and 6*s* electrons and a subsequent decrease in atomic radius. The dominant oxidation state is +3 across the lanthanide series. The Ln(III) prefer to coordinate with hard donor atoms of high electronegativity, such as the oxygen atom, explaining the ligand design for the DIAMEX process, section 1.4.

1.3.2.The Actinides

The actinides (An), containing elements actinium to lawrencium, have a more complex chemistry then the lanthanides due to their varying valence. A handful of actinides are naturally occurring, including uranium and thorium, but the rest are a consequence of transmutation in laboratory synthesis or as a by-product of thermonuclear testing, particularly during the Second World War and the Cold War.[18] Early An show comparable chemistry to the *d*-block metals and the later An show similar chemistry to the Ln(III) elements themselves. They are hard Lewis acids and therefore are strong electron acceptors.

They have unstable nuclear configurations and as a result exhibit spontaneous radioactive decay, and emit alpha particles and gamma rays. The half-life of the element quantifies its radiotoxicity and the time taken for this to reach safe levels. Through utilising the alpha decay, and resulting gamma rays emitted this can be used to identify the isotopes present, with each actinide having its own distinct energy (keV).[19] In terms of solvent extraction this can give an indication of the distribution of these elements across two immiscible phases. Within a nuclear reactor there can be two processes occurring, nuclear fission causing the splitting of a nucleus to form lighter elements, and neutron capture, resulting in the production of heavier isotopes.

The actinides have complex coordination chemistry due to their ability to lose valence electrons, leading to many oxidation states and ionic forms. Within aqueous solutions in particular, where two or more oxidation states can co-exist, it can lead to complex systems.[20] The lighter actinides, of particular interest to the nuclear industry (U, Np and Pu), can exist in multiple oxidation states in solution, +III, +IV, +V and +VI are prevalent. The heavier actinides, after plutonium, exist predominantly in a stable +III oxidation state.

The lack of shielding from the 6*s* and 6*p* electrons in the actinides results in a 5*f* orbital expansion, hence a greater ionic radii when compared to the lanthanides. As a consequence the orbitals are more readily available for overlap with ligand orbitals, which is utilised in separation techniques, section 1.4. Some of the first evidence of this increased covalent interaction, caused by greater orbital overlap, came from a ^{15}N NMR spectroscopic study utilising a ^{15}N labelled BTP ligand.[21]

This effect is somewhat limited however, as the nuclear charge increases, there is a slight contraction of the 5*f* orbitals going across the actinide series ('Actinide Contraction'), resulting in a smaller orbital overlap between the 5*f* orbitals and ligand orbitals.

1.4. Solvent Extraction

Solvent extraction has long been a dominant technique in separation experiments, in particular the purification of metals in hydrometallurgy. Liquid-liquid extraction is the most established technique within the nuclear reprocessing industry to separate the radionuclides from the waste, ensuring recycling is possible. Other separations include chromatographic methods, in which the extractant is loaded onto a solid phase, i.e. porous silica/polymer particles.[22]

Liquid-liquid extraction in the nuclear reprocessing industry involves an acidic aqueous layer, containing the radioactive waste dissolved in an aqueous acid (usually nitric acid), and an organic layer of a diluent immiscible with water, such as kerosene or 1-octanol. The process utilised dictates in which layer the extractant molecules will exist, as either a hydrophobic or hydrophilic ligand, and in which direction the radioactive species will go when moving between the two immiscible liquids. For the purpose of this project the focus will be upon hydrophobic ligands, which are dissolved within the organic phase and the separation will occur by the movement of the actinides from the aqueous into the organic phase.

Solvent extraction has advantages in terms of the development of a suitable system for the nuclear reprocessing industry, one of which being its ability to achieve quantitative recovery of the radionuclide(s) of interest. Large impacts on extraction and separation efficiency can be influenced by making small chemical and physical changes in the composition of the system, i.e. through changing the extractants utilised of altering the acidity of the aqueous phase. Various processes are under investigation within the nuclear reprocessing industry, in particular those that tackle the HLLW remaining after the PUREX process or offer a replacement. This project focuses upon novel ligands for use in the SANEX and potentially GANEX processes within Europe, Figure 5. In this section these processes, among others will be summarised to gain an

understanding of the environments the ligands are proposed to work under and current developments.

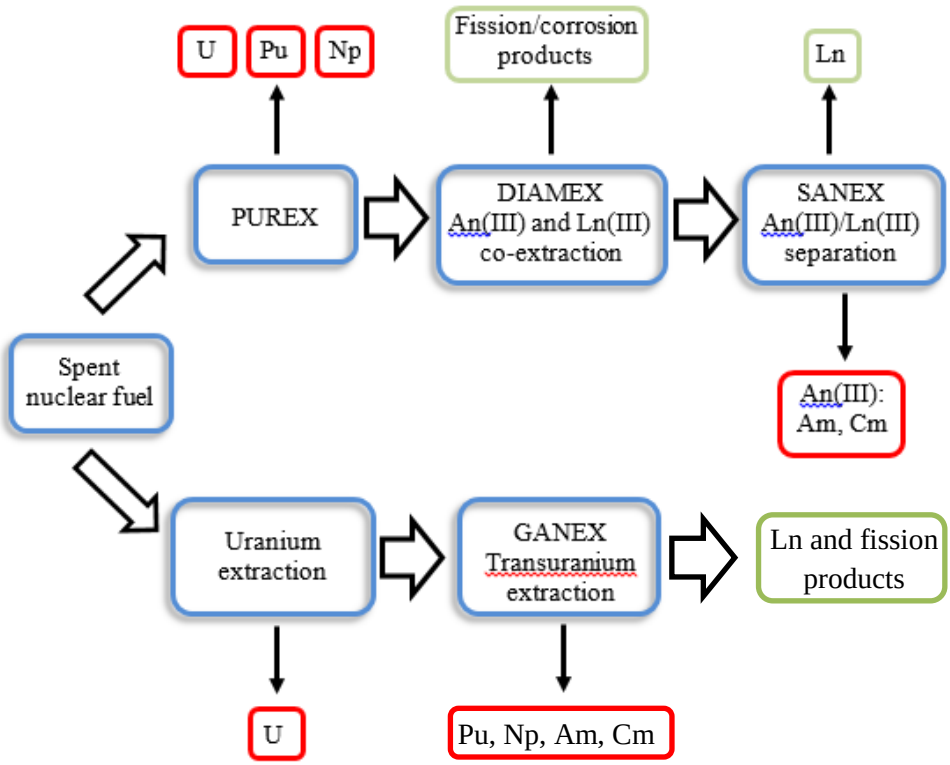

Figure 5: Outline of the proposed routes for the future processing of spent nuclear fuel.

1.4.1.PUREX

The PUREX (Plutonium and Uranium EXtraction) process involves the separation of uranium and plutonium from the spent nuclear fuel waste stream where it is then recycled as mixed oxide fuel (MOX). Since the 1960's, where it was first used at the Sellafield site in the UK, the MOX fuel has become widely used throughout Europe as a source of low enriched uranium for use in LWR.[23] As this is one of the first steps in the reprocessing of spent nuclear fuel, it is necessary to dissolve the irradiated fuel in a nitric acid (HNO_3) solution, typically at 3-4 M, and remove the insoluble solids.

The most prominent extractant used to date is tributyl phosphate **1.01** (TBP), Figure 6, which is diluted within aliphatic hydrocarbon diluents such as kerosene or dodecane, so that its typical concentration in the organic phase is 20-30%. The ligand exhibits good stability against the highly acidic aqueous phase as well as showing selectivity towards hexavalent uranium (U(VI)) and

tetravalent plutonium (Pu(IV)) to achieve quantitative recovery. The minor actinides (An(III)) and fission products remain in the aqueous phase, becoming the PUREX raffinate. A recent development sees the co-extraction of neptunium (Np) in this step in an advanced PUREX process, although with slightly lower distribution (*D*) ratios being observed than for U(VI) or Pu(IV).[24]

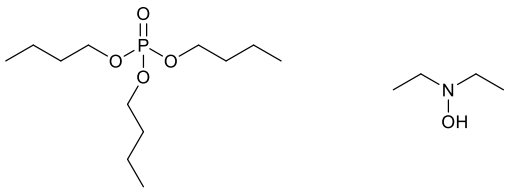

1.01 **1.02**

Figure 6: Structure of tributyl phosphate (**1.01**) and *N*,*N*-diethyl-hydroxylamine (**1.02**).

There are an additional two steps that achieve the partitioning and decontamination of the U(VI) and Pu(IV) from the HLLW. The reduction of Pu(IV) to Pu(III) using hydrazine reduces its affinity for the TBP **1.01** extractant, ensuring the element can be back-extracted into the aqueous phase. By using *N*,*N*-diethyl-hydroxylamine **1.02** as the reducing agent the simultaneous reduction of Np(VI) to Np(V) can be achieved allowing its back-extraction alongside Pu(III).[25] The final step is the back-extraction of uranium using dilute nitric acid solutions. The organic solution undergoes a solvent purification step to remove any degraded extractant before being recycled for further use. One downfall to the use of TBP **1.01** is the presence of the undesirable phosphorus atom, which can't be fully incinerated to gases at the end of its use. This ultimately leads to the production of additional waste from the process.

A drawback of the PUREX process is the sensitivity of certain species to the pH of the aqueous phase, requiring additional considerations to ensure stability is maintained, such as the specific control of the oxidation states of the actinides present in solution. At higher pH, the solubility of uranium and plutonium become a concern in the aqueous phase as a result of the formation of their insoluble oxides through hydrolysis.

1.4.2. DIAMEX

The DIAMEX (DIAMide EXtraction) process, developed in France in the 1980's, simultaneously extracts the An(III) and Ln(III) from the PUREX raffinate using *O*-donor extractants such as the malonamide and diglycoamide ligands.[26] Previous diamide extractant molecules have included *N,N'*-dimethyl-*N,N'*-dibutyltetradecylmalonamide (DMDBTDMA) **1.03** and *N,N'*-dimethyl-*N,N'*-dioctyl[(hexyloxy)ethyl]malonamide (DMDOHEMA) **1.04**, Figure 7. These ligands have the benefit of abiding by the 'CHON' principle, unlike TBP **1.01**, meaning they are only composed of the elements carbon, hydrogen, oxygen and nitrogen. This leads to minimal waste generation at the end of the cycle, as the extractant can be fully incinerated to a harmless gases. DMDOHEMA **1.04** has replaced DMDBTDMA **1.03** as the extractant of choice as a result of its increased lipophilicity and the increased solubility of its degradation products when compared to previous DIAMEX extractants.[27]

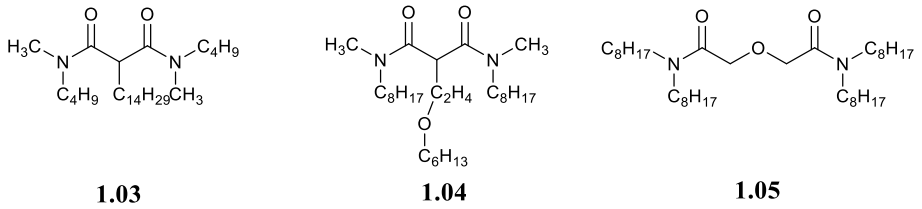

Figure 7: Structure of the DIAMEX ligands; DMDBTDMA (**1.03**), DMDOHEMA (**1.04**), and TODGA (**1.05**).

A successful 'hot-test' has been demonstrated with a PUREX raffinate using the DMDOHEMA **1.04** extractant, achieving high separation of the An(III) and Ln(III).[28] As well as co-extraction of An(III) and Ln(III), co-extraction of some of the lighter fission products; ruthenium, yttrium and technetium was observed. Prevention of this can be achieved through the addition of further chemical complexing or 'hold-back' reagents. Some examples include oxalic acid **1.06** and *N*-(2-hydroxyethyl)ethylenediamine-*N,N',N'*-triacetic acid (HEDTA) **1.07**, which avoid the co-extraction of molybdenum, zirconium and palladium, Figure 8. These additional reagents are a necessity, in some form, for most processes to ensure effective decontamination.

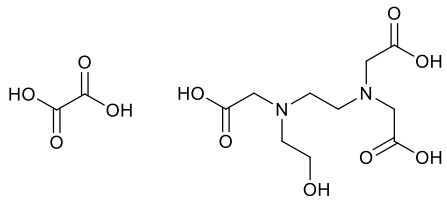

1.06 **1.07**

Figure 8: Structures of two representative hold-back reagents; oxalic acid (**1.06**) and HEDTA (**1.07**)

The current reference ligand for use in this process is the *N,N,N',N'*-tetraoctyl diglycolamide (TODGA) **1.05**. This has a notable difference in structure, when compared to the previously developed diamide extractants **1.03** and **1.04**, in which it contains an ether bridge between the carbonyl functional groups. It has been shown that the extraction efficiency of TODGA **1.05** is increased compared to other diglycolamides, as a result of increased hard O-donor ability. Its extraction affinity for the fission products has meant its concentration needs to be limited in solution, but this doesn't impact on its An(III) and Ln(III) extraction efficiency. Demonstration of this ligand in batch tests with PUREX raffinate have shown that, when combined with TBP **1.01**, the co-extraction of the actinides(III) and lanthanides(III) is successfully achieved, Figure 9.[26, 29], [30]

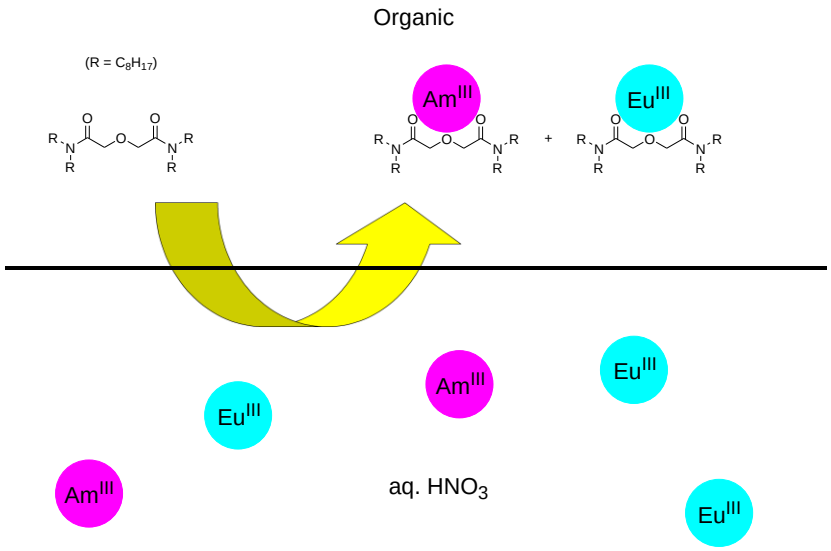

Figure 9: Diagram illustrating the principle of the DIAMEX process with a representative diglycolamide ligand.

Research through various European initiatives, e.g. ASCEPT, propose the combined use of the DIAMEX-SANEX process in the future. This will ensure that at the end of these processes, separation of the actinides alone from the PUREX raffinate will have been achieved, with the radiotoxicity of the remaining waste reduced to 300 years for disposal in geological repositories.

1.4.3. SANEX

The SANEX (Selective ActiNide EXtraction) process, proposed for use in Europe,[31] aims to use soft and selective *N*- and *S*- donor ligands to extract and separate the remaining actinides, Am(III) and Cm(III), from the lanthanide fission products, after both the PUREX and DIAMEX processes, Figure 10.[32] Due to the chemical similarity between the An(III) and Ln(III) this separation requires careful tuning with a highly An(III) selective ligand. The lanthanide to actinide ratio is approximately 40:1 in the PUREX raffinate. The process uses ligands that can take advantage of the greater overlap of the 5*f* orbitals of the An(III) with the orbitals of the ligand donor atoms, when compared to the 4*f* orbitals of the Ln(III), hence achieving separation of the two groups of elements.

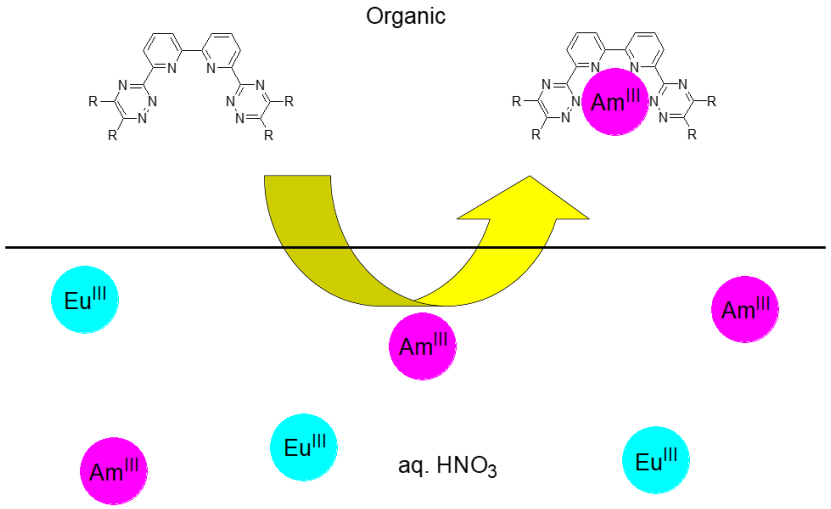

Figure 10: Diagram illustrating the principle of the SANEX process with a representative bis-1,2,4-triazine ligand.

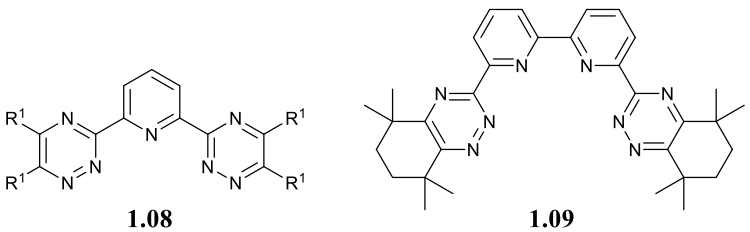

1.08 **1.09**

Figure 11: Structures of SANEX suitable reagents; a general BTP (**1.08**) and $CyMe_4$-BTBP (**1.09**).

Some of the first *N*-donor extractants capable of achieving this separation were the 2,6-bis(5,6-dialkyl-1,2,4-triazin-3-yl)pyridines (BTPs) **1.08**, which suffered from poor hydrolytic stability, Figure 11. Further advancements, discussed in detail in section 1.5, led to the development of $CyMe_4$-BTBP **1.09**, which showed high selectivity for the An(III) over Ln(III) but slow extraction kinetics. This ligand, in combination with DMDOHEMA **1.04**, shows fast kinetics, reaching equilibrium within 5 minutes of phase mixing.[33] This same ligand has been proven capable of achieving this separation in a SANEX process 'hot-test' with genuine spent fuel.[34] Further discussion regarding the SANEX process can be found in 1.5., when ligands used in this process are mentioned.

1.4.4. GANEX

Research focus has shifted towards the development of the GANEX (Grouped Actinide Extraction) process with the hope to simplify the reprocessing methods available and to close the nuclear fuel cycle. The GANEX process aims to carry out the homogeneous partitioning of the trans-uranic actinides, including Pu, Np and the minor actinides, from the lanthanides and other fission and corrosion products.[35] Currently the PUREX, and recently proposed DIAMEX-SANEX processes, offer a multi-step method for separating the actinides for recycling and disposal purposes. The GANEX proposal offers an economically beneficial and safer alternative to these. By ensuring all TRU actinides can be recovered in a single step, it ensures the number of steps is reduced and waste management simplified.

The 1st GANEX cycle extracts the bulk of the uranium, using a monoamide extractant, so that the uranium can be utilised in generation IV nuclear reactors. The second extraction step, which

separates the trans-uranic actinides, requires a combination of extractants that are capable of recovering the tri-, tetra-, penta- and hexavalent actinides simultaneously. This poses additional challenges to those of the SANEX process, where only the separation of the trivalent actinides are completed, as the varied oxidation states need to be taken into consideration when choosing suitable extractants. These extractants should still abide by the 'CHON' principle and preferably not require the use of added reagents to control the oxidation states of the elements. There are two notable processes that have been proposed as part of the European projects; the EURO-GANEX and CHALMEX processes. [36],[37]

The EURO-GANEX process has been successfully demonstrated to co-extract both the lanthanides and the actinides prior to their separation through the selective back-extraction of the actinides.[38] The hydrophobic diglycolamide, TODGA **1.05**, is known to be a successful actinide extractant that could be employed in this process,[39] but this alone is incapable of handling the high concentration of Pu that would be present.[40] The combination of DMDOHEMA **1.04** is required to prevent precipitate forming at the interphase whilst maintaining effective co-extraction.[35] Separation of the actinides is then achieved by back-extraction (stripping) of the actinides from the loaded organic phase with a hydrophilic sulfonated bis-triazinyl pyridine ligand (SO_3-Ph-BTP) **1.10**, Figure 12. This extractant is known to be effective in the aqueous *i*-SANEX (innovative-SANEX) process with a separation factor for Am(III) from Eu(III) of 1000 achieved.[41] A flowsheet for this process has successfully been tested with a spiked feed solution using the proposed solvent system.[42] There was some loss of Np into the aqueous raffinate at the end of the tested flow sheet, as a result of poor extraction conditions for this actinide. It is known that altering the acidity of the cycle can influence the oxidation state of Np and aid its extraction, which can be achieved by using acetohydroxamic acid **1.11**, Figure 12.[43]

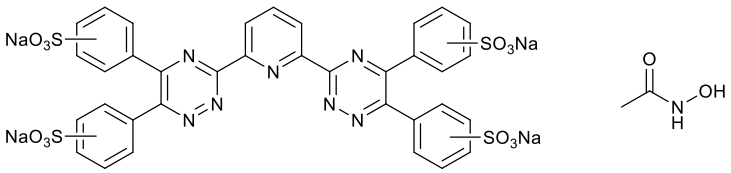

1.10 **1.11**

Figure 12: Structures of reagents used in the GANEX process; SO_3-Ph-BTP (**1.10**) and acetohydroxamic acid (**1.11**).

The Chalmers method combines two hydrophobic extractants with different properties to ensure all actinides across the series are extracted from the feed solution, suitably called the CHALMEX process.[37] The combined extractants are the bis-triazinyl-bipyridine (BTBP) ligands, which can selectively extract trivalent and pentavalent actinides, alongside the TBP ligand **1.01**, which has a proven record of extracting plutonium Pu(VI) and uranium U(VI) in the PUREX process.[44] These ligands are stable against radiolysis and hydrolysis and have been shown to extract their respective An(III) independently of each other.[45] The TBP molecule **1.01** suffers from drawbacks including not abiding by the CHON principle and plays a part in the undesirable nitric acid (HNO_3) extraction into the organic phase. Alternatives to TBP **1.01** have included *N*,*N*-di-2-ethylhexyl-butyramide (DEHBA) **1.12** as a 20% solution in cyclohexanone, which is known to extract both uranium and plutonium, Figure 13.[46] A hot test using genuine HLLW was completed at the Atalante facility in France with DEHBA **1.12** recovering more than 99.99 % of the uranium in a GANEX 1st cycle.[47] However, the use of the DEHBA **1.12** solvent was found to negatively impact the extraction of Am(III) and Eu(III) and more problematically Np, in which the distribution (*D*) ratio drops below 1 after 42 days.[48] Unlike TBP **1.01**, the degradation products of DEHBA **1.12** have a greater negative impact on the extraction of the actinides. It also sees the amplified extraction of fission and corrosion products that is not observed with the TBP extractant **1.01**, increasing the distribution ratios for all lanthanides and reducing separation efficiency.

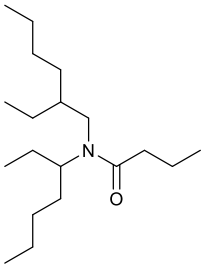

1.12

Figure 13: Structure of an alternative GANEX ligand, DEHBA (**1.12**).

The undesired co-extraction of fission and corrosion products within the GANEX process has been investigated by various research groups. An important understanding of their process behaviour is a necessity for the safe running of a future process. Palladium is known to be a problematic element as it can be extracted as a 1:1 complex with the $CyMe_4$-BTBP ligand **1.09**, preventing the ligand from coordinating to an actinide.[49] Suppressing the extraction of zirconium and palladium can be achieved using hydrophilic masking agents such as *trans*-1,2-diaminocyclohexane-*N,N,N',N'*-tetraacetic acid (CDTA) **1.13**, Figure 14.[50] Alternatively it has been found that the complexing agents of bimet **1.14** and mannitol **1.15** can suppress the extraction of molybdenum, zirconium and palladium simultaneously.[51]

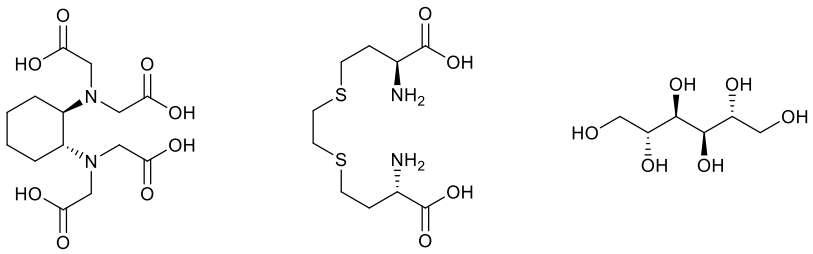

1.13 **1.14** **1.15**

Figure 14: Structures of example suppression and 'hold-back' reagents for the fission and corrosion products; CDTA (**1.13**), bimet (**1.14**) and mannitol (**1.15**).

The GANEX process still requires optimisation, but the potential of streamlining the separation of the actinides ensures a continued focus. Ligands disclosed in this thesis have the potential for application in both the CHALMERS-GANEX and SANEX processes.

1.4.5. 1c-SANEX

The 1-cycle SANEX process aims to selectively extract the trivalent actinides from a waste solution in one step, replacing the sequential DIAMEX-SANEX processes. In taking the PUREX raffinate and undertaking the extraction in a single step the number of cycles necessary for reprocessing are reduced, ensuring ease and economic benefits. A solvent mixture including $CyMe_4$-BTBP **1.09** and TODGA **1.05** has been successfully demonstrated to achieve selective actinide extraction directly from PUREX raffinate with high selectivity.[52] The undesirable co-extraction of some fission and corrosion products was observed but this could be suppressed by the addition of other hydrophilic compounds. In the case of the abundant zirconium and molybdenum fission products, oxalic acid **1.06** could be added to the aqueous phase to ensure their retention. The use of L-cysteine **1.16** could be used to strip palladium following its extraction by the BTBP ligand, Figure 15. Both oxalic acid **1.06** and L-cysteine **1.16** were found to have no impact on the selectivity towards the actinides. However, drawbacks to this process are the relatively slow kinetics of An(III) extraction. The separation from Am(III) alone from a synthetic PUREX raffinate can be achieved with minor impurities, however, there is a necessity to maintain a slow flow rate as a consequence of the slow extraction kinetics of the 1c-SANEX process.[53]

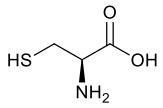

1.16

Figure 15: Structure of L-cysteine (**1.16**), a palladium suppression reagent.

More recently the combination of the hydrophobic $CyMe_4$-BTPhen ligand **1.17** with the hydrophilic extractant tetraethyldiglycolamide (TEDGA) **1.18** was observed to selectively extract Am(III) alone from a PUREX raffinate, Figure 16.[54] This included the additional separation of Am(III) from Cm(III), which is desirable for the future fabrication of a new fast reactor fuel, with a separation factor for Am(III) over Cm(III) ($SF_{Am/Cm}$) of 4.9. Cm(III) has a limited impact on the final radiotoxicity and heat-load of the sample compared to Am(III) (half-life of ^{244}Cm is 18 years) but has strong neutron radiation impacts and requires additional shielding when handling or

processing. In achieving this separation it ensures the safety of those personnel working on the new reactors.

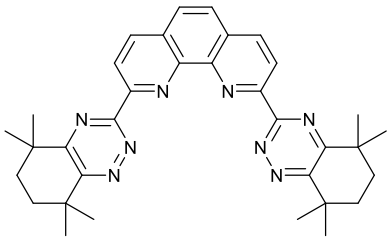

1.17

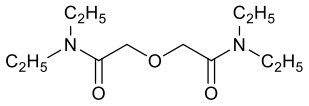

1.18

Figure 16: Structures of extractants for the 1c-SANEX process; $CyMe_4$-BTPhen (**1.17**) and TEDGA (**1.18**).

1.4.6. Processes involving selective aqueous complexation of An

Alongside the aforementioned, there are processes that achieve the An(III) partitioning by selectively retaining the An(III) in the aqueous phase, rather than selectively extracting them into the organic phase. These processes involve hydrophilic ligands that will either back-extract the An(III) selectively into the aqueous phase (after they have been extracted into the organic phase by a hydrophobic ligand), or retain the An(III) in the aqueous phase during an extraction step. Typically the co-extraction of the An(III) and Ln(III) into the organic phase is achieved at high acidity by a hydrophobic ligand before a hydrophilic ligand selectively back-extracts the An(III) into a fresh aqueous phase, with the ligand and specific conditions depending on the process employed. As hydrophilic ligands are not the focus of this thesis, these 'aqueous' processes will only be mentioned briefly here.

One of the most well-known processes involving hydrophilic ligands is the TALSPEAK (Trivalent Actinide from Lanthanide Separation by Phosphorus Reagent Extraction from Aqueous Komplexes) process which utilises polyaminocarboxylate ligands to achieve the separation.[55] In this process these ligands selectively retain the An(III) in the aqueous phase while a hydrophobic, non-selective ligand extracts the Ln(III) into the organic phase, hence achieving separation of An(III) from Ln(III). An alternative, typically using the same ligands (di[2-ethylhexyl]phosphoric acid) HDEHP **1.19** and DTPA (diethylenetriaminepentaacetic acid) **1.20**, known as the reverse

TALSPEAK process sees the co-extraction of An(III) and Ln(III) by HDEHP **1.19** prior to the partitioning of the An(III) into the aqueous phase with DTPA **1.20**, Figure 17.[56]

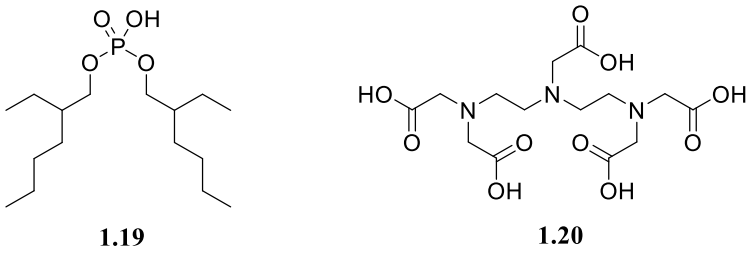

1.19 **1.20**

Figure 17: Structures of extractants used in the TALSPEAK process; HDEHP (**1.19**) and DTPA (**1.20**).

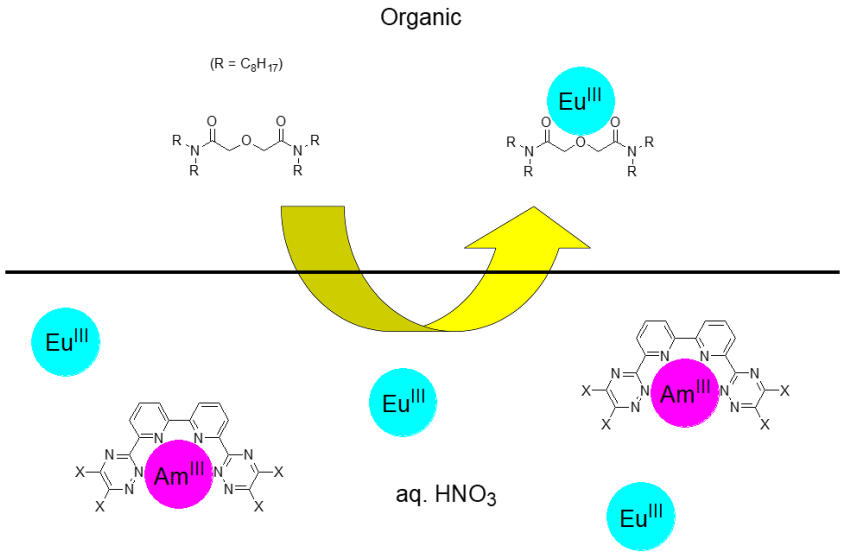

Figure 18: Diagram illustrating the principle of the *i*-SANEX process in which the lanthanides are selectively extracted into the organic phase.

An alternative process known as the innovative SANEX (i-SANEX) process involves co-extraction of the An(III) and Ln(III) prior to partitioning of the An(III), Figure 18. A diglycolamide such as TODGA **1.05** (the preferred ligand for the DIAMEX process) is used to co-extract the An(III) and Ln(III) prior to the use of a hydrophilic stripping agent, such as the sulfonated BTP **1.10**, to selectively strip the An(III) into the aqueous phase. This has additionally been considered to achieve the difficult separation of Am(III) from Cm(III), similar to what was achieved in the 1-cycle SANEX process.

The use of the hydrophilic SO_3-Ph-BTP ligand **1.10** has been found to suppress the extraction of Am(III) into the organic phase by TODGA **1.05** so that a separation factor for Am(III) over Eu(III) of approximately 1000 could be achieved.[41] The combination of SO_3-Ph-BTP **1.10** and TODGA **1.05** has demonstrated excellent separation of Am(III) and Cm(III) from Ln(III) starting from a simulated PUREX raffinate solution, with 99.8% of the An(III) recovered with minimal impurities. Additionally the BTP complexant **1.10** was found to have some selectivity for Am(III) over Cm(III) specifically with a separation factor of 2.5.[57]

This is not an exhaustive discussion of the aqueous processes available for the partitioning of An(III) but it provides a general overview of the basic principles of all aqueous solvent extraction processes. The only differences typically lie in the specific ligands, solvents and conditions used to achieve the required separations.

1.5. Ligands for Selective Actinide Extraction

In this section the complex criteria in which ligands developed for the SANEX and GANEX processes must meet is discussed, with three families standing out. Alongside the chemical ingenuity required to ensure the separation of two chemically similar groups, An(III) and Ln(III), the ligand itself has to abide by multiple criteria for future use in the nuclear fuel reprocessing industry. This has in no doubt resulted in the limited number of ligands being developed that have potential application in the reprocessing industry. Below is an indication of the criteria that has been established over the 20 years An(III) partitioning ligands have been investigated.

In terms of ligand design, they must be soluble in the required inert hydrocarbon-based organic diluents (kerosene, 1-octanol) requiring some consideration when functionalising, i.e. limiting aromaticity. It is preferred the ligand abide by the ‘CHON’ principle, dictating that a material should only be comprised of the elements; carbon, hydrogen, oxygen and nitrogen so that it can be completely incinerated to gases, hence reducing the final volume of waste for disposal in a geological repository.

In order to achieve the optimum extraction, the ligand requires a distribution (*D*) ratio, a measure of extraction affinity, high enough to ensure An(III) separation from wastes with high metal

loading. However, this *D* ratio must not be so high that it hinders the subsequent stripping of the metal from the ligand after separation, to enable ligand recycling. An ability to extract the An(III) at high acidities is essential as the partitioning is completed at acidities of >4 M nitric acid (HNO_3). In line with the conditions experienced during extraction the ligand must be resistant to radiolysis and hydrolysis, to withstand degradation.

A large dipole is favoured so that the ligand interacts more favourably at the interface between the organic and aqueous layers, facilitating a faster rate of extraction, by ensuring the ligand has more opportunity to come into contact with the metal ions. Finally, for industrial implementation, a ligand that is relatively cheap and/or easy to synthesise at scale is desirable.

With considerations made to the above criteria, a wide number of ligands have been investigated that achieve the partitioning of the An(III) from nuclear waste, albeit to varying degrees of success. Traditional ligands focused on the co-extraction of the *f*-elements and included organophosphorus compounds and diamides (i.e. diglycolamides) for use in the PUREX and DIAMEX processes, section 1.4. Most recently, ligand developments have focused on *N*-heterocyclic containing components for use in the SANEX and GANEX processes, which have been shown capable of separating the An(III) from the Ln(III). Each class of ligands have been extensively investigated with structural modifications and different solvent systems considered for optimum performance.[58]

This project focuses on ligands containing soft *N*- and *S*-donor atoms which have been found capable of distinguishing between the An(III) and Ln(III).[59],[60] They typically fall into two categories; hydrophobic or hydrophilic ligands, dependent upon which phase they are designed to dissolve in. There have been significant developments in the hydrophilic ligands, but they won't be discussed in this thesis.[61] The selectivity of the soft donor ligands is thought to be a result of the increased covalent interaction between the donor atoms of the ligands and the 5*f* orbitals of the actinides.[62],[21] These 5*f* orbitals are more diffuse and hence more available for metal-ligand bonding than the 4*f* orbitals of the lanthanides. Thermodynamic studies and X-ray crystal structures have been used to determine the difference in metal-ligand bond lengths

between the actinide and lanthanide complexes (An-M and Ln-M), to aid in the understanding of the origin of the selectivity. X-ray crystal structures have shown a shorter bond length for the actinide-ligand complexes with both the 2,2':6',2''-terpyridine (TERPY) **1.21** and 2,6-bis(5,6-dimethyl-1,2,4-triazin-3-yl)pyridines (Me-BTP) **1.22** ligands, suggesting the presence of π back-bonding interactions.[63],[64] Computational studies have supported the theory that the more diffuse *d*- and *f*-orbitals of the actinides can form bonds, covalent in character, with soft *N*-donor atoms.[65]

In the following section the 'early' classes of *N*-donor ligands and the three most prominent *N*-heterocyclic ligand classes will be discussed; from early discovery, functionalisation, extracting ability and complexation studies.

1.5.1. Early *N*-donor ligands

The TERPY **1.21** ligands were one of the earliest classes of ligands to selectively separate the An(III) from the Ln(III), Figure 19. In combination with 2,6-bis(2-pyridyl)pyridine, TERPY **1.21** was shown to form 1:1 complexes with the Ln(III) in solid state studies. At low acidities TERPY **1.21** was able to separate Am(III) from Eu(III) with a separation factor ($SF_{Am/Eu}$) of 7.2, but due to ligand protonation this decreased progressively at nitric acid acidities above 0.1 M.[66] This stoichiometry suggests their inability to completely enclose the metal and may result in their poor separation factors. Crystal structures revealed the tendency of the TERPY ligands **1.21** to form hydrogen bonds through intramolecular interactions.[67] 2,4,6-tri(2-pyridyl)-1,3,5-triazine (TPTZ) **1.23** showed slightly improved distribution (*D*) ratios of Am(III) when compared to TERPY ligands **1.21**, with a $SF_{Am/Eu}$ of above 10.[68] Similar to that observed with the TERPY ligands **1.21**, TPTZ **1.23** exhibited weak extraction ability at high concentrations of nitric acid due to the competition between metal complexation and ligand protonation.[69]

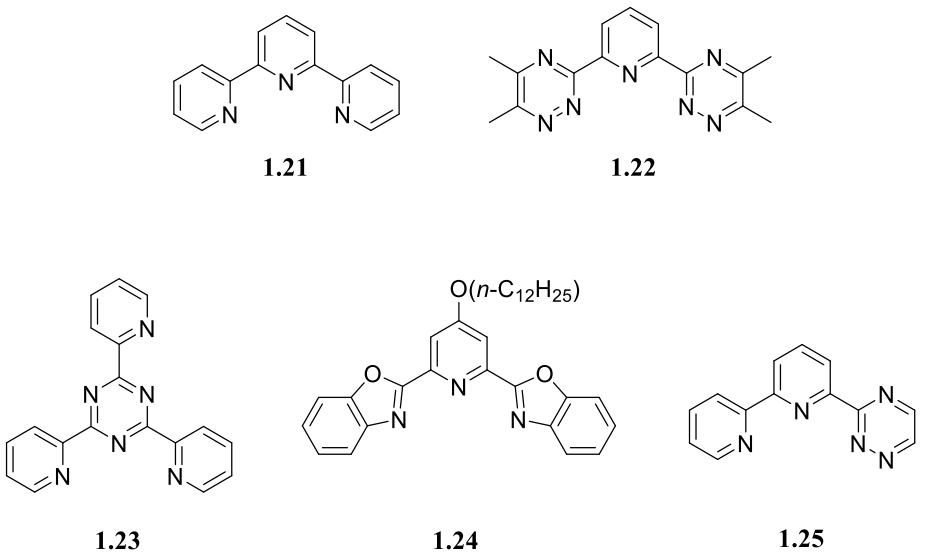

Figure 19: General structures of five classes of N-heterocyclic ligands; terpy (**1.21**), Me-BTP (**1.22**), TPTZ (**1.23)**, BODO (**1.24**) and hemi-BTP (**1.25**).

The 2,6-bis(benzoazol-2-yl)-4-dodecyloxypyridine (BODO) **1.24** and its derivatives showed comparable separation of Am(III) from Eu(III) to the previous ligands.[70] In contrast to previous ligands, BODO **1.24** showed an increased resistance to protonation at higher acidities but the distribution (*D*) of Am(III) and $SF_{Am/Eu}$ still observed a decrease, a result of increasing competition from the nitrate ions for complexation to the metal.[71]

In further developments, the hemi-BTPs **1.25** were synthesised and were shown to achieve the separation of Am(III) from Eu(III).[72] Their properties exist between those of the TERPY **1.21** and BTP families, which will be discussed in section 1.5.2. The formation of 1:1 and 1:2 lanthanide complexes were observed through crystallography and NMR studies and it was found that intramolecular bonding plays a key role in metal complexation.[73] For a complete review of ligands capable of extraction of the *f*-elements see papers by W. Verboom and co-workers or L.M. Harwood and co-workers.[58, 68]

1.5.2.Bis-triazinyl pyridine (BTP) ligands

Research by Z.Kolarik and co-workers in 1999 found that alkyl-BTPs were one of the first examples of *N*-donor 1,2,4-triazine ligands, Figure 20. These BTPs demonstrate high extraction efficiency and selectivity for the An(III) over the Ln(III), without the need of a phase transfer

agent, with separation factors ($SF_{Am/Eu}$) of close to 150 being observed, compared to that observed for terpy **1.21** and TPTZ **1.23**.[74] Electrospray ionisation mass spectrometry (ESI-MS), time-resolved laser-induced luminescence (TRLIL) and extended x-ray absorption fine structure (EXAFS) studies saw the formation of 1:3 complexes in the form of $[M(BTP)_3]^{3+}$,[75] with An(III) complexes showing increased complex stability compared to equivalent Ln(III) complexes, independent of the solvent used.[76] A ^{15}N NMR titration study with 2,6-bis(5,6-*n*-propyl-1,2,4-triazin-3-yl)-pyridine (*n*-PrBTP) **1.26** concluded that the bonding in its Am(III) complex was more covalent in character than that of a comparable Ln(III) complex, as observed by the large ^{15}N chemical shift for the coordinating atoms.[21]

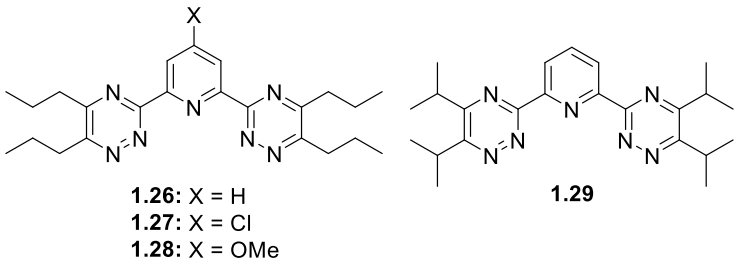

Figure 20: Molecular structures of representative alkylated-BTP ligands; *n*-PrBTP (**1.26**), Cl-Pr-BTP (**1.27**), OMe-Pr-BTP (**1.28**), *i*-Pr-BTP (**1.29**).

Functionalisation of *n*-Pr-BTP **1.26** with chlorine (Cl) **1.27** and methoxy (OMe) **1.28** groups investigated electronic effects and hence the basicity of the final ligands upon selectivity.[77] It was found that the *D* ratios and $SF_{Am/Eu}$ increased as basicity of the ligand increased, hence the ligand **1.28**, containing the OMe group, observed the greatest extraction properties as a result of the higher electron density in the pyridine ring.

These simple alkylated-BTP ligands were found to extract from high HNO_3 concentrations but had poor resistance towards radiolysis and hydrolysis in hot tests. A SANEX hot test was carried out with *n*-PrBTP **1.26**, however, it was found that some ligand degradation occurred during the 'hot-test'.[78] The degradation of the ligands was found to occur by attack of the free radical species (formed during radiolysis of the organic and aqueous phases) on the reactive benzylic positions adjacent to the triazine rings, leading to abstraction of a benzylic hydrogen. Trapping of

the resulting benzylic radical with a NO_2 radical initially forms a nitro compound before further degradation to the corresponding alcohol or ketone, as determined by gas chromatography (GC) and ESI-MS. Additional degradation ultimately leads to cleavage of the alkyl groups. Further studies found that branching of the alkyl groups at the benzylic α-position, as is the case for *i*-Pr-BTP **1.29**, can increase resistance to radiolysis and hydrolysis.

The Harwood group at Reading University found that introducing the tetramethyl cyclohexyl ($CyMe_4$) group led to the $CyMe_4$-BTP ligand **1.30** with resistance to radiolysis and hydrolysis, Figure 21, with separation factors $SF_{Am/Eu}$ of up to 5000 being observed, compared to that for *i*-Pr-BTP **1.29** which is 400. [79], [80] Unfortunately, despite the excellent extraction properties and high distribution ratio for Am(III) exhibited by $CyMe_4$-BTP **1.30**, stripping of the metal from the loaded organic phase, and subsequent recycling of the ligand in a future SANEX process, were not possible.

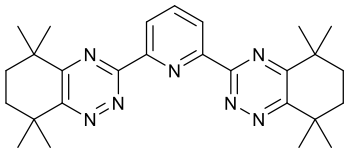

1.30

Figure 21: Molecular structure of the $CyMe_4$-BTP ligand (**1.30**).

The selectivity of these 1,2,4-triazine ligands is thought to result from the α-effect that occurs when two non-bonding nitrogen electron lone pairs are adjacent to each other, which can result in an increased covalent interaction upon complexation.[81] To confirm the impact of the α-effect the 1,2,4-triazine was replaced by 1,3,5-triazine ring to see if it impacted on the ligands extraction capability, Figure 22. It was found that upon replacement with the 1,3,5-triazine, the ligands performed significantly worse under the same solvent extraction conditions, suggesting that the 1,2,4-triazine ring is essential for good extraction and separation efficiency.[68]

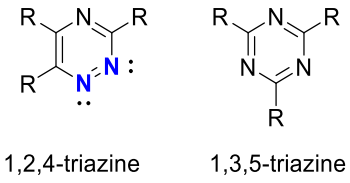

Figure 22: General structures of the 1,2,4-triazine and 1,3,5-triazine rings, showing the positioning of the adjacent lone pairs (highlighted in blue).

The development of the camphor-BTP ligand **1.31**, Figure 23, by Geist and co-workers was investigated to overcome the difficult back-extraction shown by $CyMe_4$-BTP **1.30** and the slow extraction kinetics shown by $CyMe_4$-BTBP **1.09**, as discussed in section 1.4.2. This ligand was found to be resistant to hydrolysis, in addition to showing fast extraction kinetics and high solubility in comparison to previously developed triazine ligands.[82] It has a solubility of 200 mmol/L in 1-octanol, compared to 10 mmol/L for the $CyMe_4$-BTBP ligand **1.09**. One downside was found to be the increasing tendency to form a precipitate when the organic phase was mixed with high HNO_3 concentrations in a kerosene/1-octanol diluent. The precipitate was thought to be the protonated ligand. This ligand **1.31** is discussed in more detail in chapter 3.

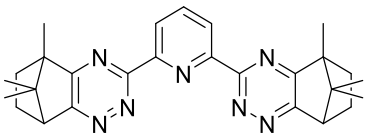

1.31

Figure 23: Molecular structure of camphor-BTP (**1.31**).

Consequently as discussed, BTPs with high *D* ratios and separation factors have been prepared and investigated. One major drawback of these ligands is the highly stable complexes, $[M(BTP)_3]^{3+}$, formed and the resulting impacts on back-extraction of the metal ions.

1.5.3. Bis-triazinyl bi-pyridine (BTBP) ligands

The BTBPs were developed by adding an additional pyridine ring to the BTP structures, extending the aromaticity and making it a tetradentate ligand. As with the BTP compounds, one of the first

BTBPs tested for selective actinide extraction was an alkylated derivative, 6,6'-bis-(5,6-dipentyl-[1,2,4]triazin-3-yl)-[2,2']bipyridinyl (C5-BTBP) **1.32**, Figure 24. This ligand has the ability to separate Am(III) from the Ln(III)s, although with lower *D* ratios then with the BTPs, with a D_{Am} of 2 at 1.0 M HNO_3, it does demonstrate that metal back-extraction is possible.[83] At the conditions back-extraction would occur, a HNO_3 concentration of 0.1 M, the C5-BTBP ligand **1.32** has a D_{Am} of 0.02. Additionally, this ligand observes some selectivity towards the transition metals; palladium and cadmium, so may have the potential to remove traces of these metals from solutions. The dependence of extraction capability on diluent choice is clearly evident in studies with the C5-BTBP extractant **1.32**, suspected to be influenced by intermolecular interactions between the ligand or metal complex with the diluent. Consistent with the alkylated-BTPs, this ligand was also susceptible to radiolysis on account of its benzylic hydrogens, making it unsuitable for future industrial use.[84]

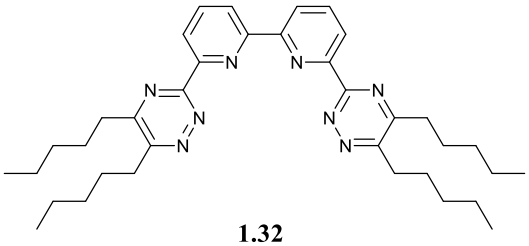

1.32

Figure 24: Structure of an alkylated-BTBP, C5-BTBP (**1.32**).

The $CyMe_4$-BTBP ligand **1.09**, which does not contain benzylic hydrogens, showed resistance to hydrolysis and radiolysis and a similar extraction selectivity to its BTP analogue **1.30**, Figure 25. Crucially however, stripping of the metal from the loaded organic phase was possible with $CyMe_4$-BTBP **1.09**, in contrast to $CyMe_4$-BTP **1.30**. On the other hand, the slow extraction kinetics observed with this family of ligands, required a contact time of one hour before reaching extraction equilibrium.[33] This impacts the final phase mixing times required to achieve separation and the ability of the ligand to extract from a waste solution with high quantities of radioisotopes. The addition of a phase transfer agent, such as DMDOHEMA **1.04** or TBP **1.01**, is required to improve the rates of extraction of the ligand by ensuring that extraction equilibrium is achieved within 5 minutes.[85] The phase transfer agent exists at the interface and can complex the

metal cation to transfer it into the bulk organic phase, where it is replaced by the $CyMe_4$-BTBP **1.09** to form a stable complex.[33]

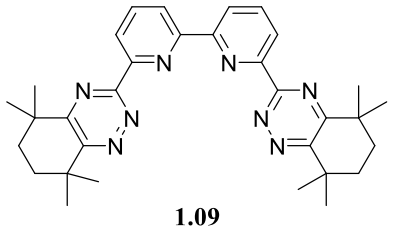

1.09

Figure 25: Structure of $CyMe_4$-BTBP (**1.09**), the current reference molecule for SANEX processes.

The combination of $CyMe_4$-BTBP **1.09** and DMDOHEMA **1.04** was analysed in a continuous counter current process using a genuine fuel solution, covering all extraction, scrubbing (Ln(III) back-extraction) and stripping (An(III) back-extraction) steps. The partitioning of the actinides was achieved with high selectivity with almost quantitative recovery of both Am(III) and Cm(III).[34] One drawback is still the slow kinetics, which results in a low flow rate during this process. For waste solutions in which large volumes are to be treated, as to be expected in industry, this would increase the time and cost of the process. These slow rates of extraction are thought to result from the conformation that the BTBPs adopt in solution. The major conformer is found to be the non-chelating *trans*-conformer or linear conformer, with a large energy barrier to overcome before rotation to the *cis*-conformer, Figure 26.[86] In addition the *trans*-conformer has a zero dipole moment, making it more hydrophobic than the *cis*-conformer and hence more likely to repel the water molecules at the interphase.

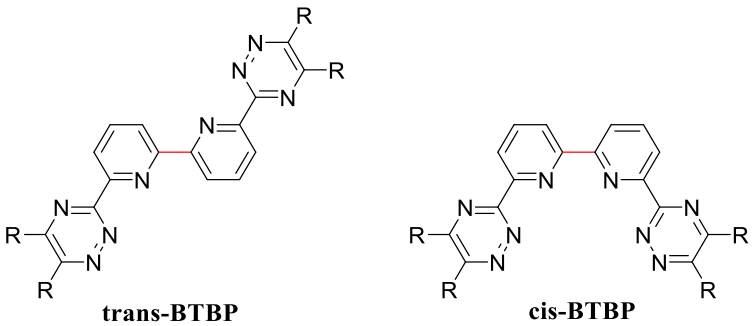

trans-BTBP **cis-BTBP**

Figure 26: The molecular conformation of a general BTBP in solution and the solid-state showing both the *trans*- and the *cis*-conformation required for metal complexation.

In attempts to influence the ligands slow extraction kinetics and solubility in preferred diluents, recent research has focused on functionalisation of the bipyridine backbone, Figure 27. Aneheim and co-workers introduced a *tert*-butyl group to the 4-position of the bis-pyridinyl backbone to produce an asymmetric ligand, *t*-BuCyMe$_4$-BTBP **1.33**. The addition of this group led to an increase in solubility (1110 mmol/L in cyclohexanone) which was found to be a consequence of the higher entropy of dissolution of the ligands.[87] Further modifications by L. M. Harwood and co-workers involved the introduction of a chloro and bromo substituent at the same position on the pyridine rings to produce two asymmetric ligands, **1.34** and **1.35** respectively.[88] Both ligands observed an increased solubility in the diluents 1-octanol (>170 mmol/L) and cyclohexanone (>230 mmol/L) compared to their predecessor **1.09**, and comparable separation factors for Am(III) and Eu(III) were observed, without the need for a phase-transfer agent.

Functionalisation in both the 4- and 4'- positions of the bis-pyridyl backbone with alkyl substituents, methyl and *tert*-butyl; leading to symmetric ligands **1.36** and **1.37** respectively, was expected to increase ligand solubility further due to the presence of the additional aliphatic groups.[89] However, the opposite was found to be the case, and both ligands **1.36** and **1.37** showed lower solubilities in several diluents and slower rates of metal-ion extraction. Am(III) distribution ratios of >1 were observed only after 30 hours of contact time, in 1-octanol and cyclohexanone. It is clear that substituent effects on the bipyridine backbone can have drastic impacts on ligand properties.

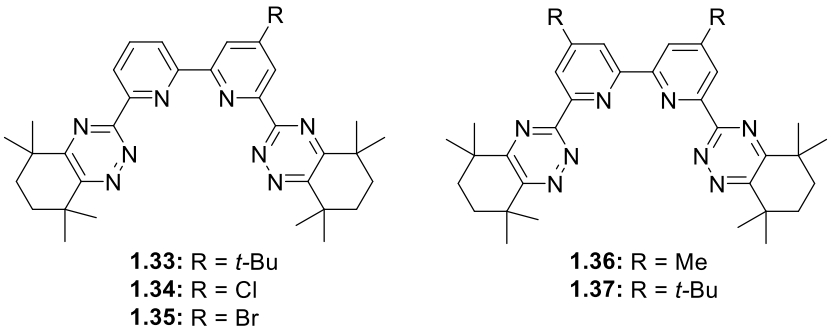

Figure 27: Molecular structures of functionalised BTBP ligands.

The structures of the complexes formed between $CyMe_4$-BTBP **1.09** and both Am(III) and Eu(III) where established by EXAFS studies to be largely constituting of $[Am(CyMe_4\text{-}BTBP)_2(NO_3)]^{2+}$ and $[Eu(CyMe_4\text{-}BTBP)_2]^{2+}$ respectively.[90] Changing the solvent system can have drastic effects on the stability of these complexes within solution and a careful balance of ligand solubility and high separation factor is necessary.[91] Again, an increased covalent interaction is indicated in theoretical studies with the actinide-BTBP complexes in comparison to the lanthanides, through the stronger interactions between Am(III) and the triazine *N*-2 atoms of the BTBP ligand.[92] A time-resolved laser fluorescence spectroscopy (TRLFS) study found a thermodynamic driving force behind the selectivity of BTBPs for the An(III) over the Ln(III), in particular the selectivity for Cm(III) over Eu(III), with stability constants of their complexes; of log K = 11.1 (for Cm(III)) and 9.0 (for Eu(III)) respectively.[93] The stability constants are consistently higher for the Cm(III)-ligand complexes suggesting there is a thermodynamic driving force for the complexation reaction, which is higher for Cm(III) than Eu(III). Further TRLFS studies have shown a 1:2 complex is formed with Eu(III) and Cm(III) in equilibrated samples and the space for the coordination of other anions and solvents can depend upon the bulkiness of ligands.[94]

Through these investigations it is clear the $CyMe_4$-BTBP **1.09** emerges as the prominent extractant of choice, with the most suited properties for the future reprocessing industry. However, this ligand suffers from poor extraction kinetics, requiring increased phase mixing times to achieve separation.

1.5.4. Bis-triazinyl phenanthroline (BTPhen) ligands

As discussed previously, $CyMe_4$-BTBP **1.09** suffers from slow extraction kinetics, even in the presence of a phase transfer agent. In order to tackle this issue the introduction of pre-organisation into the 2,2-bipyridine system led to the development of the 2,9-bis(1,2,4-triazin-3-yl)-1,10-phenanthroline (BTPhen) derivatives, Figure 28.[95] This pre-organised structure locks the 2,2'-bipyridine core of the ligand into the *cis*-conformation required for metal binding through the addition of a phenyl ring, giving rise to a 1,10-phenanthroline core. A stopped-flow technique revealed that the pre-organisation of the BTPhen observed a correlation with the kinetics of metal ion complexation.[96] X-ray crystallography of the free $CyMe_4$-BTPhen **1.17** shows a slight twist

of the two outer triazine rings out of the required conformation for metal complexation, although this would still be a significantly reduced conformational change than that required by $CyMe_4$-BTBP **1.09**.

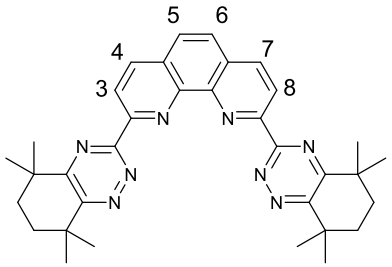

1.17

Figure 28: Molecular structure of $CyMe_4$-BTPhen (**1.17**), showing position numbering.

The extraction equilibrium with the $CyMe_4$-BTPhen **1.17** is achieved in approximately 15 minutes of phase mixing, showing a dramatic improvement on the extraction kinetics found with the equivalent $CyMe_4$-BTBP ligand **1.09**. This is in addition to increased extraction efficiency and high extraction selectivity for Am(III) over Eu(III).[97] Interfacial tension measurements reveal that a higher concentration of ligand sits at the interface during extraction, which suggests this plays a role in its improved extraction kinetics when compared to the BTBPs.

Computational studies have been completed to gain a greater theoretical understanding of the origin of the promising extraction properties of these ligands. One such study revealed that the size of the ligand cavity, influenced by the conformation of the ligands and orientation of the 1,2,4-triazine rings, can impact the ease of metal complexation.[98] In addition to the *cis*-locked structure, these ligands have a greater dipole moment than the BTBPs as well as the capability to accommodate a water molecule in the cavity, which is thought to contribute to its increased concentration at the interface.[95] The coordinated water molecule could form hydrogen bonds with water molecules at the interface leading to higher concentrations of the ligand at the interface and consequently faster extraction kinetics. The use of surface tension measurements, using the du Noüy ring method, provided further evidence for the increased activity of the $CyMe_4$-BTPhen **1.17** at the interface when compared to the $CyMe_4$-BTBP **1.09**, in which the $CyMe_4$-BTPhen observed increased surface activity in all diluents tested.

This ligand has been investigated for its potential to separate exclusively Am(III) from a PUREX raffinate. A separation factor ($SF_{Am/Cm}$) of 4.9 was observed between Am(III) and the other minor actinide Cm(III) when this ligand is used in combination with TEDGA **1.18**.[54] When silica magnetic nanoparticles functionalised with the $CyMe_4$-BTPhen **1.17** are utilised a $SF_{Am/Cm}$ of 2 is achieved at 4 M HNO_3, without the need for additional reagents.[99] This separation would be advantageous for the recycling of Am(III) alone for use as a new reactor fuel; Cm(III) has a higher neutron activity and would require additional shielding, but is relatively short-lived in comparison to Am(III).[100] The use of magnetic nanoparticles has been proposed as a viable option to reduce the secondary waste generated when using solvent extraction, as the use of large volumes of diluents are avoided.[101]

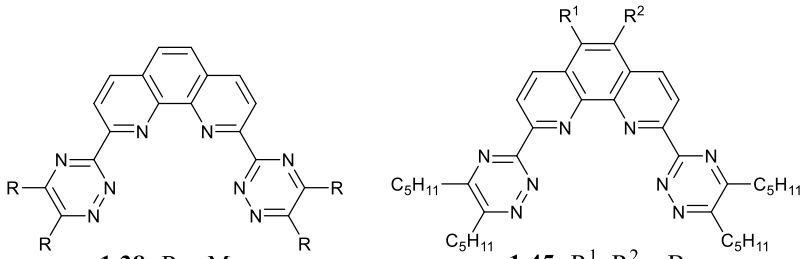

1.38: R = Me
1.39: R = *n*-Bu
1.40: R = *s*-Bu
1.41: R = pentyl
1.42: R = camphor
1.43: R = Ph
1.44: R = C_6H_4Br

1.45: R^1, R^2 = Br
1.46: R^1 = Br, R^2 = H

Figure 29: General structures of various BTPhen ligands, showing both triazine functionalisation and derivatisation at the 5,6-positions.

Investigating the impact of functionalisation on solubilities was completed with the BTPhen by modifying the triazine substituents to include alkyl, branched and cyclic groups, Figure 29. Increasing the length of the alkyl substituent chain saw a correlation with increasing solubility in all diluents investigated including; dodecane, 1-octanol and cyclohexanone, with pentyl-BTPhen **1.41** showing the greatest solubility of all ligands tested.[102] This BTPhen ligand **1.41** in particular was investigated further for the effect on electronic properties through functionalisation at the 5,6-position leading to ligands **1.45** and **1.46**. This modification resulted in a decrease in the distribution ratio of Eu(III), which consequently meant the $SF_{Am/Eu}$ was increased in comparison

to the analogous C5-BTPhen **1.41**.[103] However, based upon research regarding the alkylated-BTP **1.26**, this C5-BTPhen ligand **1.41** would also be susceptible to radiolysis on account of the benzylic hydrogens.

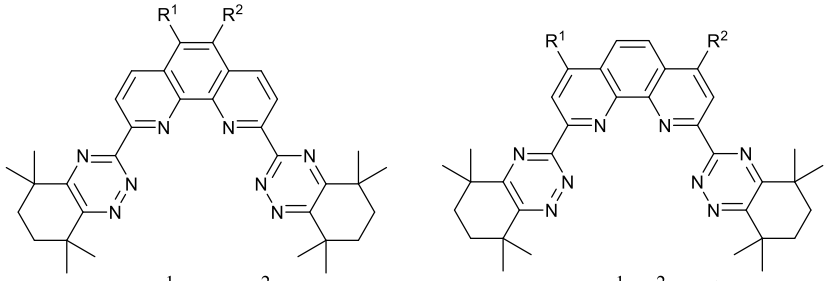

1.47: R^1 = Br, R^2 = H
1.48: R^1 = C_6H_4OH R^2 = H
1.49: R^1, R^2 = Br
1.50: R^1, R^2 = C_6H_4OH
1.51: R^1, R^2 = Cl
1.52: R^1, R^2 = MeO
1.53: R^1, R^2 = Ph
1.54: R^1, R^2 = H

Figure 30: General structures of various BTPhen ligands, showing the derivatisation at both the the 5,6- and the 4,7-positions.

The position of functionalisation on the 1,10-phenanthroline backbone can have pronounced effects on the metal ion distribution ratios at equilibrium, Figure 30. Studies into the functionalisation of $CyMe_4$-BTPhen **1.17** at the 5-position with bromine **1.47** and 4-hydroxyphenyl **1.48** substituents explored the effects on selectivity and distribution (*D*) ratios, with a focus on the selectivity between Am(III) and Cm(III).[104] The addition of bromine in **1.47** results in lower selectivity for Ln(III) than is observed with the benchmark $CyMe_4$-BTPhen **1.17** as a result of its inductive electron-withdrawing effect. This results in a decrease in the availability of the lone pair of electrons on the phenanthroline *N*-donor atom for taking part in complexation to the metal. This, in combination with the poor orbital overlap between the Ln(III) and the *N*-donor atoms, is thought to result in the lower selectivity. The 4-hydroxyphenyl substituent sees an opposite mesomeric electron-donating effect, and the lone pair of electrons on the *N*-donor atom are more available for orbital overlap with the metal ion, resulting in increased *D* values for some of the Ln(III).

A comparison of the relative position of functionalisation found that there is a greater influence on the extraction properties when there is functionalisation at the 4,7-positions over the 5,6-positions. This is proposed to result from enhanced electronic modulation due to the *para*-positioning of the substituents relative to the nitrogen atoms of the phenanthroline, which are known to coordinate to the metal ion.[105] A 1:2 metal:ligand complex species was observed exclusively for those ligands derivatised at the 4,7-positions using TRLFS studies.[106]

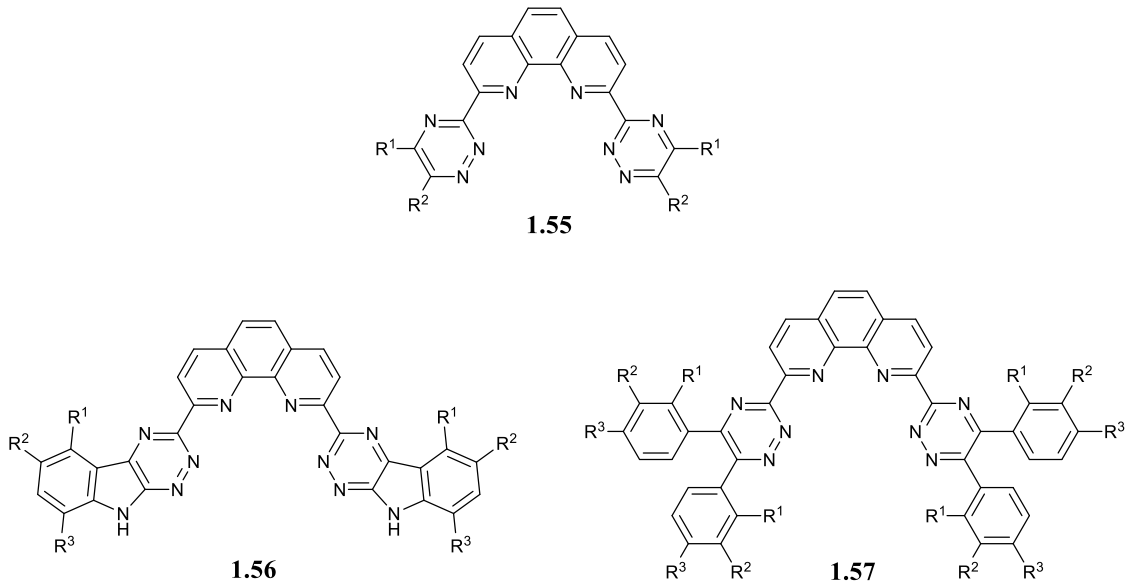

Figure 31: General structures of BTPhen derivatives functionalised at the 5,6-positions of the 1,2,4-trizaine rings by S.L.Heath and co-workers; aliphatic-BTPhens (**1.55**), isatin-BTPhens (**1.56**) and benzil-BTPhens (**1.57**).[107]

Further research has been completed into the functionalisation of the 5,6-positions of the 1,2,4-triazine rings and these studies indicate functionality can be utilised to tune properties such as solubility, extraction rate and extraction affinity. S.L.Heath and co-workers introduced further functionality using commercially available diketones to replace the $CyMe_4$ diketone such as isatin **1.56**, benzil **1.57** and various aliphatic diketones **1.55**, Figure 31.[107] Where additional aromaticity was introduced, with the isatin-BTPhens **1.56** and benzil-BTPhens **1.57**, they were all found to have poor solubility regardless of the groups at the R positions. The isatin-BTPhens **1.56** were found to co-extract Eu(III) whereas this effect was less pronounced for the benzil-BTPhens **1.57**. For the alkylated derivatives there was an increasing solubility as the alkyl chain length increased,

as observed in the research by Harwood and co-workers.[102] However, this correlated to a decreasing separation factor for Am(III) over Eu(III), potentially as a result of the negatively impacted hydrolytic and radiolytic stability.

The differences between the selectivity of the BTPhen ligands towards the An(III) and Ln(III) have been studied using various methods. X-ray diffraction (XRD), X-ray absorption spectroscopy (XAS) and luminescence spectroscopy studies revealed the formation of 10-coordinate 1:2 [M:L] complexes, with two $CyMe_4$-BTPhen **1.17** molecules surrounding the respective Ln(III) centres. Additional coordination sites usually being occupied by a bidentate nitrate ion.[32] A TRLFS study revealed both Cm(III) and Eu(III) complexes with $CyMe_4$-BTPhen **1.17** exist predominantly as 1:2 [M:L] complexes at equilibrium, with a greater stability constant observed for the Cm(III) complex.[94a] This study also provided additional evidence for the increased stability of the $CyMe_4$-BTPhen **1.17** complexes when directly compared to the $CyMe_4$-BTBP complexes **1.09**, although this is less pronounced for the Eu(III) complex.

The radiolytic stability of the benchmark BTPhen ligand, $CyMe_4$-BTPhen **1.17**, was studied in cyclohexanone-based solvents and found that, with an increasing dose of (γ) radiation, the concentration of this ligand and the respective *D* ratios for Am(III) and Eu(III) both decreased.[108] This effect is somewhat limited by the presence of ligand-diluent adducts, formed through the degradation of the parent ligand under radiolysis, with the dominant 1-octanol-ligand product observed by MS.[109] Interestingly those samples in contact with HNO_3 during irradiation observed a greater stabilisation of the distribution ratios of Am(III) and Eu(III). When the radiolytic stability of the ligand **1.17** is tested in the phenyl trifluoromethyl sulfone (FS-13) **1.58** diluent, Figure 32, an opposite trend is observed in which the distribution ratios increase with an increasing radiation dose. This is despite an increased degradation rate of $CyMe_4$-BTPhen **1.17** in comparison to $CyMe_4$-BTBP **1.09** when in contact with the acidic aqueous phase, suggesting the degradation products of the BTPhen are themselves efficient extractants.[110]

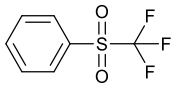

1.58

Figure 32: Structure of diluent FS-13 (**1.58**).

The functionalisations discussed in this section give a clear indication of the impact that introducing certain groups can have on the extraction properties of the ligands. Currently from those BTPhens discussed here, the $CyMe_4$-BTPhen **1.17** remains the most appropriate ligand for use in a SANEX or GANEX type process.

1.6. Project aims and objectives.

New ligands with improved solubilities and rates of extraction are needed for a feasible, economic and safe SANEX or GANEX separation process to be developed. The current European benchmark ligand, $CyMe_4$-BTBP **1.09**, has a solubility limit of approximately 10 mmol/L in 1-octanol and requires the use of a phase transfer agent to ensure sufficiently fast rates of extraction.[33] Increased solubility would reduce the chances of precipitation or third phase formation occurring during the extraction process, hence the process becomes safer to manage. Additionally less diluent would be needed to ensure dissolution of the ligand, reducing the costs of reprocessing those fuels with a higher minor actinide content, such as those that will be produced by future GEN(IV) reactors. However, attempts to increase the solubility of the BTBP, without adversely affecting the extraction kinetics, has been largely unsuccessful to date, see section 1.5.3.

Faster rates of extraction are essential in reducing the time and ultimately the costs required for an industrial process to achieve efficient extraction of the An(III). A ligand with faster rates of extraction would not require an additional phase transfer agent and hence the costs of running the process would be reduced. It would also mean that extraction can be achieved with shorter mixing times and faster flow rates, reducing the operating time and hence the cost of the process. Currently, the time taken for solutions of $CyMe_4$-BTBP **1.09** in 1-octanol to reach extraction

equilibrium is over one hour, which would be undesirable for an industrial process due to the increased costs and time necessary to ensure efficient extraction of the An(III).

This project will consider a novel approach to designing new families of bis-1,2,4-triazine ligands that show improvements on the aforementioned drawbacks. The synthesis and evaluation of these ligands will ultimately lead to validation of the design approach utilised to inform future research in this area.

1.6.1. Project Aims

Aim 1: To design and synthesise new classes of multidentate ligands based around the crucial 1,2,4-triazine moiety that will be suitable for future industrial use in the separation of the actinides from the lanthanides.

Aim 2: To investigate the ability of the new ligands to selectively extract and separate actinides from lanthanides (including measuring their solubilities and rates of extraction).

Aim 3: Where applicable, to investigate how the new ligands complex the trivalent lanthanides (used as surrogates for the trivalent actinides) and selected fission and corrosion products that are present in spent nuclear fuel.

Aim 4: To validate our approach to improving the solubilities and rates of extraction of the novel ligands using the solvent extraction data obtained in (aim 2) above.

1.6.2. Novel Ligand Design Approach

In an attempt to establish a set of guidelines to improve ligand solubility and rates of extraction in future ligand developments, a novel ligand design approach will be investigated. This approach takes inspiration from various aspects of the pharmaceutical industry and their drug discovery protocols. Christopher Lipinski formulated the "Rule of Five" (RO5) over 20 years ago to streamline drug discovery by defining what properties would make a drug orally active in humans.[111],[112],[113] The RO5 sets parameters that can predict the permeability and solubility of a compound based upon its physical and chemical properties, such as the molecular mass being

below 500 and a log *P* maximum of 5. Importantly for the design approach the focus will be on those factors relating to lipophilicity, solubility and polarity.

The number of hydrogen bond donors (HBD), those functional groups containing N-H, O-H or S-H groups in which a proton can be removed, i.e. donated, must be no more than 5. The number of hydrogen bond acceptor (HBA) functional groups, those functional groups containing heteroatoms with lone electron pairs, must be no more than 10 and include all heteroatoms with lone pairs of electrons present. These HBD/HBA functional groups are valuable in the ligand design approach as they can potentially participate in hydrogen bonding with water molecules at the phase interface, ensuring higher concentrations of the ligands exist at the interface and hence faster rates of metal extraction. As discussed in section 1.5.4, the higher polarity of the BTPhens compared to the BTBPs are beneficial to its rates of extraction by ensuring it has a higher concentration at the phase interface than BTBP, which was confirmed by surface tension measurements on $CyMe_4$-BTPhen **1.17** and $CyMe_4$-BTBP **1.09** using the du Noüy ring method.[95] In addition, the X-ray crystal structure of $CyMe_4$-BTPhen **1.17** shows a water molecule within the ligand's coordination cavity, which is suspected to be able to form hydrogen bonds with water molecules at the interface, hence aiding in its faster extraction rates compared to $CyMe_4$-BTBP **1.09**.[95]

Log *P* is used to measure the lipophilicity of a drug and is the calculated partition coefficient of a drug molecule between 1-octanol and water, or an aqueous and lipophilic phase (eq. 1.). This is significant, as one of the preferred diluents for reprocessing spent nuclear fuel is 1-octanol, so a molecule with a high log *P* value is likely to have a high solubility within this diluent. However, the value can't be taken as a predictor of absolute solubility of a ligand, as log *P* is calculated as a ratio of the relative solubility of a ligand in octanol compared to that in water. The log *P* can be calculated to predict the limitation of adding HBD/HBA functional groups (which tend to decrease log *P*) and at which point their addition can cause too large a decrease in this value. The limitation point is vital in ensuring the ligand doesn't become too polar that it partitions into the aqueous phase, rendering the lipophilic ligand ineffective for the proposed An(III) extraction. The

log *P* value will be calculated theoretically from the ligand structure using the ACD/I-labs software (ACD/Labs, 2010-2018).

$$\log P_{oct/wat} = \log(\frac{[solute]_{octanol}}{[solute]_{water}}) \qquad \text{Eq. 1}$$

Additional research by Lovering and co-workers demonstrated that there exists a correlation between drug solubility and its degree of saturation.[114] The fraction of saturated carbon atoms in the molecule (Fsp^3), calculated by taking the number of sp^3 carbons in the molecule and dividing it by the total number of carbon atoms (eq. 2.), can hence be used to predict its solubility. For the purpose of this project the degree of saturation will be investigated as a means of predicting the solubility of a ligand in an industry relevant diluent i.e. 1-octanol. Implications for ligand development in this field include limiting the development of ligands with too high a degree of unsaturation, i.e. by having too many aromatic rings, which would have low Fsp^3 values. Indeed, many such ligands are known to have very low solubilities in 1-octanol.[107] Therefore the only aromaticity to be included within the new families of ligands will be the 1,2,4-triazine rings and potentially an aromatic linker (typically one or more pyridine rings), as these are required to ensure strong metal ion coordination and high selectivity for An(III) over the Ln(III). Improving solubility will be achieved by using alkyl and cycloalkyl groups attached to the outer 1,2,4-trizine rings that follow the 'like dissolves like' principle. The relevance in designing novel ligands is that those ligands with less aromatic rings and more aliphatic groups will be structurally more 'like' the aliphatic diluent, 1-octanol, and hence should be more soluble in it. Previous research on hydrophobic ligands such as DMDOHEMA **1.04** and TODGA **1.05** for use in the DIAMEX process, section 1.4.2, has shown that these ligands which contain long alkyl chains and no aromatic rings and have very high solubilities (up to approximately 0.1 M) in the required diluents.[26] Significantly, despite being very hydrophobic, these ligands still exhibit very fast rates of metal extraction, and extraction equilibrium is typically reached within 5 minutes.[61c]

$$Fsp^3 = (\frac{\#sp^3\ hybridised\ C}{\#carbon}) \qquad \text{Eq. 2}$$

The above design criteria can be calculated from the chemical structure of the ligands themselves by using a chemical structure drawing software package such as ChemSketch, ChemDraw or the online resource ACD ILab.

In the subsequent chapters the synthesis of a variety of novel ligands will be discussed. Derivatisation of the adjacent side groups to the 1,2,4-triazine as well as changing the connecting bond between the pyridine(s) and external 1,2,4-triazines have been investigated, Figure 33. Each derivatisation or new functionality investigated has been attempted to give novel BTPs, BTBPs and BTPhen ligands.

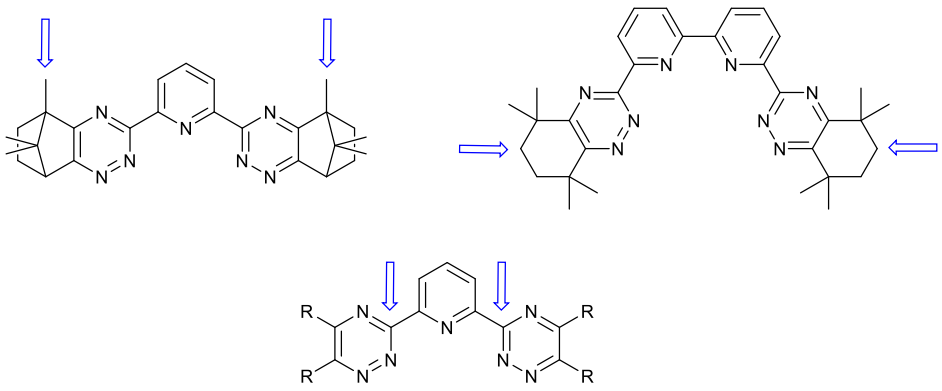

Figure 33: Example structures of BTPs and a BTBP indicating the positions where derivatisation will be focused, both on groups adjacent to the 1,2,4-triazine ring and in the connecting bond(s) between the pyridine and external 1,2,4-triazine rings.

Chapter 2

Ligands derived from 3-amino-1,2,4-triazines

2. Ligands derived from 3-amino-1,2,4-triazines

2.1. Introduction

In the 1990s, research by Buchwald and Hartwig found that palladium (Pd) can be utilised to promote the amination of aryl, vinyl and heteroaryl halides with a variety of amines.[115] The reaction provides an alternative method to traditional amination routes, such as the Ullmann coupling reaction,[116] which employ harsher reaction conditions and has limited substrate scope and versatility. Since this initial discovery, the palladium catalysed Buchwald-Hartwig C-N amination reaction has been extensively investigated, demonstrating its flexibility with a wide range of substituents on both reacting partners, including electron-withdrawing, electron-donating and sterically hindered groups. The potential of the Buchwald Hartwig reaction between 3-amino-1,2,4-triazines (**2.1.1**) and aryl halides (**2.1.2**), to synthesise novel families of ligands (**2.1.3**), will be explored, Figure 34.

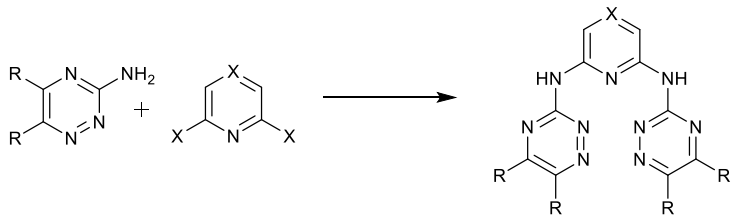

2.1.1 **2.1.2** **2.1.3**

Figure 34: Proposed Buchwald Hartwig amination reaction to form a novel family of ligands (**2.1.3**). General conditions: Palladium catalyst, ligand, base, solvent.

Various articles have explored the reaction mechanism, both experimentally and theoretically, [117] and a general outline is shown in Figure 35. Following traditional cross coupling mechanisms, after the initial formation of the Pd(0)-ligand precatalyst, oxidative addition across the C-halogen bond is achieved with the electrophile, in this case an aryl halide. The nucleophilic amine then coordinates to the Pd(II) centre in a ligand substitution step and is deprotonated by the base to leave a neutral Pd(II) complex. The base, used in excess, additionally aids in the stabilisation of the leaving anionic halide species. The final reductive elimination step sees the formation of the carbon-nitrogen bond of the product as well as regeneration of the active catalyst, Pd(0)-ligand.

The specific order of coordination and deprotonation, especially involving the base and ligand, remain unclear due to the complexity of studying an equilibrium involving many rapidly interconverting complexes. Having a detailed mechanistic understanding would undoubtedly lead to easier tuning of the amination reaction parameters to ensure maximum yields, but due to the difficulty in isolating the intermediates in solution or solid-state the catalytic cycle is still debated.

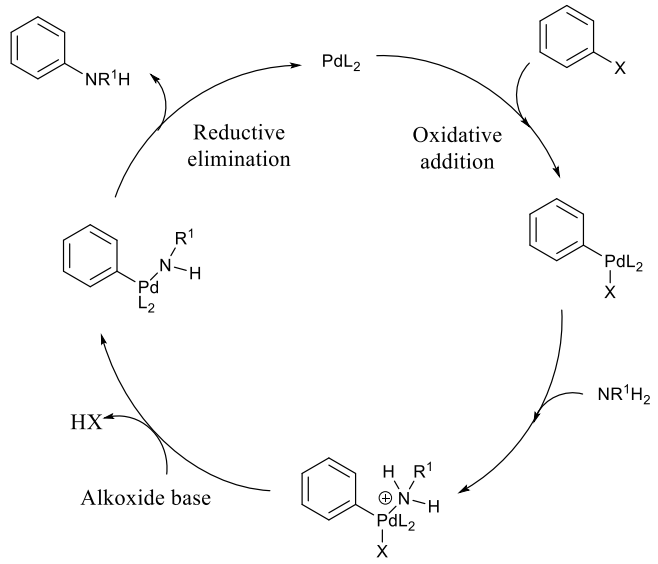

Figure 35: General scheme outlining the Buchwald Hartwig reaction mechanism.

In order to maximise the scope of the Buchwald Hartwig amination the choice of catalyst, ligand, base and other reaction parameters needs to be tailored dependent on the starting substrates. [118],[119] Due to the variable nature of the amines that can be employed in the reaction, optimising the reaction conditions can prove challenging. Each amine can have a different pK_a and nucleophilicity, which in turn alters the rate determining step of the catalytic cycle.[120] In most cases the ligand is key to the success of the reaction as it can be tuned depending on the properties of the substrates, i.e. electronic, steric etc. to limit the effect of the rate determining step.[121] For example electron-rich complexes have been found to slow down the reductive elimination step.[122]

Some isolated examples of Buchwald Hartwig amination reactions with substrates containing 1,2,4-triazine rings as the amine nucleophile have been reported in the literature. These reactions typically use tris(dibenzylideneacetone)dipalladium(0) ($Pd_2(dba)_3$) **2.1.4** and 4,5-

bis(diphenylphosphino)-9,9-dimethylxanthene (xantphos) **2.1.5**, Figure 36.[123],[124] Xantphos **2.1.5**, a bulky electron-rich, tridentate bisphosphine, is the prominent ligand for this amination due to its strong σ-donor ability and wide bite angle (110.0 °), which promotes the ease of reductive elimination of the product from the Pd(II) intermediate.[125] Xantphos **2.1.5** is additionally hemilabile, meaning one of its coordinating phosphines can be displaced from the metal centre with ease, freeing up a coordination site on the metal and lowering the energy barrier for binding, whilst the other phosphine remains bound to the Pd centre.[126] In the cases where long reaction times are necessary, an extra equivalent of ligand to metal can aid in stabilising the catalyst.

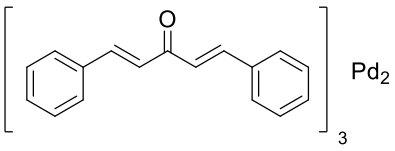

2.1.4

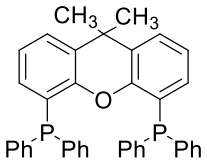

2.1.5

Figure 36: Structures of the Palladium $Pd_2(dba)_3$ **2.1.4** source and Xantphos ligand **2.1.5**.

Additionally, the palladium source needs to be considered. The presence of the coordinating dibenzylideneacetone (dba) group in $Pd_2(dba)_3$ **2.1.4** or $Pd(dba)_2$ **2.1.6** can hinder the formation of the active catalyst.[127] The use of palladium acetate, $Pd(OAc)_2$, **2.1.7** requires the reduction of Pd(II) to Pd(0) prior to entering the cross coupling cycle. The use of pre-catalyst systems have seen a greater focus due to their benefits, which include; high activity, greater stability (to air and moisture) and activation under the basic conditions used in the cross coupling reaction.[128]

Research using 1,2,4-triazines as the nucleophilic amine partner have been successfully demonstrated in Buchwald Hartwig amination reactions.[124, 129] It was decided to use caesium carbonate (Cs_2CO_3) as the preferred base, founded on similar reactions, as it offers a wide functional group tolerance and greater solubility than K_2CO_3 in organic solvents. Research recently published by the Carrick Group demonstrated the first successful double amination of functionalised heteroaryl-1,2,4-triazines **2.1.8**, Figure 37.[130] This has been achieved with various aliphatic, benzylic and functionalised amines to result in the formation of aminated-1,2,4-

triazinylpyridines **2.1.9**. Currently however, no examples of a Buchwald Hartwig double-amination reaction directly utilising 3-amino-1,2,4-triazines **2.1.1** as the nucleophile partner have been reported in the literature.

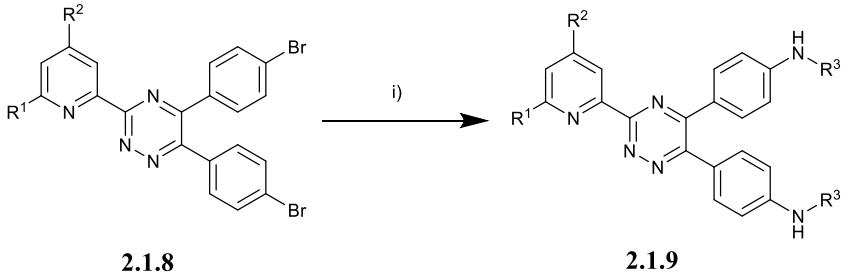

Figure 37: General reaction scheme for the di-amination *via* the Buchwald Hartwig methodology used by the Carrick group [152]. Reaction conditions; i) $Pd_2(dba)_3$ (2.5 mol%) **2.1.4**, ligand (5 mol%), NH_2R^3 (3 equiv), potassium phosphate (3 equiv).

Realising the potential of the Buchwald Hartwig amination reaction to access novel families of multidentate bis-1,2,4-triazine ligands, the Buchwald Hartwig reactions were explored with various heteroaryl halides **2.1.2** and readily synthesised 3-amino-1,2,4-triazines **2.1.1**. By building on previous work, the parameters for the successful amination involving this group will be investigated to enable the synthesis of two novel families of multidentate ligands. The amine partner will be varied based upon the diketone used to synthesise the 3-amino-1,2,4-triazine, and the aryl halide will be varied depending upon the aryl moiety used, and the desired denticity of the target ligands; pyridine, pyrazine, 2,2-bipyridine or 1,10-phenanthroline.

2.2. Ligands derived from di-amination of 2,6-dibromopyridine and related compounds

In order to establish the best synthetic protocol for the Buchwald Hartwig amination with the 3-amino-1,2,4-triazines **2.1.1**, the commercially available and inexpensive diketone, 3,4-hexanedione **2.2.1**, was used. The final ligands synthesised from this diketone will not be screened for their extraction capabilities, due to their unsuitability in the reprocessing industry. These ligands contain benzylic hydrogens on the carbon adjacent to the triazine ring which are easily abstracted by oxygen free radicals, i.e. a hydroxyl radical. These free radicals are common within

nitric acid solutions in the nuclear industry and there abstraction would result in decomposition of the ligand, as discussed in section 1.5.[131]

Due to the predominance of the $CyMe_4$ diketone **2.2.5** in currently reported bis-1,2,4-triazine ligands, it was decided to also utilise this diketone in the synthesis of the new family of ligands. Its synthesis was achieved following the procedure by Lewis and co-workers outlined in the literature, Figure 38.[95] Firstly, ethyl isobutyrate **2.2.2** was deprotonated by the *in situ* formation of lithium diisopropylamide to form an enolate. Alkylation of this is then achieved with ethylene bis(trifluoromethanesulfonate) to form diethyl 2,2,5,5-tetramethylhexanedioate **2.2.3**. The ring closure of **2.2.3** was achieved via an intramolecular acyloin type condensation with metallic sodium and chlorotrimethylsilane forming an enediolate bis-silyl ether intermediate **2.2.4**. A silyl deprotection and final oxidation, using bromine in dichloromethane, gave the final diketone **2.2.5**. An alternative diketone, 3,3,5,5-tetramethylcyclopentane-1,2-dione **2.2.7**, can be prepared through a one-step oxidation of 2,2,4,4-tetramethylcyclopentan-1-one **2.2.6** with selenium dioxide. This step was completed by a colleague in the group, Figure 39.

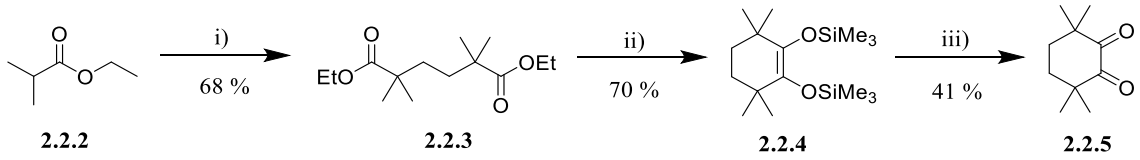

Figure 38: Reaction scheme for formation of $CyMe_4$ diketone **2.2.5**. Reaction conditions; i) LDA, ethylene bis(trifluoromethanesulfonate), anhydrous diethyl ether; ii) Na metal, Me_3SiCl, anhydrous toluene; iii) Br_2, DCM.

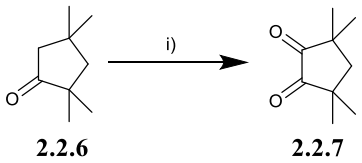

Figure 39: General synthesis of diketone **2.2.7**. Reaction conditions; i) SeO_2, 1,4-dioxane.

The final diketone under consideration as a viable alternative is the commercially available, chiral diketone (1*S*)-(+)-camphorquinone **2.2.8**, to provide an alternative to the multi-step synthesis

required to give the $CyMe_4$ diketone **2.2.5**. Other research groups have investigated racemic (±)-camphorquinone as a replacement diketone and despite an increased solubility of the camphor-BTP ligand **1.31** being observed, third phase formation occurred in extraction experiments upon contact of the organic phase with a HNO_3 aqueous phase of 3 mol/L or above.[132] Despite this, it was hoped the new family of ligands would not be susceptible to this precipitation. The selection of an enantiomerically pure diketone, (*1S)*-(+)-camphorquinone **2.2.8**, as opposed to racemic camphorquinone, will limit the potential formation of diastereomers of the final ligand.[132] The R groups from each diketone considered ultimately occupy the 5- and 6-positions of the triazine ring and this is where variability is introduced, Figure 40.

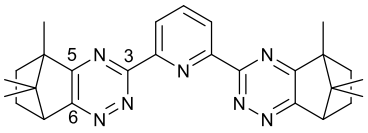

Figure 40: Molecular structure of camphor-BTP **1.31**. The absolute stereochemistry at the aliphatic carbons adjacent to carbons 5 and 6 is not specified since racemic (±)-camphorquinone was used by the authors.

For the purpose of forming the N-C bonds the 1,2,4-triazine compounds are required to have a nucleophilic amino group in the 3-position, to act as the nucleophile in the cross-coupling reaction. The commercially available and inexpensive aminoguanidine bicarbonate **2.2.9** was selected to ensure the amino group exists at the 3-position. The synthesis of the 3-amino-1,2,4-triazine compounds **2.1.1** was achieved through a condensation reaction between aminoguanidine bicarbonate **2.2.9** and each of the diketones; hexane-3,4-dione **2.2.1**, $CyMe_4$ **2.2.5**, Cy_5Me_4-diketone **2.2.7** and (1*S*)-(+)-camphorquinone **2.2.8**, Table 1 and Figure 42. Additionally utilised was 5,6-dimethyl-3-amino-1,2,4-triazine **2.2.10**, which was synthesised previously in the Lewis group. Due to four of the diketones being symmetrical the formation of only one regioisomer was observed. However, when (1*S*)-(+)-camphorquinone **2.2.8** was used, Table 1, entry 4, there is the potential for the formation of two regioisomers. In most cases this was not observed, with only one regioisomer dominating due to steric and electronic effects, Figure 41. The methyl group at the C-1 position of (1*S*)-(+)-camphorquinone **2.2.8**, results in steric hindrance around the adjacent

carbonyl group at C-2 and this is therefore the least favourable position for attack by the nitrogen nucleophile. The electronic effect across the N-C-N bond within aminoguanidine **2.2.9** makes the lone pair of the amine less available to act as a nucleophile. As a result of these effects there is some regioisomeric control in the reaction. The five 3-amino-1,2,4-triazine diketone compounds synthesised, Table 1, are used to form the final ligands through the Buchwald Hartwig reaction.

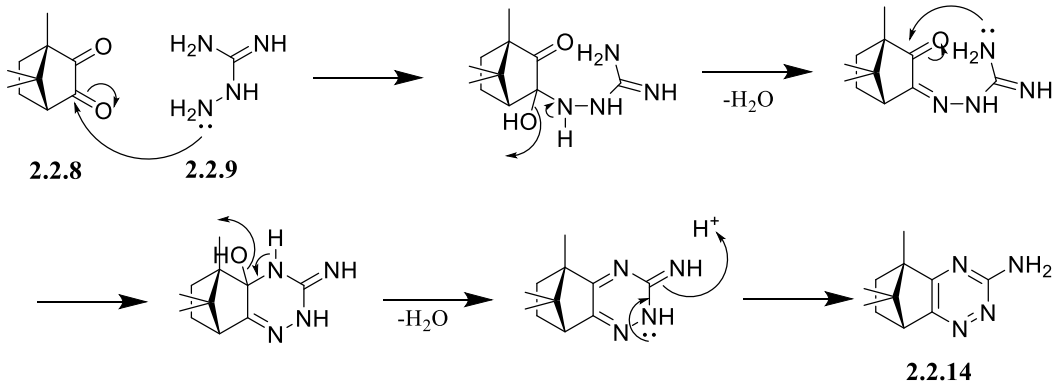

Figure 41: Reaction mechanism for the formation of the dominant regioisomer **2.2.14**.

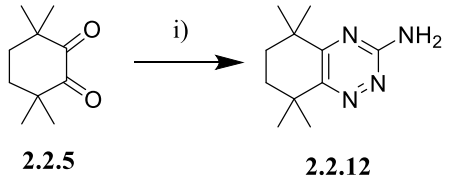

Figure 42: Example reaction scheme for the formation of 3-amino-1,2,4-triazines. Reaction conditions: i) aminoguanidine bicarbonate **2.2.9**, H_2O.

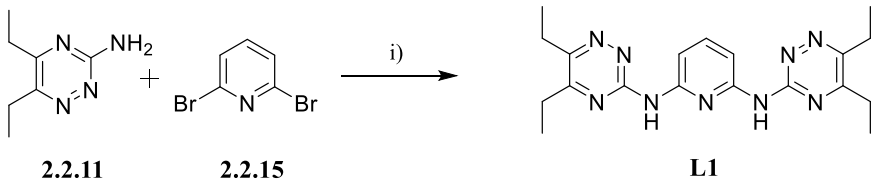

Figure 43: General reaction scheme for Buchwald Hartwig coupling. Reaction conditions: $Pd_2(dba)_3$ **2.1.4**, Xantphos **2.1.5**, $CsCO_3$, 1,4-dioxane, Δ.

The 3-amino-5,6-diethyl-1,2,4-triazine **2.2.11** and 2,6-dibromopyridine **2.2.15** were then used to optimise the reaction conditions and reagent stoichiometries in the Buchwald Hartwig reaction, to determine the optimum conditions required for the di-amination reaction, outlined in Table 3,

page 54. The optimum stoichiometry of the Pd catalyst **2.1.4** and phosphine ligand **2.1.5** were found to be 10 mol% and 20 mol% respectively to ensure the maximum yields of product were obtained, Figure 43.

Table 1: Summary of 3-amino-1,2,3-triazines formed through the condensation reaction of different diketones with aminoguanidine bicarbonate **2.2.9**.

Entry Number	Diketone	Product		Reaction Time (hr)	Yield (%)
1	**Hexane-3,4-dione** 2.2.1	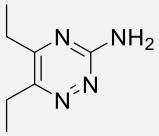	**2.2.11**	26	79
2	**CyMe$_4$-diketone** 2.2.5	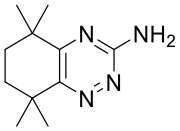	**2.2.12**	72	53
3	**Cy$_5$Me$_4$-diketone** 2.2.7	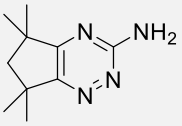	**2.2.13**	18	93
4	**(1*S*)-(+)-Camphorquinone** 2.2.8	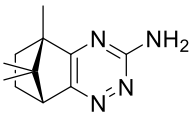	**2.2.14**	18	72

Xantphos **2.1.5** was chosen as the phosphine ligand of choice, as discussed in section 2.1, and hence further screening of other phosphine ligands was deemed unnecessary. A study by S.L. Buchwald's group found that there are two species formed when $Pd_2(dba)_3$ **2.1.4** and xantphos **2.1.5** are mixed; $Pd(Xantphos)_2$ **2.2.16** and Pd(Xantphos)(dba) **2.2.17**, Figure 44.[133] The formation of the $Pd(Xantphos)_2$ species **2.2.16** was found to significantly impact the reaction as a consequence of the large binding constant which in turn prevents the conversion to the active catalyst species, Pd(Xantphos)(dba) **2.2.17**. The xantphos **2.1.5** stoichiometry was limited at 20

mol% to limit the impact of this species. Utilising $Pd(OAc)_2$ **2.1.7** gave poorer yields than the alternative catalyst so was not considered further for this traditional route.

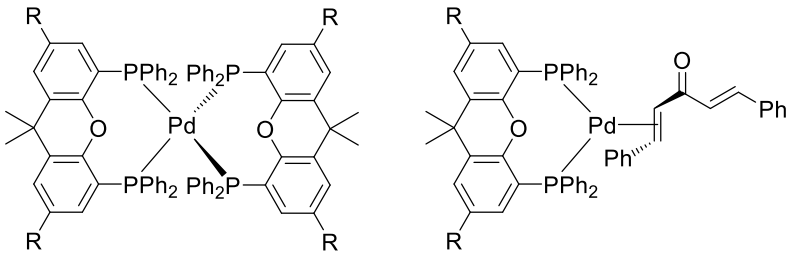

Figure 44: Structures of the two Pd-ligand species formed when $Pd_2(dba)_3$ **2.1.4** and xantphos **2.1.5** are mixed; $Pd(Xantphos)_2$ **2.2.16** and Pd(Xantphos)(dba) **2.2.17**.

The initial investigations using the 3-amino-5,6-diethyl-1,2,4-triazine **2.2.10** resulted in poor conversion to the di-aminated product **L1** in low yields. The mono-aminated product **L2** was observed initially, Figure 45, most likely resulting from the low ratio between the 3-amino-1,2,4-triazine **2.2.10** and 2,6-dibromopyridine **2.2.15**, resulting in the decision to use at least 2 equivalents of the 3-amino-1,2,4-triazine **2.2.10**. The formation of the di-aminated product **L1** could be easily observed through the integrations and number of signals in the ^1H NMR spectrum of the product as a result of the ligand's symmetry. The ^1H NMR spectrum, Figure 46, demonstrates the ease with which the mono- **L2** and di-aminated **L1** products are distinguished, in particular when focusing on the aromatic region. The mono-aminated product **L2** displays two doublets at δ 8.48 and 7.13 ppm and a broad signal at δ 7.87 ppm as a result of the lack of symmetry, each with an integration of 1H. A convergence of the two doublets at δ 7.74 ppm and a downfield shift of the broad singlet to δ 9.27 ppm indicate the presence of the di-aminated product **L1**, supported by a doubling of their respective integrations.

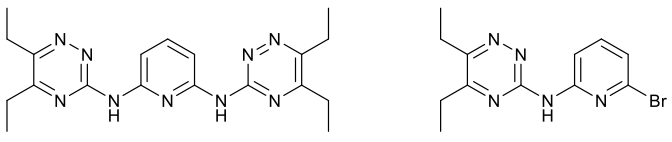

Figure 45: Structures of the di-aminated **L1** and mono-aminated **L2** products of the Buchwald Hartwig reaction.

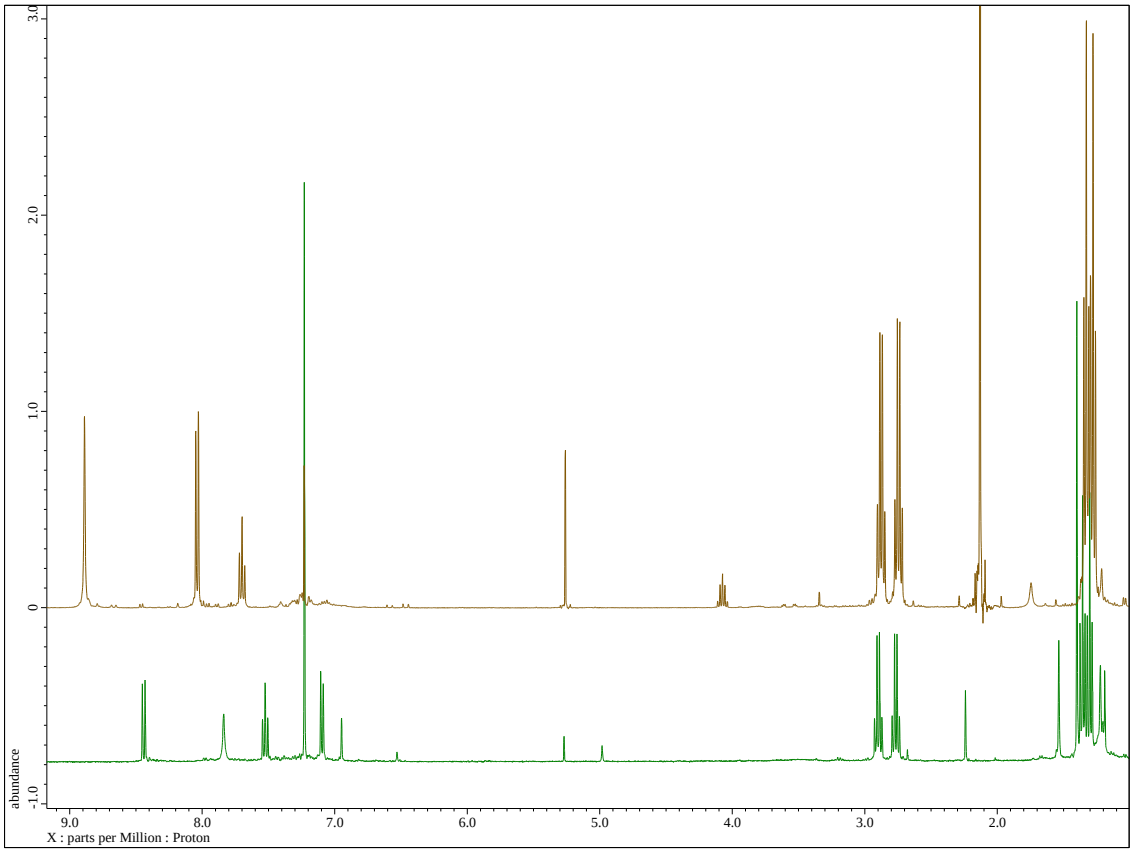

Figure 46: Overlaid ^{1}H NMR spectra for the a) mono-aminated ligand **L2** (bottom spectrum) and b) di-aminated ligand **L1** (top spectrum). Solvent impurities present.

Table 2: Assignment of signals for the comparison of the mono-aminated ligand **L2** and di-aminated ligand **L1**.

Mono-aminated ligand L2		**Di-aminated ligand L1**	
^{1}H (ppm)	**Proton integration and multiplicity (Hz)**	**^{1}H (ppm)**	**Proton integration and multiplicity (Hz)**
8.48	1H, d, *J* = 7.79 Hz	9.27	1H, s, br
7.87	1H, s, br	8.07	1H, t, *J* = 8.24 Hz
7.56	1H, t, *J* = 7.79 Hz	7.74	1H, d, *J* = 8.24 Hz
7.13	1H, d, *J* = 7.79 Hz	-	-
2.93	4H, q, *J* = 7.79, 7.33 Hz	2.91	4H, q, *J* = 7.79, 7.33 Hz
2.80	4H, q, *J* = 7.33 Hz	2.78	4H, q, *J* = 7.33 Hz
1.39	6H, t, *J* = 7.79, 7.33 Hz	1.37	6H, t, *J* = 7.79, 7.33 Hz
1.34	6H, t, *J* = 7.33 Hz	1.31	6H, t, *J* = 7.33 Hz

Table 3: Summary of reaction conditions attempted for Buchwald Hartwig reactions of 3-amino-1,2,4-triazines with different electrophiles; R = representative diketone. a) Mono-aminated compound formed only.

Entry	Nucleophile		Electrophile		Pd catalyst	Ligand	Base	Solvent	Reaction Time (hr)	Yield
1	2.2.10	2.0 eq	**2.2.15**	1.5 eq	$Pd_2(dba)_3$ 5 mol%	Xantphos 15 mol%	Cs_2CO_3	1,4-dioxane	21	14 % [a] **L2**
2	2.2.10	2.5 eq	**2.2.15**	1.0 eq	$Pd_2(dba)_3$ 4 mol%	Xantphos 12 mol%	Cs_2CO_3	1,4 -dioxane	71	14 % **L1**
3	2.2.10	2.5 eq	**2.2.15**	1.0 eq	$Pd_2(dba)_3$ 5 mol%	Xantphos 15 mol%	Cs_2CO_3	1,4-dioxane	48	26 % **L1**
4	2.2.14	2.0 eq	**2.2.15**	1.0 eq	$Pd_2(dba)_3$ 10 mol%	Xantphos 20 mol%	Cs_2CO_3	1,4-dioxane	72	81 % **L3**
5	2.2.18	1.0 eq	**2.2.19**	2.2 eq.	$Pd(OAc)_2$ 10 mol%	Xantphos 20 mol% CuMeSal (4 eq)	t-BuOK	Toluene	22	-
6	2.2.18	1.2 eq.	**2.2.19**	2.2 eq.	$Pd(OAc)_2$ 10 mol%	Xantphos 20 mol% CuMeSal (4 eq)	K_2CO_2	Toluene	24	-
7	2.2.18	1.2 eq.	**2.2.19**	2.2 eq.	$Pd_2(OAc)_3$ 10 mol%	Xantphos 20 mol% CuMeSal (4 eq)	Cs_2CO_3	Toluene	20	-

Attempts to further improve the yield involved increasing the reaction time and altering the stoichiometry of the catalyst **2.1.4** and phosphine ligand **2.1.5**, however this was to no avail, Table 3, entry 2 and 3. It is suspected that the weak nucleophilicity of the 3-amino-1,2,4-triazine compounds could be hindering the reaction, hence the coordination of the amine to the Pd centre may be the rate determining step. Hartwig and co-workers found that a large difference in the electronic properties of the reagents can result in an increased rate of reductive elimination, with electronic-withdrawing groups slowing the rate of reductive elimination.[134]

The use of the stronger base potassium *tert*-butoxide was investigated due to the evidence that amines more resistant to deprotonation, such as dialkyl amines, require a stronger base to achieve the reaction.[135] Its use in the reaction with **2.2.10** and **2.2.15** revealed a greater conversion of the starting reagents to the final ligand **L1** through examination of the ^{1}H NMR spectrum of the crude product, Figure 47. It is clear when utilising potassium *tert*-butoxide that there is a greater conversion to the product by examining the CH_2 of the ethyl groups, in which the peak intensities of the CH_2 groups from the starting material are significantly reduced. As this is a crude NMR spectrum, the other peaks within this region are a result of solvent impurities. Purification of the crude mixture resulted in comparable yields as observed previously. Going forward, Cs_2CO_3 will be utilised as a result of the high yield obtained for the camphor ligand **L3**, Table 3.

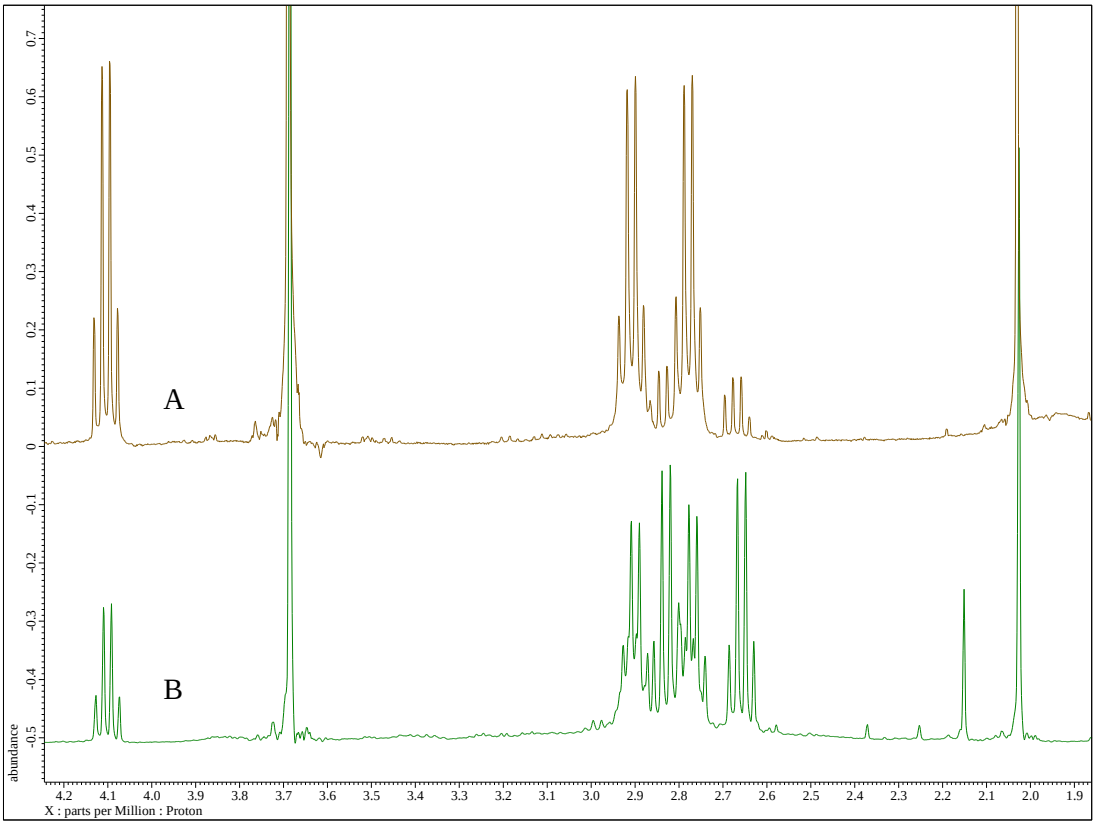

Figure 47: ^{1}H NMR overlaid spectra of the crude material for **L1** in the aliphatic region representing the CH_2 signals of the diethyl chain when a) using *t*-BuOK and b) Cs_2CO_3.

To determine whether poor nucleophilicity of the 3-amino-1,2,4-triazine is a limiting factor in this synthetic methodology and in an attempt to improve the yields of the reaction, an alternative synthetic method was considered. This involved carrying out the Pd-catalysed cross-coupling reaction between 2,6-diaminopyridine **2.2.18** and 3-methylthio-5,6-diethyl-1,2,4-triazine **2.2.19**, Figure 48. A role reversal of the 1,2,4-triazine from nucleophile to electrophile was hoped to limit the effect of the presumed poor nucleophilicity of the 3-amino-1,2,4-triazine. Having the nucleophilic amino-groups directly attached to the pyridine, as in 2,6-diaminopyridine **2.2.18**, which is less electron withdrawing than the 1,2,4-triazine ring, should increase the nucleophilicity of the nitrogen lone pairs and make them more readily available for the cross coupling reaction.[136] Electron withdrawing groups attached to one of the reactive partners has been found to result in an increased strength of the bond between this partner and the metal centre; this increase in bond strength can slow the rate of reductive elimination.[137] As the 3-amino-1,2,4-

triazine would fit into this electron withdrawing criteria, there is a potential that the reductive elimination step may also be hindering the reaction.

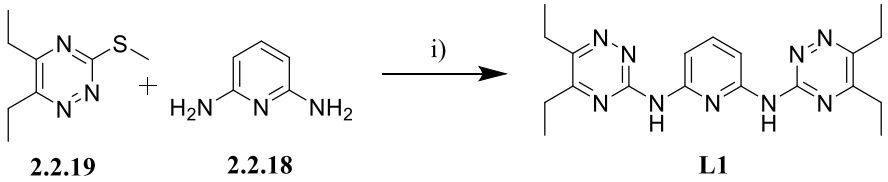

Figure 48: Alternative Pd(0)-catalysed C-N cross coupling reaction to synthesise **L1**. Reaction conditions: i) $Pd(OAc)_2$ **2.1.4**, Xantphos **2.1.5**, CuMeSal **2.2.20**, *t*-BuOK, toluene.

The alternative methodology uses copper(I) 3-methylsalicylate (CuMeSal) **2.2.20** alongside xantphos **2.1.5** and palladium(II) acetate **2.1.7** as the catalytic system. It has been shown that CuMeSal **2.2.20** is necessary in this reaction, in which the electrophilic methylthio compound **2.2.19** is used, to aid the oxidative addition of Pd(0) across the C-S bond, which is less susceptible to oxidative addition than a C-Br bond.[136a] The starting electrophile, 3-methylthio-5,6-diethyl-1,2,4-triazine **2.2.19** was synthesised in a two-step reaction starting with an initial methylation of thiosemicarbazide **2.2.21** using iodomethane followed by a condensation reaction with hexane-3,4-dione **2.2.1** to form the 1,2,4-triazine ring **2.2.19**, Figure 49.

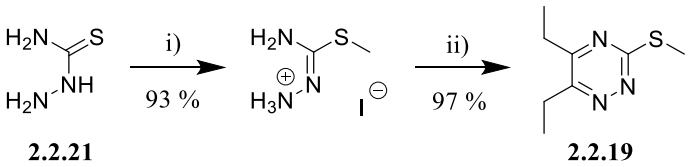

Figure 49: Reaction scheme to form triazine **2.2.19**. Reaction conditions: i) iodomethane, ethanol; ii) hexane-3,4-dione **2.2.1**, sodium bicarbonate, ethanol, H_2O.

The C-N palladium-catalysed amination of 3-methylthio-1,2,4-triazines, like **2.2.19**, has been reported previously using a combination of $Pd(OAc)_2$ **2.04**, xantphos **2.02** and CuMeSal **2.2.20**.[136] The CuMeSal **2.2.20** is an important addition in the cross coupling reaction as it promotes the displacement of the methylsulfur (SMe) group and aids oxidative addition. Generally it was found that electron-rich amines, such as 4-methoxyaniline and 5-amino-2-methoxypyridine, produced the best yields in this reaction under microwave conditions.

Employing 2,6-diaminopyridine **2.2.18** and the electrophile **2.2.19** in this C-N bond forming reaction resulted in unreacted starting material, and none of the desired product **L1** was formed, Figure 48. The most likely cause is an imbalance in the stoichiometry of the different reagents, in particular the base and CuMeSal **2.2.20** equivalents. Further investigations would be necessary to optimise the reaction by combining two alternative procedures alongside employing microwave conditions.

Coinciding with this line of research, the (1*S*)-(+)-camphorquinone **2.2.8** was successfully employed in the cross-coupling reaction following the established method, Figure 43, leading to the successful synthesis of the camphor-1,2,4-triazine ligand **L3** in an 81% yield, see Table 3, entry 4. In subsequent reactions, the optimised Buchwald Hartwig method using 2.1 eq. 3-amino-1,2,4-triazine, 10 mol% Pd catalyst **2.1.4**, 20 mol% xantphos **2.1.5** and 4 eq. $CsCO_3$, was determined to be the most effective and versatile to synthesise further novel bis-1,2,4-triazine ligands, as outlined in Figure 50. Replacement of 2,6-dibromopyridine **2.2.15** with 2,6-dibromopyrazine **2.2.22** was considered to investigate the effect of an additional nitrogen atom within this bridging group synthesising **L6**. The ^{1}H NMR, ^{13}C NMR and HRMS were all used to confirm the presence of the di-aminated ligands with example ^{1}H NMR spectra shown in Figure 51 and Figure 52 for the ligands **L3** and **L5** respectively.

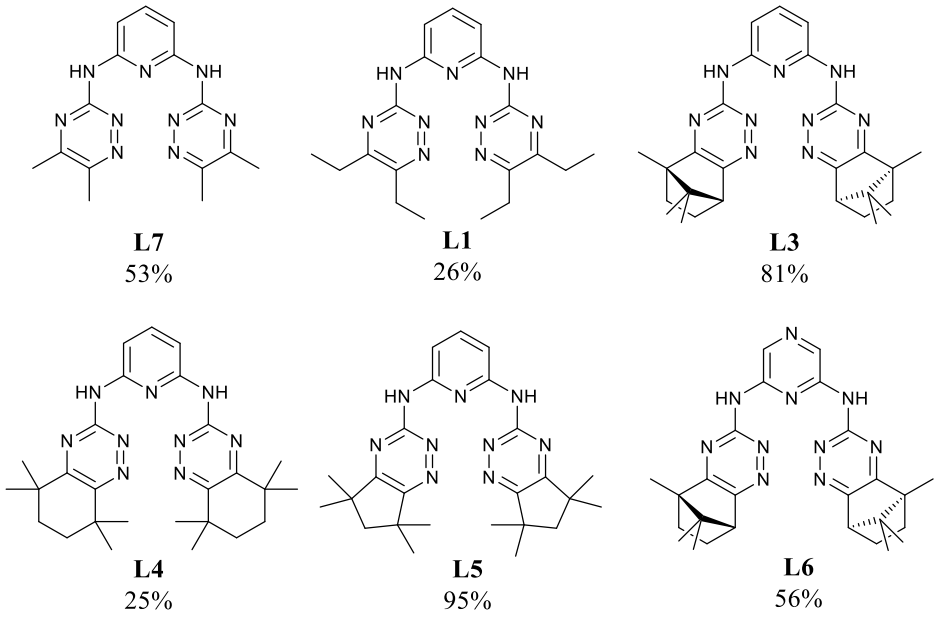

Figure 50: Novel bis-1,2,4-triazine ligands formed via the Buchwald Hartwig cross-coupling reactions of 3-amino-1,2,4-triazines with dibromoheteroarenes.

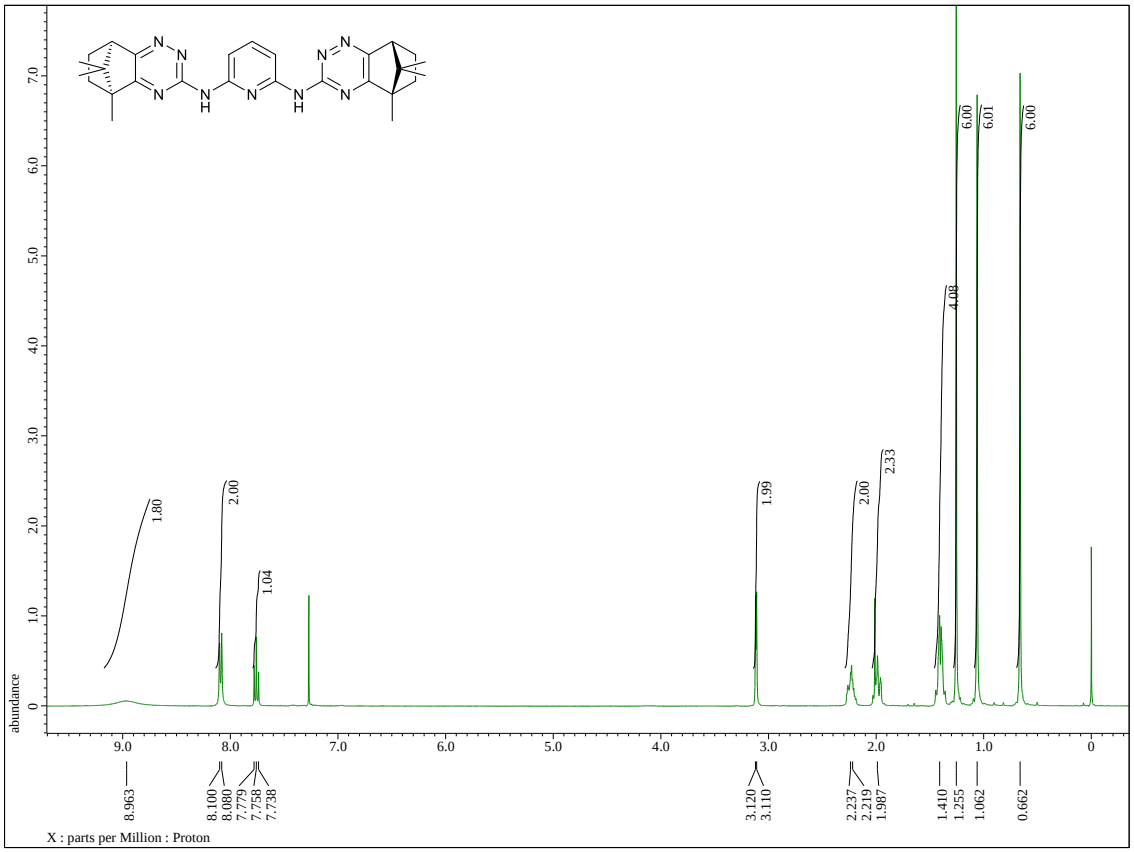

Figure 51: ^{1}H NMR spectrum of ligand **L3**, in $CDCl_3$.

Table 4: Assignment of NMR signals for ligand **L3**.

^{1}H (ppm)	**Proton integration and multiplicity (Hz)**	**^{13}C (ppm)**	**Assignment**
8.98	2H, s, br	-	2 x NH
8.09	2H, d, *J* = 8.02	107.4	2 x ArCH
7.76	1H, t, *J* = 8.02	140.2	ArCH
3.12	2H, d, *J* = 4.12	50.6	CH
2.27 – 2.19	2H, m	31.4	2 x CH_{exo}
2.03 – 1.96	2H, m	24.6	2 x CH_{exo}
1.45 – 1.36	4H, m	24.6, 31.4	4 x CH_{endo}
1.26	6H, s	20.1	2 x CH_3
1.06	6H, s	18.3	2 x CH_3
0.66	6H, s	9.1	2 x CH_3

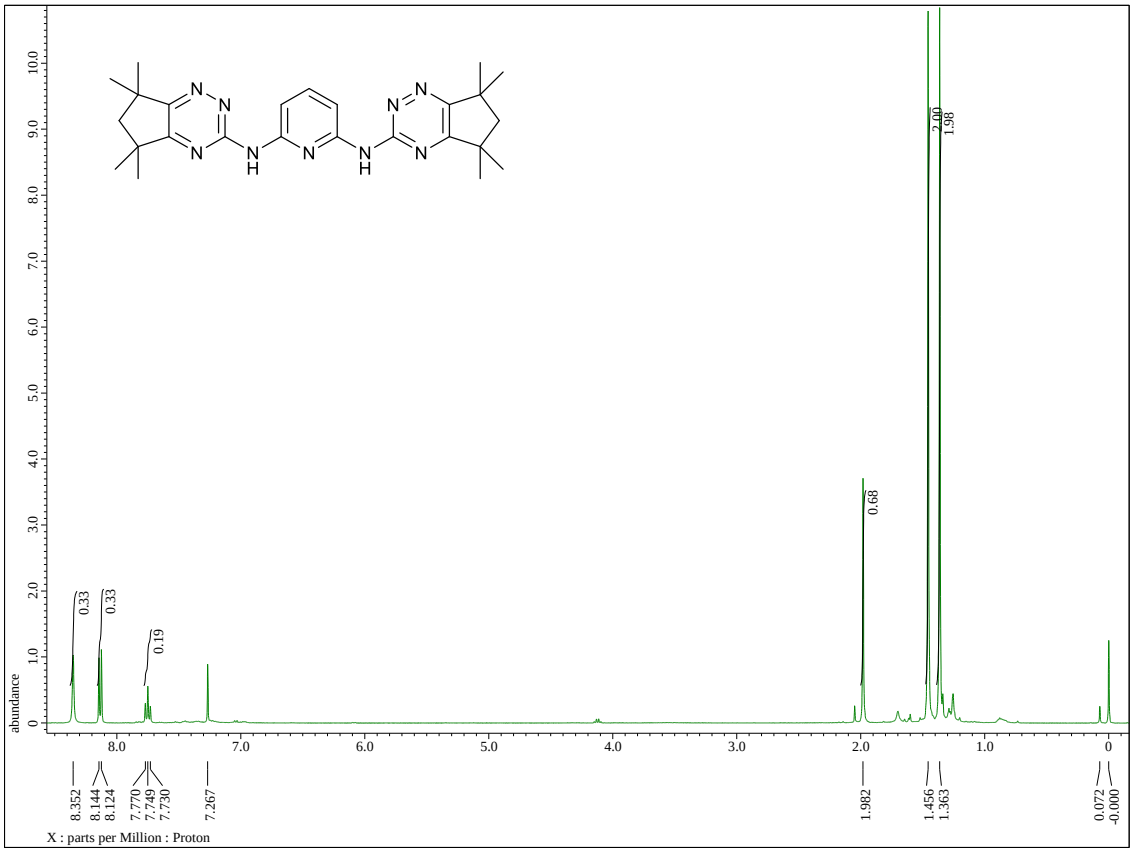

Figure 52: ^{1}H NMR spectrum of ligand **L5**, in $CDCl_3$.

Table 5: Assignment of NMR signals for ligand **L5**.

^{1}H (ppm)	Proton integration and multiplicity (Hz)	^{13}C (ppm)	Assignment
8.35	2H, s, br	-	2 x NH
8.13	2H, d, *J* = 8.24	107.0	2 x ArCH
7.75	1H, t, *J* = 8.24	140.3	ArCH
1.98	4H, s	53.1	2 x CH_2
1.46	12H, s	29.8	4 x CH_3
1.36	12H, s	28.8	4 x CH_3

The use of the commercially available 6,6'-dibromo-2,2'-bipyridine **2.2.23** as the electrophile instead of 2,6-dibromopyridine **2.2.15** was considered to synthesise a new family of potentially tetradentate ligands, closely related to the BTBPs, Figure 53. It was hoped that having the two N-donor atoms of the bipyridine group, known to complex to the metal in the BTBPs, would aid in the ability of this ligand to act as a strong chelating ligand and hence as an efficient extractant of the An(III).

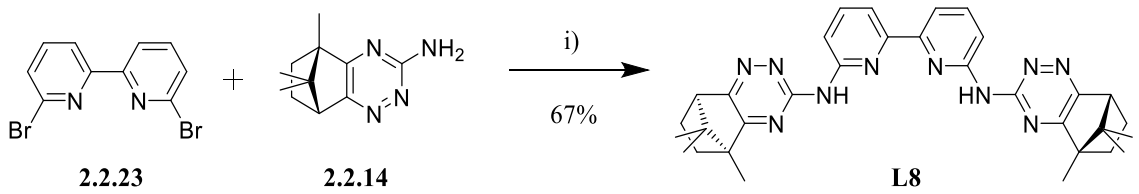

Figure 53: Reaction scheme to synthesise ligand **L8**. Reaction conditions; $Pd_2(dba)_3$ **2.1.4**, Xantphos **2.1.5**, Cs_2CO_3, 1,4-dioxane, Δ.

Initially, the Buchwald Hartwig reaction of 6,6'-dibromo-2,2'-bipyidine **2.2.23** with **2.2.14**, using the standard conditions mentioned previously, failed to produce the desired product **L8.** After 48 hours at reflux, only starting material remained. It was deemed necessary to ensure the separate formation of the active catalyst by combining $Pd_2(dba)_3$ **2.1.4** and xantphos **2.1.5** in a separate flask, prior to the addition of the aryl halide **2.2.23**. This ensures that the aryl halide **2.2.23**, itself a strong chelating ligand, doesn't outcompete the xantphos ligand **2.1.5** in binding to the palladium centre, and prevent its participation in the formation of the C-N bond. In achieving this slightly modified reaction set up, the product **L8** was successfully formed in a yield of 67% using the same conditions as previously, as easily observed via a bright yellow spot on the TLC plate. A triplet at δ 7.72 ppm and an overlapped doublet at δ 7.40 ppm were observed for the protons of the 2,2'-bipyridine backbone in the ^{1}H NMR spectrum of the crude product. The integrations of all the relevant peaks confirmed the production of the ligand **L8**, Figure 54.

Further synthesis of related ligands derived from commercially available but expensive 6,6'-dibromo-2,2'-bipyridine **2.2.23** were not investigated until the extraction capability of ligand **L8** had been determined.

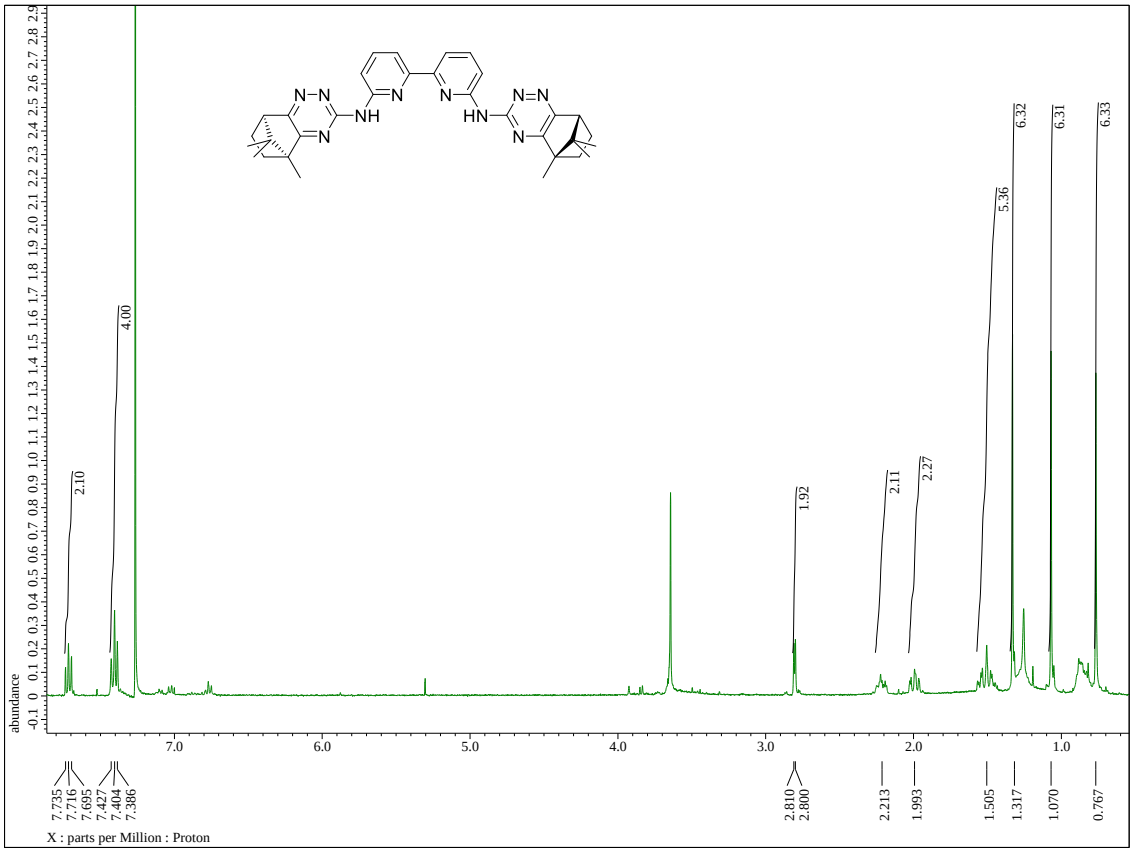

Figure 54: ^{1}H NMR spectrum of the ligand **L8** in $CDCl_3$.

Table 6: Assignment of NMR signals for ligand **L8**.

^{1}H (ppm)	Proton integration and multiplicity (Hz)	^{13}C (ppm)	Assignment
7.72	2H, t, *J* = 7.79	136.6	2 x ArCH
7.40	4H, m	124.9, 112.3	4 x ArCH
2.81	2H, m	50.3	CH
2.25 – 2.18	2H, m	31.4	2 x CH_{exo}
2.02 – 1.97	2H, m	24.8	2 x CH_{exo}
1.57 – 1.47	4H, m	31.4, 24.8	4 x CH_{endo}
1.33	6H, s	9.3	2 x CH_3
1.07	6H, s	18.2	2 x CH_3
0.77	6H, s	20.5	2 x CH_3

After the successful synthesis of the novel bis-1,2,4-triazine ligands with the pyridine, pyrazine and bipyridine linkers, attempts were made to synthesise the related 1,10-phenanthroline **2.2.24** based ligand **L9**, Figure 56. The synthesis of the aryl halides, 2,9-dichloro-1,10-phenanthroline **2.2.27** and 2,9-dibromo-1,10-phenanthroline **2.2.28**, was achieved according to literature procedures in three steps, Figure 55. The first step sees the formation of a salt **2.2.25** by reaction

of 1,10-phenanthroline **2.2.24** with 1,3-dibromopropane in nitrobenzene prior to its oxidation to give **2.2.26**. The initial oxidation reaction, using potassium ferricyanide was found to be low yielding. However, following a procedure first reported by Zhengand co-workers the yield was found to be quadrupled using a combination of *tert*-butanol, potassium *tert*-butoxide and air as the oxidising agent.[138] The final chlorinated **2.2.27** and brominated **2.2.28** products could be obtained in high yields. The aromatic region of the ^{1}H NMR spectrum for both compounds showed two doublets and a singlet from the symmetrical phenanthroline backbone. The chlorinated product **2.2.27** showed the two doublets at δ 7.66 and δ 8.22 ppm with the brominated **2.2.28** compound showing signals with a chemical shift to δ 7.81 and δ 8.11 ppm respectively, Figure 57.

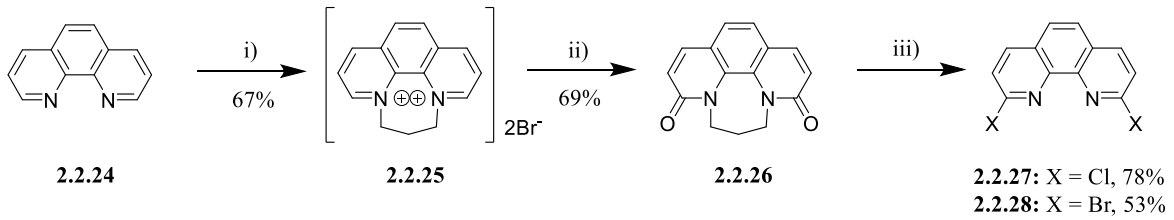

Figure 55: Optimised reaction scheme to synthesise the 2,9-dihalo-1,10-phenanthroline compounds **2.2.27** and **2.2.28**. Reaction conditions; i) 1,3-dibromopropane, nitrobenzene, ii) *t*-butanol, *t*-BuOK, air iii) phosphorus oxychloride, phosphorus pentachloride or phosphorus oxybromide, phosphorus pentabromide.

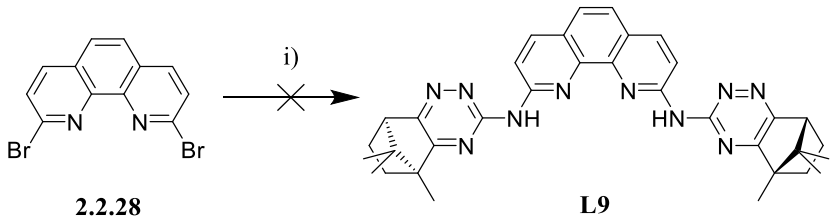

Figure 56: Proposed reaction scheme for the Buchwald Hartwig coupling using 2,9-dibromo-1,10-phenanthroline **2.2.28** as the electrophile to give **L9**. Reaction conditions: i) 3-amino-1,2,4-triazine **2.2.14**, $Pd_2(dba)_3$ **2.1.4**, xantphos **2.1.5**, Cs_2CO_3, 1,4-dioxane.

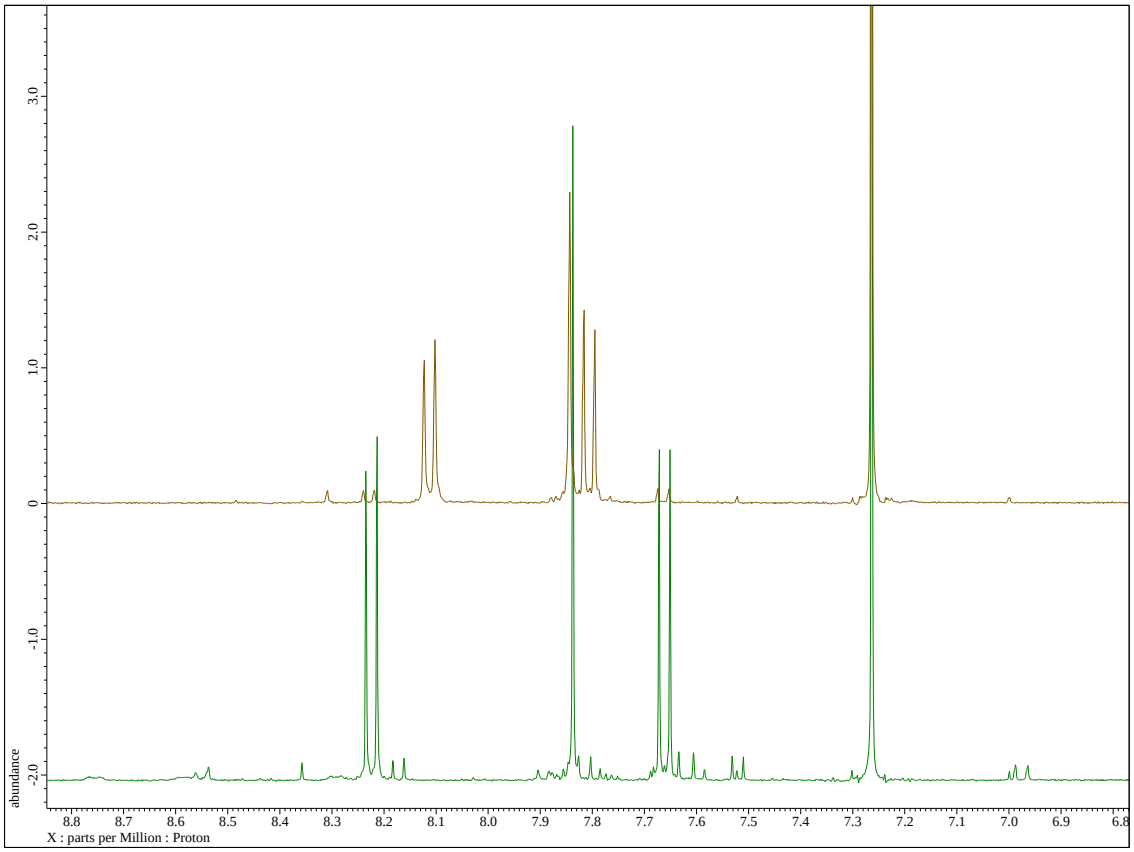

Figure 57: Overlaid ^{1}H NMR spectra of 2,9-dichloro-1,10-phenanthroline **2.2.27** (bottom spectrum) and 2,9-dibromo-1,10-phenanthroline **2.2.28** (top spectrum).

The chlorinate phenanthroline **2.2.27** was initially utilised as the electrophile within the Buchwald Hartwig reactions using conditions depicted in Figure 56. The reactive catalytic species was formed prior to the addition of the phenanthroline compound **2.2.27**, as carried out previously with the 6,6'-dibromo-2,2'-bipyridine **2.2.23**. Unfortunately, evidence from both TLC measurements and ^{1}H NMR data, showed that the reaction was unsuccessful, with the starting 3-amino-1,2,4-triazine **2.2.14** remaining unreacted. A similar outcome was observed when utilising 2,9-dibromo-1,10-phenanthroline **2.2.28** as the electrophile.

1,10-Phenanthroline **2.2.24** is known to act as a catalyst in other reactions acting as a *N*,*N*-bidentate chelator for a variety of metals.[139a, 139b] This includes a copper-catalysed *N*-arylation reaction which found that the addition of 1,10-phenanthroline **2.2.24** and dibenzylideneacetone is crucial to the success of the process. Although the role of the ligands is not clear, it is suspected they are involved in the stabilisation of the Cu(I) complex or that they prevent aggregation.[140] It is proposed that the stability of the intermediate complex formed between the catalytic palladium

species and the phenanthroline-halide **2.2.27** or **2.2.28** may be hindering further reaction with the amine compound and hence terminating the cross-coupling reaction. Due to the poor solubility of the palladium complexes formed in these reactions, which can be collected *via* filtration, the determination of the species present was unable to be completed.

Further derivatisation of the secondary amine group of the bis-1,2,4-triazine ligands synthesised above was next carried out to explore the effects of *N*-alkyl substituents on the solubility of the compounds. It was decided to consider both short and long alkyl chain derivatives by using two representative electrophiles; iodomethane and 1-iodobutane. The *N*-alkylation reaction involves the deprotonation of the secondary amine with sodium hydride prior to subsequent addition of the alkylating agent. Potassium carbonate was also explored as a milder base to achieve this deprotonation. The electron-withdrawing resonance effects of the surrounding 1,2,4-triazine and pyridine rings was expected to stabilise the anion formed. However, reaction of ligand **L3** with potassium carbonate and iodomethane failed to generate substantial amount of product **L10** and the starting material **L3** was recovered. The use of sodium hydride as the base gave more encouraging results.

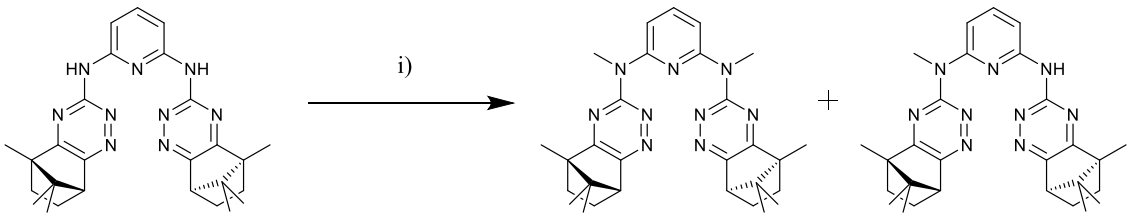

L3 **L10** 23% **L11** 12%

Figure 58: Reaction scheme for the *N*-alkylation of the ligand **L3** using iodomethane. Reaction conditions: i) sodium hydride, iodomethane, THF.

It was noted after an overnight reaction with ligand **L3** and iodomethane that the *N*-alkylation reaction proceeded to give both a mono- **L11** and a bis-alkylated ligand **L10**. The combined yields of the ligands was collectively below 50% for the methylated ligands (**L10**, **L11**), Figure 58. However, the mono-alklated product **L11** could be separated by column chromatography. The sacrifice in the overall yield obtained was made to ensure the formation of both products for each reaction, although undoubtedly a higher yield could have been obtained by employing longer

reaction times and using more forceful conditions. However, previous research published by Chalmers University,[87] found that unsymmetrical BTBP ligands resulted in higher solubilities compared to their symmetrical analogues, such as $CyMe_4$-BTBP **1.09**. As a consequence, it was decided to continue with the proposed conditions to obtain both symmetrical and unsymmetrical ligands in the present *N*-alkylation reactions, enabling the screening of each of these for minor actinide extraction and ligand solubility. In addition to ligand solubility, it was hoped that adding the alkyl chains could influence the hydrophobicity of the ligands (and hence their extraction affinity, as measured by the metal distribution ratios), and possibly their preferred conformation. The *N*-alkylation with 1-iodobutane successfully gave the di- and mono-butylated ligands **L12** and **L13**, respectively, Figure 59.

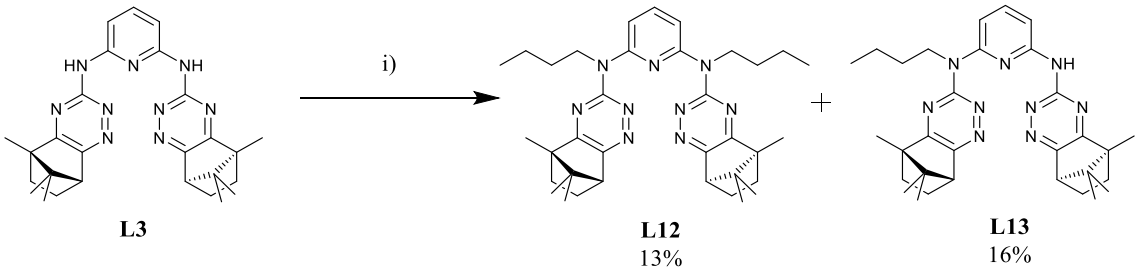

Figure 59: Reaction scheme for the *N*-alkylation of the ligand **L3** using 1-iodobutane. Reaction conditions: i) sodium hydride, 1-iodobutane, THF.

2.3. Ligands derived from mono-amination of 3-(6-bromo-2-pyridyl)-1,2,4-triazines

3-(6-Bromo-2-pyridyl)-1,2,4-triazines have been previously reported in the literature by the Carrick group.[141] Realising their potential use in the above Pd-catalysed Buchwald Hartwig reactions described above, their reaction with 3-amino-1,2,4-triazines **2.1.1** in the cross-coupling reactions was studied, to access another novel family of terdentate triazines ligands, Figure 60.

The ligands were synthesised in order to determine whether these unsymmetrical ligands would have beneficial extraction properties compared to the symmetrical ligands synthesised above. A notable difference between these ligands and those described above was the removal of one NH group, and its replacement with a direct C-C bond between the pyridine and triazine rings, Figure 61. This could reduce the torsional energy barrier needed for both rings to rotate into the

conformation required to chelate the metal. With this in mind, a range of ligands were synthesised based upon starting 3-(6-bromo-2-pyridyl)-1,2,4-triazine scaffolds; **2.3.3** and **2.3.4**, Table 7.

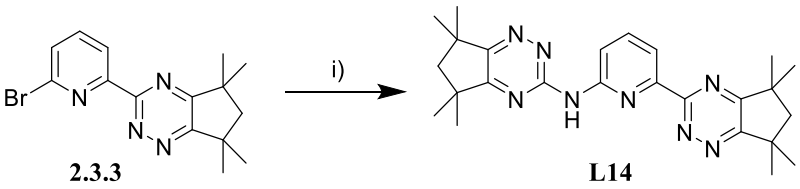

Figure 60: Reaction scheme to form the final ligand **L14**. Reaction conditions; i) 3-amino-1,2,4-trazine **2.2.13**, $Pd_2(dba)_3$ **2.1.4**, xantphos **2.1.5**, Cs_2CO_3, 1,4-dioxane, Δ.

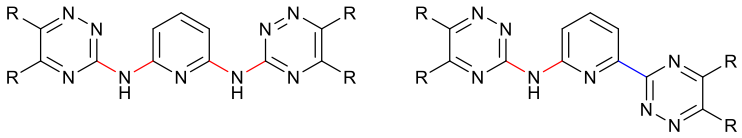

Figure 61: Comparison between symmetrical ligands discussed in Section 2.2 and the unsymmetrical ligands discussed in Section 2.3, showing the different bond torsions; C-N-C in red and C-C in blue.

The precursor to the 3-(6-bromo-2-pyridyl)-1,2,4-triazine scaffolds **2.3.1** and **2.3.2** was synthesised by treatment of 6-bromopyridine-2-carbonitrile **2.3.1** with hydrazine hydrate to obtain the hydrazonamide **2.3.2** as described by the Carrick Group.[142] The condensation reaction of this product with the representative diketone Cy_5Me_4-diketone **2.2.7** and the hydrazonamide **2.3.2** gave **2.3.3**, Figure 62. This same reaction was completed with (1*S*)-(+)-camphorquinone **2.2.8** to synthesise **2.3.4**. The 3-amino-1,2,4-triazines used to form the final ligands were synthesised in a condensation reaction of each diketone with aminoguanidine bicarbonate **2.2.9**, as discussed in section 2.2. The Buchwald Hartwig procedure, established previously, was used to form the final ligands between the 3-(6-bromo-2-pyridyl)-1,2,4-triazine scaffolds, **2.3.3** and **2.3.4**, and the 3-amino-1,2,4-triazines, Table 7. Synthesis of all ligands was verified through ^{1}H NMR, ^{13}C NMR and HRMS, with example ^{1}H NMR spectra shown in Figure 63 and Figure 64 for ligands **L14** and **L16**, respectively.

The use of the scaffold **2.3.4** appears to yield a disparity in the yields of the final reaction to produce the ligands **L15** and **L16** when compared to the use of the scaffold **2.3.3** under the same conditions.

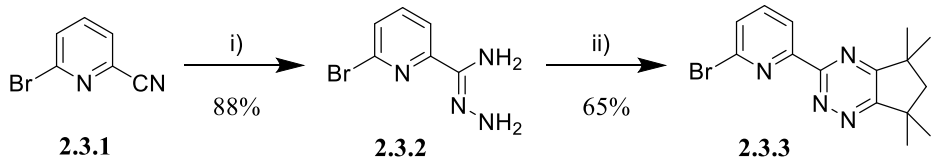

Figure 62: Reaction scheme to form the 3-(6-bromo-2-pyridyl)-1,2,4-triazine **2.3.3**. Reaction conditions; i) hydrazine hydrate, ethanol, ii) Cy_5Me_4-diketone **2.2.7**, AcOH.

Table 7: Reaction yields for the ligands derived from 3-(6-bromo-2-pyridyl)-1,2,4-triazine. General reaction conditions: $Pd_2(dba)_3$ **2.1.4** 10 mol%, Xantphos **2.1.5** 20 mol%, $CsCO_3$, 4 equivalents.

Aryl Halide	Aryl Amine	Product	Yield
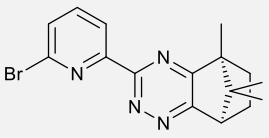 **2.3.4**	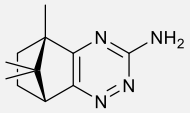 **2.2.14**	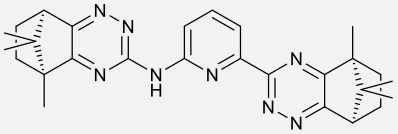 **L16**	27 %
	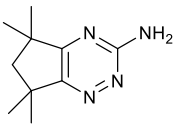 **2.2.13**	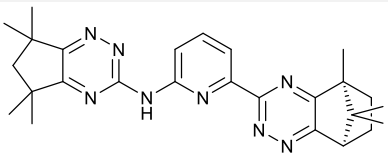 **L17**	36 %
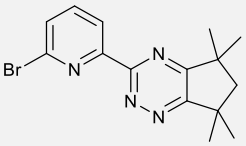 **2.3.3**	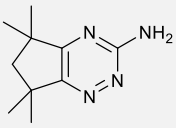 **2.2.13**	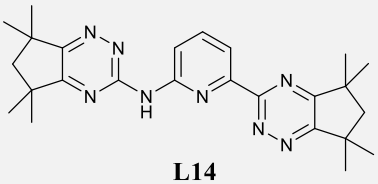 **L14**	80%
	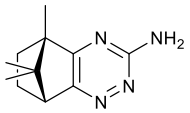 **2.2.14**	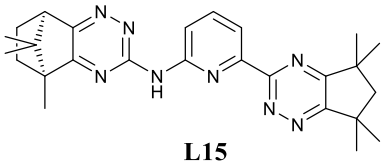 **L15**	70 %

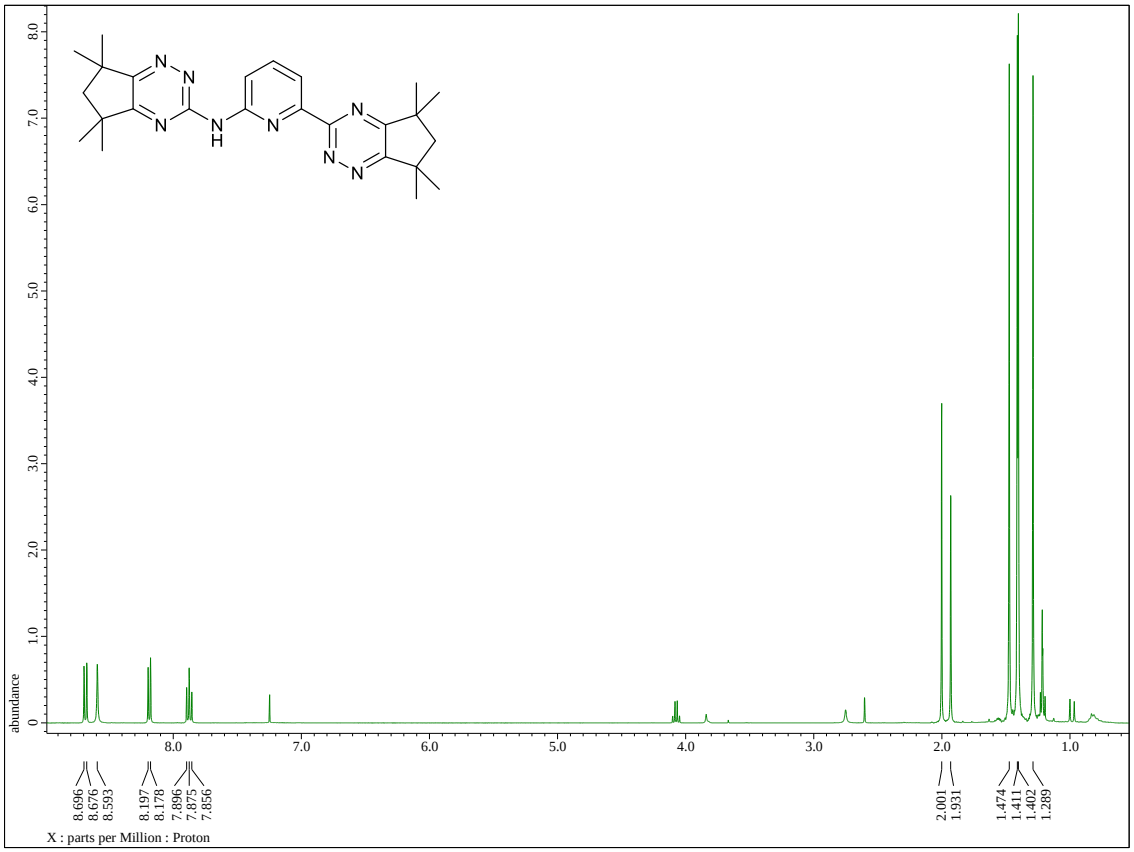

Figure 63: ^{1}H NMR spectrum of **L14**, in $CDCl_3$.

Table 8: Assignment of NMR signals for ligand **L14**.

^{1}H (ppm)	Proton integration and multiplicity (Hz)	^{13}C (ppm)	Assignment
8.73	1H, d, *J* = 8.24	114.7	ArCH
8.64	1H, s, br	-	NH
8.24	1H, d, *J* = 7.79	118.1	ArCH
7.92	1H, dd, *J* = 8.24, 7.79	139.1	ArCH
2.05	2H, s	53.0	CH_2
1.98	2H, s	52.9	CH_2
1.52	6H, s	29.8	CH_3
1.46	6H, s	29.7	CH_3
1.45	6H, s	29.0	CH_3
1.34	6H, s	28.7	CH_3

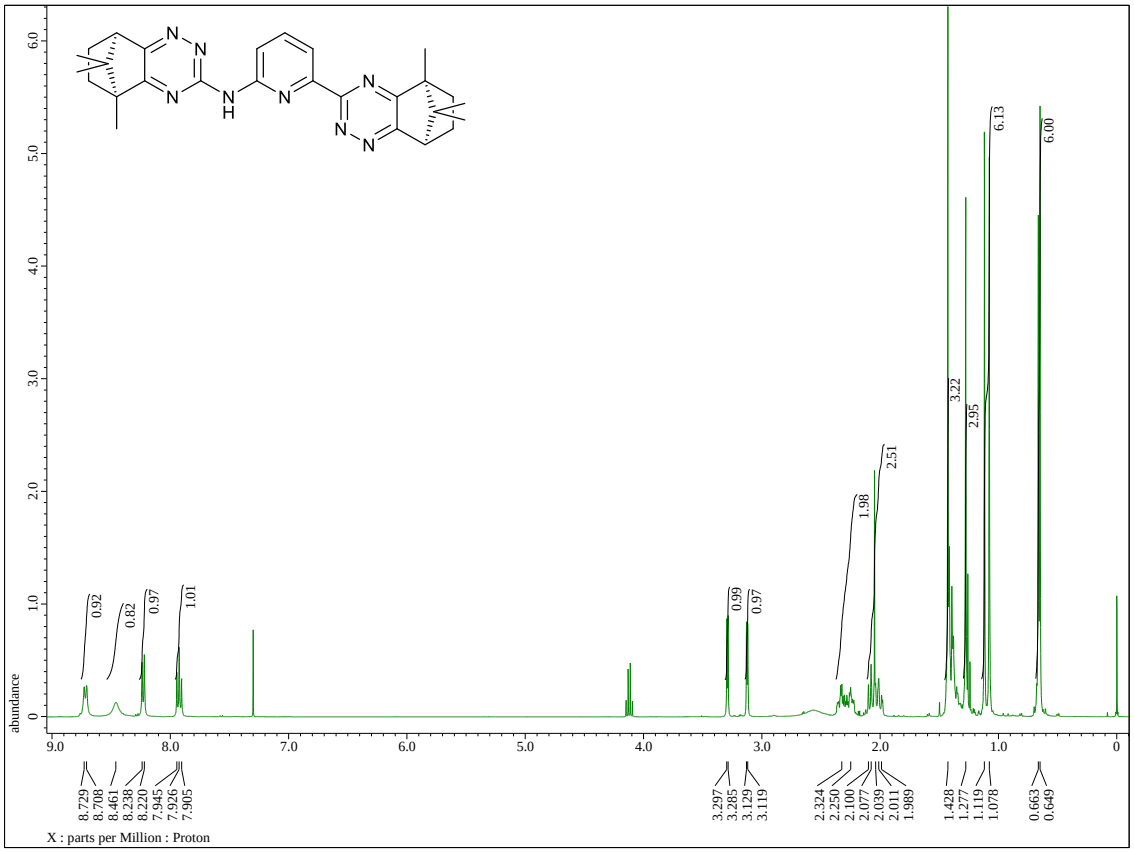

Figure 64: ^{1}H NMR spectrum of **L16** in $CDCl_3$.

Table 9: Assignment of NMR signals for ligand **L16**.

^{1}H (ppm)	Proton integration and multiplicity (Hz)	^{13}C (ppm)	Assignment
8.72	1H, d, *J* = 8.24	115.0	ArCH
8.46	1H, s, br	-	NH
8.23	1H, d, *J* = 7.79	118.0	ArCH
7.92	1H, dd, *J* = 8.24, 7.79	139.2	ArCH
3.29	1H, d, *J* = 4.58	51.2	CH
3.12	1H, d, *J* = 4.12	50.6	CH
2.36 – 2.22	2H, m	24.6, 24.3	2 x CH_{exo}
2.10 – 2.99	2H, m	31.4, 31.2	2 x CH_{exo}
1.43 – 1.38	4H, m	31.4, 31.2, 24.6, 24.3	4 x CH_{endo}
1.43	3H, s	9.1	CH_3
1.28	3H, s	9.3	CH_3
1.12	3H, s	18.3	CH_3
1.08	3H, s	18.4	CH_3
0.66	3H, s	20.2	CH_3
0.65	3H, s	20.2	CH_3

As described above with the symmetrical ligands, *N*-alkylation was successfully achieved by treatment of **L15** with sodium hydride and iodomethane using the same method as stated in

section 2.2, Figure 65. Formation of the product was observed on ^{1}H NMR spectrum, but was not purified completely, with minor impurities remaining. It was decided that further ligands would not be alkylated until initial extraction results on this family of ligands were obtained.

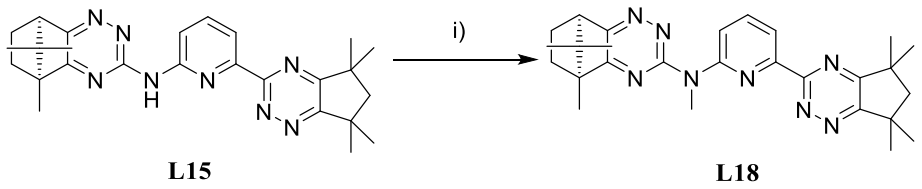

Figure 65: Reaction scheme for the *N*-alkylation reaction of **L15** to give the target ligand **L18**. Reaction conditions: i) NaH, iodomethane, THF.

The ligands described above are anticipated to have quite different properties compared to the BTP ligands. They are anticipated to have a higher basicity (ie: higher pKa) than the BTPs, due to the resonance delocalisation of the NH lone pairs into the aromatic rings. This may also lead to each of the C-NH bonds having a substantial degree of double bond character, which may increase the energy barrier to rotation about these bonds. These factors will likely influence the ligand extraction properties and solubility.

2.4. Calculated Ligand Parameters

For each of the ligands synthesised in sections 2.2 and 2.3, their ligand parameters have been calculated to enable comparisons between theoretical and experimental data in line with the project objectives. It is hoped that a set of predictive guidelines can be established that allows the prediction of the potential solubility and extraction kinetics of a given ligand prior to its synthesis. This will be based upon the theoretical values and in the case of this project, backed up with experimental data if there is a strong correlation between the two.

Based upon the theoretical results, specifically the Fsp^3 and Log *P* values, in Table 10, the ligands **L1** and **L7** would be expected to have a low lipophilicity and hence solubility in 1-octanol. A low log *P* is predictive of an increased solubility in the aqueous phase and decreased solubility in 1-octanol, and a low Fsp^3 value can correlate to its solubility. Opposing this, ligands **L4** and **L13**

have a log *P* value above 6 in addition to an Fsp^3 value above 0.59. Of the ligands synthesised in this chapter it is expected that these are the most lipophilic and would therefore have the greatest solubility in 1-octanol. In between these extreme values, where the log *P* values range from 4-6, there is very little trend between the log *P* and Fsp^3 values to indicate the potential ligand solubility. Ligand **L5** has a high log *P* value of 5.95 but an Fsp^3 value of 0.48, suggesting a contradiction in the prediction of its solubility. Although the calculated parameters may give a good predictability of solubility in the extreme cases, it should be taken as only an indication, as these calculations may have minimal accuracy.

When considering the addition of HBD/HBA groups, which could indicate the potential for a ligand to form hydrogen bonds at the interface, there is an increase in these numbers across all ligands synthesised in this chapter, when compared to the benchmark ligands. Based upon the novel design approach discussed in section 1.7, it is hoped that the higher the number of HBD/HBA groups, the greater the concentration of the ligand that may exist at the interphase. It is here that the log *P* value can also give an indication to the limitation point of the addition of these groups. Based principally on increasing the number of HBD/HBA groups it would be expected that ligands **L6** and **L8** have the fastest extraction kinetics. However, this increase may result in these ligands becoming so polar, as to partition into the aqueous phase. The mono-aminated ligands **L14**, **L15**, **L16** and **L17** have the lowest HBD/HBA groups of the novel target ligands and may show the slowest extraction kinetics based upon the theoretical principle outlined.

In the next two sections the solubility and extraction results will be discussed for the ligands synthesised in this chapter. Upon obtaining these results, they will be compared back to the theoretical results calculated below in Table 10.

Table 10: Table showing calculated parameters (Log *P* and Fsp^3) for novel ligands. The log *P* value was calculated using the ACD ILabs online software.

Ligand	Ligand Number	Log *P*	Fsp^3	HBD	HBA
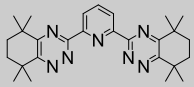	**1.30**	5.45	0.59	0	7
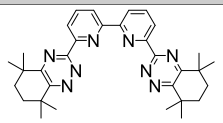	**1.09**	6.01	0.50	0	8
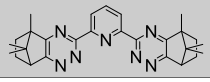	**1.31**	3.69	0.59	0	7
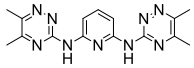	**L7**	2.66	0.27	2	9
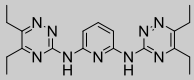	**L1**	3.79	0.42	2	9
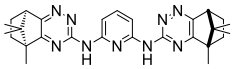	**L3**	5.46	0.59	2	9
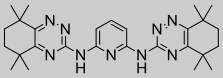	**L4**	6.77	0.59	2	9
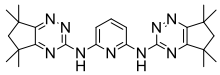	**L5**	5.95	0.48	2	9
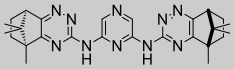	**L6**	4.71	0.62	2	10
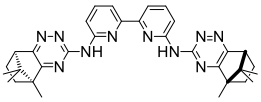	**L8**	5.77	0.50	2	10
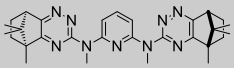	**L10**	5.37	0.62	0	9
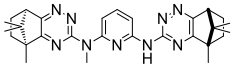	**L11**	5.24	0.61	1	9
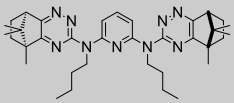	**L12**	7.53	0.69	0	9
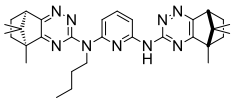	**L13**	6.62	0.65	1	9
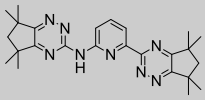	**L14**	5.03	0.56	1	8
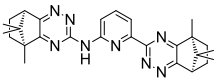	**L16**	4.64	0.59	1	8
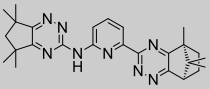	**L17**	4.80	0.58	1	8
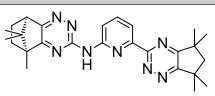	**L15**	4.81	0.58	1	8
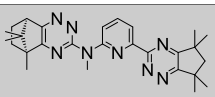	**L18**	4.81	0.59	0	8

2.5. Solubility Studies

Solubility studies were completed as outlined in Chapter 6 in 1-octanol. Results were compared to the analogous ligand **1.31** to evaluate whether an improvement in solubility was achieved with any of the ligands synthesised. Table 11 shows the novel terdentate ligands synthesised through the Buchwald Hartwig cross-coupling reactions alongside their individual Fsp^3 values and measured solubilities. The applicability of the Fsp^3 value, in addition to the log *P* values, in predicting the solubility of the ligands will be considered based upon the experimental results shown, as discussed in section 1.6. Ultimately these results will be compared to the theoretical data to determine whether the proposed design approach has established the necessary criteria to determine ligand solubility. The camphor-BTP ligand **1.31** has a solubility of 200 mmol/L in 1-octanol.[82]

A graph showing the correlation between the measured ligand solubility in 1-octanol and Fsp^3 values is presented in Figure 66. There is a generally good correlation observed between the Fsp^3 values of the ligands and their measured solubilities, although individual data points have not been assigned to the graph, the corresponding data can be found in Table 12. As suspected during their synthesis, ligands **L1** and **L7** have very low solubilities, so much so that the final solubility result for **L7** was unable to be obtained. This is an expected result as observed from the Fsp^3 value and ligand structure, and aligns with the proposed hypothesis, section 1.6. The alkylation at the secondary amine in ligands **L10**, **L11**, **L12** and **L13** was suspected to result in an improved solubility compared to the parent ligand **L3**. The solubility results confirm this, with the solubility increasing in parallel to the increasing alkyl chain length. Interestingly, and in contradiction to previous work by Aneheim and coworkers,[87] there is no distinct increase in measured solubility for the unsymmetrical ligands **L11** and **L13**. Despite this, the solubility results for the alkylated derivatives do show a correlation between the Fsp^3 value and their resulting solubilities, supporting the hypothesis proposed in the novel design approach. With regards to the mono-aminated terdentate ligands, there is a distinct decrease in solubility for those ligands with different groups adjacent to the 1,2,4-triazine rings, as in **L15** and **L17**.

When compared to the camphor-BTP **1.31** there is a decrease in solubility observed for those ligands containing the (1*S*)-(+)-camphorquinone **2.2.8**. However, all ligands containing **2.2.8** show an improved solubility in comparison to the $CyMe_4$-BTP analogue **1.30**. Direct comparison of **L8** with the benchmark ligand $CyMe_4$-BTBP **1.09** shows a slight improvement in solubility. Surprisingly the use of the diketone **2.2.7** doesn't appear to impact the solubility of the ligand **L5** as might be expected in the removal of a CH_2 from the well utilised diketone $CyMe_4$ **2.2.5**.

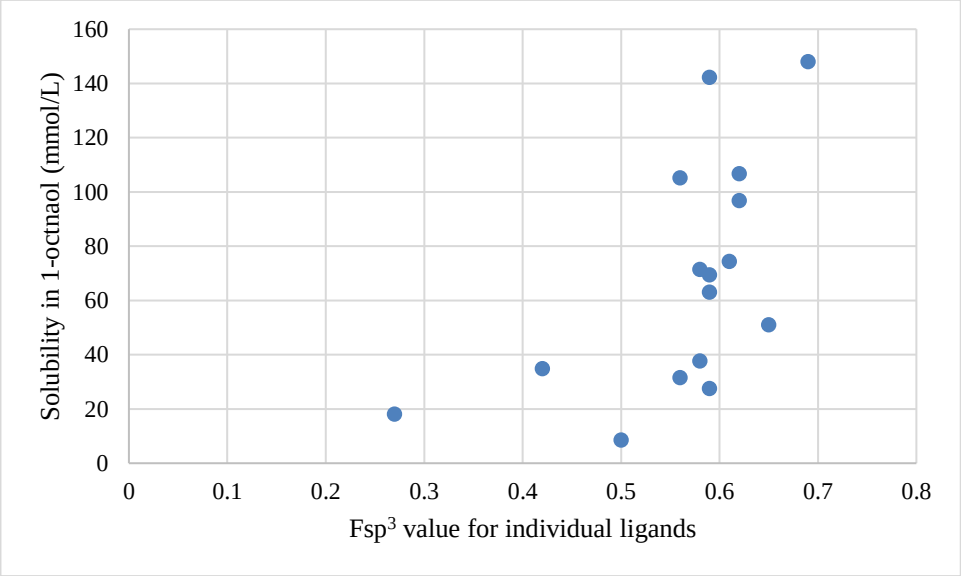

Figure 66: Graph showing the correlation between a ligands calculated Fsp3 value and its measured solubility in 1-octanol. Each data point represents a ligand, see Table 11 for further information.

The following section discusses the extraction data obtained for the ligands discussed in this chapter.

Table 11: The respective Fsp^3 value and measured solubility for each novel terdentate ligand.

Code	Structures	Solubility mmol/L in 1-octanol	Fsp^3 value
L1	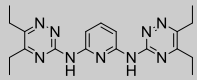	34.8	0.42
L3	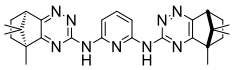	69.4	0.59
L4	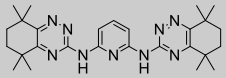	27.5	0.59
L5	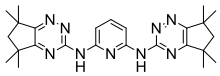	105.2	0.56
L6	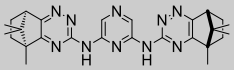	106.7	0.62
L7	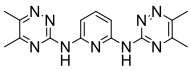	-	0.27
L8	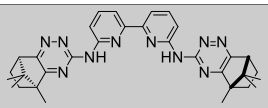	8.5	0.50
L10	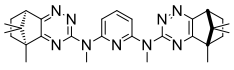	96.8	0.62
L11	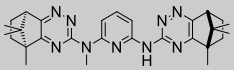	74.7	0.61
L12	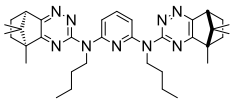	148.8	0.69
L13	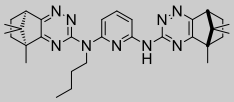	51.0	0.65
L14	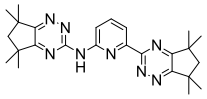	151.3	0.56
L15	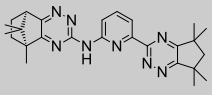	37.3	0.58
L16	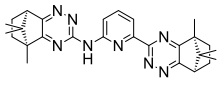	63.0	0.59
L17	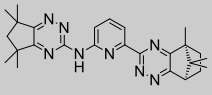	71.4	0.58

2.6. Extraction Studies

Extraction studies were carried out to determine the ability of this new family of ligands to selectively extract the An(III) over the Ln(III) from nitric acid (HNO_3) solutions. Solutions of the ligands were prepared in 1-octanol at a concentration of 0.01 M and subsequently contacted with HNO_3 solutions containing all the Ln(III) (10^{-5} mol/L) and the radiotracers ^{241}Am, ^{152}Eu and ^{244}Cm. See Chapter 6 for a detailed description of this study. The distribution (*D*) ratio for each radioisotope is a quantitative measurement of their relative radioactivity, as analysed by both α- and γ-spectroscopy, in both the organic and aqueous phase. It gives an indication of how a metal ion distributes between two immiscible phases, and is thus a measure of extraction affinity of a ligand for that metal ion. The separation factor ($SF_{Am/Eu}$ and $SF_{Cm/Am}$) is a measure of the separation between two radioisopes; i.e. $SF_{Am/Eu} = D_{Am} / D_{Eu}$ and this is a measure of the extraction selectivity of a ligand. For potential future use in a selective actinide extraction (SANEX) process, the ligand should ideally show a distribution ratio for Am(III) (D_{Am}) of ≥ 1, a distribution ratio for Eu(III) (D_{Eu}) of < 1, and a separation factor for Am(III) over Eu(III) ($SF_{Am/Eu}$) as high as possible (ideally at least 5).

Under the standard conditions used, the ligand **L3** gave very low *D* ratios for all radioisotopes and a resulting negligible separation factor ($SF_{Am/Eu}$) at all concentrations, Figure 67. This indicates that none of the radioisotopes have been extracted into the organic phase by the ligand **L3** and hence remain in the aqueous phase. This result is mimicked when ligands **L4** and **L6** were screened, suggesting that the structures of the aliphatic parts of the ligands, which are derived from the diketones used in the synthesis, have no impact upon the final extraction properties. Additionally it appears that varying the aromatic linker, whether it be pyridine or pyrazine, between the external triazine rings has no influence upon the extraction properties of these ligands.

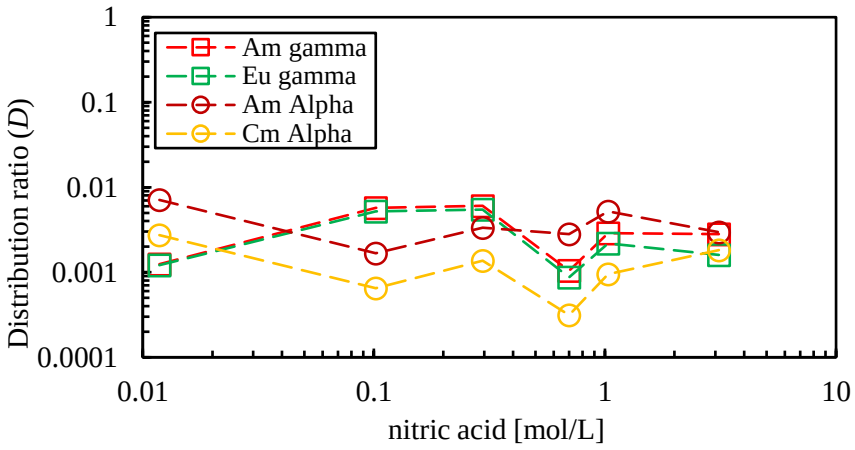

Figure 67: Distribution ratios for extraction of ^{152}Eu, ^{241}Am, ^{244}Cm by **L3** measured by α- and γ-spectroscopy as a function of the nitric acid concentration of the aqueous phase (1 hr, 22 °C at 2,200 rpm). Organic phase: 10 mM **L3** in 1-octanol.

Those ligands derived from (1*S*)-(+)-camphorquinone **2.2.8** showed no precipitation under contact with the nitric acid solutions, Figure 68. This is in contrast with the extraction results previously published for camphor-BTP **1.31**, which was susceptible to forming precipitates in contact with nitric acid solutions.[82]

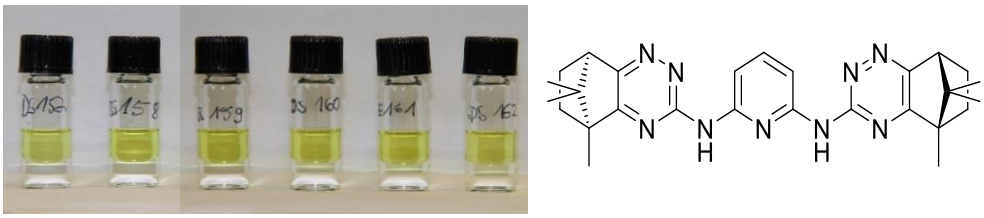

Figure 68: (a) Photographs of the sample tubes after the first screening test using **L3**, c with increasing [HNO_3] from left to right; (b) molecular structure of **L3**.

It was hoped that the addition of the *N*-alkyl chain(s) in ligands **L10**, **L11**, **L12** and **L13** would influence the preferred conformation of the ligands and improve their extraction properties, Figure 69. Upon completion of the extraction tests using standard conditions, both low *D* ratios and low $SF_{Am/Eu}$ values were observed for ligand **L13**, in agreement with the previous screening results with this family of ligands, Figure 70. All *D* ratios remain below 0.1 across all nitric acid concentrations used for all four of the alkylated ligands (**L10**, **L11**, **L12** and **L13**); further extraction data can be found in the appendix. For effective extraction of the An(III) from the Ln(III) the $D_{(Am)}$ should be above 1, with the $D_{(Eu)}$ remaining below to 1.

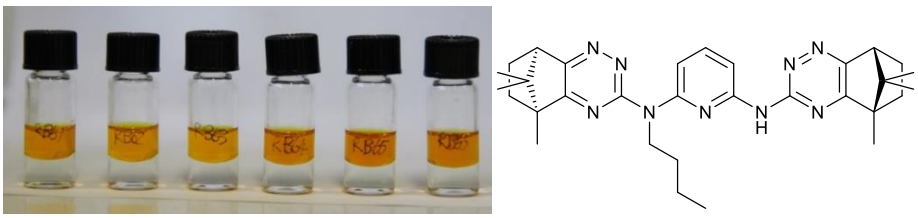

Figure 69: (a) Photographs of the sample tubes after first screening test using **L13**, with increasing [HNO_3] from left to right; (b) molecular structure of **L13**.

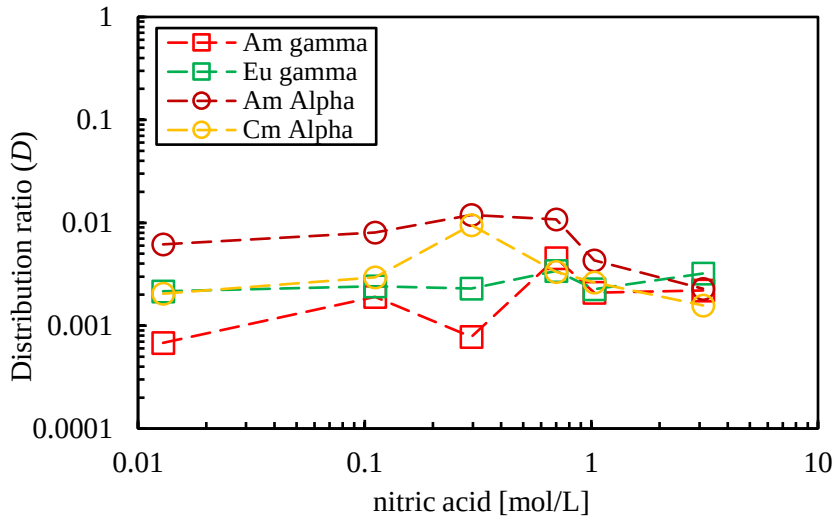

Figure 70: Distribution ratios for extraction of ^{152}Eu, ^{241}Am, ^{244}Cm by **L13** measured by α- and γ-spectroscopy as a function of the nitric acid concentration of the aqueous phase (1 hr, 22 °C at 2,200 rpm). Organic phase: 10 mM **L13** in 1-octanol.

The synthesis of the 2,2'-bipyridine-derived ligand **L8** was hoped to influence the extraction capability of those ligands containing the amine bridge, by having two N-donor atoms in the 2,2'-bipyridine group that could coordinate initially. Unfortunately, low *D* ratios were again obtained for all radioisotopes across all HNO_3 concentrations, showing that all radioisotopes remained in the aqueous phase, Figure 71. The resulting $SF_{Am/Eu}$ values were negligible as well. As a result, further investigations into using the 2,2'-bipyridine group to derive further ligands were not considered.

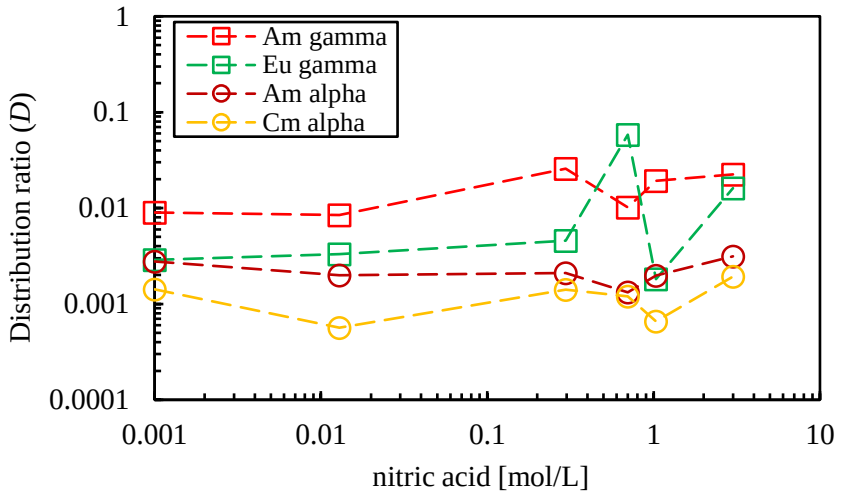

Figure 71: Distribution ratios for extraction of ^{152}Eu, ^{241}Am, ^{244}Cm by **L8** measured by α- and γ-spectroscopy, as a function of the [HNO_3] of the aqueous phase (1hr, 22 °C at 2,200 rpm). Organic phase: 10 mM **L8** in 1-octanol.

Unfortunately this trend of low *D* ratios and negligible $SF_{(Am/Eu)}$ was observed across all these ligands containing the amine bridge (see the appendix for the full data set). Consequently, it was decided to no longer investigate further variations into this family of ligands for the extraction of the An(III) over the Ln(III). It was clear that the addition of an amine bridge between the pyridine rings and the 1,2,4-triazine rings negatively impacted the extraction capability of the ligands, when compared to the analogues BTP and BTBP ligands, section 1.5.

Potential reasons for the poor extraction capability of the above ligands may be that there is a competition between metal ion coordination and ligand protonation as a result of the ligands being more basic than the BTP/BTBP ligands. When in contact with the HNO_3 solution, the basic nitrogen atoms of the pyridine and triazine groups can undergo protonation, preventing their ability to coordinate to the actinide ions. Due to the introduction of the amine bridge, it could be expected that the resulting ligands are more basic than the BTP analogues due to the delocalisation of electron density from the NH lone pairs into the adjacent pyridine and triazine rings, Figure 72. This additionally gives the C-N-C bridge some double bond character, preventing the free rotation of this bond as would be observed for the BTP ligands, where there is a C-C bond with no double bond character. In addition, they might be poorer π-acceptor ligands than the BTP

ligands due to the electron donating resonance effect of the nitrogen in the amine bridge and the hence impact on both the metal-ligand bond strength and complex stability.

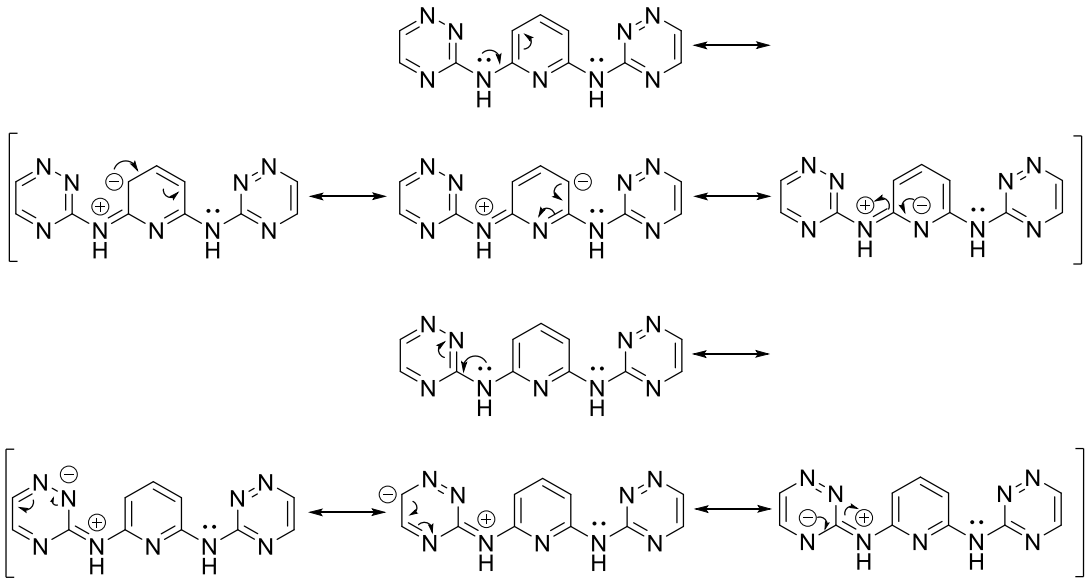

Figure 72: Resonance structures of the novel ligand family synthesised by Buchwald Hartwig reactions of 3-amino-1,2,4-triazines, showing the delocalisation of the NH lone pairs into both the 1,2,4-triazine and pyridine rings.

Alternatively, it could be the ligands adopt the non-chelating *trans-trans* conformation as the preferred conformation in solution, preventing the coordination of the outer 1,2,4-triazine 2-N atom with the metal. Potential conformations are summarised in Figure 73, with the *cis-cis* conformation being the only conformation that has the potential for chelating the metal in a tridentate fashion. Indeed the obtained X-ray crystal structure for ligand **L3**, Figure 74, shows that the ligand is adopting the non-chelating *trans-trans* conformation in the solid state and this could be the dominant conformation in solution. The outer triazine rings are twisted away from the conformation necessary for metal ligation. This conformation is in contrast to that observed for the $CyMe_4$-BTP ligand **1.30** which, despite showing the *trans-trans* conformation, has only one torsion to consider, that of the pyridine-triazine C-C bond.[80] Once the $CyMe_4$-BTP ligand **1.30** is protonated it adopts the *cis-cis* conformation which may suggest a lower rotational energy is required then rotation across the C-N bonds of the amine bridge of ligand **L3**. With the help of computational studies, this could imply that this is the most stable conformation of the ligand and not a crystal packing effect.

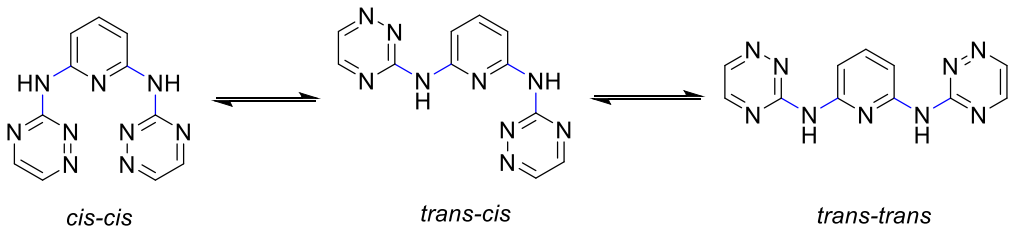

Figure 73: Possible conformations of the novel ligand family synthesised by Buchwald Hartwig reactions of 3-amino-1,2,4-triazines. Different conformers are due to rotation across the $C_{pyridine}$-N bonds (denotated in blue).

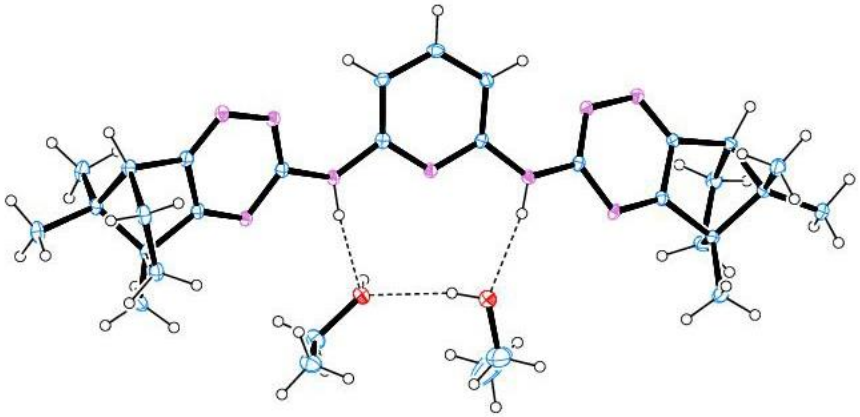

Figure 74: X-ray crystal structure of terdentate ligand **L3**.

Computational studies were completed by Dr Mark Sims at Northumbria University on $CyMe_4$-BTBP **1.09** and $CyMe_4$-BTPhen **1.17**. It was confirmed that there is a small energy barrier that needs to be overcome to rotate the 1,2,4-triazine rings into their chelating conformations.[96] Further computational studies were completed at Northumbria University on **L3** to investigate the possible conformations that may exist in solution. A relaxed potential energy scan around the four dihedral angles, Table 12, was completed. A 30 ° rotation between the dihedral angle of 0 and 180 ° resulted in a total of 2401 (7^4) structures investigated at their respective optimised geometries. Those conformations within 10 kJ mol^{-1} of the minimum energy structure, at 298 K, were taken forward for fully relaxed geometry optimisations.

Table 12: Table showing lowest energy conformations and their populations of the novel ligand family synthesised by Buchwald Hartwig reactions of 3-amino-1,2,4-triazines, with torsion angles; respective to triazine-N, N-pyridine, pyridine-N and N-triazine. Studies completed by Dr Mark Sims of Northumbria University. Alll density functional theory calculations were performed using Gaussian 09 software package (Revision C.01).

Structure	Torsion Angles (°)	Population (%)
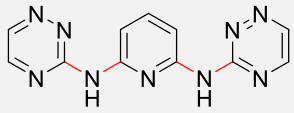	180-180-180-180	35
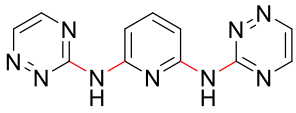	0-180-180-180	50
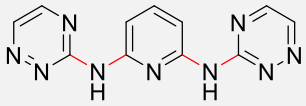	0-180-180-0	15

It was found that only 3 conformations dominated the population at 298 K, Table 12, in agreement with the conformation observed in the crystal structure of ligand **L3** (*trans-trans*). It should be noted that these calculations were completed on simplistic structures and don't consider any of the aliphatic side groups attached to the triazine rings, which could influence dominant conformations based upon steric effects. In recalculating the populations based upon the three conformations, the percentage populations are also given. The *cis-cis* conformations, which would be expected to coordinate the metal ions, are approximately 70 kcal mol^{-1} higher in energy then the *trans-trans* conformations. This is a substantial increase from those conformations shown in the table and a considerable barrier to overcome in order to achieve the conformation for metal ion complexation.

A further extraction study was completed on these ligands using a 3.1 mol/L simulated waste solution containing various fission and corrosion products present in spent nuclear fuel such as nickel, palladium, and cadmium. This comes as a consequence of an NMR titration study completed with $AgNO_3$ and **L3** in which a 1:1 complex was observed, section 2.7. This solution was diluted to a concentration of 0.031 mol/L for subsequent ICP-MS measurements and the extraction screening was completed using the same conditions as previously (varying HNO_3

concentration, 22 °C, phase mixing for 1 hour at 2,200 rpm). Results from this study will be published in due course once completed by colleagues at the Forschungszentrum Jülich.

The ligands derived from 3-(6-bromo-2-pyridyl)-1,2,4-triazines **L14, L15**, **L16** and **L17** were synthesised in order to off-set the poor extraction properties shown above for the symmetrical ligands derived from 2,6-dibromoheteroarenes. It was proposed that by removing one of the C-NH-C bridges, the extraction properties for this family of ligands may be positively impacted. The low rotational energy barrier across the bond highlighted in blue, Figure 75, as seen with the BTPs, BTBPs and BTPhens, freely rotates even at room temperature, allowing for the two highlighted nitrogens in the triazine rings to be orientated for coordination to the metal.[96]

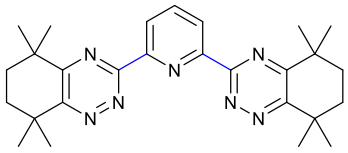

1.30

Figure 75: Molecular structure of $CyMe_4$-BTP **1.30**, with the bond required to rotate highlighted (blue).

Despite the above hypothesis, the extraction experiments carried out with ligands **L14, L15** and **L17** indicated no extraction of Am(III) or Cm(III) across all nitric acid concentrations, Figure 76 and Figure 77. The *D* ratios remained below 0.1, as observed with the ligands discussed previously. The external aliphatic groups attached to the triazine rings have no impact on the ligands extraction capabilities or ability to separate the An(III) from the Ln(III). These $SF_{Am/Eu}$ values were uniformly low for all three ligands tested (see appendix for the full data set).

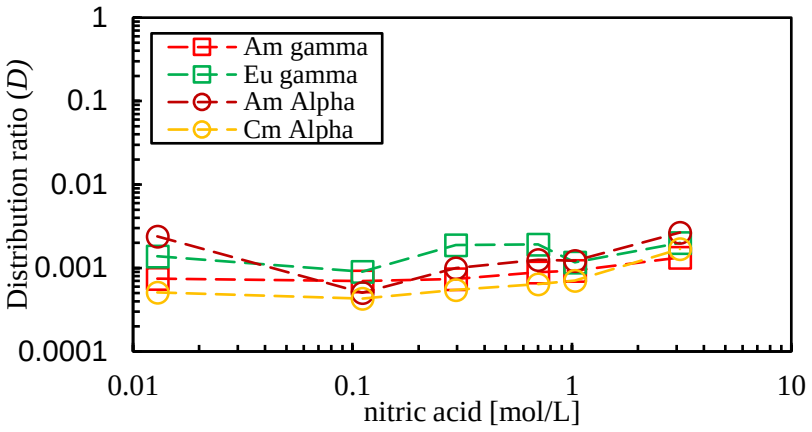

Figure 76: Distribution ratios for extraction of ^{152}Eu, ^{241}Am, ^{244}Cm by **L17** measured by α- and γ-spectroscopy, as a function of the [HNO_3] of the aqueous phase (1 hr, 22 °C at 2,200 rpm). Organic phase: 10 mM **L17** in 1-octanol.

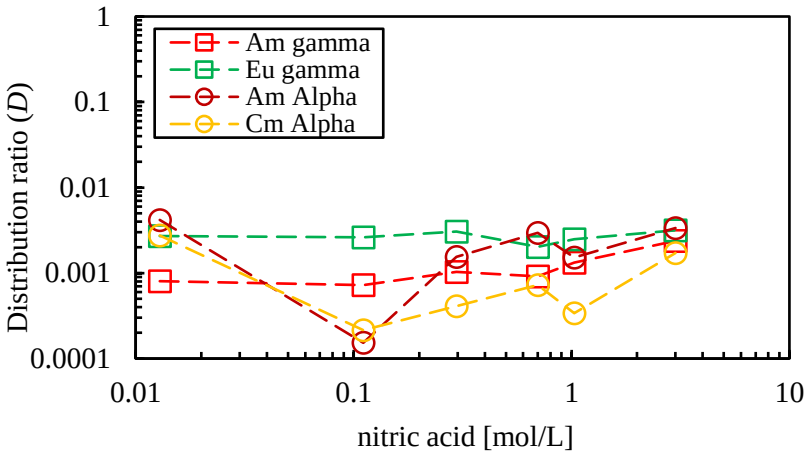

Figure 77: Distribution ratios for extraction of ^{152}Eu, ^{241}Am, ^{244}Cm by **L14** measured by α- and γ-spectroscopy, as a function of the [HNO_3] of the aqueous phase (1 hr, 22 °C at 2,200 rpm). Organic phase: 10 mM **L14** in 1-octanol.

It was hypothesised that similar reasons to that discussed above are the consequence of the poor extraction capability of these ligands. The removal of one of the C-NH-C bridges has no positive impact on the extraction properties using these ligands, suggesting that the conformational properties of the ligand may still play a role. An X-ray crystal structure has not being successfully obtained for any of these ligands to verify this hypothesis.

As a consequence of the data obtained through the extraction screening of these ligands, it is clear that the addition of an amine (C-NH-C) bridge between the pyridine and triazine rings has an

unquestionably negative impact on the extraction abilities of these ligands. Subsequently, no further ligands containing this bridge were considered.

2.7. NMR Titration Studies

In order to determine the potential species that could be present in an extraction experiment, NMR titration studies were completed with the lanthanide nitrate salts acting as actinide surrogates. Lanthanum (La(III)) and lutetium (Lu(III)) were selected as the lanthanide salts, along with ytterbium (Yb(III)) and yttrium (Y(III)) (all as nitrate salts) due to their diamagnetism and the subsequent likelihood of obtaining well resolved NMR spectra.

A methanol-d_4 solution of $La(NO_3)_3$ was titrated against a 0.01 M solution of **L3** in the same solvent. The resulting spectra were overlaid to give stacked ^1H NMR spectra, Figure 78. The disappearance of the free ligand resonances, and the appearance of new resonances for a complex species, as the metal is added to the ligand would be expected if ligand **L3** formed complexes in solution with La(III). In this event, no new resonances were observed upon titration of ligand **L3** with 0.8 eq. addition of the $La(NO_3)_3$ solution. Under the conditions of the titration experiment, the ligand shows no complexation with the La(III) metal present, despite an attempt to force complexation by increasing the temperature. This is in agreement with the evidence obtained during the solvent extraction tests, in which these ligands observed no extraction capability for the An(III) or Ln(III)'s present. As a consequence, further di-aminated ligands were not studied by NMR titrations with the lanthanide salts.

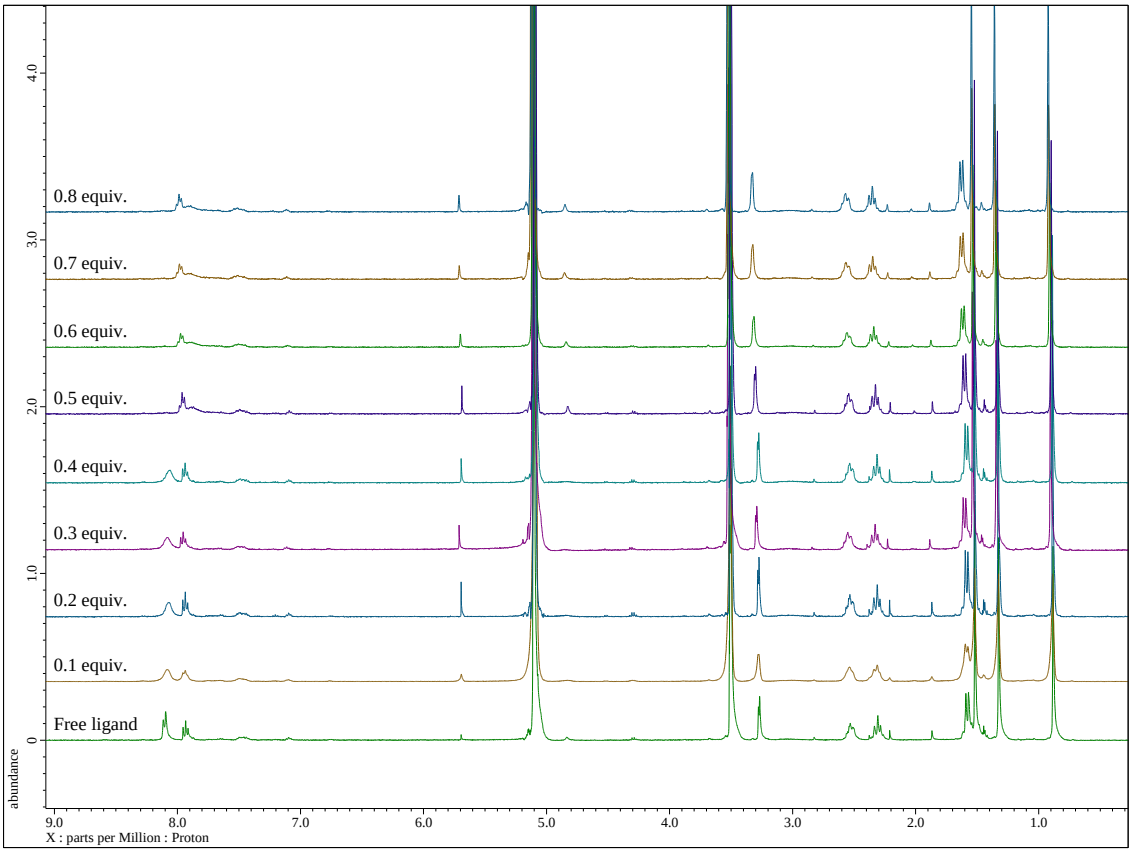

Figure 78: Stack plot for the ^{1}H NMR titration of **L3** with increasing equivalents of $La(NO_3)_3$ showing no complex formation.

In further studies it was decided to test the **L3** ligand with a deuterated solution of the transition metal, silver nitrate ($AgNO_3$), to ascertain the potential scope of these ligands for fission and/or corrosion product extraction. As Ag^+ is a soft Lewis acid it prefers to complex with soft Lewis bases, such as the nitrogen atoms of the *N*-donor ligands, forming stable complexes. Previously, it has been shown that BTBPs can complex the Ag^+ fission product with high distribution ratios during extraction testing.[49] An X-ray crystal structure revealed a 2:2 stoichiometry with a BTBP (C2-BTBP) as a $[Ag_2(C2\text{-}BTBP)_2]^{2+}$ complex.[49] Each Ag^+ metal ion coordinates to two nitrogen atoms from each ligand, one from the pyridine and one from the triazine resulting in a distorted square pyramidal geometry. NMR titrations revealed little influence from the side groups of the BTBP ligands in the same study. In aqueous solutions, hydrophilic bidentate bis-1,2,4-triazine ligands have been shown to complex the Ag^+ ion and can act as a masking agent, in order to supress its extraction by the BTBPs into the organic phase.[143] Further investigation with the **L3**

ligand would open up the potential for these ligands to act as masking agents of the transition metals during actinide extractions.

An NMR titration of ligand **L3** with $AgNO_3$ in methanol-d_4 shows a shift in the signals in the aromatic region upon addition of increasing equivalents of the $AgNO_3$ stock solution, Figure 79. The first spectrum of the free ligand shows three signals in the aromatic region at δ 8.0, 8.4 and 8.6 ppm, although the multiplicity is unclear. There is a gradual upfield shift in the signal at δ 8.6 to 8.0 ppm upon addition of 0.4 eq. of Ag^+ with the other signals remaining unchanged. After addition of 0.6 eq. of Ag^+ a new doublet appears at δ 7.3 ppm. There are no notable changes in the aliphatic region. A high-resolution mass spectrum (HRMS) was obtained for the sample containing 1.2 eq. of $AgNO_3$ to confirm the presence of a complex, Figure 80. The mass spectrum shows mass peaks for both the protonated free ligand [$C_{27}H_{33}N_9 + H^+$] at 484.2920 m/z, with a further peak at 590.1892 m/z indicative of a 1:1 or 2:2 complex. The smaller peak at 1075.4762 m/z is indicative of a 2:1 species, in which two ligand molecules surround the Ag^+ ion. Further understanding into the mode of binding could be discovered by obtaining an X-ray crystal structure of the complex, but unfortunately this was not obtained due to time constraints.

A further NMR titration was completed on **L10** with $Ni(NO_3)_2$ in deuterated acetonitrile, but no complexation was observed for this ligand, see appendix for details. It is believed that the Ag^+ ion may be interacting with the amine (C-NH-C) during coordination. Once the position is alkylated it is less able to coordinate to the Ag^+ ion as a consequence of the hindrance from the alkyl chain.

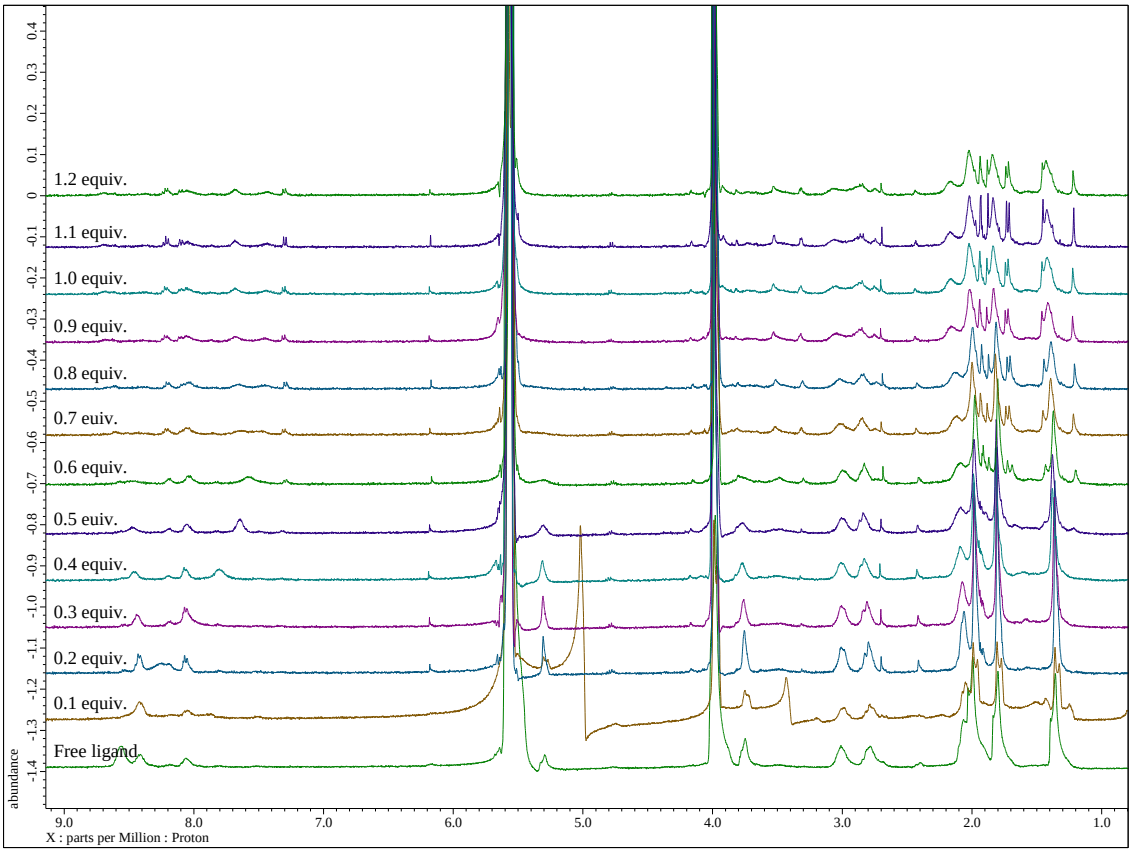

Figure 79: Stack plot for the ^{1}H NMR titration of **L3** with increasing equivalents of $AgNO_3$ in deuterated methanol.

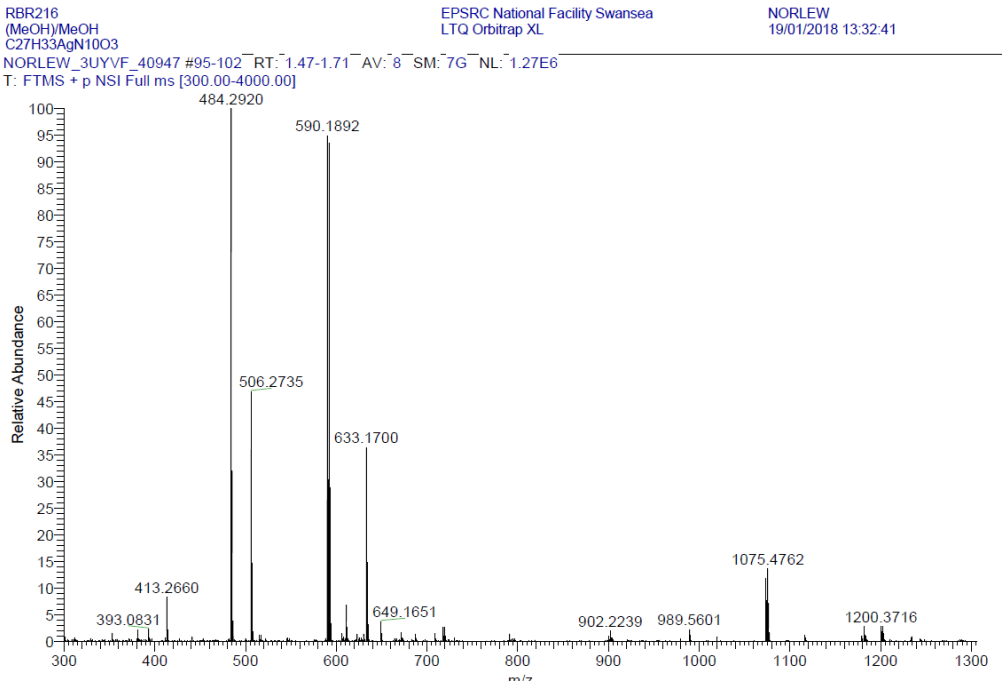

Figure 80: HRMS of the NMR tube sample from the NMR titration of **L3** with $AgNO_3$ after addition of 1.2 eq. $AgNO_3$ showing the mass peaks for the protonated ligand, a 1:1 or 2:2 complex and 1:2 complex.

The purpose of investigating the ligands derived from 3-(6-bromo-2-pyridyl)-1,2,4-triazines **L14**, **L15**, **L16** and **L17** was to gain a more complete understanding of how these ligands may, or may not, be interacting with the actinide metal ions. These non-symmetrical ligands can be considered a hybrid between the BTP ligands and the symmetrical ligands such as **L3**, and they could have a conformational rigidity that falls in between the two. It was proposed that this may aid in the coordination of these ligands with the An(III) metal ions, in parallel to the previous hypothesis regarding the lanthanide ions. An NMR titration of ligand **L15** with $La(NO_3)_3$ in deuterated acetonitrile was completed. During the titration, an upfield chemical shift of one of the proton signals in the aromatic region was observed from δ 8.8 to 8.2 ppm, potentially caused by interaction of the metal with the ligand. Figure 81 shows the stacked ^1H NMR spectra. However, a HRMS of the final sample, containing 1.2 eq. of $La(NO_3)_3$ was obtained and showed only the mass peak for the protonated free ligand. As it stands this is not enough evidence for complexation.

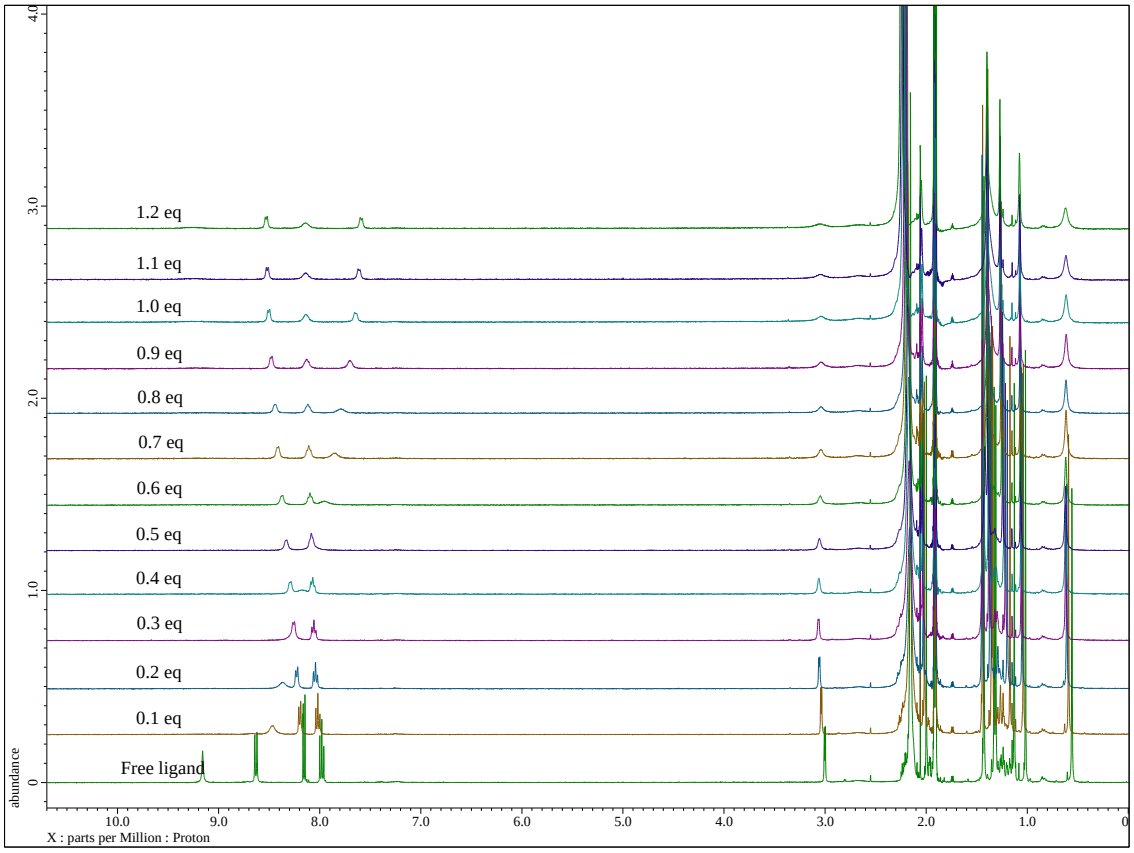

Figure 81: Stack plot for the ^1H NMR titration of **L15** with increasing equivalents of $La(NO_3)_3$ in deuterated methanol.

Following on from the results obtained from the NMR titration of **L3** with $AgNO_3$, it was decided to test the unsymmetrical ligands **L15** and **L17** with $AgNO_3$ in CD_3CN-d_3. For the titration completed with **L17**, the spectrum of the free ligand shows four signals in the aromatic region at δ 9.81, 8.25, 7.82 and 7.60 ppm. There is a gradual upfield shift of the signal at δ 8.25 to 7.60 ppm, and a gradual downfield shift of the doublet at δ 7.60 to 7.81 ppm, Figure 82, upon addition of 1.0 eq. of Ag^+. Additionally the broad singlet representative of the NH signal at δ 9.80 shifts upfield to 8.66 ppm. A similar observation was made for **L15** (refer to the appendix). Most likely the Ag^+ is interacting with the N atom of the pyridine and that of the amine (C-NH-C), although an X-ray crystal structure would be required to confirm this.

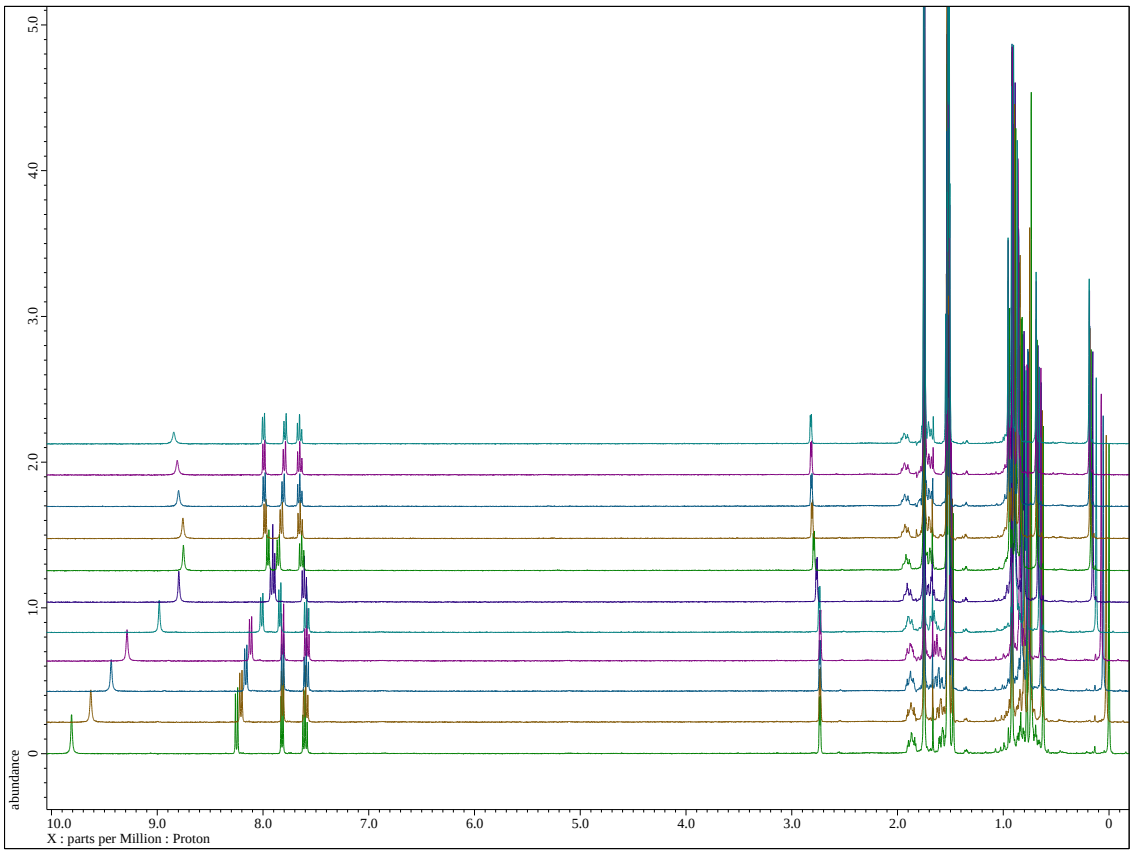

Figure 82: Stack plot for the ^1H NMR titration of **L17** with increasing equivalents of $AgNO_3$ in deuterated acetonitrile.

2.8. Conclusion

In this chapter two families of novel multidentate bis-1,2,4-triazine ligands have been synthesised, linked by various aromatic groups; pyridine, pyrazine and 2,2-bipyridine. This is the first time 3-amino-1,2,4-triazines have been employed as the nucleophilic partner directly in a Buchwald Hartwig double amination reaction.

From the ligands synthesised in this chapter, the majority observe higher solubilities when compared to the current benchmark ligand $CyMe_4$-BTBP **1.09**, with the exception of **L7**. Upon the addition of alkyl chains there was a positive correlation between the Fsp^3 value and their respective measured solubilities, with this general trend observed across all ligands, suggesting some evidence for the proposed hypothesis, section 1.6. For the mono-aminated ligands **L14**, **L15**, **L16** and **L17** there is a distinct difference in solubilities if two different diketone groups are attached, adjacent to the 1,2,4-triazine ring, with the highest solubilities obtained when these groups are the same.

Since the ligands did not extract any metals in our extraction experiments, conclusions about whether or not the added amino-groups in these ligands have a beneficial effect on extraction kinetics were unable to be made. The dominant *trans-trans* conformers of the ligands, as revealed through computational studies, are unable to rotate to the *cis-cis* conformers to complex the metal centre, due to a high C-N rotational energy barrier. As a consequence, it was concluded that the addition of an amine bridge between the pyridine and triazine rings should no longer be considered in future developments for the separation of the An(III) from the Ln(III).

An investigation into the potential for these ligands to coordinate with transition metals is underway with colleagues at the Forschungszentrum Jülich. The results of this study will be published in due course. Those results obtained will indicate the potential applicability of these ligands as fission or corrosion product extractants.

Chapter 3

Ligands derived from a modified camphorquinone diketone

3. Ligands derived from a modified camphorquinone diketone

3.1. Introduction

In research to replace the $CyMe_4$-diketone **2.2.5**, the commercially available diketone (1*S*)-(+)-camphorquinone **2.2.8** was selected as a potentially viable option, Figure 83. Previously, this diketone has been used by Geist and co-workers to synthesise the camphor-BTP ligand **1.31**, Figure 84. This ligand showed a number of advantages over $CyMe_4$-BTBP **1.09** in extraction experiments, namely significantly higher solubilities in organic diluents (up to 200 mM in diluent 1-octanol), faster extraction kinetics, good selectivity for the An(III) over the Ln(III) and hydrolytic stablity.[82] The ligand observed no degradation over a period of 100 days in contact with 1 M nitric acid (HNO_3) and the extraction equilibrium was achieved in a tetrahydropyran/1-octanol system within approximately 10 minutes of phase mixing. Despite this, these investigations found that camphor-BTP **1.31** exhibited third phase formation in contact with higher concentrations of HNO_3 solutions, dependent upon the diluent used. When the ligand was dissolved in a kerosene/1-octanol mixture (7:3 vol. ratio), a precipitate was observed when contacted with 1 M HNO_3. Utilising the more polar 1-octanol diluent, the precipitate was not observed up until contact with 4 M HNO_3. However, in spite of this improved solubility in 1-octanol, there was a decrease in the distribution (*D*) ratios of Am(III) (D_{Am}) in comparison to when the same ligand was dissolved in the kerosene/1-octanol diluent. The BTPs are known to exhibit some HNO_3 extraction and it is proposed that the precipitate observed in these solutions is a consequence of precipitation of the protonated ligand.[144] In Section 2.0, where the (1*S*)-(+)-camphorquinone **2.2.8** was utilised as the diketone, showed no solubility or precipitation issues when the ligand came into contact with the HNO_3 aqueous phase. As a result, derivatives of this group will be considered for their potential application in actinide extractions.

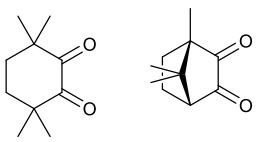

2.2.5 **2.2.8**

Figure 83: Molecular structure of $CyMe_4$ **2.2.5** and (1*S*)-(+)-camphorquinone **2.2.8**.

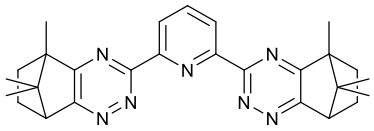

1.31

Figure 84: Molecular structure of camphor-BTP **1.31**.

Due to the presence of chirality within the diketone it exists as two enantiomers; *R*- or *S*-camphorquinone. The aforementioned work completed by Geist and co-workers was carried out using a racemic (±)-camphorquinone, meaning the final camphor-BTP **1.31** ligand may exist as diastereomers within solution, Figure 84. Research by D.D. Ensor and co-workers found that using a racemic mixture of camphorquinone, as opposed to a single R or S enantiomer, had a negative impact on the distribution ratios observed during extraction testing with camphor-BTP **1.31** in the polar solvent FS-13 **1.58** (page 38).[132] In order to investigate the application of the camphorquinone group as a viable alternative to $CyMe_4$ **2.2.5** the enantiomerically pure compounds; (1*S*)-(+)-ketopinic acid **3.1.2** and (1*S*)-(+)-10-camphorsulfonyl chloride **3.1.3**, will be utilised to synthesise a range of novel multidentate ligands containing the core group, Figure 85. This will limit the potential formation of diastereomers as well as potentially maximising the distribution ratios that may be observed during solvent extraction experiments, depending upon the starting material utilised.

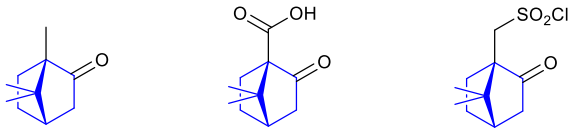

3.1.1 **3.1.2** **3.1.3**

Figure 85: Comparison between the molecular structures of (+)-camphor **3.1.1**, (+)-ketopinic acid **3.1.2** and (1*S*)-(+)-10-camphorsulfonyl chloride **3.1.3**; with the common structure highlighted in blue.

(1*S*)-(+)-Ketopinic acid **3.1.2** was selected as the starting material of choice for the synthesis of modified derivatives of camphorquinone **2.2.8** as it allows for functionalisation at the carboxylic acid moiety. Although ketopinic acid **3.1.2** is a more costly starting material in comparison to

camphorquinone **2.2.8**, it avoids the multi-step synthesis that would be required to achieve the derivatisation of camphor **3.1.1** itself, Figure 86.[145] Alternatively, camphorsulfonyl chloride **3.1.3** can be purchased at a reasonable cost and oxidised to give ketopinic acid **3.1.2** to provide an even more economically beneficial alternative to using ketopinic acid **3.1.2** itself as the starting material.

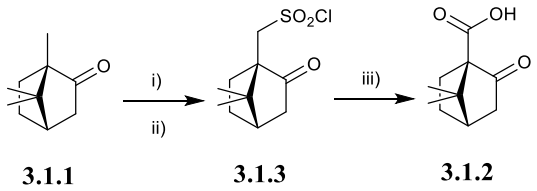

Figure 86: Synthetic scheme for the synthesis of (+)-ketopinic acid **3.1.2** from (+)-camphor **3.1.1**. [170-172]. Reaction conditions: i) H_2SO_4, Ac_2O; ii) $SOCl_2$; iii) $KMnO_4$, Na_2CO_3, H_2O.

In line with the aims and objectives of the project, converting the acid functionality of ketopinic acid **3.1.2** into an amide will ensure the inclusion of additional HBD/HBA functional groups into the resulting bis-1,2,4-triazine ligands. The introduction of the amide functionality is based on previous research into the amide containing extractants; TODGA **1.05** and DMDOHEMA **1.04**. Both ligands are known to have very high solubilities in the required diluents (octanol, dodecane, kerosene). They additionally, despite their hydrophobicity, show very fast rates of metal extraction, section 1.4. Amide bonds have traditionally been used where Am/Eu selectivity was not required such as in the DIAMEX process. The oxygen atom, as a hard donor, observes no selectivity between the An(III) and Ln(III). However, as the amide group will not be part of the coordination cavity in these novel ligands and not likely to take part in metal coordination, it is anticipated they will have minimal impact on their subsequent selectivity for An(III) over Ln(III). Despite this, the amide group should enable the ligands to have a high surface concentration at the phase interface, and hence increase the rates of metal extraction, due to its ability to form hydrogen bonds with the water molecules at the phase interface.

This chapter will consider a variety of ligands based upon the functionalised ketopinic acid **3.1.2** that are analogous of the BTP, BTBP and BTPhen ligands. The ketopinic acid **3.1.2** will be coupled with a variety of primary and secondary amines to form amides, which will subsequently

be oxidised to form a variety of the final 1,2-diketones, section 3.3. Utilising a variety of amines enables us to tune the solubilities and extraction properties of the ligands, which will hopefully lead to the discovery of novel camphorquinone-derived ligands suitable for further development. In addition, the analogous ligands camphor-BTBP **L28** and camphor-BTPhen **L29**, Figure 87, will also be synthesised and screened for comparison purposes, as these ligands have never been investigated for their ability to extract and separate An(III) from Ln(III). Camphor-BTPhen **L29** has previously been reported in work by L.M. Harwood and co-workers in which its solubility was investigated (18.6 mM in diluent 1-octanol).[102]

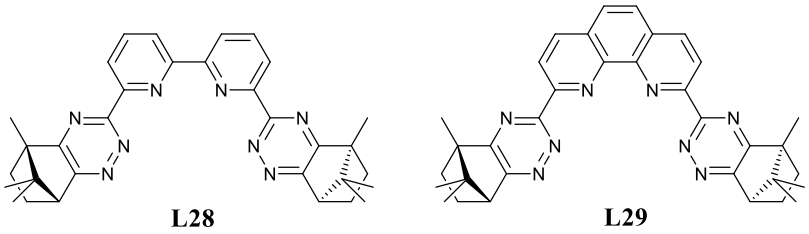

Figure 87: Structures of analogous ligands camphor-BTBP **L28** and camphor-BTPhen **L29**.

3.2. Synthesis of the bis-amidrazones

In order to synthesise the final ligands in this Chapter and following (Chapter 4), the bis-amidrazones, corresponding to the final BTP and BTPhen ligands, first need to be synthesised. Following a procedure by Therien and co-workers.[146] hydrazine hydrate was added to pyridine-2,6-dicarbonitrile **3.2.1** to produce the known pyridine-2,6-dicarboxamidrazone **3.2.2** in a 64% yield, Figure 88.[147] The corresponding 2,2'-bipyridine-6,6'-dicarboxamidrazone **3.2.5** was synthesised previously within the Lewis goup, via the dinitrile compound **3.2.4**, and was used as obtained, Figure 89.[61c]

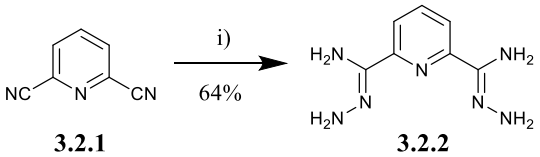

Figure 88: Reaction scheme for the synthesis of **3.2.2**. Reaction conditions: i) hydrazine hydrate, ethanol.

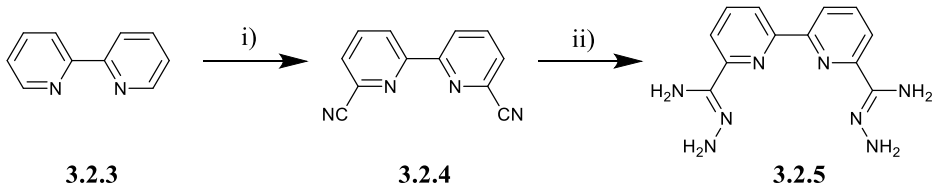

Figure 89: Synthesis of the 2,2'-bipyridine-6.6'-dicarboxamide dihydrazone **3.2.5**, as completed previously within the Lewis group. Reaction conditions: i) hydrogen peroxide, AcOH, potassium cyanide, benzoyl chloride, THF, H_2O; ii) hydrazine hydrate, EtOH.

The 1,10-phenanthroline-2,9-dicarboxamidrazone **3.2.10** was initially synthesised in three steps following the procedure of Harwood and co-workers, Figure 90.[95] The formation of the dialdehyde **3.2.7** was achieved by oxidising the starting neocuproine **3.2.6** with selenium dioxide. The dialdehyde **3.2.7** was converted to the dinitrile **3.2.9** in a one pot synthesis via the intermediate dioxime **3.2.8**. The final formation of the bis-amidrazone **3.2.10** was achieved in 88% yields.

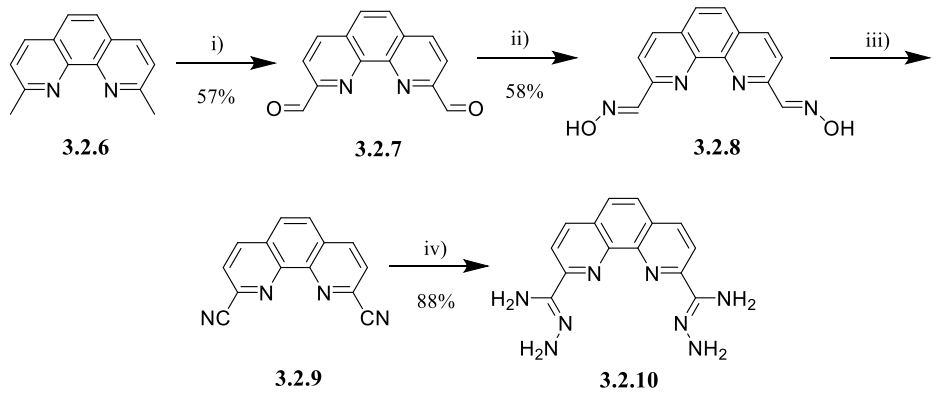

Figure 90: Reaction scheme for the synthesis of bis-amidrazone **3.2.10**. Reaction conditions: i) SeO_2, 1,4-dioxane, ii) hydroxylamine hydrochloride, triethylamine, MeCN, iii) p-toluenesulfonyl chloride, DBU, iv) hydrazine hydrate, EtOH.

Due to the cumbersome nature of this synthesis, which involves multiple triturations of the dialdehyde **3.2.7** in the first step to remove selenium-derived impurities, an alternative synthesis of **3.2.10** was explored, as described again by Harwood and co-workers, Figure 91.[148] Although this procedure involves a higher number of steps, the ease in completing the reactions and higher yields of each step make it appealing to investigate. There is the added benefit of avoiding the use of toxic SeO_2 in the first step, in which its use results in a more intensive purification process to ensure the complete removal of any selenium impurities. This modified route proceeds via the

free radical chlorination of the two methyl groups of neocuprione **3.2.6** using *N*-chlorosuccinimide and 3-chloroperbenzoic acid to give **3.2.11** prior to hydrolysis to produce the diester **3.2.12**. The formation of the diamide **3.2.13** was achieved with ammonium chloride in concentrated ammonium hydroxide prior to its dehydration to form the dinitrile **3.2.9**. The final step was completed as above to give final yields of bis-amidrazone **3.2.10** of 84%, Figure 91.

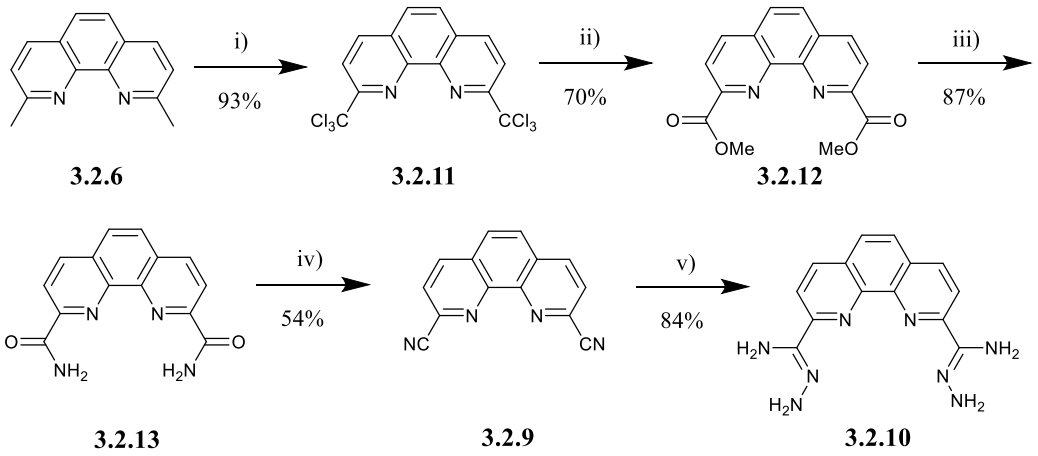

Figure 91: Reaction scheme for the alternative synthesis of bis-amidrazone **3.2.10**. Reaction conditions: i) *N*-chlorosuccinimide, 2,2'-azobis(2-methylpropionitrile), $CHCl_3$, ii) H_2SO_4, MeOH, iii) NH_4Cl, NH_4OH, iv) phosphorus oxychloride, v) hydrazine hydrate, DMSO.

The above bis-amidrazones **3.2.2**, **3.2.5** and **3.2.10** were utilised in the synthesis of a range of ligands described throughout this Chapter and the subsequent Chapter 4.

3.3. Synthesis of modified camphorquinone ligands.

In the first efforts to synthesise a range of amide derivatives of ketopinic acid **3.1.2**, it was decided to initially form the C-N bond via traditional amidation conditions, followed by the oxidation reaction to give the final 1,2-diketones. Following procedures reported by S.M. Cerero and co-workers,[149] the amidation was explored using the carboxyl activating reagent EDC (1-ethyl-3-[3-dimethylaminopropyl]carbodiimide) and DMAP (4-dimethylaminopyridine).[149] The DMAP is a nucleophile that acts in a preventative measure to stop the unwanted formation of the unreactive *N*-acylurea, through acyl transfer, by reacting faster with the carbodiimide.[150] This method produced yields of 19, 52 and 42% for the reactions of (+)-ketopinic acid **3.1.2** with the

secondary amines morpholine, piperidine and diethylamine, respectively, Figure 92. As a result of the low yields, an alternative methodology was considered.

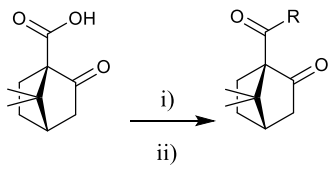

3.1.2

3.3.1: R = morpholine
3.3.2: R = piperidine
3.3.3: R = diethylamine

Figure 92: Synthesis of the amides showing the two alternative pathways, where R represents the amine. Reaction conditions: i) amine (R), EDC.HCl, DMAP, DCM; ii) amine (R), $SOCl_2$, triethylamine, DCM.

B.J. Uang and co-workers demonstrate an alternative pathway in which the acid **3.1.2** is activated as the acid chloride prior to forming the amide.[151] The acid chloride forms readily through the addition of thionyl chloride ($SOCl_2$) to **3.1.2**, prior to the addition of the respective amine and triethylamine. This procedure led to improved yields for the formation of the amides using the amines morpholine, piperidine and diethylamine, with yields of 86, 90 and 84% being observed, respectively. Several amides were successfully synthesised using the amines; morpholine, piperidine, diethylamine, isopropylamine, methylamine, propylamine and hexylamine, Figure 93.

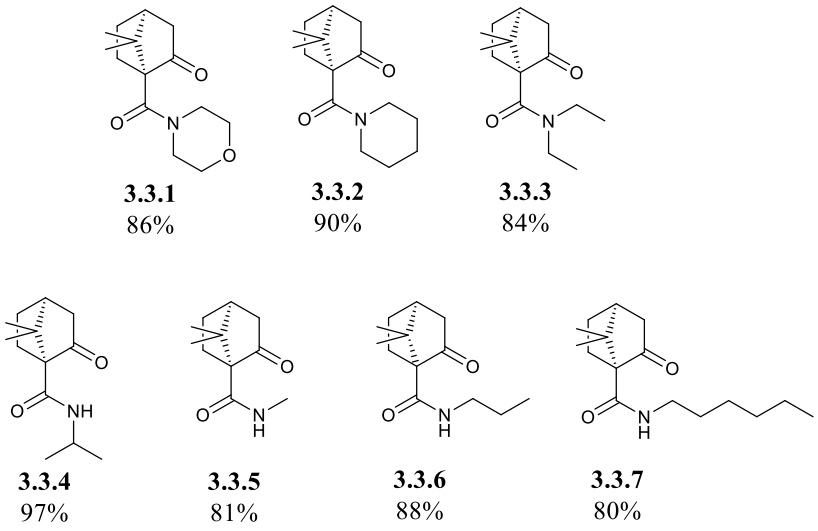

3.3.1 86%
3.3.2 90%
3.3.3 84%
3.3.4 97%
3.3.5 81%
3.3.6 88%
3.3.7 80%

Figure 93: Molecular structures and yields of the amide-derivatives of (+)-ketopinic acid **3.1.2**.

The oxidation step to obtain the final 1,2-diketone compounds proved challenging. Following traditional oxidation conditions, selenium dioxide (SeO_2) in 1,4-dioxane was employed. Using a slight excess of SeO_2 resulted in no conversion to the oxidised product **3.3.8** as perceived through ^1H NMR spectroscopy. Minimal impact on conversion was observed when the starting stoichiometry of SeO_2 was increased. Additionally changing the solvent to acetic acid, as observed with similar reactions,[152] had no impact in product conversion. It was subsequently decided to sequentially add 2 equivalents of SeO_2 to the reaction vessel every 2-3 hours, leading to the synthesis of **3.3.8** in 58% yield, after the total addition of 6 equivalents, Figure 94. The success of the reaction can be clearly observed through ^1H NMR spectroscopy with the disappearance of the doublet at δ 1.9 ppm representing the 3-CH_2 group that is oxidised to give the second ketone carbonyl group. Additionally, upon the formation of the 1,2-diketone the other signals see a change in the chemical shifts, Figure 95. A further indication is the doublet at δ 2.6 ppm of the product, with an integration of 1H (CH), representing the single proton CH at the α-carbon (C4) with respect to the new carbonyl group.

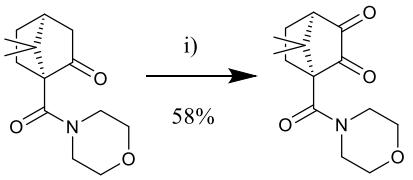

3.3.1 **3.3.8**

Figure 94: Oxidation of **3.3.1** to form **3.3.8**. Reaction conditions: i) SeO_2, AcOH.

This method did not reproduce the desired results when utilised to oxidise the other ketopinic acid-amides. The addition of excess SeO_2 had minimal impact in facilitating the oxidation reaction with these compounds, with only minor conversions to product being observed. As a consequence of the low yielding oxidation, and subsequent difficult separation of the product from the crude mixture in sufficient quantities, an alternative route was considered.

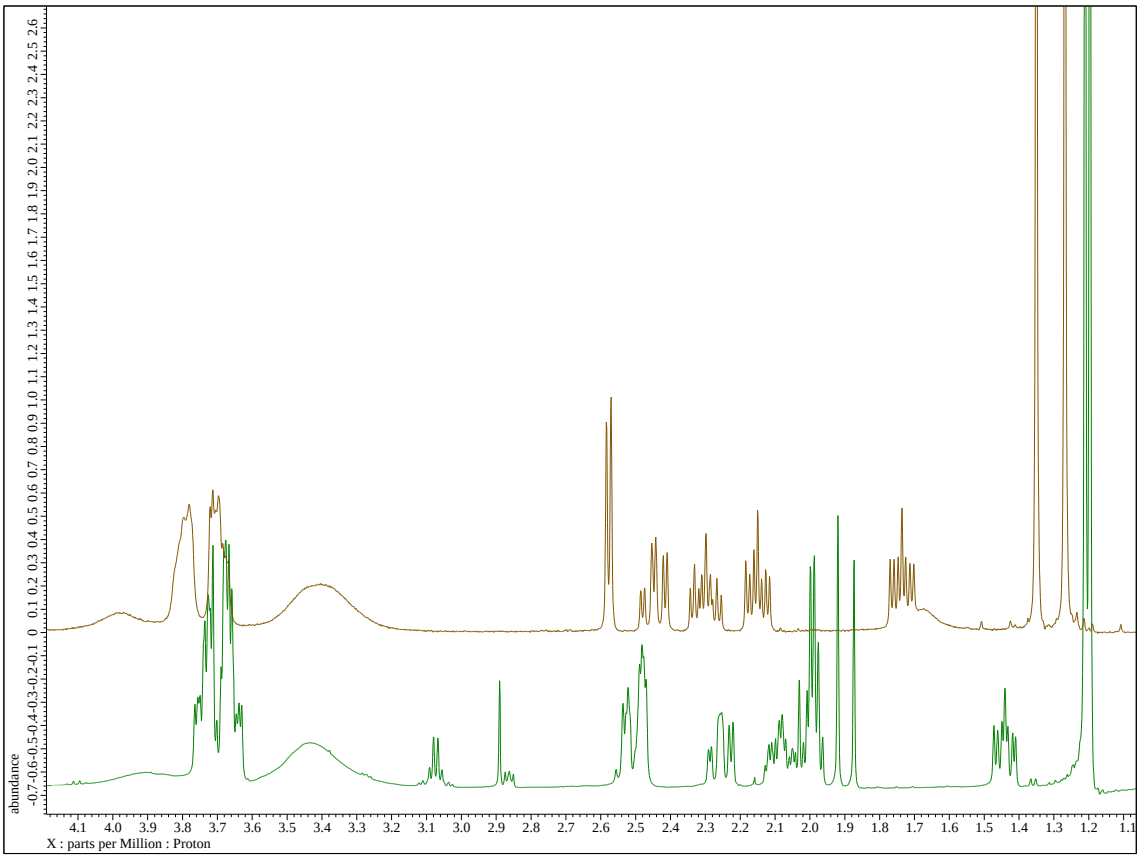

Figure 95: Overlaid ^{1}H NMR spectra showing the starting material **3.3.1** (bottom spectrum) and the product **3.3.8** (top spectrum).

Improving the overall synthetic methodology was necessary to give a reliable procedure to synthesise a variety of amides from ketopinic acid **3.1.2** regardless of the amine used, Figure 96. As a consequence, the oxidation of ketopinic acid **3.1.2** to the diketone, a known reaction completed by multiple research groups, was considered prior to the amidation reaction.[152-153] This reaction again employed SeO_2 in acetic acid, beginning with an equimolar amount of the oxidising agent and successively adding 0.2 equivalents. In comparison to the previous attempts to synthesise the final 1,2-diketones, the oxidation of ketopinic acid **3.1.2** could be achieved with a lower overall quantity of SeO_2. In addition to the reduced quantities of SeO_2 used, purification proved to be much simpler. It was found that **3.3.9** could easily be recrystallized in high purity and with reasonable yields from an ethyl acetate-hexane mixture. The ^{1}H NMR spectrum is shown in Figure 98.

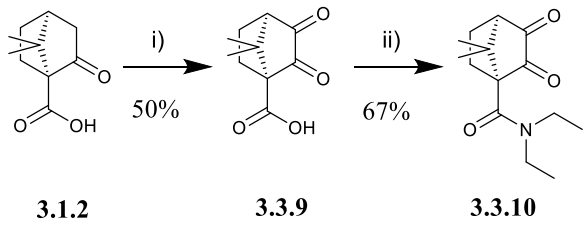

Figure 96: Alternative synthetic pathway to the final ketopinic acid-amide **3.3.10**. Reaction conditions: i) SeO_2, dioxane, ii) $SOCl_2$, triethylamine, diethylamine, DCM.

Using the oxidised ketopinic acid **3.3.9**, the amidation reaction was again performed via the intermediate acid chloride to form **3.3.10**. The final 1,2-diketones were synthesised via this more reliable route with reasonably high yields obtained, Figure 97. In some cases, purification of the final product proved more complex than previously observed when forming the amide bond. There was a notable decrease in the yields of the final pure compounds when the primary amines, methylamine, propylamine and isopropylamine were used to synthesise the 1,2-diketones **3.3.12**, **3.3.13**, and **3.1.14.**

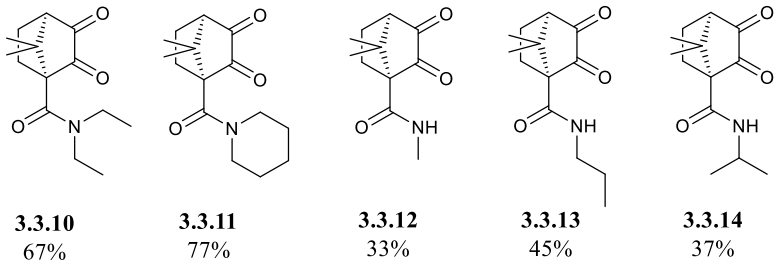

Figure 97: The molecular structure of the amido-camphor 1,2-diketones synthesised. Yields shown are for the amide forming step only.

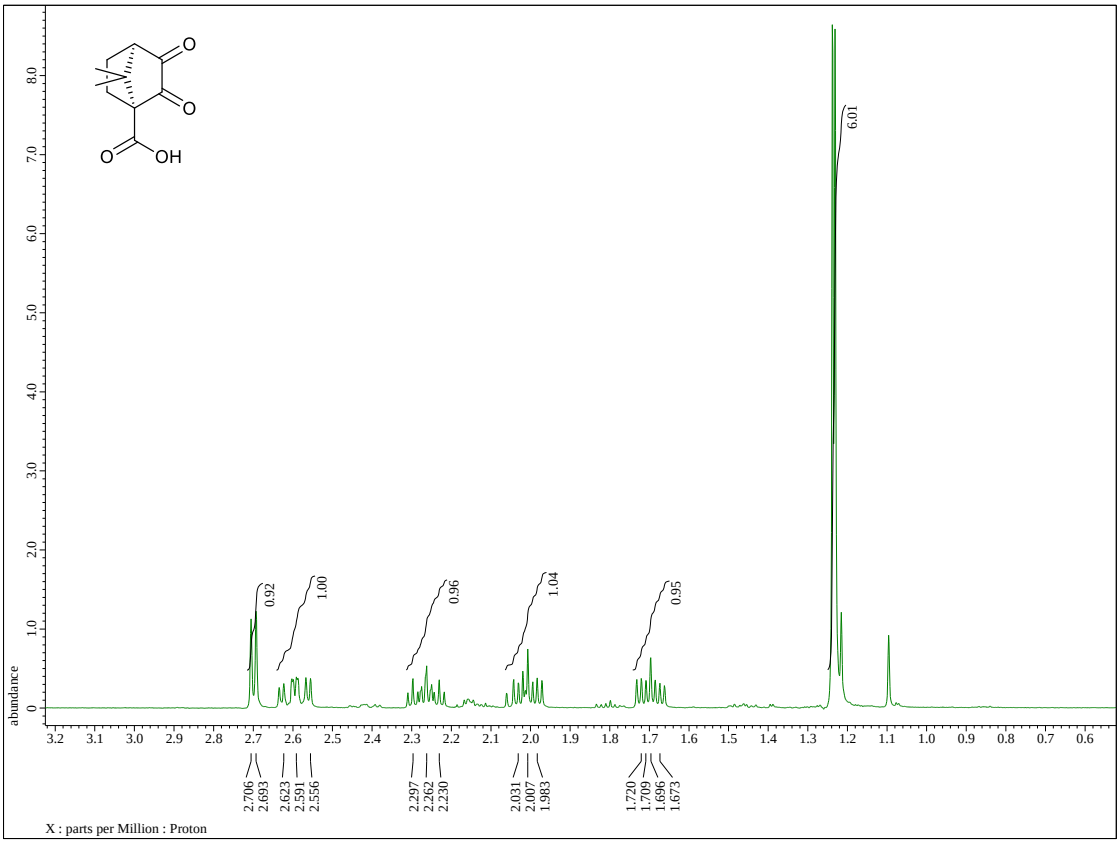

Figure 98: ^{1}H NMR spectrum of oxidised (+)-ketopinic acid **3.3.9**.

Table 13: Assignment of NMR signals for (+)-ketopinic acid **3.3.9**.

^{1}H (ppm)	Proton integration and multiplicity (Hz)	^{13}C (ppm)	Assignment
2.72	1H, d, *J* = 5.04	58.1	CH
2.61	1H, td, *J* = 4.58	26.7	CH_{exo}
2.29	1H, tt, *J* = 5.04	21.5	CH_{exo}
2.06 – 1.99	1H, m	26.7	CH_{endo}
1.75 – 1.68	1H, m	21.5	CH_{endo}
1.25	3H, s	22.2	CH_3
1.25	3H, s	18.5	CH_3

Due to the toxicity of SeO_2 and the difficulty arising in ensuring the complete removal of the selenium by-products from the diketones, an alternative method was investigated for the oxidation reaction that utilises bromine, Figure 99. The first step in the reaction is the bromination of ketopinic acid **3.1.2** itself to form the *endo*-3-bromo-ketopinc acid **3.3.15**.[154] This was used *in situ* to form **3.3.9** via air-oxidation using sodium iodide as a catalyst in DMSO, as following the procedure demonstrated by Miyakoshi and co-workers in oxidising 3-bromocamphor to give camphorquinone.[155] The resulting low yield obtained in the synthesis of **3.3.9** from ketopinic

acid **3.1.2** of 20% was thought to result from the method used to introduce air into the system. We used a water-pump to introduce air into the reaction mixture, which may have resulted in the ineffective distribution of oxygen into the reaction mixture. Alternative procedures in the final oxidation step can use catalysts such as cobalt(II) acetate[128] or tetrabutylammonium iodide to achieve the same oxidation as discussed by Miyakoshi and co-workers.[156] Going forward it was decided to continue to carry out the oxidation reaction using SeO_2 in order to obtain the required 1,2-diketones, which despite being the more toxic reagent, offered the highest yields.

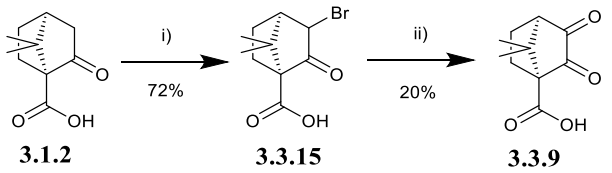

Figure 99: Alternative oxidation protocol to diketone **3.3.9**. Reagents and conditions; i) Bromine, AcOH, ii) Sodium iodide, DMSO, air.

As discussed briefly in section 3.1, the preparation of ketopinic acid **3.1.2** from the cheaper starting material (+)-camphor-10-sulfonyl chloride **3.1.3** was also considered, Figure 100. This was deemed necessary for cost considerations should a scaled-up synthesis of any of the ligands need to be carried out, both in the present work as well as in future industrial use. Current procedures to synthesise ketopinic acid **3.1.2**, directly from the (+)-camphor **3.1.1** starting material, are cumbersome.[145a] The final step, involving oxidation of camphorsulfonyl chloride **3.1.3** with potassium permanganate, has previously yielded ketopinic acid **3.1.2** in yields of 38-43%.[157] Due to the low cost of (+)-camphor sulfonyl chloride **3.1.3**, this final oxidation step will be considered as an alternative method to purchasing the much more expensive ketopinic acid **3.1.2**. Following a literature procedure,[130] first established in 1965, the successful synthesis of ketopinic acid **3.1.2** using potassium permanganate was achieved in yields of 35%. This methodology can be applied in the future scaled-up synthesis of the final target ligands that may have future industrial application.

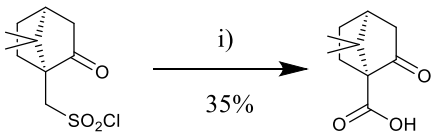

3.1.3 3.1.2

Figure 100: Synthesis of ketopinic acid **3.1.2**. Reaction conditions: i) $KMnO_4$, Na_2CO_3, H_2O

The final 1,2-diketones successfully synthesised are shown in Figure 97 (page 106) with yields ranging from 33 – 77% dependant on the amine. These will be used in the condensation reactions with the relevant bis-amidrazones to form the final bis-1,2,4-triazine ligands containing the 1,2,4-triazine moiety. Efforts to realise analogues of the $CyMe_4$-BTP **1.30**, $CyMe_4$-BTBP **1.09** and $CyMe_4$-BTPhen **1.17** will be made to directly compare their solubility and rates of extraction results.

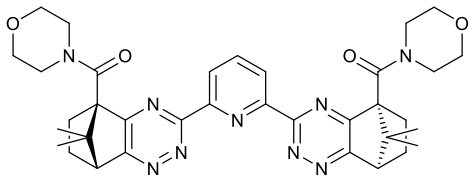

L19

Figure 101: Structure of **L19**.

Synthesis of the final ligands was achieved through a condensation reaction between the novel diketones and the appropriate bis-amidrazone. An initial experiment using **3.3.8** and pyridine-2,6-dicarboxamidrazone **3.2.2** was carried out through refluxing in ethanol and resulted in minimal conversion to the final ligand **L19**, Figure 101. As a consequence of the steric hindrance exhibited by the amide group on the C2-carbonyl group of **3.3.8**, Figure 102, it was proposed that the reaction may require a higher boiling point solvent in order to improve conversion to the product. The reaction was thus repeated in 1,4-dioxane in attempts to encourage the reaction to proceed. The ^{1}H NMR spectrum of the crude product exhibited an unusual mass of signals between δ 3.5 – 5.5 ppm that did not appear when the reaction was completed in ethanol. It is proposed that this may be a consequence of degradation of the solvent or impurities present within the solvent.

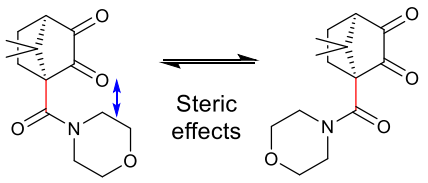

Figure 102: Representative conformers of a ketopinic acid-derived diketone **3.3.8**, dependent on the bond rotation (red) and the resulting steric hindrance (blue) caused by the bulky amide group.

In an effort to confirm whether the aforementioned signals are a consequence of the reaction or due to of solvent degradation or impurities, two parallel condensation reactions were completed in ethanol and 1,4-dioxane. It was decided to investigate the condensation reaction between pyridine-2,6-bisamidrazone **3.2.2** and (1*S*)-(+)camphorquinone **2.2.8** to form camphor-BTP **L30** following the previously reported procedure, with the only variable being the solvent used, Figure 103.[80] The reaction between the two reagents was chosen as a result of the chemical similarity to the reaction under consideration in this chapter, as well as being a known reaction in literature. Interestingly, in ethanol the reaction proceeds almost to completion after 3 days at reflux as observed by the ^{1}H NMR spectroscopy. In 1,4-dioxane the same phenomena as seen previously was observed, Figure 104. There is potential that the bottle of 1,4-dioxane utilised may have degraded or contained impurities, but at the time of carrying out the reaction, this was not checked.

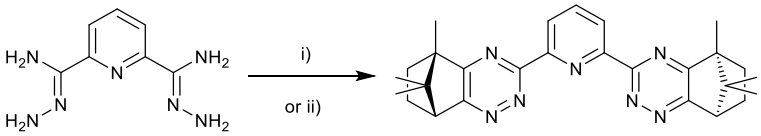

Figure 103: Reaction scheme for the formation of camphor-BTP **L30**. Reaction conditions: (i) (1*S*)-(+)-camphorquinone **2.2.8**, ethanol, (ii) (1*S*)-(+)-camphorquinone **2.2.8**, 1,4-dioxane.

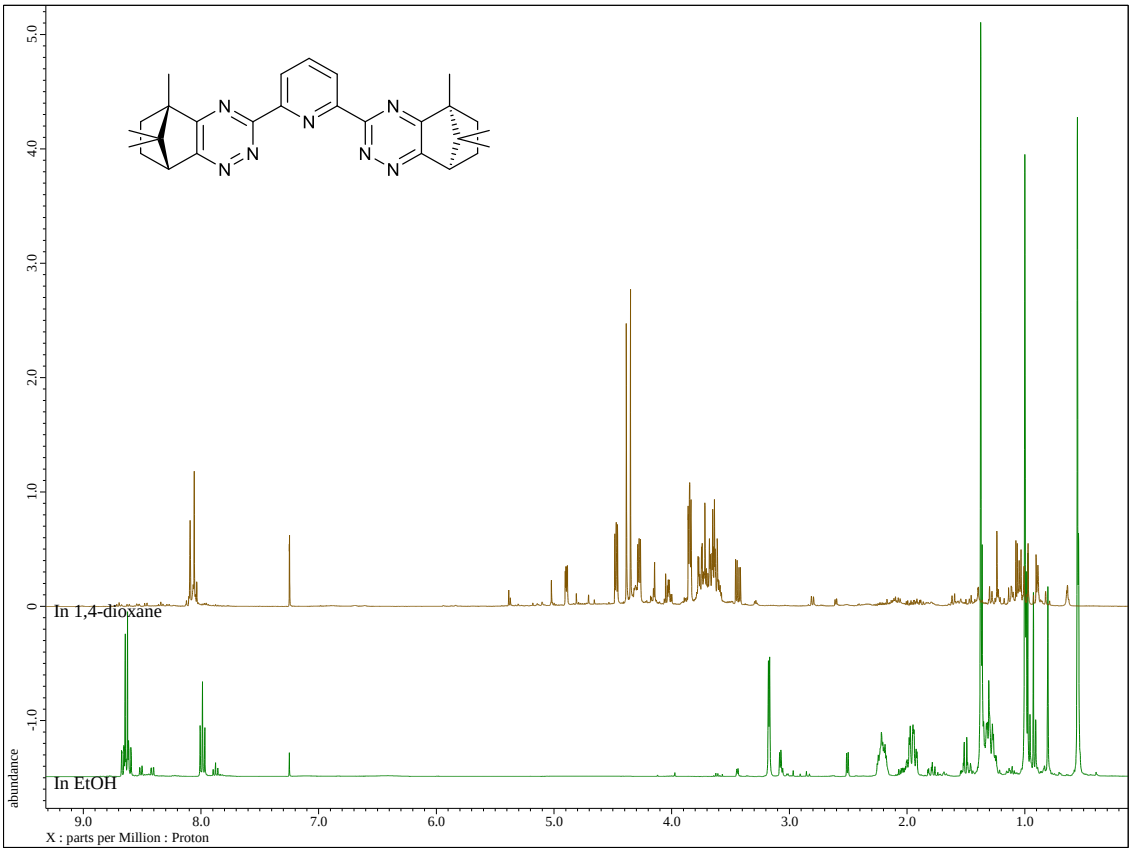

Figure 104: Overlaid ^{1}H NMR spectra of crude products from the condensation reaction between **3.2.2** and **2.2.8** to form **L30** in ethanol (bottom spectrum) and 1,4-dioxane (top spectrum).

As 1,4-dioxane appears to be unsuitable for the reaction and ethanol gives limited conversion to the product when using the derivatised camphor-diketones, it was decided to use acidic conditions by utilising acetic acid as the solvent. As a condensation reaction is, in simplest terms, a nucleophilic addition reaction, it is anticipated the use of acetic acid may aid the reaction by protonation of the carbonyl group oxygen atom, to encourage attack on the carbonyl group by the nucleophilic amino groups of the bis-amidrazones. This is in addition to its increased boiling point in comparison with ethanol, both of which should drive the condensation reactions to completion.

The successful synthesis of a range of novel ligands was achieved using acetic acid as the solvent, with variable yields being obtained dependent upon on the starting 1,2-diketone used, Figure 105. The successful observation of the products was confirmed through full characterisation of the ligands (^{1}H NMR, ^{13}C NMR and HRMS).

The use of the diketone **3.3.8** resulted in the successful formation of the novel BTP **L19**, BTBP **L20** and BTPhen **L21** ligands, Figure 106. Similarly the diketone **3.3.10** was used successfully in the preparation of the BTP **L22**, BTBP **L23** and BTPhen **L24** ligands. It was notable that the yields observed in this case were significantly lower than those observed when utilising the diketone **3.3.8**.

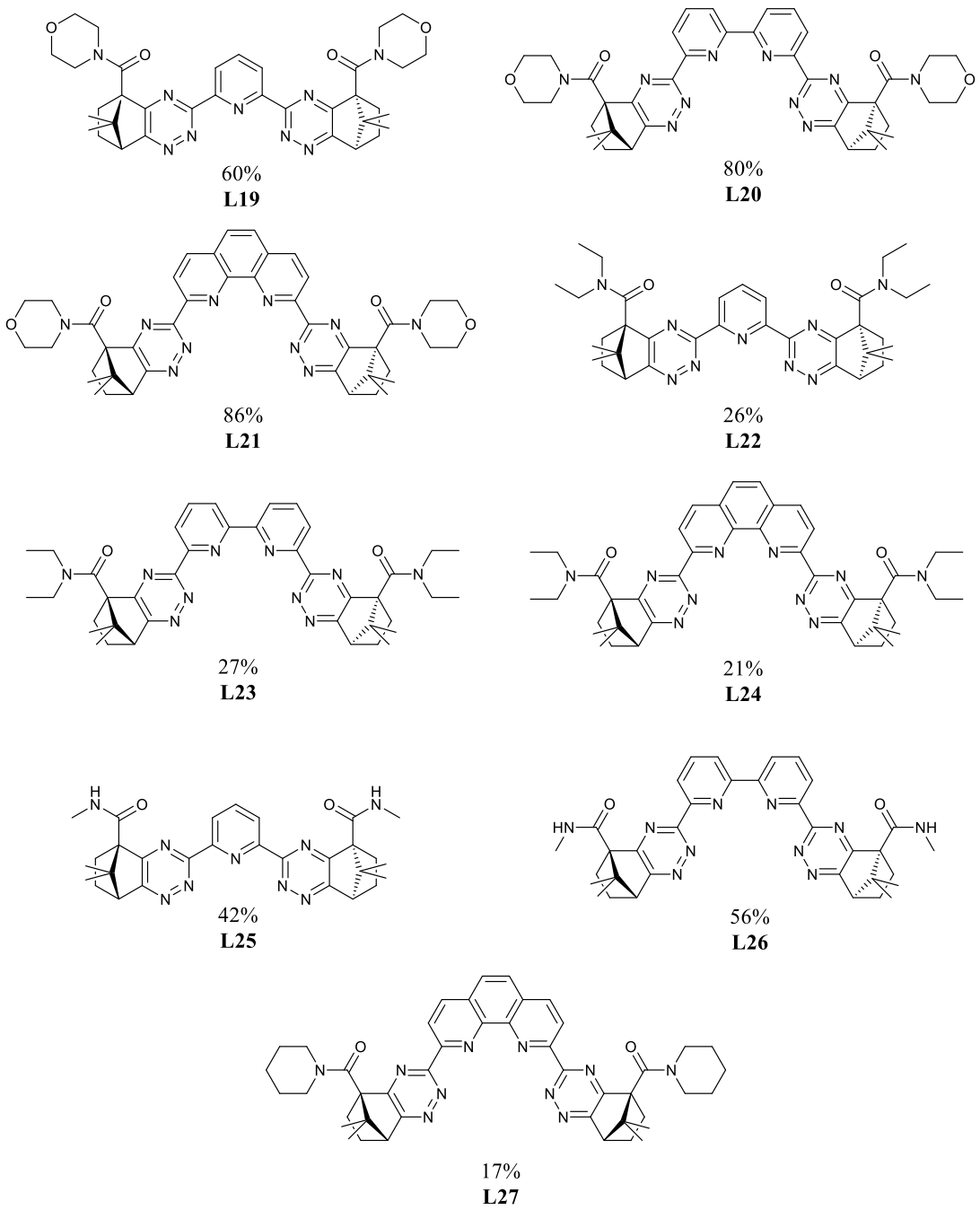

Figure 105: Structures of successfully synthesised ligands. Yields are for the condensation reaction step alone.

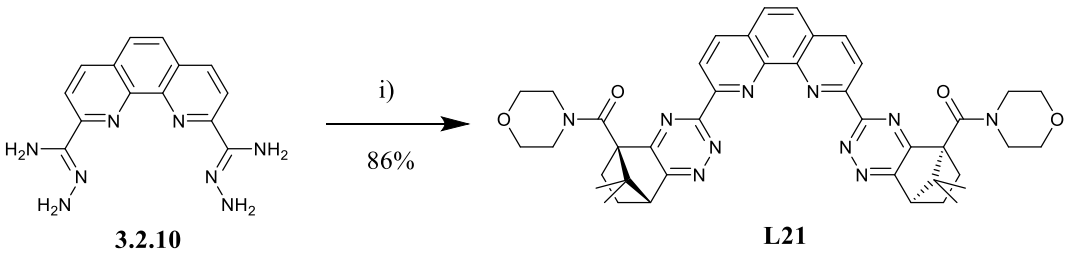

Figure 106: Synthesis of morpholine-derived ligand **L21**. Reaction conditions: i) morpholine-derived diketone **3.3.8**, acetic acid, reflux.

The use of the diketone **3.3.11** resulted in only the BTPhen **L27** ligand being isolated with the required purity for extraction testing. The purification of the BTP **L31** and BTBP **L32** was unsuccessful through either recrystallization or column chromatography. The use of the diketone **3.3.12** resulted in the isolation of the BTP **L25** and BTBP **L26** successfully, Figure 107.

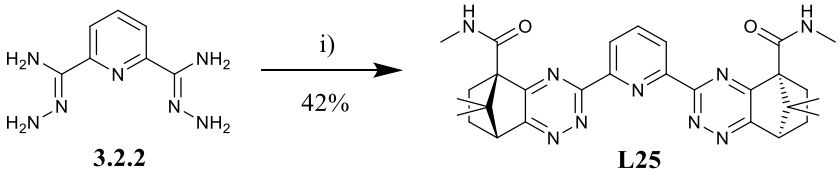

Figure 107: Synthesis of methylamine-derived ligand **L25**. Reaction conditions: i) methylamine-derived diketone **3.3.12**, acetic acid, reflux.

Unfortunately, the ligands derived from diketones **3.3.13** and **3.3.14** could not be obtained as pure samples. Those proposed ligands that were unable to be obtained are shown in Figure 108.

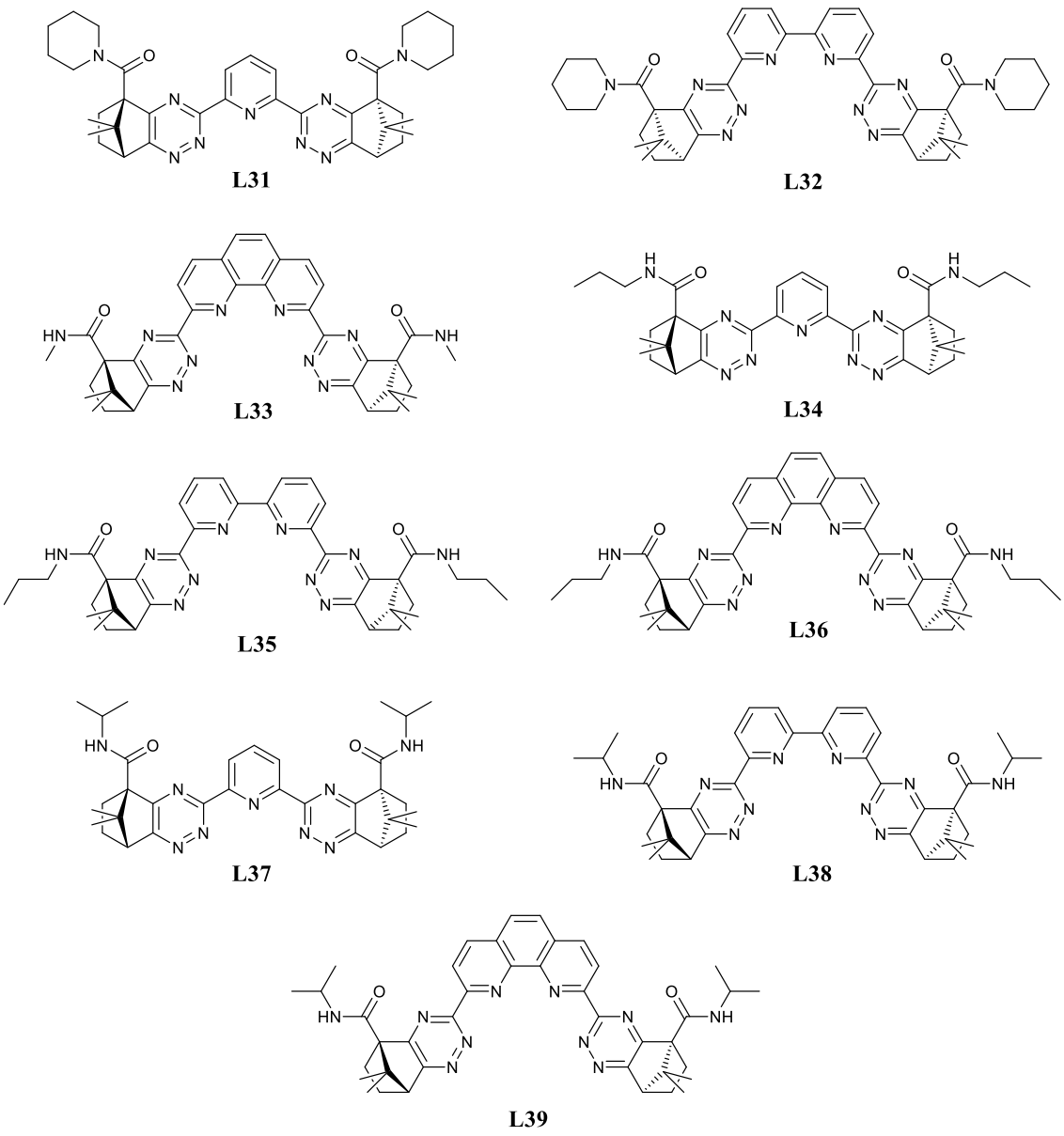

Figure 108: Molecular structures of proposed ligands unsuccessfully synthesised using the amide-derived ketopinic acid compounds.

In order to draw effective comparisons between the extraction properties of these novel ligands and those of the ligands derived from camphorquinone **2.2.8** itself, such as camphor-BTP **1.31**, it was decided to also synthesise and screen the analogues of the novel BTBP and BTPhen ligands discussed in these chapters; camphor-BTBP **L28** and camphor-BTPhen **L29**. The effect of the amide group on the solubilities, extraction properties and extraction kinetics can be discovered through the direct comparison to the 'parent' ligands derived from an enantiomerically pure sample of camphorquinone **2.2.8**. The synthesis of camphor-BTBP **L28** and camphor-BTPhen

L29 was achieved by a condensation reaction between the respective bis-amidrazone and (1*S*)-(+)-camphorquinone **2.2.8** in refluxing acetic acid, Figure 109 and Figure 110. The camphor-BTBP **L28** and camphor-BTPhen **L29** were obtained in 53 and 59% yields, respectively, which is similar to the yield obtained for the camphor-BTP ligand **1.31** (56%).

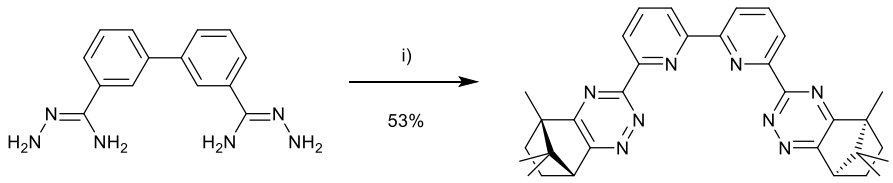

Figure 109: Reaction scheme for the formation of camphor-BTBP **L28**. Reaction conditions: (i) (1*S*)-(+)-camphorquinone **2.2.8**, AcOH, reflux.

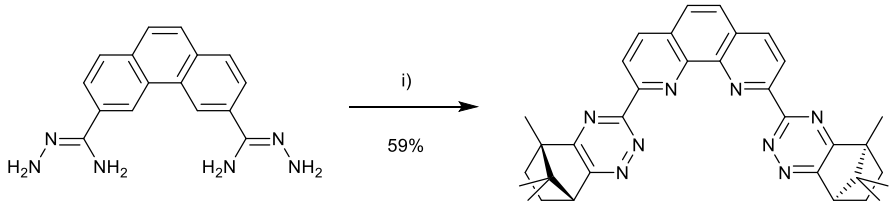

Figure 110: Reaction scheme for the formation of camphor-BTPhen **L29**. Reaction conditions: (i) (1*S*)-(+)-camphorquinone **2.2.8**, AcOH, reflux.

The new ligands based upon the BTP, BTBP and BTPhens synthesised above, are anticipated to exhibit faster extraction kinetics than the benchmark ligand $CyMe_4$-BTBP **1.09** and camphor-derived ligands **1.31**, **L28** and **L29** through the addition of the amide functional group. The addition of the HBD and HBA amide functionality should enable increased hydrogen bonding with the water molecules at the aqueous/organic interface, hence influencing their extraction kinetics.

3.4. Calculated Ligand Parameters

For each of the ligands synthesised in section 3.3, their ligand parameters have been calculated to enable comparisons between theoretical and experimental data in line with the project objectives. Using the experimental data obtained for solubility and extraction kinetics for a given ligand, which will be compared to the theoretical data, the potential for using the proposed ligand design

guidelines can be established. The theoretical log *P* values of the ligands were obtained through the ACD I-lab software. The calculated properties are shown in Table 14.

Based upon the theoretical values, specifically the Fsp^3 and log *P* values obtained for the methylamine-derived ligand **L25** and **L26**, these ligands would be expected to have poor lipophilicity and hence low solubility within the 1-octanol diluent. In comparison, those ligands functionalised with diethylamine (**L22**, **L23** and **L24**) have the greatest calculated log *P* and Fsp^3 values suggesting they will observe the highest solubility. Those ligands functionalised with piperidine (**L27**) should be expected to show similar solubilities as the diethylamine based upon the calculated values.

There is a contradiction in the log *P* value and Fsp^3 obtained for the morpholine-derived ligands **L19**, **L20** and **L21**, Table 14. The log *P* values suggest a low lipophilicity and hence poor solubility in 1-octanol but the Fsp^3 values, if it is established to be a good indication of ligand solubility, suggests the opposite. The addition of additional HBA atoms in the amide functionality may impact the solubility outside of what the data can predict. Directly comparing **L21** and **L27** will indicate the effect of having two HBA oxygen atoms, from the morpholine rings, can have upon solubility and the subsequent extraction ability.

Across all the ligands there is a general trend in increasing log *P* values along the series BTPs < BTBPs < BTPhens, with BTPhens having the highest calculated log *P* values. This trend is reversed for the Fsp^3 values in which there is a decrease in this value along the series BTPs > BTBPs > BTPhens. This is to be expected based upon the increasing aromaticity as you add an additional pyridine ring in going from a BTP to a BTBP and as you add an additional phenyl ring in going from a BTBP to a BTPhen. Based upon the Fsp^3 values, it is expected that the BTPs **L19** and **L22** should have the highest solubilities.

Table 14: Table showing calculated Log *P* and Fsp^3 parameters alongside the HBD and HBA values for all novel ligands synthesised. Calculated values of log *P* were obtained using the ACD ILabs online software.

Ligand	Ligand Number	Log *P*	Fsp^3	HBD	HBA
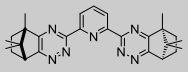	**1.31**	3.69	0.59	0	7
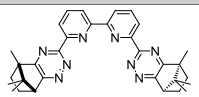	**L28**	4.59	0.50	0	8
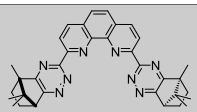	**L29**	5.33	0.47	0	8
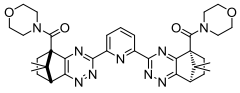	**L19**	1.46	0.63	0	13
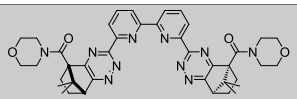	**L20**	2.24	0.55	0	14
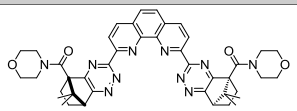	**L21**	2.86	0.52	0	14
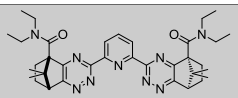	**L22**	3.20	0.63	0	11
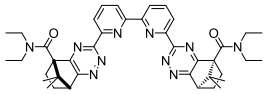	**L23**	3.99	0.55	0	12
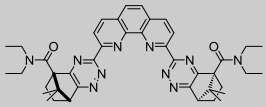	**L24**	4.67	0.52	0	12
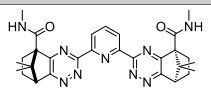	**L25**	1.23	0.55	2	11
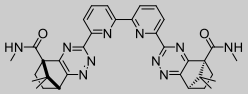	**L26**	2.06	0.47	2	12
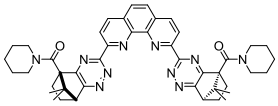	**L27**	4.62	0.52	0	12

In the next two sections the solubility and extraction results will be discussed for the ligands synthesised in this chapter. Upon obtaining these results, they will be compared back to the theoretical results calculated below in Table 14.

3.5. Solubility Studies

The solubility of the ligands were measured in 1-octanol as outlined in Chapter 6. By changing the external groups adjacent to the 1,2,4-triazine rings, the influence on the solubilities can be determined. These results will then be compared to those of the camphor-BTP **1.31** and the synthesised 'parent' camphor-BTBP **L28** and camphor-BTPhen **L29** ligands. Table 15 shows the novel terdentate ligands synthesised in this chapter alongside the calculated Fsp^3 values and the measured solubilities. The applicability of the Fsp^3 and log *P* values in predicting the solubility of the ligands will be considered based upon the experimental results shown. Ultimately these results will be compared to the theoretical data to determine if a correlation exists between the two, and hence whether the proposed ligand design approach can be validated as a means to predict ligand solubility more generally.

There is a general trend, Figure 111, of increasing solubility in 1-octanol as the calculated Fsp^3 increases for each ligand. The lowest measured solubility was for **L26**, which also has the lowest Fsp^3 value. This is an expected measurement based upon the ligand structure, which contains only an addition CH_3 group as part of the methylamine functionality. The ligand **L22** observes the greatest solubility in 1-octanol, correlating to its high Fsp^3 value. In the case of the outlier, in which an Fsp^3 value above 0.6 correlates to a lower solubility, is representative of **L19**. This may indicate the addition of the morpholine group negatively impact the ligands solubility in 1-octanol when compared to **L22**. When compared to the camphor-BTP **1.31**, there is a decrease in solubility, suggesting that the maximum solubility of the novel ligands may not have been found. Comparison of the functionalised BTBPs, **L20** and **L23**, with the 'parent' camphor-BTBP **L28** shows an increased solubility with amide functionalisation. The methylamine-derived ligand **L26** opposes this trend, with a decreased solubility when compared to camphor-BTBP **L28**, however, this decreased solubility correlates to a lower Fsp^3 value in comparison to **L28**. This result is

replicated when comparing the 'parent' camphor-BTPhen **L29** to the functionalised BTPhens; **L21**, **L24** and **L27**.

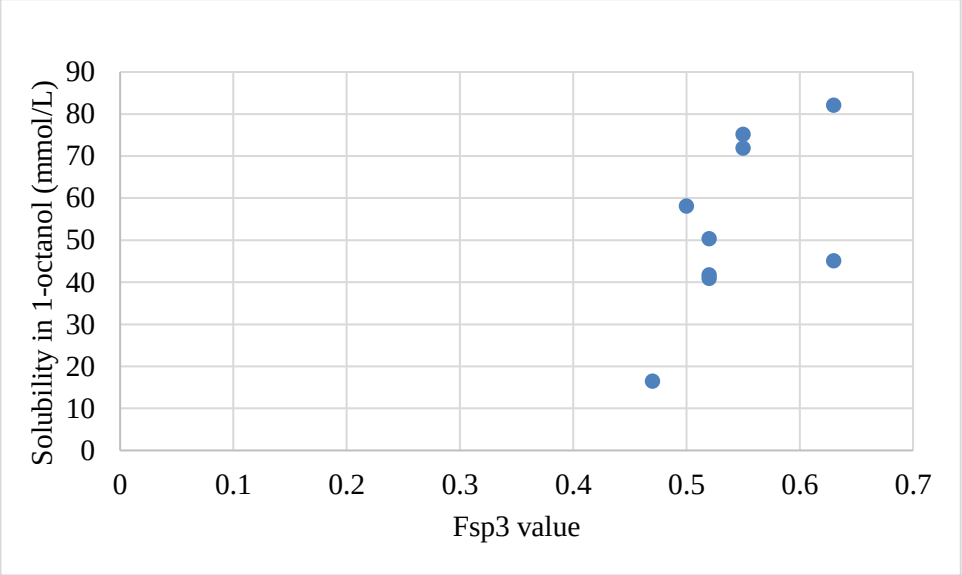

Figure 111: Graph showing the correlation between a ligands calculated Fsp^3 value and its measured solubility in 1-octanol (mmol/L). Each data point represents a ligand, see Table 15 for further information.

In most cases there is an improved solubility when compared to the camphor-derived parent ligands upon introducing the amide functionality, with the exception of the methylamine-derived ligand, **L26**. In the following section the novel BTP, BTBP and BTPhen ligands will be screened for their extraction ability to confirm whether the introduction of the amide functional group has a positive impact on the extraction of An(III) over the Ln(III) when compared to the 'parent' camphor-derived ligands.

Table 15: The respective Fsp^3 value and measured solubility for each novel camphor-derived ligand.

Number	Structures	Solubility mmol/L in 1-octanol	Fsp^3 value
1.31	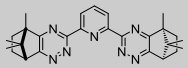	200[82]	0.59
L28	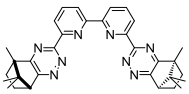	58.1	0.50
L29	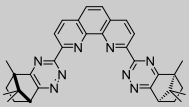	18.6[102]	0.47
L19	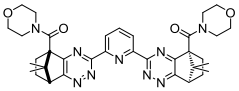	45.1	0.63
L20	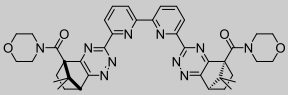	71.4	0.55
L21	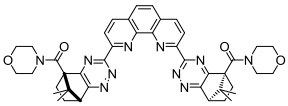	41.8	0.52
L22	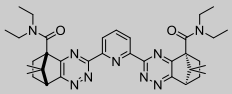	82.1	0.63
L23	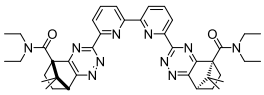	75.2	0.55
L24	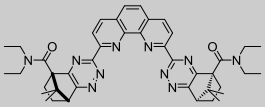	50.4	0.52
L25	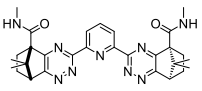	-	0.55
L26	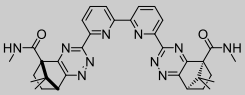	16.5	0.47
L27	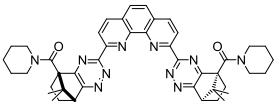	40.9	0.52

3.6. Extraction Studies

Extraction studies with the novel ligands were carried out to determine the ability of the ligands to selectively extract the actinides (An(III)) over the lanthandies (Ln(III)), see Chapter 6 for a detailed description. The key focus of this thesis is the separation of, in terms of these radioisotopes, Am(III) from Eu(III). Therefore the separation of Am(III) from Cm(III) will only be discussed if there is a notable separation achieved by one of the ligands, i.e. $SF_{Am/Cm}$ of 1.5 and above. Extraction experiments were completed using 1-octanol as the organic diluent unless otherwise specified.

The extraction studies of the 'parent' camphor-BTBP **L28** and camphor-BTPhen **L29** ligands were also completed for comparison with the extraction results for the amide functionalisaed ligands discussed in this Chapter. The camphor-BTP **1.31** has been investigated previously for its extraction capabilities as discussed in section 1.5.2 and 3.1. When comparing the data obtained for the novel BTP ligands discussed in this chapter, considerations will be taken on their different concentrations. The camphor-BTP **1.31** was tested at 60 mmol/L and 50 mmol/L in kerosene/1-octanol and 1-octanol alone, respectively.[82] The novel ligands were all tested at a concentration of 10 mmol/L in each diluent used unless specified. The camphor-BTPhen **L29**, although the synthesis and solubility measurements have previously been described,[102] its extraction properties have yet to be reported.

Both the 'parent' ligands camphor-BTBP **L28** and camphor-BTPhen **L29** observed significant precipitation at all HNO_3 concentrations after 1 hour of contact time with the HNO_3 phase, Figure 112. The top phase is the respective ligand in 1-octanol with the bottom phase being HNO_3, containing the radioisotopes. This is most likely a consequence of ligand protonation and precipitation of the insoluble protonated ligands, as observed previously with the camphor-BTP ligand **1.31**. As the radioisotope mass balances are indicative of the concentration of these across both the aqueous and organic phase, should the precipitate be a ligand complex we would observe a decrease in the radioisotope mass balances within the sample. However, this was not observed after the screening test for each ligand; **L28** and **L29**.

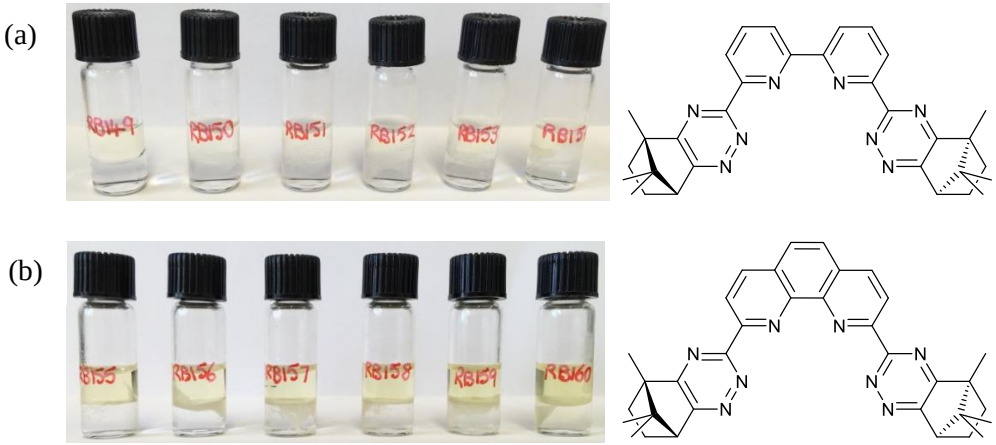

Figure 112: Photographs of the sample tubes after the first screening test with increasing [HNO_3] from left to right with (a) camphor-BTBP **L28**; (b) camphor-BTPhen **L29**. Molecular structures are shown alongside the respective photographs.

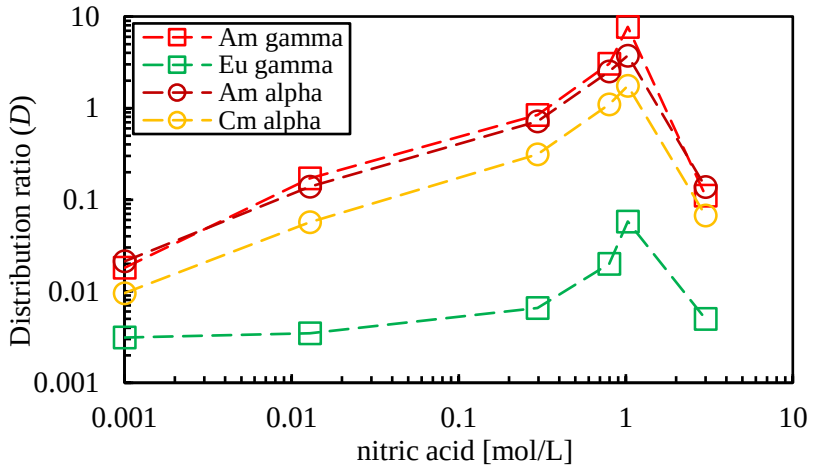

Figure 113: Distribution ratios for extraction of ^{152}Eu, ^{241}Am, ^{244}Cm by **L28** measured by α- and γ-spectroscopy as a function of the nitric acid concentration of the aqueous phase (1 hr, 22 °C at 2,200 rpm). Organic phase: 10 mM **L28** in 1-octanol.

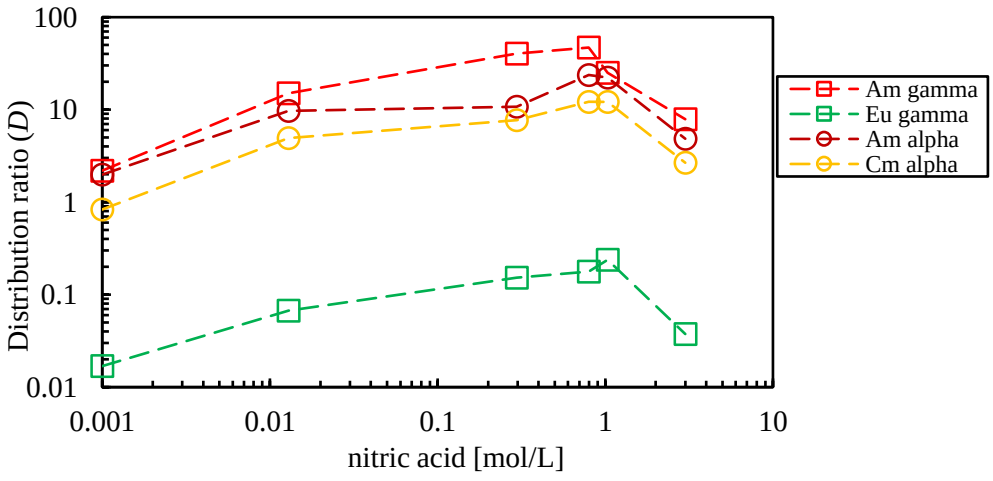

Figure 114: Distribution ratios for extraction of ^{152}Eu, ^{241}Am, ^{244}Cm by **L29** measured by α- and γ-spectroscopy as a function of the nitric acid concentration of the aqueous phase (1 hr, 22 °C at 2,200 rpm). Organic phase: 10 mM **L29** in 1-octanol.

The camphor-BTBP ligand **L28** had increasing distribution ratios for all radioisotopes up until a concentration of 1.0 M HNO_3, after which they decreases again, Figure 113. The separation factor, $SF_{Am/Eu}$, is over 120 between 0.2 and 1.0 M HNO_3, decreasing to 22 at 3.0 M HNO_3 as a consequence of the fall in distribution ratios. In comparison, for the camphor-BTPhen ligand **L29** the distribution ratios for Am(III) and Cm(III) are significantly higher, indicating more effective extraction of these isotopes into the organic phase by the BTPhen ligand **L29**, Figure 114. The subsequent separation factors are in the region of 200 – 250 at 0.1 – 0.8 M HNO_3, greater than those for the BTBP **L28**. These extraction results mirror those of the equivalent $CyMe_4$-ligands, section 1.5, where it was found that the *D* values of all metal ions (Am(III), Cm(III) and Eu(III)) for $CyMe_4$-BTPhen **1.17** were approximately two orders of magnitude higher than those of $CyMe_4$-BTBP **1.09**.[95] After 1 M HNO_3, as observed with the BTBP **L28**, there is a drop in the distribution ratios, which is most likely due to competing ligand protonation at high HNO_3 concentrations. What is noticeable with this ligand is the deviance in the results obtained by α- and γ-spectroscopy for Am(III). This is most likely caused by the increased level of precipitate observed after screening this ligand, which can have significant impacts on the α-measurements. Solid deposits will prevent the formation of a uniform layer on the alpha disc during analytical sample preparation, ensuing some of the alpha particles are unable to pass through the material to reach the detector. Within the series of camphor-BTP **1.31**, camphor-BTBP **L28** and camphor-BTPhen **L29** ligands there is an increased level of precipitate observed when moving from the BTP **1.31** to the BTPhen **L29** when in contact with the HNO_3 phase, which correlates to the decrease in Fsp^3 values.

It is difficult to directly compare the camphor-family of ligands to the corresponding $CyMe_4$-ligands in terms of their extraction ability, due to the tendency of the former ligands to form precipitates. A phase modifier or co-diluent could be added to the organic phase to improve their solubility and reduce precipitate formation. However, the observed precipitate formation would prevent the ligands being considered for future industrial use as a consequence of the safety implications that would result from this effect. Going forward, a discussion of the derivatised ligands will be made.

The novel ligand **L19** was tested under the standard conditions in 1-octanol as above, see Chapter 6, and observed a gradual increase in the *D* values for Am(III), Cm(III) and Eu(III) as the HNO_3 concentration increases, Figure 116. This trend has been observed previously with other bis-1,2,4-triazine ligands, and is to be expected, as metal ion extraction (as nitrate salts) becomes more thermodynamically favoured as the nitric acid (and hence nitrate ion) concentration increases. At a concentration of 0.30 M HNO_3 and above, the *D* values begin to decrease again. This is probably due to competing ligand protonation as the HNO_3 concentration increases. The maximum *D* ratios for Am(III) and Eu(III) are 3.41 and 0.65, respectively at 0.3 M HNO_3, with a $SF_{Am/Eu}$ of 5.22. At lower concentrations the separation factor is at approximately 30, but this is drastically lower at higher HNO_3 concentrations, at approximately 3 above 0.7 M HNO_3. The process conditions the ligands have to operate in a future SANEX process are between 3-6 M HNO_3, suggesting this ligand would be an unsuitable choice for the future reprocessing industry.

Upon completion of the extraction test with **L19** there was a noticeable colour leaching from the organic into the aqueous phase upon contact with 1.0 M HNO_3, Figure 115. It is assumed that this may reflect the suspected dissolution of the protonated ligand into the aqueous phase at higher acidities. If the ligand protonation is outcompeting metal complexation, there would be less ligand available to complex and extract in Am(III) leading to a reduction in the distribution ratios. As precipitation was only observed after contact with the HNO_3 the protonated ligand is the likely cause.

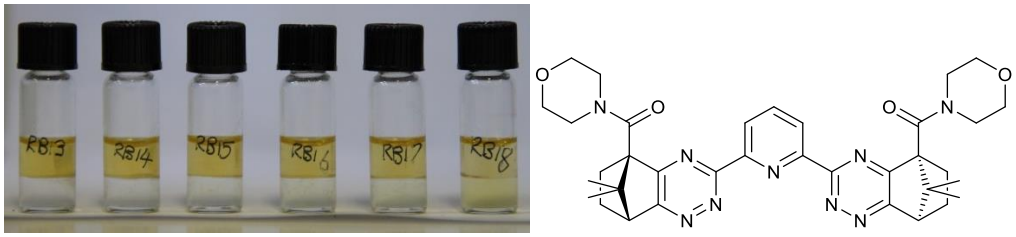

Figure 115: (a) Photograph of the sample tubes after the first screening test using **L19** with increasing [HNO_3] from left to right; (b) molecular structure of **L19**.

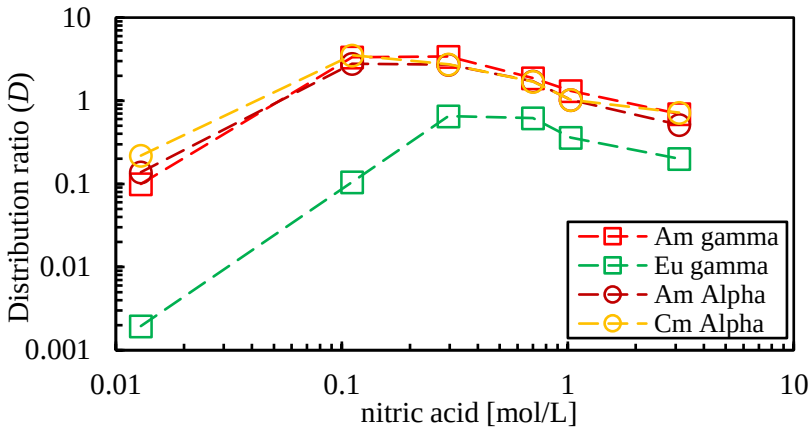

Figure 116: Distribution ratios for extraction of ^{152}Eu, ^{241}Am, ^{244}Cm by **L19** measured by α- and γ-spectroscopy as a function of the nitric acid concentration of the aqueous phase (1 hr, 22 °C at 2,200 rpm). Organic phase: 10 mM **L19** in 1-octanol.

Following the work by Geist and co-workers on camphor-BTP **1.31** it was decided to complete the extraction with ligand **L19** in a TPH/1-octanol (7:3 vol. ratio) mixture to investigate the impact of this solvent system. As discussed in the introduction, camphor-BTP **1.31** saw higher distribution ratios in TPH/1-octanol in contrast to 1-octanol alone despite observing a poorer solubility in this diluent. The complete dissolution of ligand **L19** at a concentration of 0.1 M HNO_3 was achieved in this diluent mixture. However, upon instant contact with the HNO_3 phase there was precipitation observed at HNO_3 concentrations above 1 M. After completion of the screening test, there was a significant brown precipitate observed at HNO_3 concentrations up to and including 1 M HNO_3, Figure 117. At a 3.0 M HNO_3 concentration, where no precipitation was observed, there was significant discolouration of the aqueous phase, as perceived in the 1-octanol screening test. This indicates that the precipitate has dissolved in the aqueous phase at higher acidities. The obtained extraction data shows low *D* ratios for the radioisotopes across all concentrations, Figure 118. There is a 10-fold decrease in the *D* ratios in comparison to the same ligand when the diluent considered was 1-octanol, in contrast to the reversed observation by Geist and co-workers. This is undoubtedly correlated to the decreased solubility of the ligand in this diluent mixture.

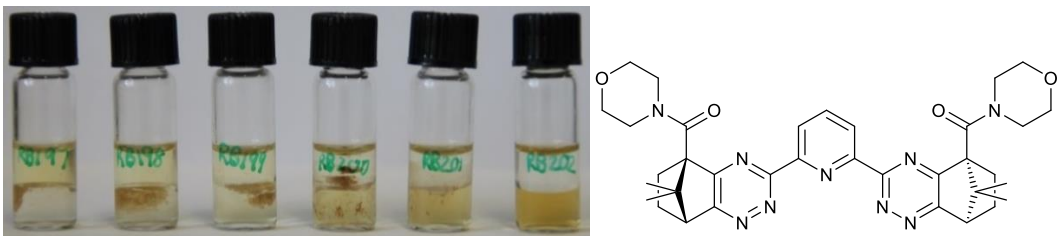

Figure 117: a) Photographs of the sample tubes after the first screening test using **L19** after phase mixing, increasing [HNO_3] from left to right; (b) molecular structure of **L19**.

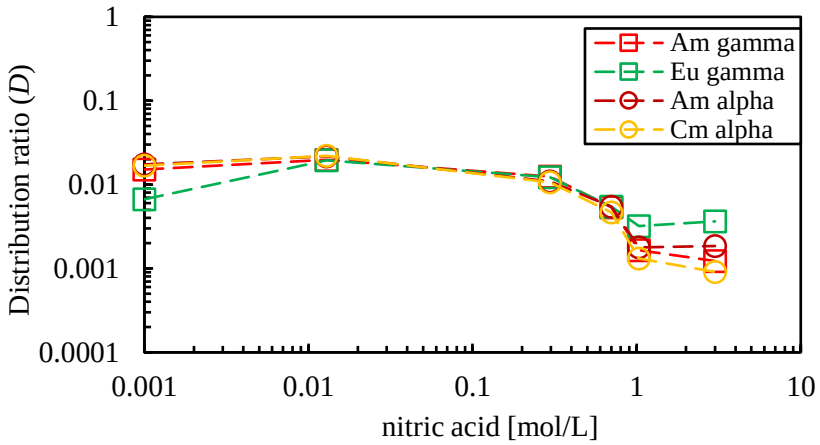

Figure 118: Distribution ratios for the extraction of ^{152}Eu, ^{241}Am, ^{244}Cm by **L19** measured by α- and γ-spectroscopy as a function of the nitric acid concentration of the aqueous phase (1 hr, 22 °C at 2,200 rpm). Organic phase: 10 mM **L19** in TPH/1-octanol (7:3 vol. ratio)

The functionalisation in **L19** with morpholine thus has a negative impact on the extraction results when directly compared to camphor-BTP **1.31**. This poor extraction capability may be explained by the increased precipitation observed for **L19**, which would prevent the ligand from taking part in the extraction of An(III) into the organic phase. As the camphor-BTP **1.31** was screened at a higher concentration than the **L19** in both diluents, this suggests that the precipitate would be considerable if tested at the same concentration.

The ligand **L20** observed a similar solubility trend to **L19**, with increasing precipitation as the HNO_3 concentration increases, with the exception of the highest HNO_3 concentration at 3.0 M, Figure 119. Again, at this concentration the same phenomena was noted, in which there was colour leaching into the aqueous phase, Figure 120. The *D* values for all radioisotopes are considerably lower than the camphor-BTBP **L28**, at 2 orders of magnitude across all concentrations. The D_{Am} value reaches a maximum value of 0.04 at 1.0 M HNO_3 indicating there

is negligible extraction of Am(III) or Cm(III). As a result, the $SF_{Am/Eu}$ values are all low and essentially meaningless due to the fact that no radioisotopes are being extracted from the aqueous phase into the organic phase. In terms of future industry potential, the ligand **L20** would thus be unsuitable for further development.

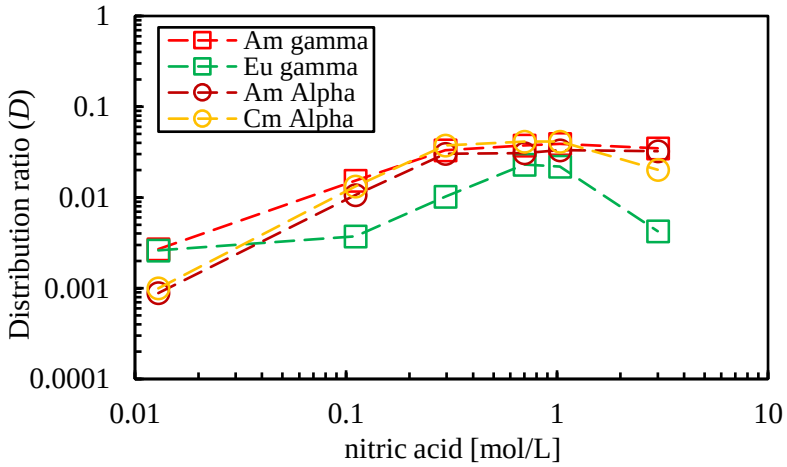

Figure 119: Distribution ratios for the extraction of ^{152}Eu, ^{241}Am, ^{244}Cm for **L20** measured by α- and γ-spectroscopy as a function of the nitric acid concentration of the aqueous phase (1 hr, 22 °C at 2,200 rpm). Organic phase: 10 mM **L20** in 1-octanol.

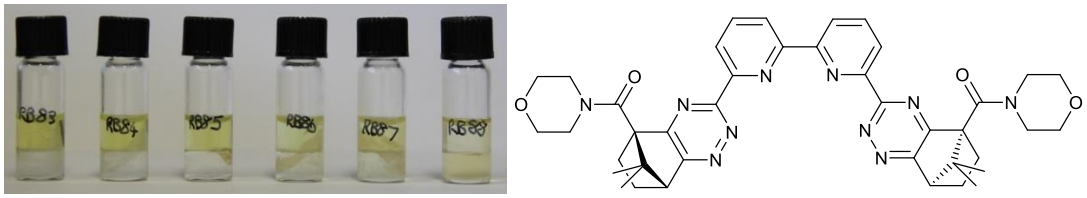

Figure 120: a) Photographs of the sample tubes after the first screening test using **L20** after phase mixing, increasing [HNO_3] from left to right; (b) molecular structure of **L20**.

The ligand **L21** observed the greatest quantity of precipitate formation after the screening test of all the morpholine functionalised ligands, the extraction data can be found in the appenxdix. This can be attributed to the increased basicity of the BTPhen **L21** ligand. At the highest HNO_3 concentration, 3.0 M, the same discolouration of the aqueous phase is observed as with the other morpholine-derived ligands (**L19** and **L20**). Again the same reduction in the visual amount of precipitation at this HNO_3 concentration (3.0 M) is observed, Figure 121. Clearer for this ligand **L21,** is the gradual colour change from deep yellow to a faint yellow as the HNO_3 concentration increases, and in correlation with the increasing precipitate.

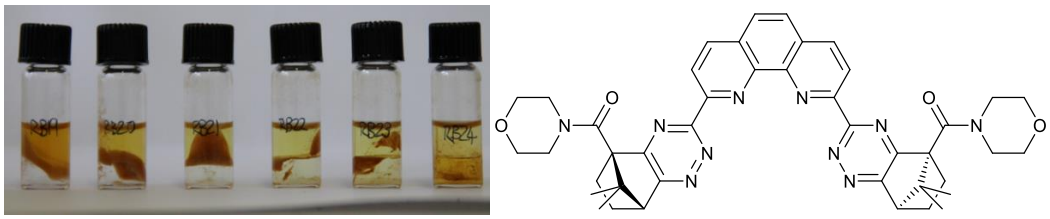

Figure 121: (a) Photographs of the sample tubes after the first screening test using **L21**, increasing [HNO_3] from left to right; (b) molecular structure of **L21**.

The results from γ-spectroscopy can be found in the appendix, with low D_{Am} and D_{Eu} observed across all concentrations, indicating the radioisotopes remain in the aqueous phase, as was observed for similar ligands **L19** and **L20**. The mass balances attained for the γ-measurements, in which the precipitate was avoided, are consistent across all HNO_3 concentrations. This suggests the precipitation is not a consequence of a ligand complex with either Am(III), Cm(III) or Eu(III) and subsequently it is a sensible suggestion that this precipitation is a consequence of the protonated ligand coming out of the solution upon contact with the HNO_3 aqueous phase. To gain confirmation of the precipitate composition, a technique such as X-ray crystallography or NMR spectroscopy would be beneficial. Unfortunately this was not carried out due to the presence of the radioisotopes.

The sensitivity of α-spectroscopy to solid deposits on the plates means the analysis was limited to γ-spectroscopy. Although this limits the ability to analyse for Cm(III), a good indication of the distribution of Am(III) and Eu(III) across the two phases in each sample and hence the ligand's extraction capability was still obtained.

An alternative secondary amine considered was piperidine in which the BTPhen **L27** was successfully purified to be screened for its extraction capabilities, Figure 122. The extraction test for ligand **L27** showed an increase in the *D* values for Am(III) and Cm(III) with increasing HNO_3 concentration, apart from one decrease at 0.7001 M HNO_3, Figure 123. At the higher HNO_3 concentrations, a decrease in the distribution ratios for Eu(III) was observed, indicating that a greater concentration of this radionuclide remains in the aqueous phase and the subsequent

$SF_{Am/Eu}$ increases dramatically. As stated previously, in industry this extraction would be completed at HNO_3 concentration ranges of 3-6 M HNO_3, and at the highest HNO_3 concentration this ligand has an excellent $SF_{Am/Eu}$ value of 230. An additional benefit with this ligand **L27** is the low *D* ratios of Am(III) and Cm(III) observed at low HNO_3 concentrations. In a future SANEX process, the back-extraction (or stripping) of Am(III) and Cm(III) would be carried out at low HNO_3 concentrations (0.1 M HNO_3) following the extraction step. The low *D* values for Am(III) and Cm(III) observed for **L27** at low HNO_3 concentrations would facilitate this stripping step.

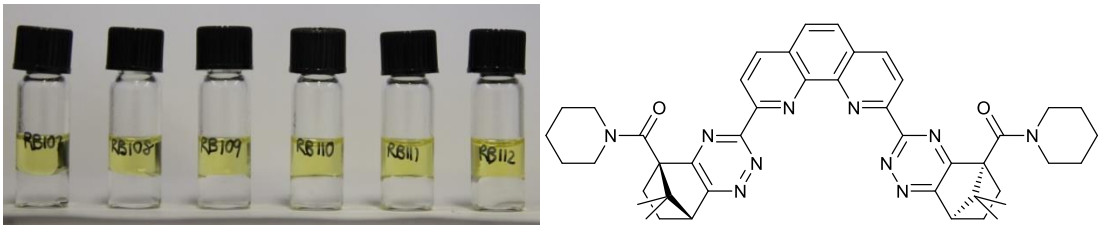

Figure 122: a) Photographs of the first screening test using **L27**, increasing nitric acid concentration from left to right; b) molecular structure of **L27**.

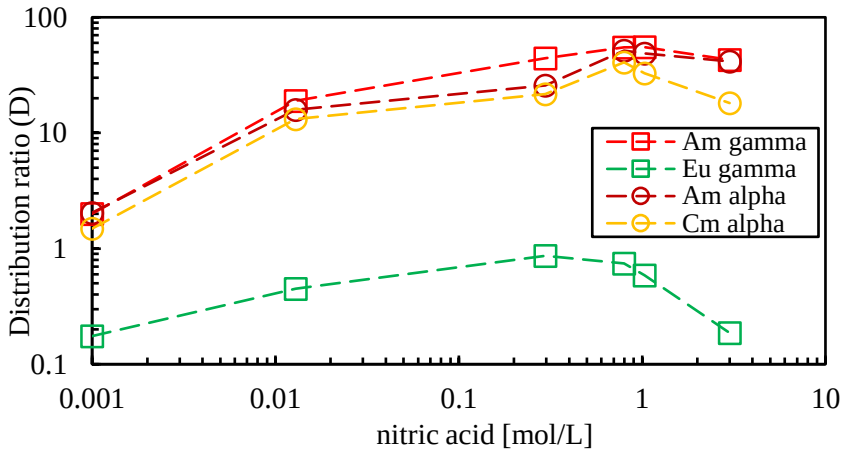

Figure 123: Distribution ratios for extraction of ^{152}Eu, ^{241}Am, ^{244}Cm using **L27** measured by α- and γ-spectroscopy as a function of the nitric acid concentration of the aqueous phase (30 min, 22 °C at 2,200 rpm). Organic phase: 10 mM **L27** in 1-octanol.

Unlike the morpholine-BTPhen **L21**, there was no precipitation observed with BTPhen ligand **L27** indicating an increased solubility of this ligand **L27** when the organic phase is in contact with the HNO_3 aqueous phase. The addition of the oxygen atom in the morpholine-derived ligands lowers the log *P* value of **L21** by more than 2 when compared to the **L27**, suggesting a lower lipophilicity, Table 16. The lower lipophilicity would decrease the solubility of the protonated

ligand in 1-octanol and perhaps increases its solubility in a HNO_3 aqueous phase, resulting in movement of the ligand across the organic/aqueous interface and hindering its ability to extract the An(III). During the extraction screening of **L21**, it is noted that with an increasing HNO_3 concentration, there is an increased colour change for the aqueous phase and a decrease in the level of precipitation observed. This suggests the precipitate is dissolved in the acidic aqueous phase, and would support the lower theoretical lipophilicity obtained for **L21**, from the log *P* values. The piperidine-derived BTP **L31** and BTBP **L32** were unfortunately not tested for their extraction properties due to difficulties in the purification of the samples, subsequently comparisons beyond the theoretical values cannot therefore be made. Considering the extraction data received for the ligand **L27**, the piperidine group has a significant impact on the *D* values and hence the $SF_{Am/Eu}$ in comparison to the use of the morpholine, potentially as a result of the increased solubility of the ligand when in contact with the HNO_3 phase. This may be a consequence of an increased basicity of **L21** which contains the morpholine group, although the pKa values for these ligands were not measured.

Table 16: Respective calculated log *P* values of the morpholine- and piperidine-derived bis-1,2,4-triazine ligands from the ACD I-lab software.

Ligand	Code	Log *P* (ACD I-lab)
Morpholine-BTP	**L19**	3.06
Morpholine BTBP	**L20**	3.34
Morpholine BTPhen	**L21**	3.84
Piperidine BTP	**L31**	517
Piperidine BTBP	**L32**	5.45
Piperidine BTPhen	**L27**	5.95

Finally, the BTP **L22**, BTBP **L23** and BTPhen **L24** ligands synthesised from the diethylamine-derived diketone **3.3.10** were screened. The BTP **L22** observed an increase in the distribution ratios for all radionuclides up until 0.296 M HNO_3, after which a decrease was observed. This suggests that as the nitric acid concentration is increasing, ligand protonation is outcompeting

metal complexation, with the *D* value for Am(III) dropping below 2 at 3 M HNO_3. This is a well-known phenomenon for the BTP ligands and to a lesser extent the BTBPs and BTPhens, as a consequence of the BTP ligand basicity. The $SF_{Am/Eu}$ increases from 53.52 to average at approximately 75.00 at higher HNO_3 concentrations, Figure 124. Despite the large D_{Am}, D_{Cm} and $SF_{Am/Eu}$, values the D_{Am} falling below 3 at 3.0 M HNO_3 isn't ideal for industrial application. In comparison to the corresponding camphor-BTP, this shows an improved extraction capability in 1-octanol then seen in research by Geist and co-workers, as no precipitate was observed across all concentrations tested, Figure 125.[82]

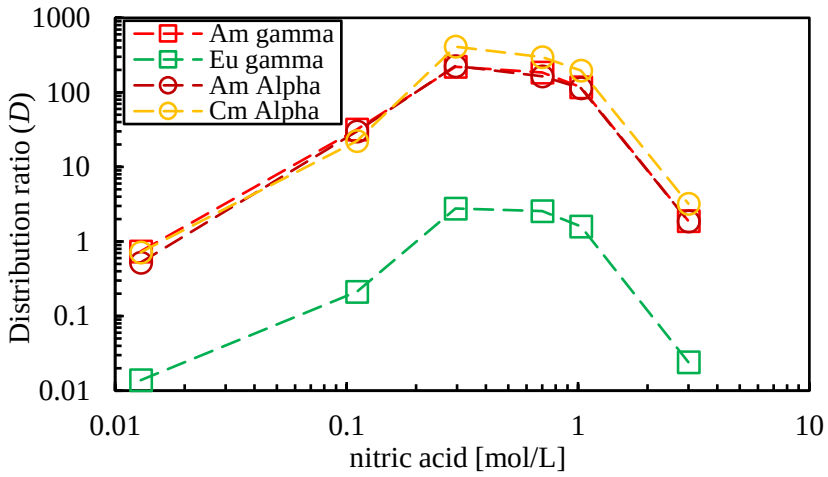

Figure 124: Distribution ratios for extraction of ^{152}Eu, ^{241}Am, ^{244}Cm using **L22** measured by α- and γ-spectroscopy as a function of the nitric acid concentration of the aqueous phase (30 min, 22 °C at 2,200 rpm). Organic phase: 10 mM **L22** in 1-octanol.

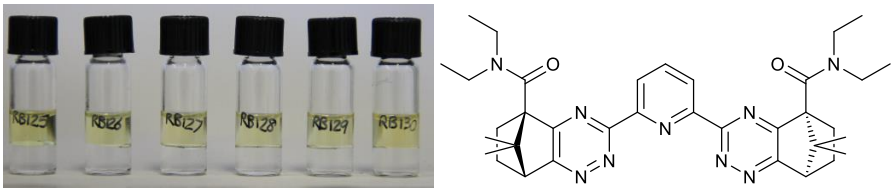

Figure 125: Photographs of the sample tubes after the first screening test using **L22**, with increasing [HNO_3] from left to right; (a) molecular structure of **L22**.

For the ligand **L23**, the screening for extraction capability was completed at a lower concentration, 0.006 M, as a result of a limited quantity of the purified ligand sample being obtained. This must be taken into consideration when comparing its results with those of the other ligands. At this lower concentration there was no precipitate observed after 1 hour of phase mixing, Figure 126. Despite the slightly lower concentration of the sample, at 6 mmol/L organic

solution of **L23**, the separation factor for Am(III) over Eu(III) ($SF_{Am/Eu}$) was consistently greater than 100 when in contact with ≥ 0.3 M HNO_3 aqueous phase, Figure 127. The *D* ratio for Am(III) increases until reaching a maximum of 4.68 at 1.0 M HNO_3, where it subsequently decreases again to 1.31 at 3 M HNO_3. This decrease in the *D* ratio, although it has minimal impact on the separation factor, may be a concern for future industrial implementation. Those waste solutions with a high metal loading would require a greater *D* ratio in order to achieve effective separations in the required phase mixing times. Since *D* values depend on the ligand concentration, the *D* values for ligand **L22** should increase if a higher concentration of the ligand **L22** within the organic phase was used than that trialled here, providing ligand solubility doesn't then pose an issue.

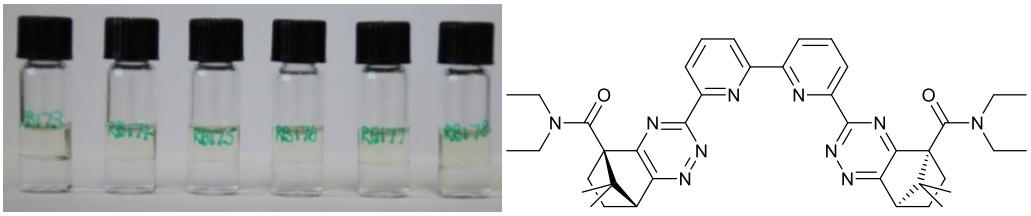

Figure 126: (a) Photographs of the sample tubes after the first screening test using **L23**, with increasing [HNO_3] from left to right; (b) molecular structure of **L23**.

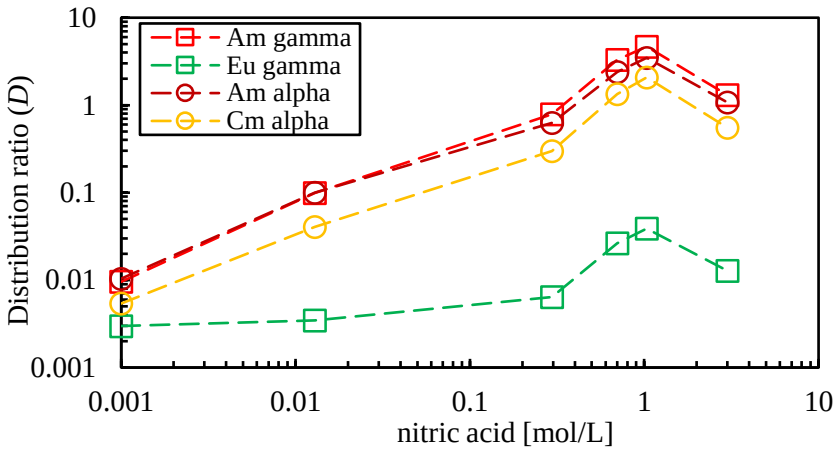

Figure 127: Distribution ratios for extraction of ^{152}Eu, ^{241}Am, ^{244}Cm by **L23** measured by α- and γ-spectroscopy as a function of the nitric acid concentration of the aqueous phase (1 hr, 22 °C at 2,200 rpm). Organic phase: 10 mM **L23** in 1-octanol.

The extraction test for the BTPhen ligand **L24** showed a continuous increase in the *D* values for Am(III) and Cm(III) across the HNO_3 concentrations, using the same conditions as dictated in

Chapter 6 apart from the contact time, which was reduced to 30 minutes. The *D* ratio of Eu(III) increases up until 0.296 M HNO_3, where it then decreases again, a phenomena observed with the previous BTPhen ligands, at the highest HNO_3 concentration, Figure 128.[95] As a consequence, the $SF_{Am/Eu}$ is significantly increased to 111 at 3.0 M HNO_3, with the *D* value for Am(III) being two orders of magnitude higher than that for Eu(III) at this HNO_3 concentration. These results show that at higher concentrations of HNO_3, above 1.0 M HNO_3, high selectivity between Am(III) and Eu(III) is achieved with this ligand **L24**, comparable to that of the benchmark ligand $CyMe_4$-BTBP **1.09**, but without the need for a phase transfer agent. There was no selectivity observered between Am(III) and Cm(III), with $SF_{Cm/Am}$ values falling between 0.89 – 1.38. The ligand showed clear phase separation and no precipitation upon contact with the HNO_3 aqueous phase, unlike that observed for the camphor-BTPhen **L29**, Figure 129.

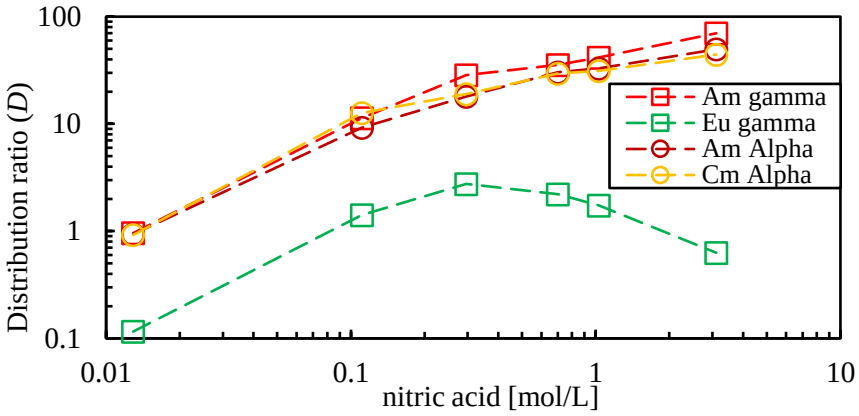

Figure 128: Distribution ratios for extraction of ^{152}Eu, ^{241}Am, ^{244}Cm by **L24** measured by α- and γ-spectroscopy as a function of the nitric acid concentration of the aqueous phase (30 min, 22 °C at 2,200 rpm). Organic phase: 10 mM **L24** in 1-octanol.

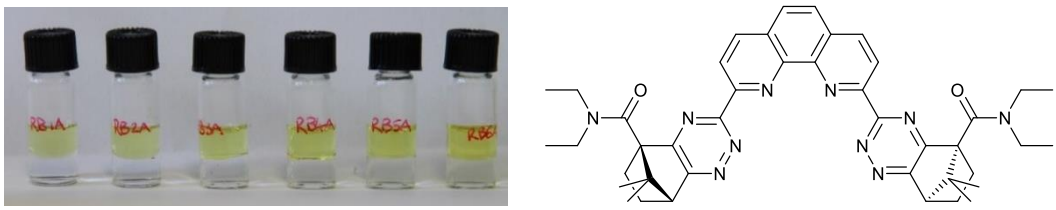

Figure 129: (a) Photographs of the sample tubes after the first screening test using **L24**, increasing [HNO_3] from left to right; (b) molecular structure of **L24**.

The ligand **L24** does have lower *D* values and separation factors than those observed for the related ligand $CyMe_4$-BTPhen **1.17**, but this is not necessarily a hindrance to the ligands potential within a future industrial process. When the *D* values are increasingly high this could cause issues

for the back-extraction (or stripping) of the metal from the ligand, so that the ligand can be recycled and re-used. Having lower *D* values is desired to avoid the addition of a hydrophilic stripping agent (such as glycolic acid) which would increases costs of the process. Ideally, for the purposes of stripping, *D* values of below 1 are desirable at low HNO_3 concentrations, the conditions utilised for the metal back-extraction in a process. At 0.01 M HNO_3 the D_{Am} and D_{Cm} values fall just below 1, indicating stripping of both An(III) is possible at these HNO_3 concentrations. Investigation into the ligands extraction kinetics, section 3.6, will give a further indication of the plausibility of its potential in industry, as specified in the aims and objectives.

Interestingly, both the piperidine-BTPhen **L27** and diethylamine-BTPhen **L24** ligands observe the same trend regarding the decreasing *D* ratio of Eu(III) at higher HNO_3 concentrations, similar to the $CyMe_4$-BTPhen ligand **1.17**. This phenomenon isn't yet fully understood but it is proposed that ligand protonation out-competes metal complexation with regards to the formation of a ligand complex with Eu(III). The use of TRLFS found that the $CyMe_4$-BTPhen **1.17** forms a 1:2 complex with Cm(III) that has an increased stability constant when compared the complex formed with Eu(III), with log beta values of 13.8 and 11.6 for the Cm(III)-$CyMe_4$-BTPhen **1.17** and Eu(III)-$CyMe_4$-BTPhen **1.17**, respectively.[94a]

The BTP **L25** and BTBP **L26** ligands derived from the primary amine, methylamine, were next tested for their extraction abilities. The **L25** observed increasing *D* ratios with regards to Am(III) and Cm(III) with increasing HNO_3 concentration up until 1.0 M HNO_3, whereafter these values decline, Figure 130. Despite the observation of no precipitation across all samples, there were notably low *D* ratios observed for all radioisotopes, remaining below 0.1 across all concentrations. Observation of the sample tubes after the screening test showed a notable colour change as the HNO_3 concentration increased, although this was less notable then previous ligands tested (morpholine-derived ligands) Figure 131. This suggests that some degree of ligand dissolution into the aqueous phase is occurring, which would reduce its ability to act as an extractant, in agreement with the low *D* ratios. Alternatively, the ligand may not be hydrophobic enough to extract the Am(III) or Cm(III) or forms complexes which are thermodynamically weak. Further

studies could investigate the reasoning for this ligands poor solubility including TRLFS and EXAFS.

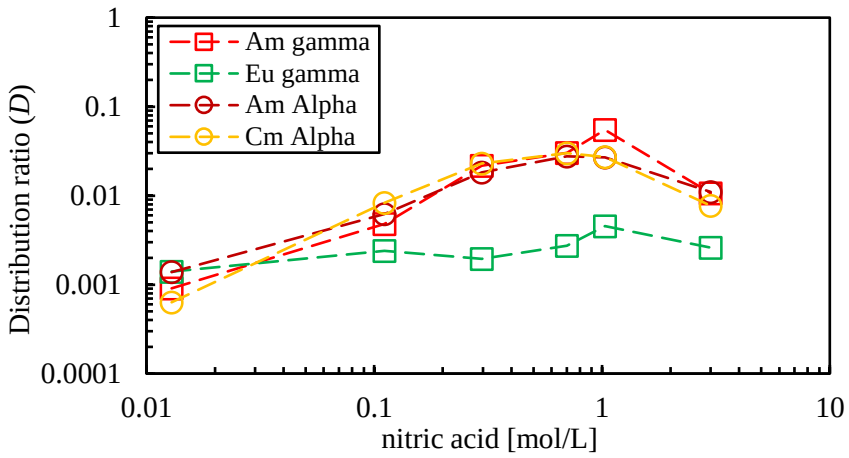

Figure 130: Distribution ratios for extraction of ^{152}Eu, ^{241}Am, ^{244}Cm by **L25** measured by α- and γ- spectroscopy as a function of the nitric acid concentration of the aqueous phase (60 min, 22°C at 2,200 rpm). Organic phase: 10 mM **L25** in 1-octanol.

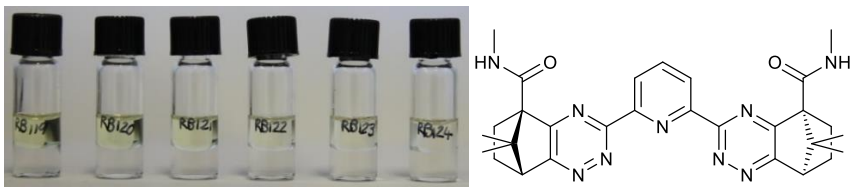

Figure 131: (a) Photograph of the sample tubes after the first screening test using **L25**, increasing [HNO_3] from left to right; (b) molecular structure of **L25**.

The methylamine-derived BTBP ligand **L26** displays increasing *D* ratios for Am(III) and Cm(III) across all HNO_3 concentrations, which is less pronounced for Eu(III), Figure 132. However, the *D* ratios all remain below 0.1 as was observed for **L25**. Thus the addition of a *N*-methyl amide substitutent to the camphor backbone has a negative impact on the extraction capabilities or corresponding BTP and BTBP ligands when compared to the extraction properties of the corresponding secondary amide derivatives. The discolouration of the aqueous phase, as observed with **L25** again correlate to the ligands decreased lipophilicty and hence improved solubility in the aqueous phase. Significant precipitation was observed at the highest HNO_3 concentration of 3.0 M, suggesting ligand protonation, Figure 133.

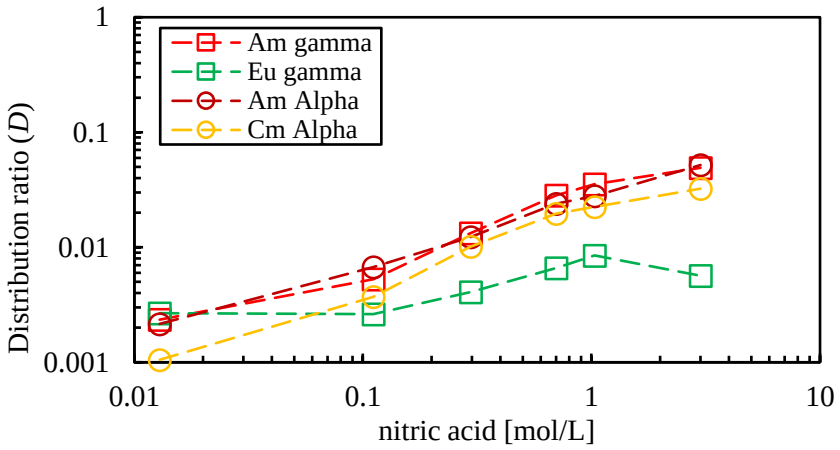

Figure 132: Distribution ratios for extraction of ^{152}Eu, ^{241}Am, ^{244}Cm by **L26** measured by α- and γ- spectroscopy as a function of the nitric acid concentration of the aqueous phase (60 min, 22°C at 2,200 rpm). Organic phase: 10 mm **L26** in **1**-octanol.

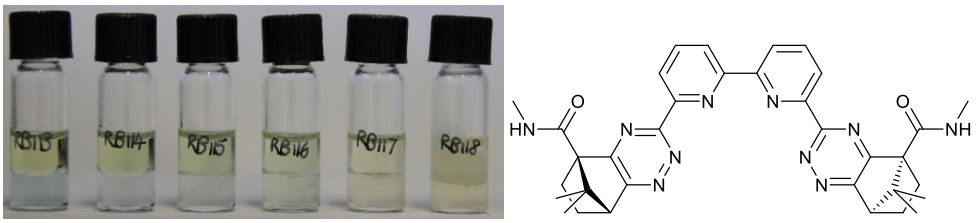

Figure 133: (a) Photograph of the sample tubes after the first screening test by **L26**, increasing [HNO_3] from left to right; (b) molecular structure of **L26**.

Based upon the extraction data obtained for the ligands discussed in this chapter it is clear that functionalisation of the camphor moiety can have significant impacts on the extraction properties of the ligands. Where poor extraction performance was observed this was generally related to ligand precipitation in contact with the HNO_3 phase and correlated to a lower calculated log *P* value. Suggesting this may, in future, give an indication for a ligands ability to extraction Am(III) and Cm(III) from the aqueous phase containing Eu(III). The extraction kinetics of some ligands will be discussed in the following section.

3.7. Kinetics studies

Where reasonably encouraging *D* values and $SF_{Am/Eu}$ values were observed in the initial extraction experiments upon varying the nitric acid concentration, it was decided to complete a kinetics study. This would gain an insight into the extraction kinetics, or rates of metal extraction, of these ligands as stated in the project aims. The rate of extraction of a given metal by a ligand can be measured by the time taken for the *D* value to reach its equilibrium value. The rates of metal extraction are significant and important to measure when designing a future extraction process, since the *D* values for all metal ions need to be at thermodynamic equilibrium during a process. The rates of extraction were investigated at specific HNO_3 concentrations, typically 0.30 M or 1.00 HNO_3 over the time period of 60 minutes, in order to establish how long the phases need to be mixed for before extraction equilibrium is reached. The benchmark ligand $CyMe_4$-BTBP **1.09** requires a contact time of approximately 60 minutes to reach equilibrium, while $CyMe_4$-BTPhen **1.17** achieves equilibrium after 15 minutes of phase contact time, without the need for a phase-transfer agent in both cases.

The ligand **L24** shows very fast extraction kinetics for Am(III) and Cm(III) at 0.30 M HNO_3, Figure 134, with the distribution ratios reaching equilibrium within 5 minutes of phase mixing. This shows significantly faster kinetics than $CyMe_4$-BTPhen **1.17**, which observes comparable *D* values for Am(III) but requires longer to reach its equilibrium. Direct comparisons should be judged with care due to the different nitric acid concentrations utilised, $CyMe_4$-BTPhen **1.17** was tested at 1.0 M HNO_3. The data obtained for **L24** demonstrates the ligands ability to selectively extract Am(III) and Cm(III) with short contact times, whilst still achieving a D_{Am} and D_{Cm} of greater than 20 and a $SF_{Am/Eu}$ of 8. A comparable extraction as obtained for $CyMe_4$-BTPhen **1.17** as this concentration.[95] The separation factor ($SF_{Cm/Am}$) was found to average at 1 for **L24**, a value not significant enough to suggest the ligand could be utilised to achieve this separation.

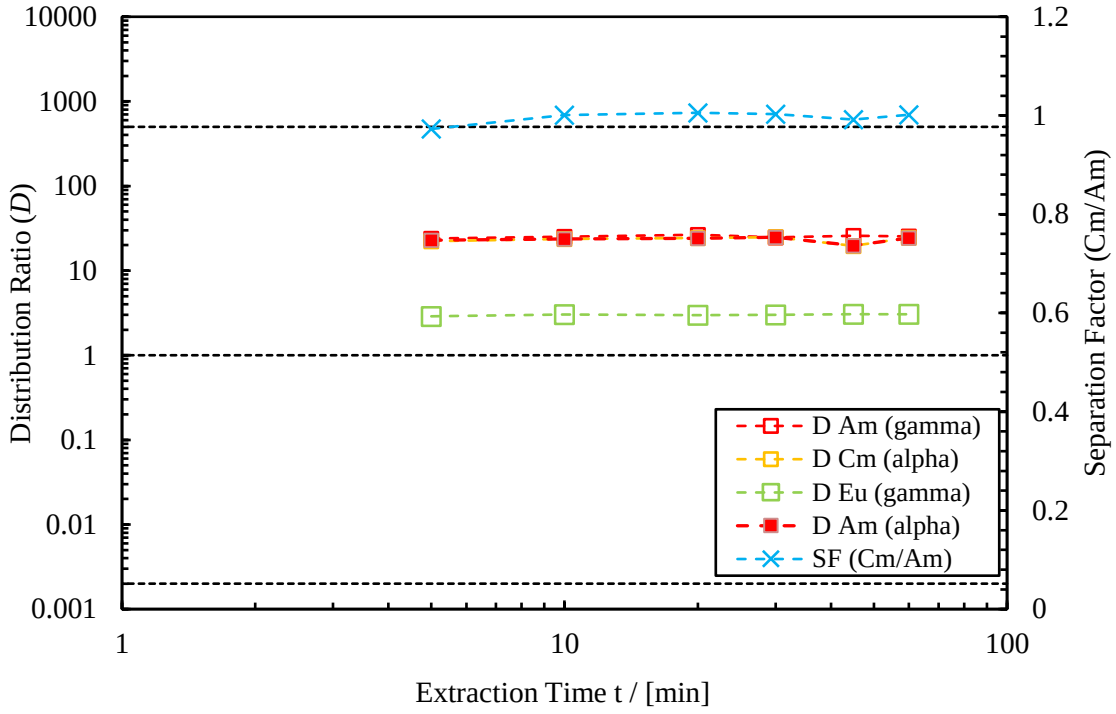

Figure 134: Distribution ratios and $SF_{Cm/Am}$ for the extraction of ^{241}Am, ^{244}Cm and ^{152}Eu by **L24** as a function of contact time. (0.296 M, 22 °C at 2,200 rpm) Organic phase: 10 mM **L24** in 1-octanol.

The ligand **L19**, which showed the least precipitation amongst the morpholine-derived ligands, was examined for its extraction kinetics in the screening for its extraction of Am(III) and Cm(III) from the aqueous phase at 0.30 M HNO_3, Figure 135. The equilibrium distribution ratios were reached within 5 minutes for both the An(III) and Eu(III), but with a lower $SF_{Am/Eu}$ of approximately 3, then was observed for **L24**. A similar $SF_{Cm/Am}$ of 1 was observed for **L19**. These extraction kinetics are slightly improved on the comparable camphor-BTP **1.31**, as reported in the work by Geist and co-workers,[82] in which extraction equilibrium was reached within 10 minutes at a HNO_3 concentration of 1 M, using the diluent TPH/1-octanol (7:3 vol.).

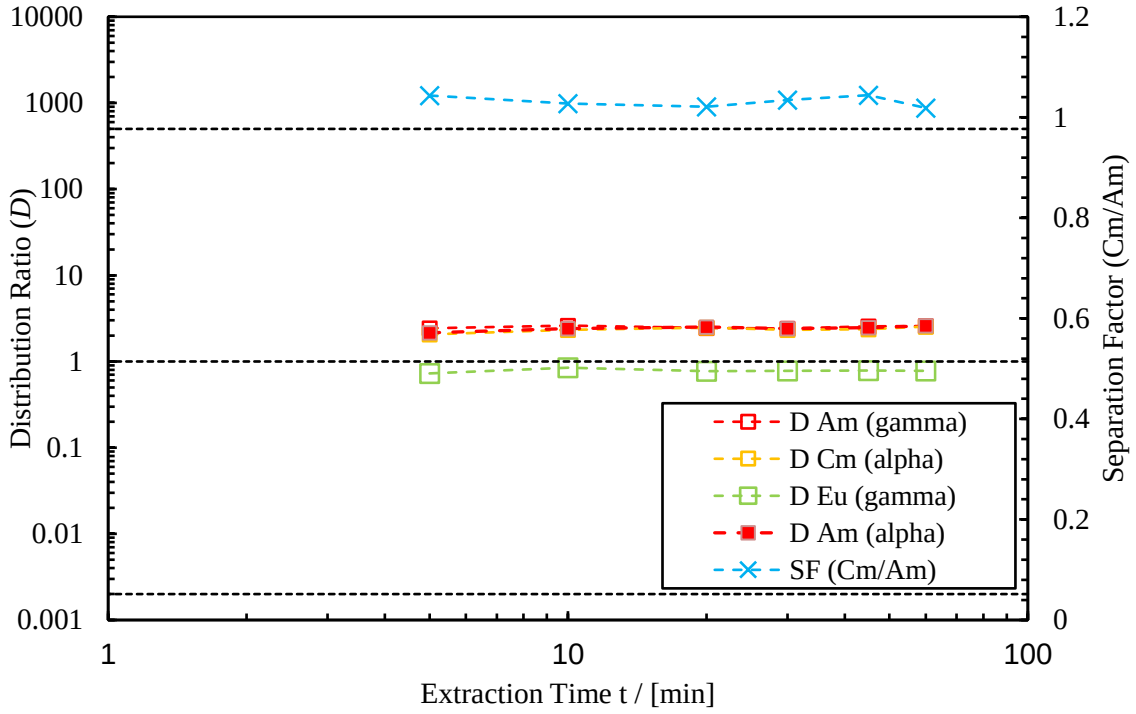

Figure 135: Distribution ratios and $SF_{Cm/Am}$ for the extraction of ^{241}Am, ^{244}Cm and ^{152}Eu by **L19** as a function of contact time. (0.296 M, 22 °C at 2,200 rpm) Organic phase: 10 mM **L19** in 1-octanol.

3.8. NMR Titration Studies

In order to establish the potential species that may be present during an extraction experiment, NMR titration studies were completed with the lanthanide nitriate salts acting as actinide surrogates. Lanthanum (La(III)) and lutetium (Lu(III)) were selected as the lanthanide salts, along with yttrium (Y(III)) (all as nitrate salts) due to their diamagnetism and the subsequent likelihood of obtaining a well resolved spectra. A CD_3CN-d_3 solution of $La(NO_3)_3$, $Y(NO_3)_3$ and $Lu(NO_3)_3$ were individually titrated against solutions of the ligands functionalised in this chapter, in the same solvent. In this section the most significant titrations will be discussed and a complete data set for all ligand titrations can be found in the Appendix.

A ^1H NMR titration of a CD_3CN-d_3 solution of **L19** with $La(NO_3)_3$ was completed, and the formation of a 1:2 metal-ligand complex was observed, Figure 136. The initial spectrum shows the free ligand species with a doublet at δ 6.87 ppm and a triplet at δ 8.15 ppm. Upon addition of 0.3 equivalents of $La(NO_3)_3$ the appearance of new signals at δ 9.12, 8.90 and 8.49 ppm were observed with complete disappearance of the free ligand resonances occurring upon addition of

0.4 equivalents of the lanthanide salt. There were no further spectroscopic changes on further addition of the lanthanide salt. This observation corresponds to the 1:3 metal-ligand complex suggesting three ligand molecules surround the lanthanum metal centre, as complete disappearance of the starting material is seen. A similar observation was made for **L22**, see appendix for the full data set.

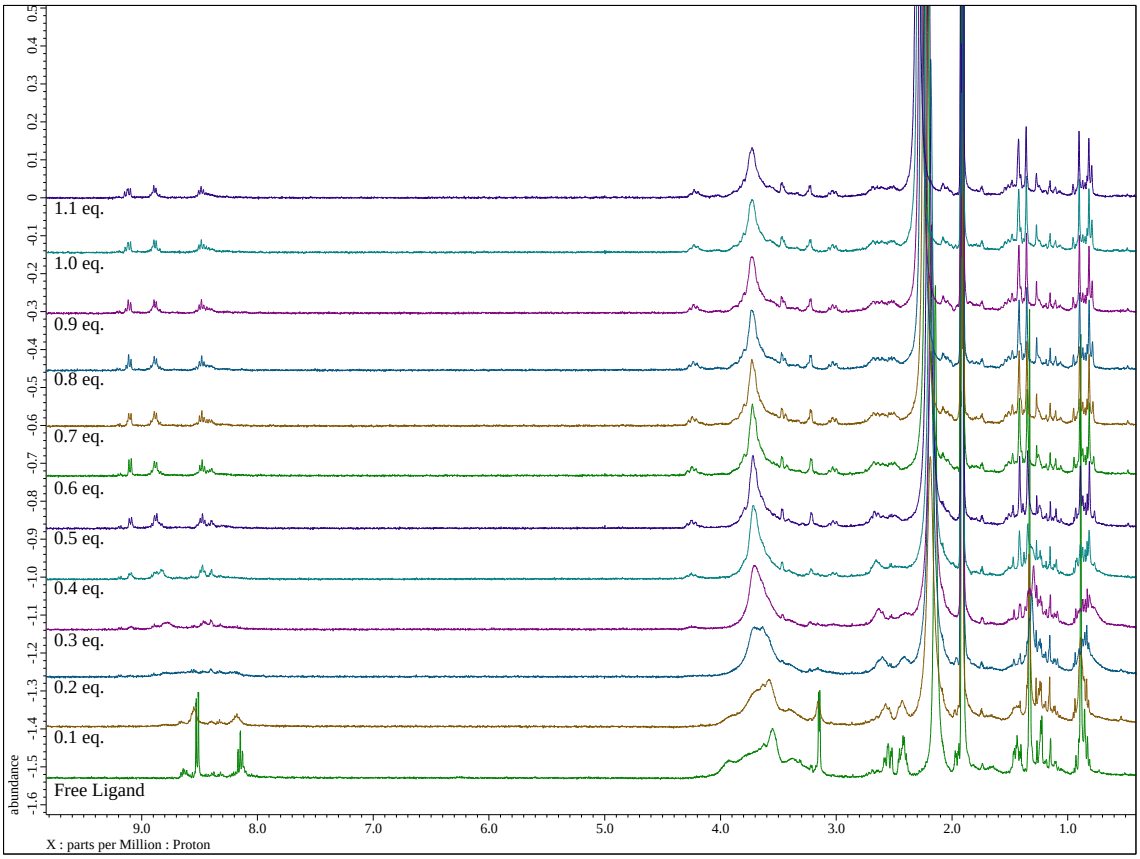

Figure 136: ^{1}H NMR titration of **L19** with increasing equivalents of $La(NO_3)_3$ showing a 1:3 complexation formation after the addition of 0.3 eq. $La(NO_3)_3$.

A ^{1}H NMR titration of ligand **L24** with $La(NO_3)_3$ in CD_3CN-d_3 shows the formation of metal-ligand complexes. After 0.1 eq. addition of the lanthanide salt the formation of a 1:2 complex is observed with signals appearing at δ 9.09, 8.82 and 8.46 ppm. Complete disappearance of the free ligand signals is perceived after 0.5 eq. of La(III) had been added, indicating the initially formed complex is a 1:2 metal:ligand complex. Formation of a 1:2 complex was also observed on further additions of the lanthanide salt and complete saturation with this complex is achieved after 0.9 eq. of the lanthanide salt had been added. When using $Lu(NO_3)_3$ in a similar titration study, the formation of both 1:1 and 1:2 complexes was also observed after a total of 1.2 equivalents addition

of the lanthanide nitrate had been added, Figure 137. La(III) is a larger lanthanide then Lu(III), as a consequence of the lanthanide contraction, and may aid in the explaining why a 1:1 complex was still observed after 1.2 equivalents addition. The high *D* values obtained in the extraction experiments, section 3.6 may be attributed to the formation of these 1:2 bis-complexes.

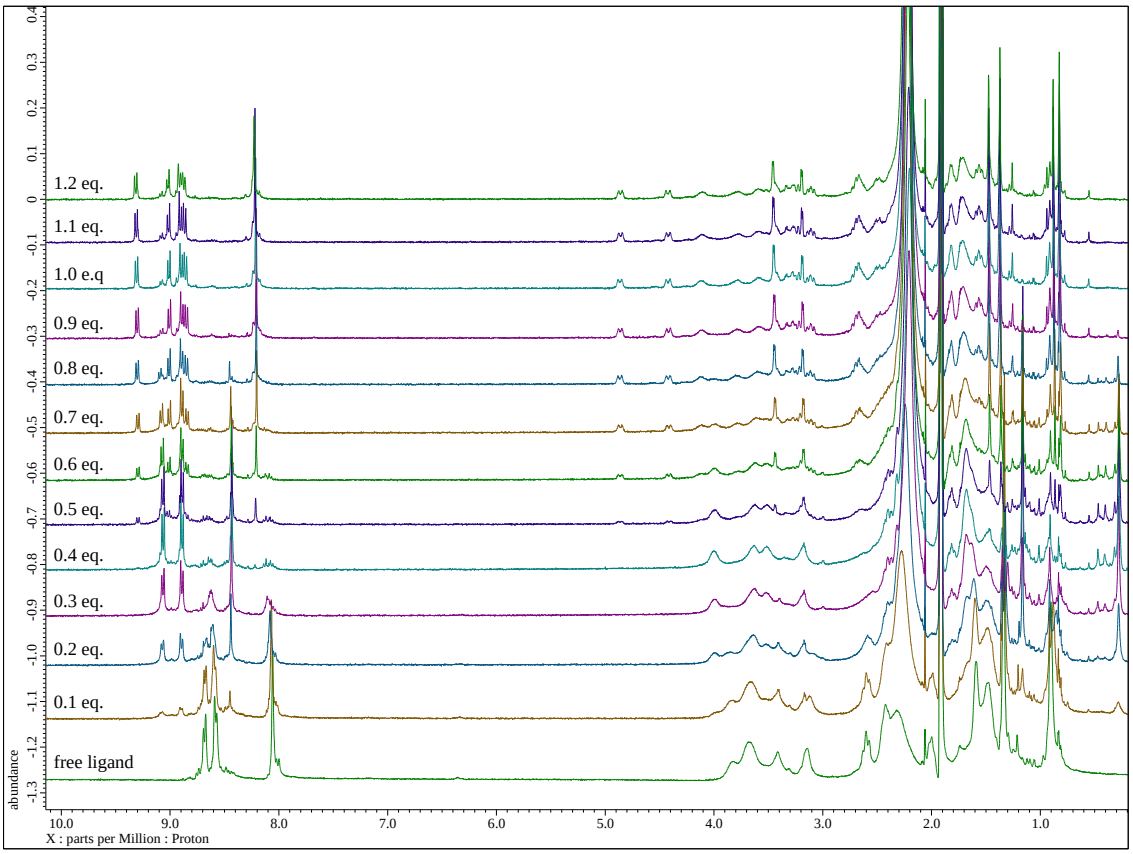

Figure 137: ^{1}H NMR titration of **L24** with increasing equivalents of $Lu(NO_3)_3$ showing a 1:2 complex forming upon addition of 0.1 eq. and 1:1 complex upon addition of 0.4 eq.

The ^{1}H NMR titration of **L27** with $La(NO_3)$ shows the same 1:2 and 1:1 complex formation upon increasing addition of the lanthanide nitrate, Figure 137. The 1:2 complex is initially observed upon addition of 0.1 equivalents of $La(NO_3)_3$, with the 1:1 complex being observed after 0.5 equivalents of the lanthanide salt had been added. Upon addition of 1.2 equivalents of the lanthanide salt there is almost complete saturation with the 1:1 complex. This shows a similar trend to that observed for **L24**. This could potentially be a significant result in explaining why these ligands show slightly lower distribution ratios during extraction screening for Am(III) and Cm(III). The $CyMe_4$-BTBP **1.09** and $CyMe_4$-BTPhen **1.17** don't observe this almost complete

disassociation of the 1:2 complexes upon increasing equivalents of the lanthanide salt, suggesting the 1:2 complexes formed from the novel ligands **L27** and **L24** may be less stable.[96]

3.9. Conclusion

In this chapter a versatile two-step synthesis has been established to obtain a range of amide-diketone derivatives of ketopinic acid using both primary and secondary amines. These diketones were used to synthesise the corresponding BTP, BTBP and BTPhen ligands from the corresponding bis-amidrazones, in most cases. Mixed solubility results were observed that correlate to the ligand families, with increasing solubility being found generally across the series of BTPs > BTBPs > BTPhens.

In solvent extraction experiments the BTPhen derivatives observed the greatest separation factor for Am(III) over Eu(III) of all the ligand families tested; BTP, BTBP or BTPhen. In particular, those ligands containing the diethyl amide and piperidine amide groups showed the most encouraging extraction properties, with no precipitates being observed in contact with the HNO_3 aqueous phase. It is apparent that the addition of the morpholine amide group negatively impacts ligand solubility upon contact with the HNO_3 phase. This may suggest that consideration of the log *P* values can give a good indication as to the potential solubility of a ligand when in contact with the HNO_3 phase, with the calculated log *P*s for the morpholine ligands being some of the lowest considered.

The diethylamide-derived BTPhen ligand **L24** observed high *D* ratios for Am(III) and Cm(III) with a $SF_{Am/Eu}$ OF 111.17 at 3.0 M HNO_3, in addition to reaching equilibrium within 5 minutes of phase mixing. This is significantly improved extraction kinetics compared to the benchmark ligand $CyMe_4$-BTPhen **1.17**, which achieves extraction equilibrium within 15 minutes. Despite the *D* ratios being lower than those of the $CyMe_4$-BTPhen **1.17**, they are still high enough to achieve effective and efficient extraction of Am(III) and Cm(III) and can be considered as a viable alternative to the benchmark ligands. The piperidine amide-derived BTPhen ligand **L27** additionally shows the same extraction capabilities, with a $SF_{Am/Eu}$ at 3 M HNO_3 of 231. This will

need to be further investigated to gauge the kinetics of this particular ligand and how it compares to both the $CyMe_4$-BTPhen ligand **1.17** and **L24**.

The NMR titrations give evidence to the presence of both 1:1 and 1:2 complex formations under the titration conditions. The slightly decreased *D* ratios in comparison to $CyMe_4$-BTPhen may be explained by the apparent decreased stability of the 1:2 complexes within solution. However, this wouldn't prevent the potential future implementation of these ligands in a process, as these *D* ratios would still allow for quantitative separation.

Chapter 4

Modified $CyMe_4$ ligands derived from modified $CyMe_4$ diketones.

4. Modified $CyMe_4$-ligands derived from modified $CyMe_4$-diketones.

4.1. Introduction

The tetramethylcyclohexyl ($CyMe_4$) group **4.1.1** has emerged as the dominant aliphatic side group of the bis-triazinyl-pyridine (BTP), bis-triazinyl-bipyridine (BTBP) and bis-triazinyl-phenanthroline (BTPhen) ligands, section 1.5, Figure 138. When incorporated into the ligands, the $CyMe_4$ group confers good radiolytic and hydrolytic stability to bis-1,2,4-triazine ligands, in contrast to simple *n*-alkyl groups. This is due to the absence of any hydrogen atoms at the benzylic positions adjacent to the triazine rings. As a result, the final ligands, in particular $CyMe_4$-BTBP **1.09** and $CyMe_4$-BTPhen **1.17**, are the leading candidates for industrial implementation in the SANEX process. However, the complex and time-consuming synthesis of the $CyMe_4$ diketone intermediate **4.1.1** used to synthesise these ligands, the limited solubility of the ligands in preferred diluents (1-octanol, dodecane etc.) and the relatively slow rates of metal extraction are some issues that still remain. New ligand developments have focused in two areas, on replacing the $CyMe_4$ moiety **4.1.1** of the ligands altogether or on the functionalisation of the bis-1,2,4-triazine backbones, both discussed in section 1.5. Currently a satisfactory replacement for the $CyMe_4$ diketone **4.1.1** has not been identified that includes its beneficial properties but improves on its drawbacks.

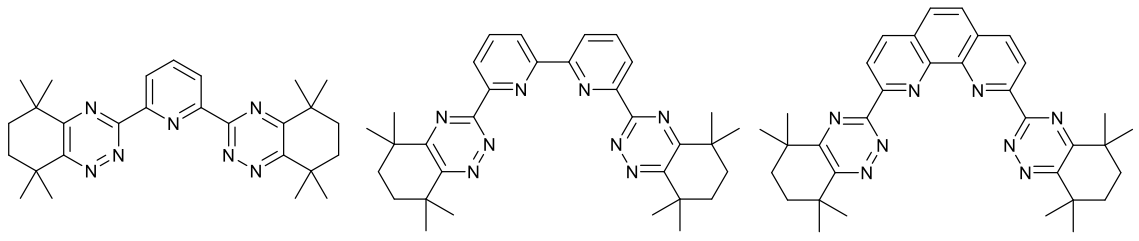

1.30 **1.09** **1.17**

Figure 138: Dominant ligand from each family; $CyMe_4$-BTP **1.30**, $CyMe_4$-BTP **1.09** and $CyMe_4$-BTP **1.17**.

The $CyMe_4$ group **4.1.1** was first utilised in the synthesis of a bis-triazinyl-pyridine (BTP) ligand **1.30** as a result of insufficient chemical stability to radiolysis and hydrolysis of previous *n*-alkyl substituted BTP derivatives, section 1.5.2. This group has the benefit of having no benzylic

hydrogens, which can be abstracted by free radicals, nitrite ions or nitrogen oxides when in contact with the HNO_3 aqueous phase. Upon exposing the $CyMe_4$-BTP **1.30** to boiling nitric acid (3 M) there was no degradation after 24 hours. In contrast the alkylated *i*-Pr-BTP **1.29** ligand showed extensive degradation.[80] The addition of an extra aromatic ring in **1.09**, improved the resistance to radiolysis of the BTP ligands, which was thought to result from the distribution of excess energy from the absorbed gamma radiation across the aromatic π-system.[80] The $CyMe_4$-BTBP **1.09** was found to be resistant to hydrolysis for up to 90 days.[86]

There has been no attention paid to developing new synthetic protocols that lead to modified derivatives of the $CyMe_4$ group **4.1.1** itself. In the current research, the general structure of the $CyMe_4$-diketone **4.1.1** will be the basis for modified derivatisatives **4.1.2**, Figure 139, with the highlighted tetramethylcyclohexane ring being the common feature through all the modified diketones. Alternative synthetic methods will be investigated to functionalise the $CyMe_4$-diketone **4.1.1** with moieties that are intended to improve the solubility and increase the rates of extraction of the derived ligands. The introduction of additional hydrogen bond donor and acceptor groups (HBD/HBA) should influence the polarity of the ligands when compared to the analogous benchmark ligands **1.30**, **1.09** and **1.17**. This increased polarity may enable a higher concentration of the ligand to exist at the phase interface and hence improve the rates of extraction. Introducing these groups will also increase the Fsp^3 value (if these groups contain sp^3-hybridised aliphatic carbon atoms), which is thought to directly correlate to ligand solubility. Previous developments, such as the addition of the *tert*-butyl group on the $CyMe_4$-BTBP ligand **1.09** saw an increase in solubility but a decrease in the rates of extraction of the resulting ligand **1.37**.[87, 89, 158] Thus is has been difficult to increase ligand solubility without simultaneously decreasing the ligand's rates of extraction. It is hoped that, through the addition of HBD/HBA functional groups (eg: amide, ether, alkoxy groups etc) containing sp^3-hybridised carbon atoms, the solubility and rates of extraction of the ligands can be simultaneously increased. This could pave the way for the rational design of future bis-1,2,4-triazine ligands with improved extraction properties.

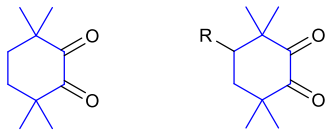

4.1.1 **4.1.2**

Figure 139: Molecular structure of the $CyMe_4$ diketone **4.1.1** and the general structure of the functionalised $CyMe_4$-diketones containing the (R) at the 4-position **4.1.2**. The common structure in both is highlighted in blue.

Discussed in this chapter is the synthesis of novel functionalised $CyMe_4$-diketones that are utilised to form novel BTP, BTBP and BTPhen ligands. The subsequent solubility and extraction results are discussed for those ligands successfully synthesised and compared to the analogous unfunctionalised ligands $CyMe_4$-BTP **1.30**, $CyMe_4$-BTBP **1.09** and $CyMe_4$-BTPhen **1.17**.

4.2. Synthesis of modified $CyMe_4$ diketones and ligands

The lost-cost reagent 5,5-dimethylcyclohexane-1,3-dione (dimedone) **4.2.1** was chosen as the starting material for the synthesis of all derivatives, due to the presence of the dimethylated-cyclohexane ring and its similarity to the $CyMe_4$-diketone **4.1.1**. Dimedone **4.2.1** was initially di-methylated with iodomethane in the presence of base to remove the hydrogens present to give the 2,2,5,5-tetramethylcyclohexan-1,3-dione **4.2.2**, Figure 140.[159] The alkylation proceeds to give **4.2.2** in yields of 80% and above, dependent on the batch.

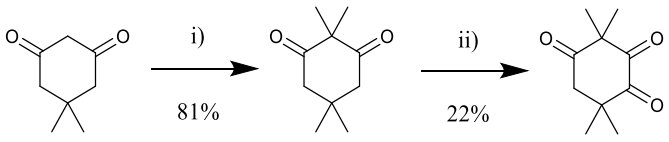

4.2.1 **4.2.2** **4.2.3**

Figure 140: Reaction scheme for the synthesis of **4.2.3**; Reaction conditions: (i) iodomethane, K_2CO_3, $EtOH/H_2O$, (ii) SeO_2, toluene.

From the product formed **4.2.2** a variety of reactions can be completed to give novel diketones, involving synthetic manipulation of one of the carbonyl groups, followed by oxidation of the products with selenium dioxide (SeO_2). One of these strategies involves the oxidation of **4.2.2** with SeO_2 to form the 3,3,6,6-tetramethylcyclohexane-1,2,4-trione **4.2.3**. Following a procedure

by Wenkert and co-workers,[160] this oxidation was initially attempted using 2 equivalents of SeO_2 in refluxing toluene. The over-oxidation that would result in the formation of the corresponding tetra-ketone was hoped to be avoided. Only a 12% yield of the final product **4.2.3** was obtained after an overnight reaction, with the ^{1}H NMR spectrum of the crude product showing that starting material remained. An increase in the SeO_2 stoichiometry to 2 and then 3 equivalents, saw an increase in the yield to 26%, Table 17, entries 1-3. There was limited, if any, observation of the tetra-ketone forming under these conditions. Furthering efforts to improve product conversion, alternative solvents were explored which included 1,4-dioxane and acetic acid. The use of either solvent resulted in the disappearance of the starting material as followed by ^{1}H NMR with additional signals being observed in the aliphatic region. In particular, the use of acetic acid resulted in various impurities observed in the ^{1}H NMR spectrum which were not observed in 1,4-dioxane, in which a cleaner crude product was obtained. The final yields of **4.2.3** when utilising 1,4-dioxane or acetic acid were similar, at 30 and 32% respectively, Table 17, entries 4-5. Going forward it was decided to utilise 1,4-dioxane as the solvent based upon the improvement in the purity of the crude product obtained.

Table 17: Reaction conditions trialled for the formation of the tri-ketone **4.1.3**.

Entry	Selenium Dioxide	Solvent	Reaction Time (hr)	Yield
1	**2.0 eq.**	Toluene	24	12 %
2	**3.0 eq.**	Toluene	20	15 %
3	**2.5 eq.**	Toluene	24	26 %
4	**2.0 eq.**	1,4-dioxane	24	30 %
5	**2.0 eq.**	Acetic acid	24	32 %
6	**1.0 eq.**	1,4-dioxane	72	26 %

The SeO_2 stoichiometry was again varied in the chosen solvent, 1,4-dioxane, but it was found that reducing the stoichiometry negatively impacted the product yield. There appears to be little sensitivity in the amount of SeO_2 used in the reaction, with only trace amounts of the tetra-ketone

being observed. Based upon the product yields obtained and observation of the crude ^{1}H NMR spectra, there appears to be some loss of product during work up. Column chromatography fractions included the starting material **4.2.2**, product **4.2.3** and then a third fraction containing multiple aliphatic impurities. For the purpose of obtaining the final ligands, it was decided to use these reaction conditions, regardless of the yield. Should a scaled-up synthesis of any of the ligands need to be developed, this reaction will need to be optimised further by investigating alternative, less toxic oxidising reagents.

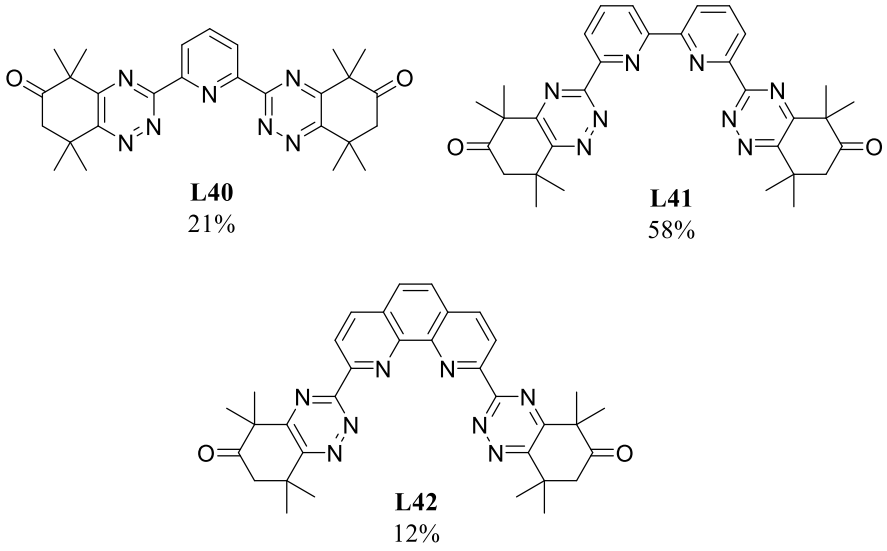

Figure 141: Molecular structures of the ligands derived from the condensation reactions of the triketone **4.2.3** with bis-amidrazones, with one representative regioisomer shown in each case a) **L31**, b) **L32** and c) **L33**

The condensation reactions between the triketone **4.1.3** and the bis-amidrazone compounds (**3.2.2**, **3.2.5** and **3.2.10**) in acetic acid successfully yielded the novel final ligands **L40**, **L41** and **L42**, Figure 141. Since the diketone **4.2.3** is non-symmetrical, different regioisomers could in principle be formed in the condensation reactions of **4.2.3** with the bis-amidrazones. The purification of the BTBP **L41** was the easiest to achieve via filtration of the crude product as a solid, with one major regioisomer being observed through ^{1}H NMR spectroscopy. The filtrate was analysed by ^{1}H NMR which showed the presence of unreacted starting diketone **4.2.3**. The purification of the BTP **L40** proved more complicated, with a dark oil produced upon filtration which mainly constituted of starting material. Recrystallisation from diethyl ether gave a pure sample of the BTP **L40**, with two regioisomers being detected through ^{1}H NMR, Figure 143, with major and minor

regioisomers observed in a ratio of 4:1. Considering the singlets observed for the methyl groups at δ 1.70 and 1.52 ppm (minor isomer), δ 1.65 and 1.56 ppm (major isomer), it appears that two symmetrical regioisomers have formed. Further product purification to increase the yield was unsuccessful with unreacted starting tri-ketone **4.2.3** obtained. The three possible regioisomers that could form during the synthesis of the BTP ligand **L40** are represented in Figure 142.

Further difficulties in ligand purification were encountered when the BTPhen **L42** was synthesised, which upon purification through recrystallization and trituration gave a yellow solid as the product contaminated with minor aliphatic impurities. It was decided to attempt column chromatography on the sample, with increasing solvent polarity used to elute the ligand. Unfortunately, the emergence of the required product was not observed. Ultimately it was deemed that the sample had a greater affinity for the silica than the eluting solvent. Repeating the condensation reaction of **4.2.3** and **3.2.10** again resulted in product formation, with the ^{1}H NMR spectrum of the crude product again showing the presence of aliphatic impurities, Figure 144.

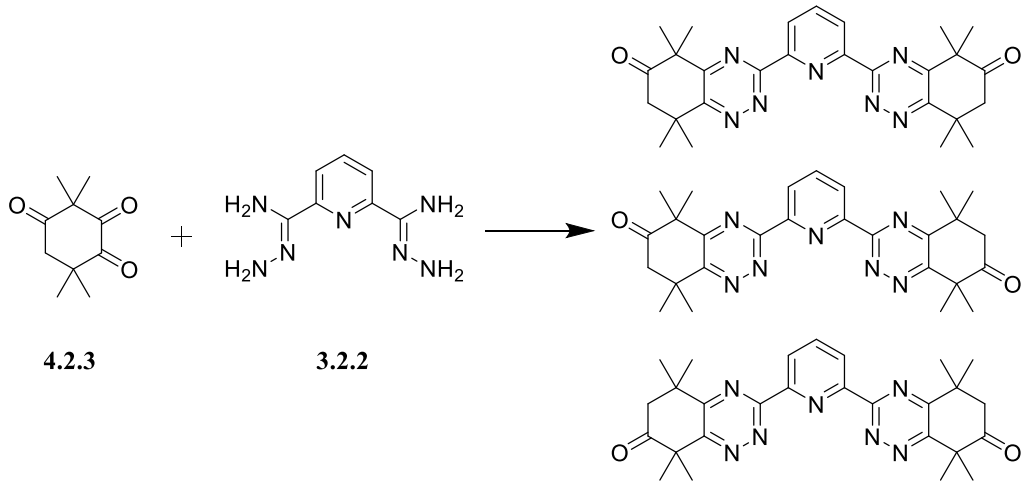

Figure 142: Reaction scheme for the condensation reaction between triketone **4.2.3** and bis-amidrazone **3.2.2** to form the ligand **L40**, showing the three regioisomers that could be formed. Reaction conditions: i) AcOH.

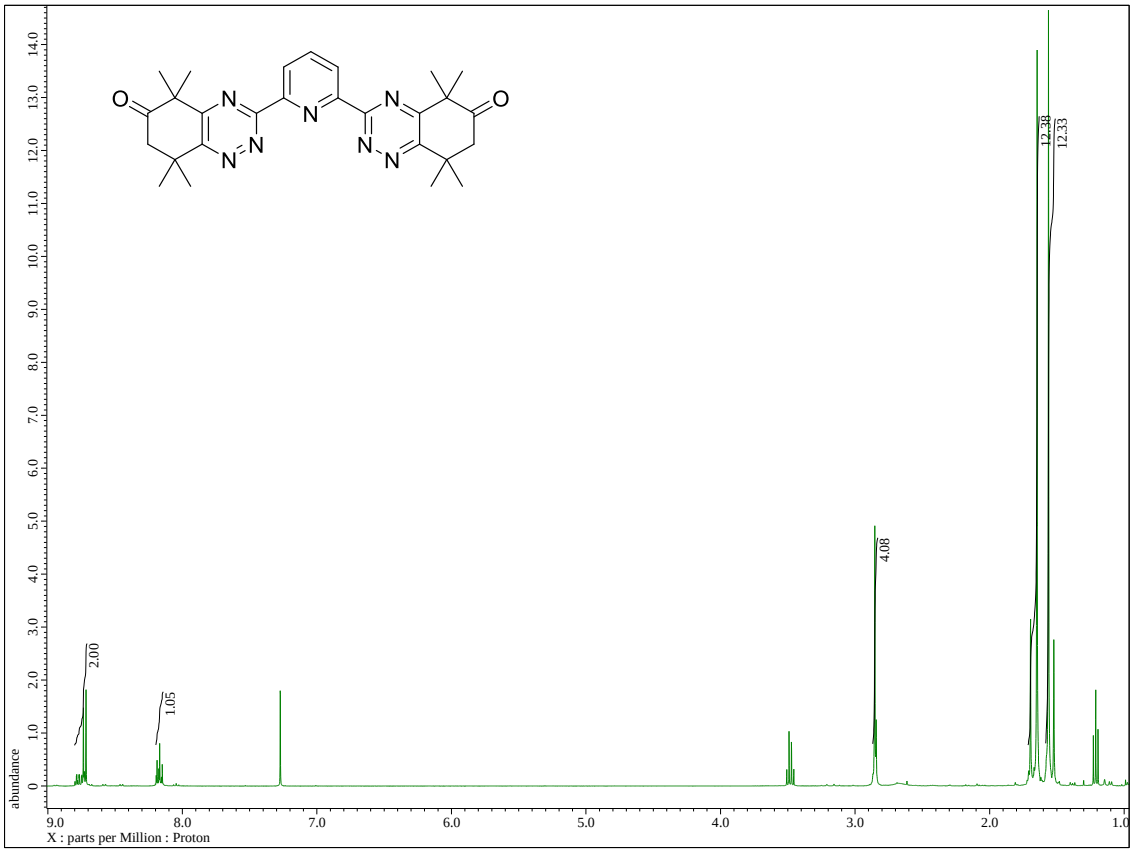

Figure 143: ^{1}H NMR spectrum of two regioisomers of BTP ligand **L40**, with one example structure shown.

Table 18: Assignment of NMR signals for the major regioisomer of the BTP ligand **L40**.

^{1}H (ppm)	**Proton integration and multiplicity (Hz)**	**^{13}C (ppm)**	**Assignment**
8.73	2H, d, *J* = 7.79 Hz	138.4	2 x ArCH
8.17	1H, t, *J* = 7.79 Hz	125.5	ArCH
2.85	4H, s	50.7	2 x CH_2
1.65	1.65, s	26.1	4 x CH_3
1.56	1.56, s	28.7	4 x CH_3

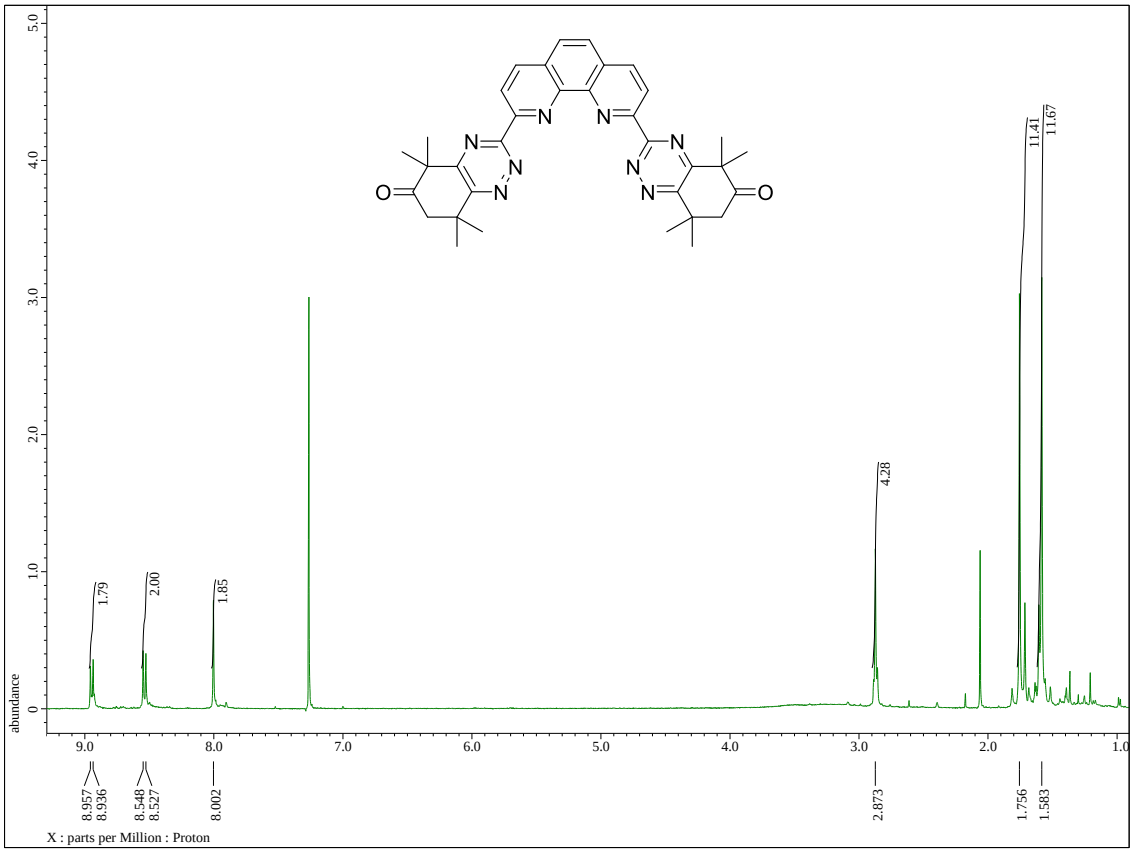

Figure 144: ^{1}H NMR spectrum of the BTPhen ligand **L42**, showing aliphatic impurities.

Table 19: Assignment of NMR signals for the BTPhen ligand **L42**.

^{1}H (ppm)	Proton integration and multiplicity (Hz)	^{13}C (ppm)	Assignment
8.98	2H, d, *J* = 7.79 Hz	123.4	2 x ArCH
8.58	2H, d, *J* = 7.79 Hz	124.3	2 x ArCH
8.10	2H, s, *J* = 7.79 Hz	138.2	2 x ArCH
2.87	4H, s	50.7	2 x CH_2
1.66	12H, s	26.2	4 x CH_3
1.58	12H, s	28.7	4 x CH_3

Introducing an amide functional group into the $CyMe_4$-diketone **4.1.1** was next considered *via* the Wittig reaction of a phosphonium ylide **4.2.6** with **4.2.2**. The intended synthesis of the final diketone is shown in Figure 147. The ylide was prepared in a two-step synthesis following a procedure by Vicente and co-workers to give the final product **4.2.6** in 58% yield.[161] An initial reaction between 2-chloro-*N*,*N*-dimethylacetamide **4.2.4** and triphenyl-phosphine prior to deprotonation of the resulting phosphonium salt yields the final ylide **4.2.6**, Figure 145.

Unfortunately, on reaction of the ylide **4.2.5** with **4.2.2**, there was no observed formation of the alkene product **4.2.7**. As the initial nucleophilic attack of the ylide onto the carbonyl carbon is the rate determining step, Figure 146, it is suspected that the stabilised ylide is reacting very slowly or in this case not at all, with the sterically hindered ketone **4.2.2**. The presence of the electron withdrawing amide group stabilises the carbanion formed when the ylide is deprotonated. As a consequence, the ylide has a lower nucleophilicity compared to non-stabilised ylides and their reactions with sterically hindered ketones (eg: ketones with a tertiary carbon in the alpha position) are much less common. An alternative procedure that can be considered is the Horner-Emmons reaction.

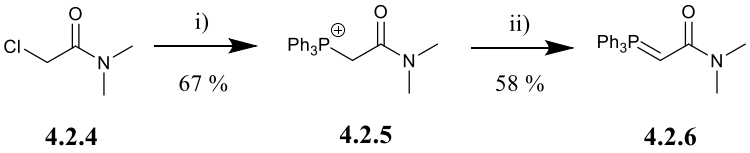

Figure 145: General synthesis of the Wittig reagent **4.2.6**. Reaction conditions: i) Triphenylphosphine, $CHCl_3$, ii) NaH, DCM (anhy).

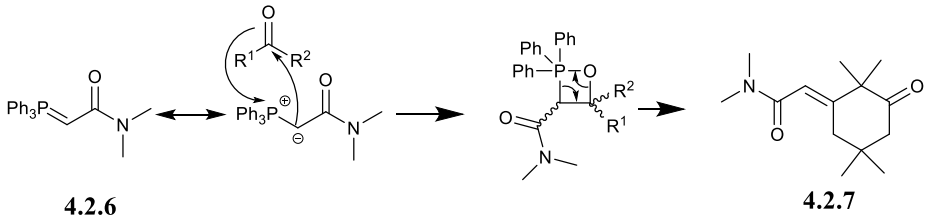

Figure 146: Proposed mechanism for the Wittig reaction to **4.2.6** form **4.2.7**.

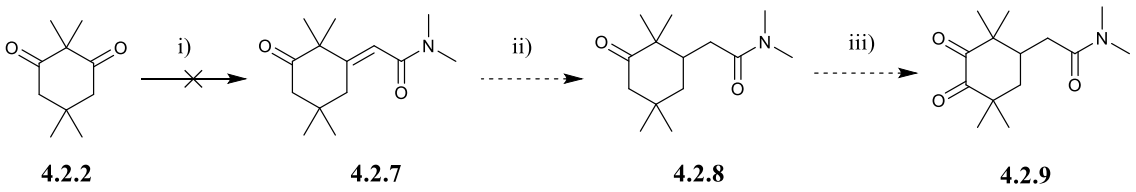

Figure 147: Intended synthesis of the final functionalised diketone **4.2.9**. Reaction conditions: i) phosphonium ylide **4.2.5**, NaH, THF; ii) Pd/C, H_2, MeOH; iii) SeO_2, AcOH.

The Horner-Wadsworth-Emmons (HWE) olefination reaction was examined as an alternative method to introduce the amide group into the diketone **4.2.2**. In replacement of the stabilised ylides of the Wittig reaction above, the more nucleophilic phosphonate ester **4.2.10** was utilised,

Figure 148. The phosphonate ester **4.2.10** was synthesised via the Arbuzov reaction of the commercially available 2-chloro-*N*,*N*-dimethylacetamide **4.2.4** with triethyl phosphite. [162]

Initially the reaction was completed in THF with considerable starting material remaining upon work up of the reaction. The molar equivalents of the phosphonate ester and sodium hydride, were increased from 1.2 to 4 equivalents, in an attempt to drive the reaction towards product formation. Again, no conversion to the final desired product **4.2.7** was observed. It was thought that the sterically hindered nature of the diketone **4.2.2** due to the adjacent dimethyl groups, may have prevented this reaction from proceeding.

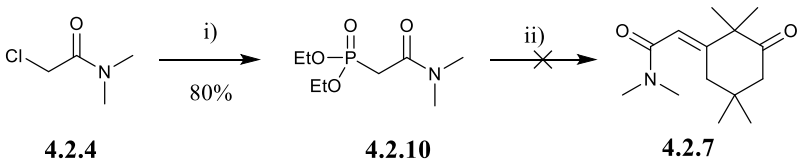

Figure 148: Proposed synthesis of **4.2.7** by Horner Wadsworth Emmons Olefination of **4.2.4** with the phosphonate ester **4.2.10**. Reaction conditions: i) triethyl phosphite; ii) NaH, **4.2.2**, THF.

Following the above unsuccessful approaches to alkene **4.2.7** *via* the Wittig and HWE reactions of **4.2.2** with stabilised ylides and carbanions, respectively, an alternative Wittig reaction using a non-stabilised ylide was studied. The commercially available phosphonium salt; methyltriphenylphosphonium bromide **4.2.11**, was considered, to generate a more reactive non-stabilised phosphonium ylide, which would convert the carbonyl group into a simple unfunctionalised alkene **4.2.12**. Hydrogenation of the alkene, followed by the oxidation of **4.2.13** would then generate the novel target diketone **4.2.14**, Figure 149. Although this approach would not allow introduction of an amide group, it was considered to introduce additional alkyl groups into the final diketone **4.2.14**, with the aim of increasing the solubility of the final ligands. Following procedures by U. Quabeck and co-workers[163] the Wittig reaction of methyltriphenylphosphonium bromide with **4.2.2** was initially attempted with potassium *tert*-butoxide (*t*-BuOK) as the base to form the ylide through deprotonation, observed by the formation of a yellow mixture in the reaction vessel. The reaction proceeded with a slight excess of the base

and ylide (1.3 equivalents) in toluene to give the alkene in 15% yield. Improving the yield was attempted by altering the stoichiometric equivalent of the base. At 1.5 equivalents this led to the observation of the dialkene compound **4.2.15**, Figure 150. An alternative base, *n*-butyllithium (*n*-BuLi) was considered. However, this ultimately led to the formation of no product. Consequently, it was decided to continue using *t*-BuOK as the base of choice.

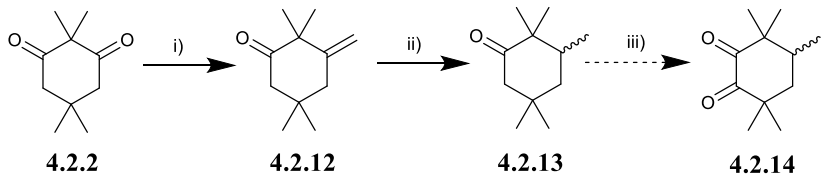

Figure 149: Proposed reaction scheme for the formation of X. Reaction conditions: i) methyltriphenylphosphonium bromide, t-BuOK, toluene; ii) H_2, Pd/C, methanol; iii) SeO_2, 1,4-dioxane.

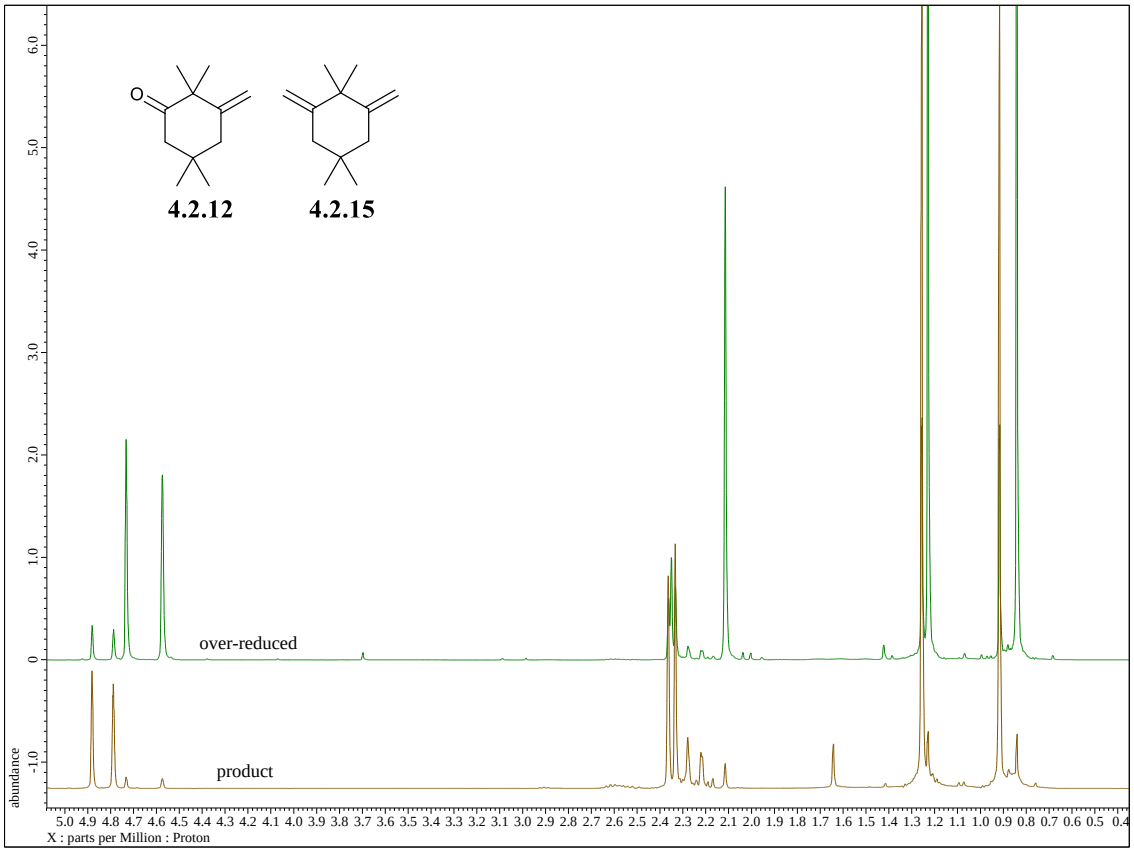

Figure 150: ^{1}H NMR spectra overlaid showing the desired alkene product **4.2.12** (bottom spectrum) and the formation of the dialkene compound **4.2.15** (top spectrum).

The ylide was formed in a separate flask, as observed by the vivid colour change (cloudy to yellow), before it was added in aliquots to the 1,3-diketone **4.2.2** in a separate vessel. As the

yield was very low, at 15%, alternative solvents were considered to toluene; in particular THF and diethyl ether. Diethyl ether was chosen as a low boiling point solvent as it was suspected that the alkene could be a volatile compound and hence evaporating during the evaporation of the solvents in the work-up. Utilising this solvent resulted in a doubling of the yield of alkene **4.2.12** to 31%. Analysis of the ^{1}H NMR spectrum proves that a balance is required in this reaction, in which the yield is sacrificed either by starting material remaining or the formation of the dialkene compound **4.2.15.** Attempts to improve this yield would have been considered if the final diketone was obtained.

The reduction of the alkene **4.2.12** was next investigated through a hydrogenation reaction using H_2 and palladium on activated carbon. The formation of the chiral product **4.2.13** can be clearly observed in the ^{1}H NMR spectrum by the disappearance of the olefinic proton signals of the starting material **4.2.12** and the appearance of an AB proton system for the diastereotopic methylene protons at C-4, Figure 151. Purification and further investigations could not be completed due to time constraints near the end of the project.

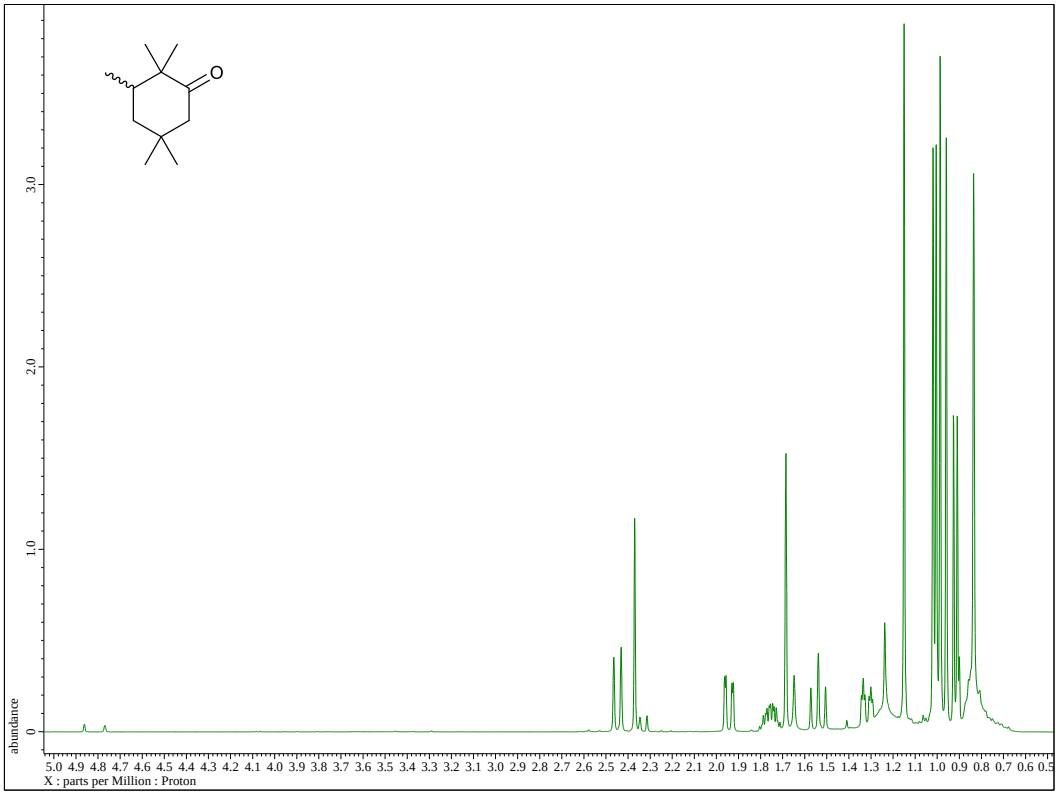

Figure 151: ^{1}H NMR spectrum of the crude product **4.2.13** from the hydrogenation of alkene **4.2.12**, showing the presence of traces of starting material remaining.

Reductive amination was considered as an alternative method of introducing an amide functional group into the $CyMe_4$-diketone **4.1.1** to study its effects on extraction kinetics, by converting one of the ketone carbonyl groups into a secondary amine, and then into a tertiary amide *via N*-acetylation of the amide. The use of the mild reducing agent, sodium triacetoxyborohydride ($NaBH(OAc)_3$) and a selected primary alkyl amine was investigated following procedures proposed by M.E. Flanagan and co-workers.[164] The use of hexylamine as the amine in the reductive amination reaction of ketone **4.2.2** proceeded in 20% yields with the ^{1}H NMR spectrum of the crude product **4.2.16** displaying significant starting material, Figure 152. Unsuccessful attempts at the reductive amination of **4.2.2** were made with propylamine and methylamine under the same conditions, again the ^{1}H NMR spectrum of the crude products showed the presence of unreacted starting materials in each case. It has been shown previously that reductive aminations with sterically hindered ketones can be low yielding if at all, such as the reaction with camphor.[165] As the starting material generally remains it is suspected that the imine formation is the rate limiting step in this reaction.

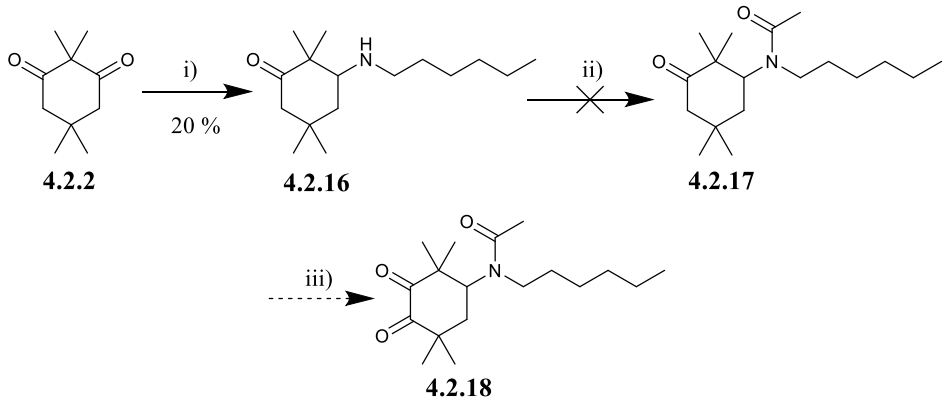

Figure 152: Proposed synthesis of novel diketone **4.2.18**. Reaction conditions: i) $NaBH(OAc)_3$, hexylamine, THF; ii) acetic anhydride, triethylamine, DCM; iii) SeO_2, 1,4-dioxane.

An alternative reaction was the acylation of the amine to form an amide bond with acetic anhydride, Figure 152. However, attempted *N*-acylation of amine **4.2.16** with acetic anhydride was unsuccessful and the starting material was recovered. Due to the low yielding nature of the

reductive amination reaction, and the limited literature available on the reductive amination reactions of sterically hindered ketones, this reaction was not developed any further.

Other efforts to derivatise the diketone **4.2.2** were studied involving oxime formation from the reaction of diketone **4.2.2** with hydroxylamine hydrochloride in the presence of base. If successful, the resulting oxime **4.2.19** could be further manipulated to derive amides (by *N*-acylation), hydroxylamines (by reduction) or alkoxyamines (by *O*-alkylation), Figure 153. Initial efforts following procedures reported by S. Lochyński and co-workers which utilised pyridine as the base, resulted in no conversion of **4.2.2** to the oxime **4.2.19**.[166] The use of sodium bicarbonate as the base resulted in some conversion of **4.2.2** to the product **4.2.19**.[167] The use of sodium acetate resulted in the best conversion of starting material, but the bis-oxime **4.2.20** was generally formed, even when utilising 1 equivalent of hydroxylamine hydrochloride. Obtaining the required product **4.2.19** required a reduction in the reaction time. It was difficult to obtain a reasonable yield of the desired product **4.2.19** in order to take forward in the subsequent steps as the bis-oxime **4.2.20** formed very readily within solution, so this approach was not studied further. The crude ^{1}H NMR spectrum, Figure 154, shows the observation of two broad signals at δ 10.7 and 10.5 ppm, from the –OH groups of the required oxime **4.2.19** and bis-oxime **4.2.20** compounds, respectively.

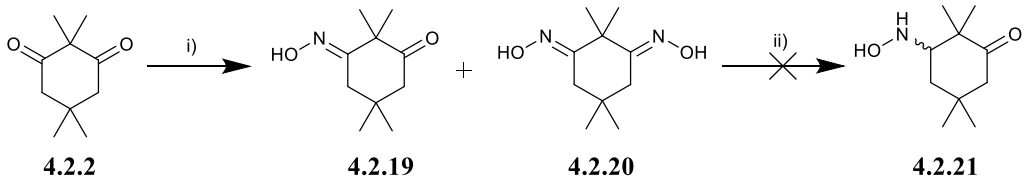

4.2.2 **4.2.19** **4.2.20** **4.2.21**

Figure 153: Proposed synthesis of compound **4.2.21**. Reaction conditions: i) hydroxylamine hydrochloride, NaOAc, EtOH, ii) ammonium acetate, sodium cyanoborohydride, titanium chloride, MeOH.

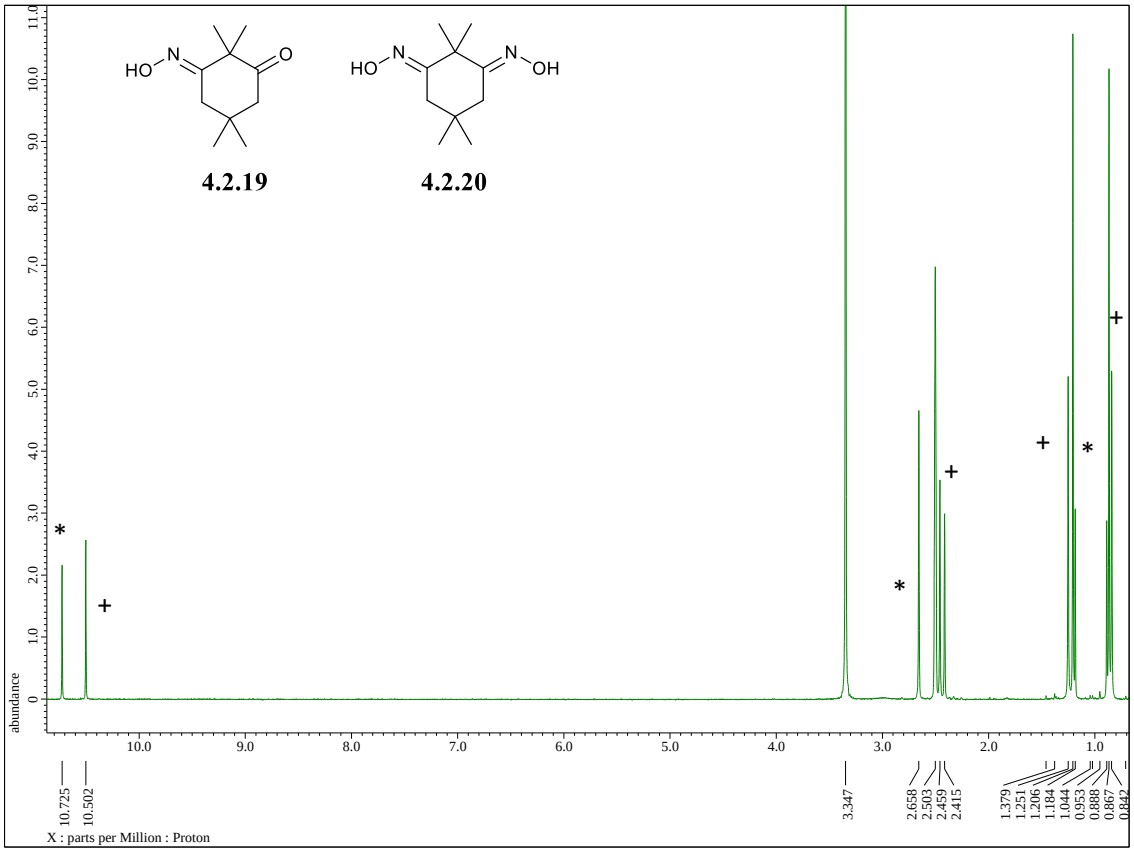

Figure 154: [1]H NMR spectrum of the crude product from the reaction of **4.2.2** with hydroxylamine hydrochloride to give the oximes **4.2.19** and **4.2.20**; where (*) represents the required product and (+) the bis-oxime **4.2.20**.

Next studied was the partial reduction of diketone **4.2.2** with sodium borohydride ($NaBH_4$) to obtain the hydroxyketone **4.2.22**, which could be then oxidised (SeO_2) to derive a novel diketone **4.2.23**, Figure 155. The formation of hydroxyketone **4.2.22** was achieved successfully using 0.25 equivalents of $NaBH_4$ following procedures reported by J. Petrova and co-workers.[162] A maximum yield of 68% of the desired product **4.2.22** was obtained in this reaction. In obtaining this yield various conditions were trialled such as low temperatures of 0 °C to control the product formation, varying equivalents of $NaBH_4$ and different solvents (ethanol, methanol and water). It was found that completing the reaction at room temperature, using a solvent mixture of ethanol/water obtained the best yields with the reaction completed in 15 minutes. An overlay of the [1]H NMR spectra, Figure 156, shows that as the starting material **4.2.2** disappears completely the formation of significant amounts of the over-reduced compound, diol **4.2.24** are observed. This is a recurring theme in many of the reactions used in this Chapter to functionalise the 1,3-diketone **4.2.2**. Fortunately, the starting 1,3-diketone **4.2.2**, desired hydroxyketone **4.2.22** and diol

4.2.24 compounds could be cleanly separated by careful column chromatography. The oxidation of the hydroxylketone **4.2.22** with selenium dioxide to give the novel diketone **4.2.23** was successful in a 46% yield for subsequent use in the condensation reactions to form the final target ligands.

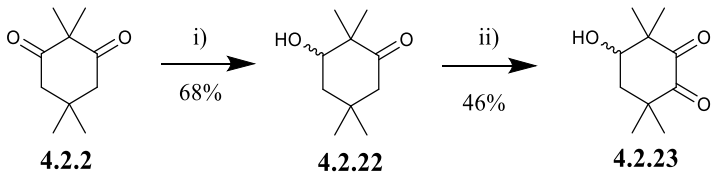

Figure 155: Reaction scheme showing the formation of novel dikeotne **4.2.23**. Reaction conditions: i) $NaBH_4$, H_2O, methanol; ii) SeO_2, 1,4-dioxane.

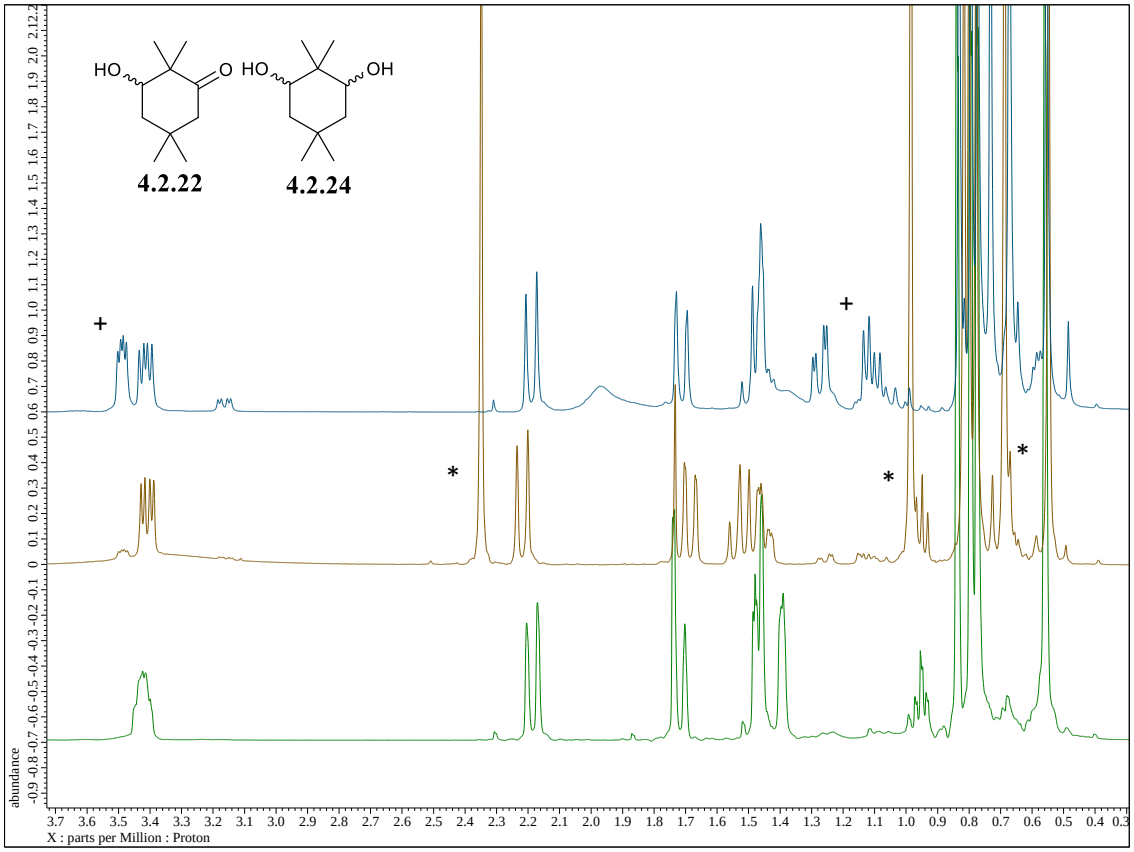

Figure 156: ^1H NMR overlaid spectra of the 3-hydroxyketone reaction stages; the desired hydroxyketone **4.2.22** (bottom spectrum), the desired **4.2.22** and the starting material **4.2.2** (denoted by *) (central spectrum) and the desired compound **4.2.22** and the diol **4.2.24** (denoted by +) (top spectrum).

The final condensation reactions between the diketone **4.2.23** and each of the three bis-amidrazones **3.2.2**, **3.2.5** and **3.2.9** were completed in ethanol, Figure 158. In the formation of the hydroxy-BTPhen **L45**, Figure 159, only one isomer was isolated which gave a well resolved NMR spectrum. It is suspected that there were more soluble isomers forming within the crude reaction mixture that were unable to be isolated and characterised. Similarly, the hydroxy-BTBP **L44** and hydroxy-BTP **L43** were obtained in relatively poor yields of 15 and 22%, respectively after recrystallization, Figure 157 and Figure 158. Further purification of the filtrate, in which product peaks were observed by ^{1}H NMR spectrum, was attempted by column chromatography. However, products were not eluted from the column due to the high polarity of the molecules, even when utilising the highly polar solvent methanol. It is proposed that reverse phase silica is a necessity for use in these purifications, to increase product yields. In terms of the possible isomers that could be obtained in these condensation reactions, they include regioisomers, enantiomers and diastereoisomers, Figure 160. Three regioisomers are possible as the diketone is non-symmetrical. In addition, as the diketone is chiral but racemic, each regioisomer could be obtained as a mixture of diastereomers (each existing as a pair of enantiomers). Obviously, this would be expected to lead to very complex NMR spectra for the crude products.^{1}H NMR spectroscopy can easily be used to distinguish between symmetrical and non-symmetrical regioisomers, as many of the proton's environments would be equivalent in the symmetrical regioisomers. On the other hand, the non-symmetrical regioisomer would display a higher number of non-equivalent proton resonances due to the lack of a plane of symmetry. The different diastereomers of a given regioisomer may not be as easy to distinguish by NMRspectroscopy if some of the resonances for each diastereomer overlap. However, all the regio- or stereoisomers of a given ligand should in principle exhibit very similar extraction properties as the changes made to the ligand structure are far removed from the *N*-donor atoms that coordinate to the metal.

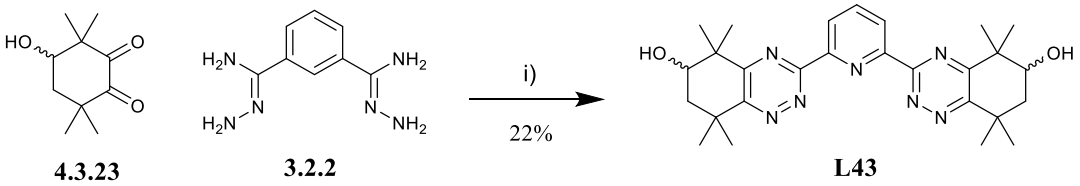

Figure 157: Synthesis of final BTP ligand **L43** *via* condensation reaction of **4.3.23** with **3.2.2**. The absolute stereochemistry at the chiral carbon atom is not shown. Reagents and conditions: i) EtOH, reflux.

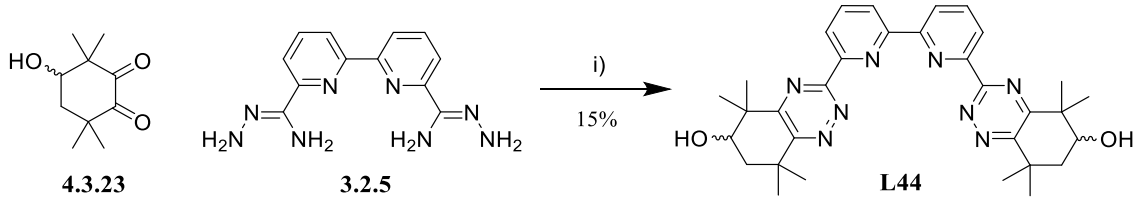

Figure 158: Synthesis of final BTBP ligand **L44** *via* condensation reaction of **4.3.23** with **3.2.5**. The absolute stereochemistry at the chiral carbon atom is not shown. Reagents and conditions: i) EtOH, reflux.

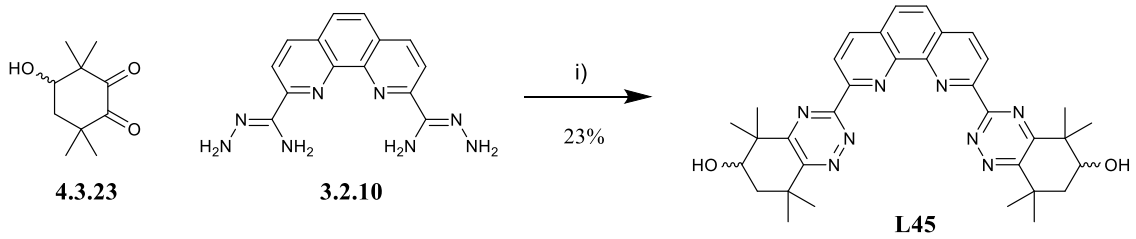

Figure 159: Synthesis of final BTPhen ligand **L45** *via* condensation reaction of **4.3.23** with **3.2.10**. The absolute stereochemistry at the chiral carbon atom is not shown. Reagents and conditions: i) EtOH, reflux.

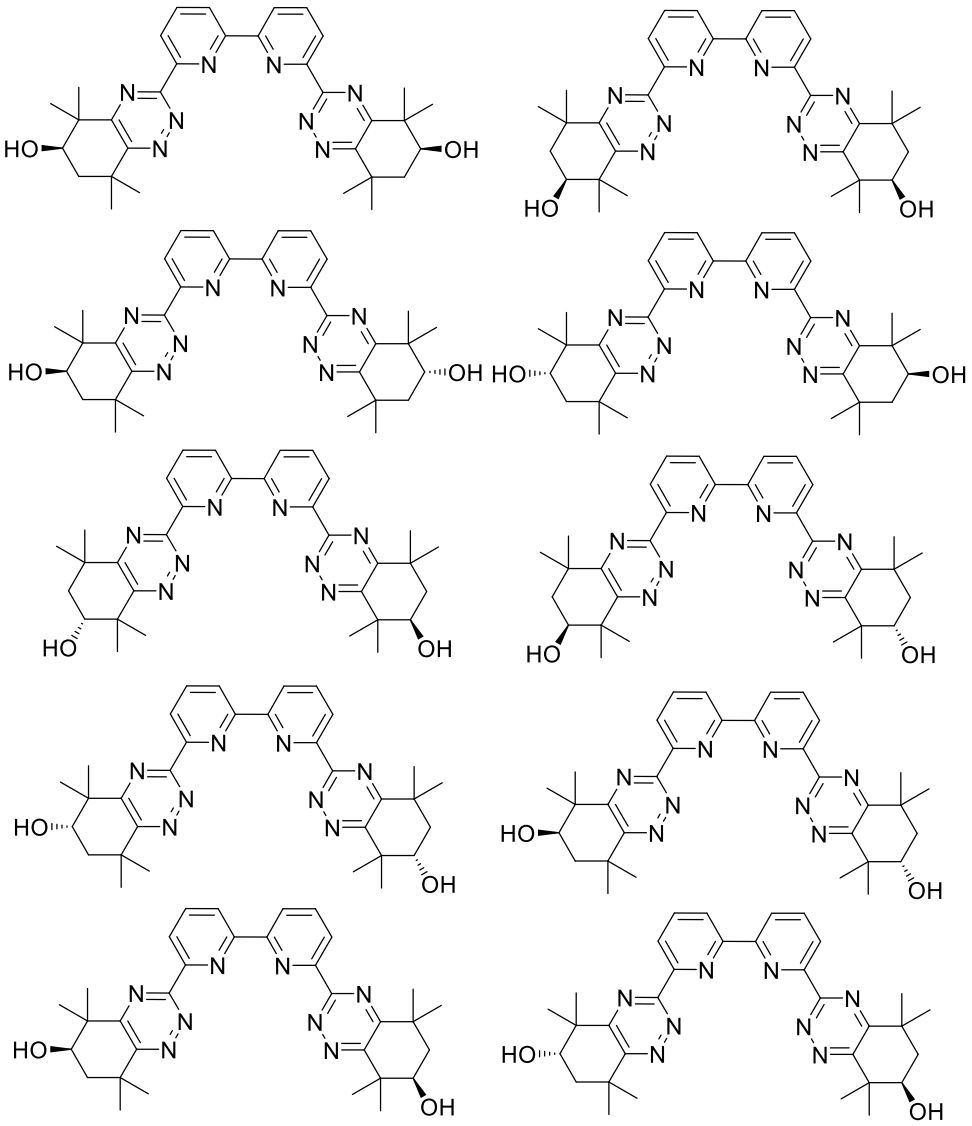

Figure 160: Representation of the possible regioisomers and diastereoisomers of BTBP ligand **L44**.

With the hydroxyketone **4.2.22** in hand, we next considered that an *O*-alkylation reaction of this compound to afford alkyl ether derivatives would be a useful way to tune the solubilities of the final bis-1,2,4-triazine ligands. Thus the *O*-alkylation of the hydroxy-ketone **4.2.22** with iodomethane and NaH as the base was achieved in reasonable yields of 51% to give the methyl ether **4.2.25**, Figure 161. The ^{1}H NMR spectrum of the crude product showed that some starting material remained in this reaction and it was suspected that some of the iodomethane (b.p. 42 °C) had evaporated prior to the reaction reaching completion. In an effort to force the reaction towards completion, the reaction was completed at a lower temperature, to ensure loss of the iodomethane

by evaporation was avoided. Additionally the iodomethane was added sequentially over the period of the reaction, improving the isolated yields of the methyl ether **4.2.25** to 82%. The oxidation of **4.2.25** using SeO_2 in 1,4-dioxane was a high yielding reaction that gave the diketone **4.2.26** in 86% yield.

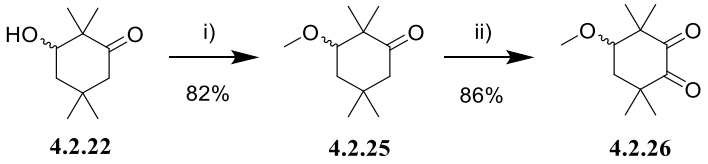

Figure 161: Synthesis of novel methoxy-diketone **4.2.26**. Reagents and conditions: i) iodomethane, NaH, THF; ii) SeO_2, 1,4-dioxane.

Finally the condensation reactions of diketone **4.2.26** with each of the bis-amidrazones **3.2.2**, **3.2.5** and **3.2.10** in refluxing acetic acid gave the final novel ligands **L46**, **L47** and **L48**, Figure 162 and Figure 163. The methoxy-BTPhen ligand **L48** was isolated as a solid following removal of the unreacted amidrazone **3.1.10** by trituration of the filtrate with diethyl ether. The methoxy-BTP **L46** and methoxy-BTBP **L47** were unable to be obtained as a suitably pure sample, as observed in the ^{1}H NMR spectrum, for extraction testing through trituration, recrystallisation or column chromatography.

Further alkylation reactions of ketone **4.2.22** with different alkyl iodides would have been investigated had time allowed, in order to gain a greater understanding of how increasing the alkyl chain length impacts the extraction properties (especially solubility) in the solvent extraction experiments.

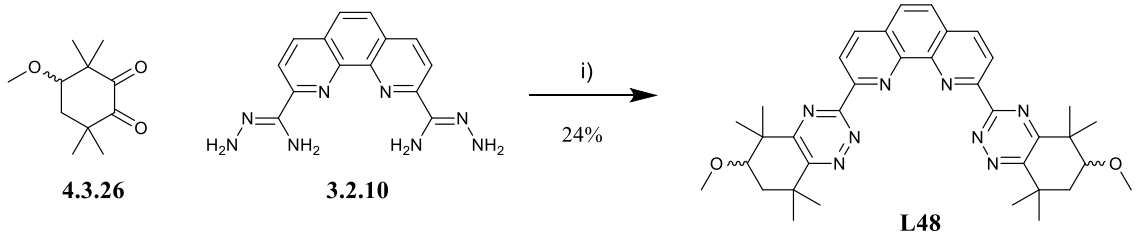

Figure 162: Condensation reaction of diketone **4.3.26** with **3.2.10** to form the final novel BTPhen ligand **L48**. Reaction conditions: i) AcOH, reflux.

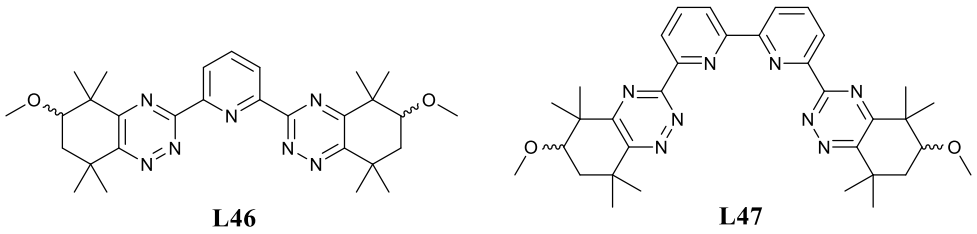

Figure 163: Molecular structures of the methoxy-bis-1,2,4-triazine ligands **L46** and **L47**.

The methoxy-BTPhen ligand **L48** was purified by a recrystallisation from diethyl ether. The ligand ^{1}H NMR spectrum observes a broad signal at δ 3.30 ppm, indicative of a water molecule. Completing a D_2O shake upon the NMR sample resulted in a complete disappearance of this signal, Figure 164. The deuterium in D_2O will exchange with those exchangeable protons present in the sample, such as those from H_2O. The presence of such a water molecule in the ligands coordination cavity was similarly observed with $CyMe_4$-BTPhen **1.17**, which may aid in the ability of this ligand sitting to reside at the phase interface.

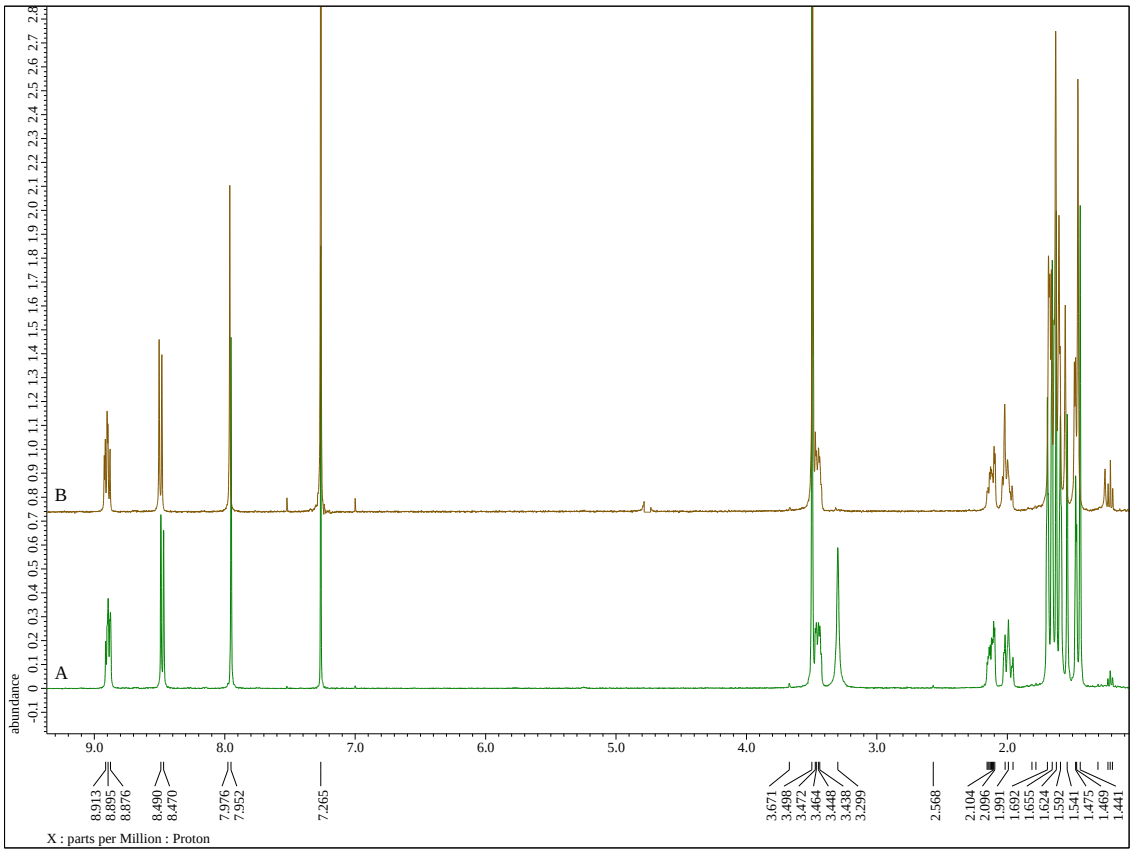

Figure 164: Overlaid ^{1}H NMR spectra of the methoxy-$CyMe_4$BTPhen ligand **L48**; (a) before and (b) after a D_2O shake.

Table 20: Assignment of NMR signals for the major isomer of the methoxy-CyMe$_4$-BTPhen **L48**.

^{1}H (ppm)	Proton integration and multiplicity (Hz)	^{13}C (ppm)	Assignment
8.90	2H, t, *J* = 7.79	137.3	2 x ArCH
8.48	2H, d, *J* = 7.79	127.6	2 x ArCH
7.95	2H, s	123.5	2 x ArCH
3.50	6H, s	81.2	2 x CH_3
3.46	2H, dd, *J* = 6.41, 3.67	57.6	2 x CH
3.30	2H, br, s	-	H_2O
2.15 – 2.10	2H, m	36.6, 36.5	2 x CH
2.03 – 1.96	2H, m	36.6, 36.5	2 x CH
1.69 – 1.44	24H, m	31.4, 31.0, 30.7, 30.2, 26.4, 25.9, 23.6, 23.0	8 x CH_3

Introduction of an *N*,*N*-dimethylamide group into the hydroxy-ketone **4.2.22** was next investigated through an *O*-alkylation reaction using 2-chloro-*N*,*N*-dimethylacetamide **4.2.4**, Figure 165. Following procedures by K. Ohgane and co-workers this was achieved in a 60% yield to give compound **4.2.27**, Figure 166.[168] The final oxidation step to the novel diketone **4.2.28** using SeO_2 was achieved in a 44% yield and could be monitored via ^{1}H NMR spectroscopy by the disappearance of the AB system adjacent to the carbonyl group in **4.2.27**, Figure 166.

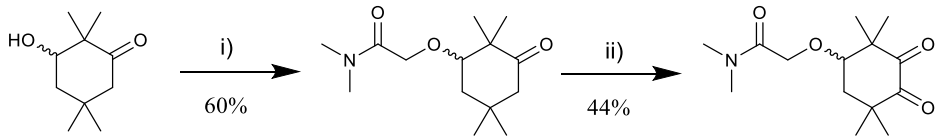

4.2.22 **4.2.27** **4.2.28**

Figure 165: Synthetic pathway to form novel diketone **4.2.28.** Reaction conditions i) 2-chloro-*N*,*N*-dimethylacetamide, NaH, THF, ii) SeO_2, dioxane.

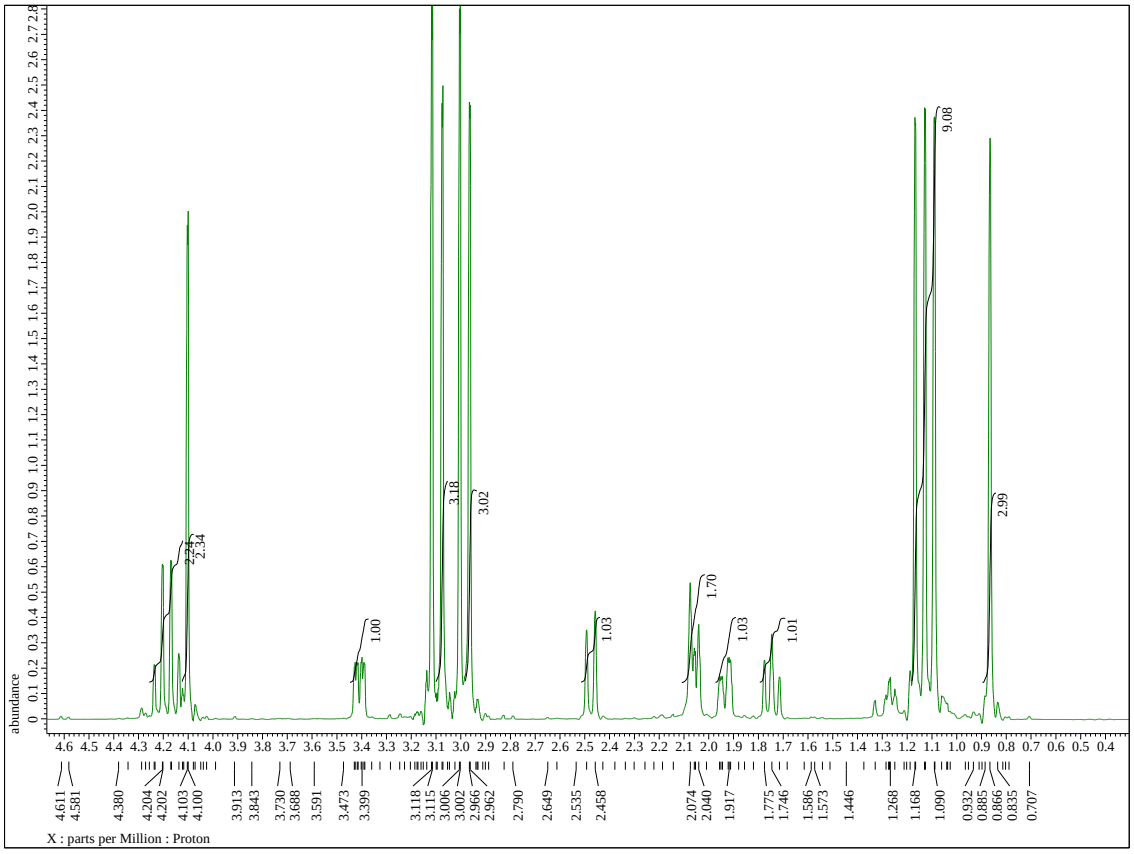

Figure 166: ^{1}H NMR spectrum of compound **4.2.27**.

The condensation reaction of diketone **4.2.28** with the bis-amidrazones **3.2.2** to form the final ligand acetamide-BTP **L49** was attempted in acetic acid, Figure 167. In this reaction the crude ^{1}H NMR spectrum suggested product formation, with the disappearance of the broad NH_2 peaks from the respective amidrazone being observed. However, obtaining a clean, well resolved NMR spectrum proved difficult in the deuterated solvents available, with broad and unclear signals being observed and further attempts at purification were unsuccessful. As a result, these ligands were not taken forward for solvent extraction testing.

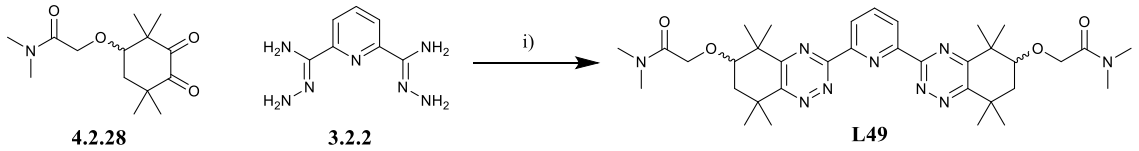

Figure 167: Representative condensation reaction of **4.2.28** with the bis-amidrazone **3.2.2** to give the target ligand **L49**.

The *O*-alkylation of the hydroxy-ketone **4.2.22** with poly-ethylene glycol (PEG) based alkylating agents were then explored as an alternative method of introducing an ether group(s) as hydrogen bond acceptors into the ligands. The reaction of **4.2.22** with 2-bromoethyl methyl ether resulted in the formation of **4.2.29** in a 16% yield, Figure 168. The final oxidation step to the novel diketone **4.2.30** was completed in 51% yield using SeO_2, but in order to obtain enough sample of the dikeone **4.2.30** for ligand synthesis to be completed, it was necessary to first try and improve the yield of the *O*-alkylation step. The disappearance of the AB system next to the carbonyl group in **4.2.29** can be clearly observed when comparing ^{1}H NMR spectra of **4.2.29** and **4.2.30**, Figure 169.

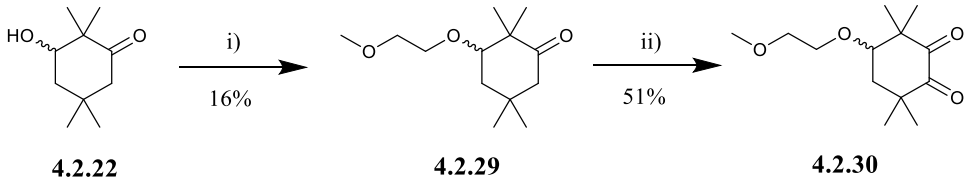

4.2.22 **4.2.29** **4.2.30**

Figure 168: Synthesis of the novel diketone **4.2.30** *via O*-alkylation of **4.2.22**. Reaction conditions: i) 2-bromoethyl methyl ether, NaH, THF (anhy.) ii) SeO_2, 1,4-dioxane.

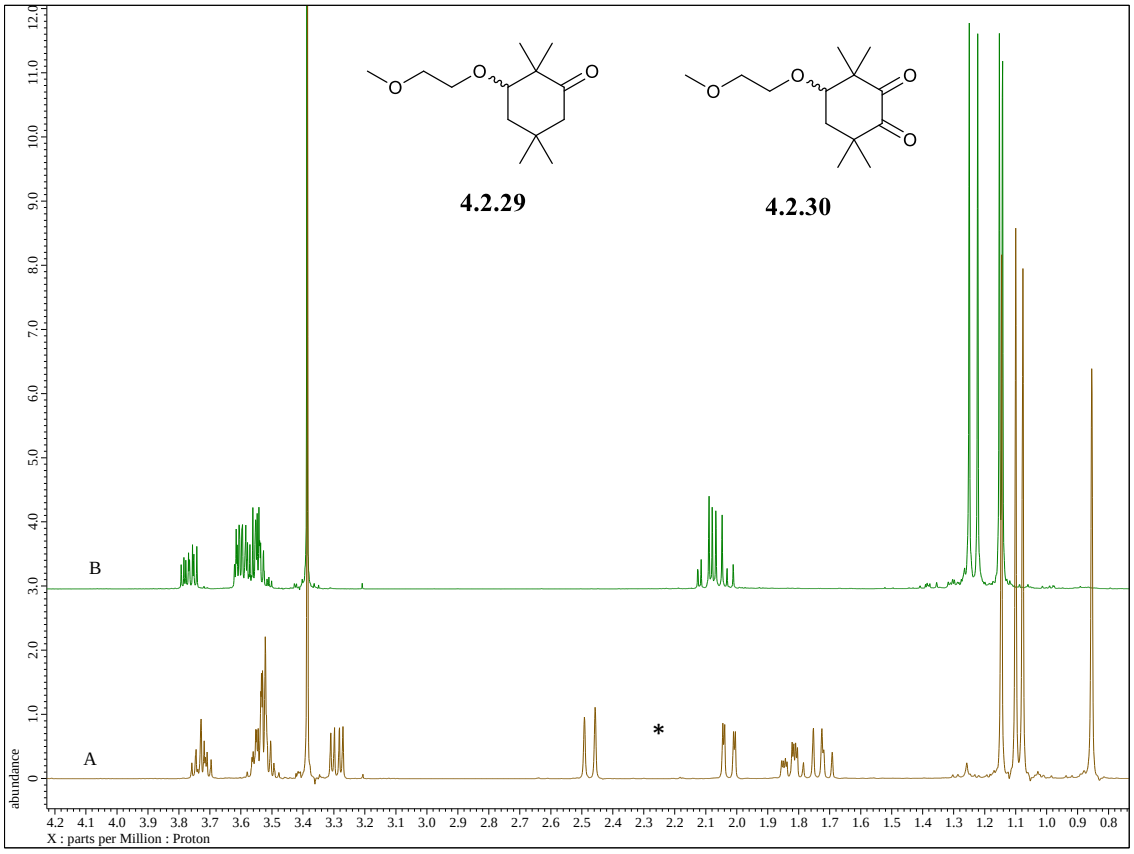

Figure 169: Overlaid ^{1}H NMR spectra of (a) compound **4.2.29** and (b) diketone **4.2.30** showing disappearance of AB proton system (*).

The synthetic chemistry discussed in this section led to the successful formation of novel BTP, BTBP and BTPhen ligands derived from modified derivatives of $CyMe_4$-diketone **4.1.1**. Due to the symmetrical nature of the starting 1,3-diketone dimedone **4.2.2** some of the reactions proved difficult to obtain the required diketone, and mixtures of products were obtained. A protecting group strategy could be considered, wherein one of the carbonyl groups could be protected (eg: as an acetal). Continued optimisation of the synthesis could lead to the successful synthesis of the 1,2-diketones discussed above that can then be taken forward for further investigations. In subsequent sections, the solubilities and solvent extraction properties of the obtained ligands are discussed.

4.3. Calculated ligand parameters

For each of the ligands synthesised in section 4.2, their ligand parameters that could be used as predictors of ligand solubility and rates of extraction have been calculated to enable comparisons between theoretical and experimental data in line with the project objectives. It is hoped that a set

of general guidelines can be established from this based upon the theoretical values that can be used indicate the solubility and rates of extraction of a given ligand prior to its synthesis. For the ligands successfully synthesised in section 4.2, their theoretical results are given in Table 21.

Of those ligands synthesised, the ketone-substituted ligands (**L40**, **L41** and **L42**) would be expected to have a decreased solubility in comparison to the benchmark ligands due to a reduction in their theoretical Fsp^3 and log *P* values. On the other hand, the theoretical data for the methoxy-ligands (**L46**, **L47** and **L48**) indicate that an increased solubility should be expected in 1-octanol, constituting an improvement on the corresponding benchmark $CyMe_4$ ligands **1.30**, **1.09** and **1.17**. There is, as observed previously, a contradicting trend in the log *P* and Fsp^3 values when considering the different ligand families derived from the same diketone. There is an increase in calculated log *P* values across the series BTP < BTBP < BTPhen, with the opposite trend being observed for the corresponding calculated Fsp^3 values.

As dictated in the aims and objectives the addition of HBD and HBA functional groups was intended to confer an increased concentration of the ligand at the phase interface, in order to increase the rates of metal extraction (extraction kinetics). With this in mind, a variety of different functional groups, (ketone, hydroxyl and methoxy groups) were introduced into the benchmark $CyMe_4$-ligands so their effects on ligand solubility and rates of extraction could be investigated. Based upon the HBD and HBA values in Table 22, all ligands would be expected to have improved extraction kinetics based upon the discussed hypothesis. Of these ligands the hydroxyl-substituted ligands would be expected to have the greatest increase in rates of extraction.

Table 21: Table showing calculated ligand parameters for the novel $CyMe_4$-ligands. Only one regioisomer is represented in each case.

Ligand	Code	Log P	Fsp^3	HBD	HBA
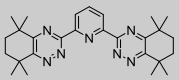	**1.30**	5.45	0.59	0	7
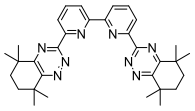	**1.09**	6.01	0.50	0	8
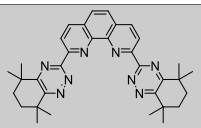	**1.17**	7.04	0.47	0	8
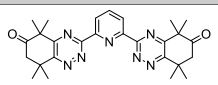	**L40**	3.01	0.52	0	9
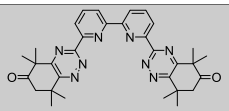	**L41**	3.76	0.44	0	10
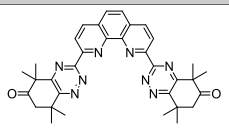	**L42**	4.43	0.41	0	10
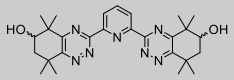	**L43**	3.49	0.59	2	9
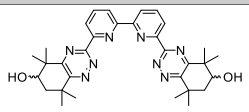	**L44**	4.40	0.50	2	10
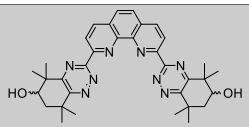	**L45**	5.34	0.47	2	10
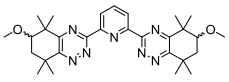	**L46**	5.17	0.67	0	9
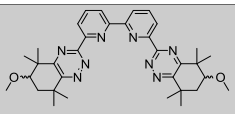	**L47**	5.89	0.56	0	10
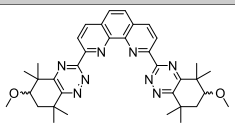	**L48**	6.78	0.53	0	10

4.4. Solubility Studies

The solubilities of the novel ligands were investigated in 1-octanol using the procedure disclosed in Chapter 6. These ligands will be compared to the benchmark ligands; $CyMe_4$-BTP **1.30**, $CyMe_4$-BTBP **1.09**, $CyMe_4$-BTPhen **1.17**. Table 22 present the novel functionalised $CyMe_4$-ligands synthesised, alongside their individual Fsp^3 and measured solubility values. The applicability of the Fsp^3 and log *P* values for individual ligands in predicting the solubility will be considered based upon the experimental results shown, as discussed in section 1.5.

Increasing the number of aromatic rings on moving from BTP to BTBP to BTPhen decreases the measured solubilities in line with a decreasing Fsp^3 value. The lowest solubility that was able to be obtained was for the hydroxy-$CyMe_4$-BTPhen **L45**. In contrast, the methoxy-$CyMe_4$-BTPhen **L48** shows a much greater solubility in 1-octanol, suggesting the addition of the methyl groups has drastically improved the solubility. Similar observations have been made when investigating the effect of increasing alkyl chain length with BTPhen ligands against solubilities.[102]

Table 22: The respective Fsp^3 values and measured solubilities for the novel $CyMe_4$-functionalised ligands.

Number	Structures	Solubility mmol/L in 1-octanol	Fsp^3 value
L40	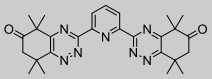	101.6	0.52
L41	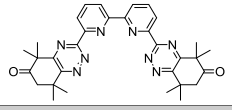	13.6	0.44
L42	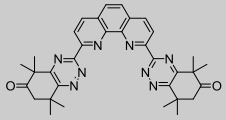	-	0.41
L43	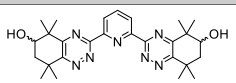	-	0.59
L44	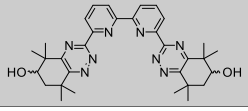	20.3	0.50
L45	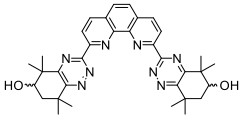	4.9	0.47
L48	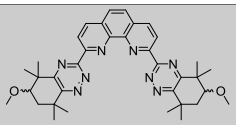	70.6	0.53

4.5. Extraction Studies

The hydroxy and ketone-substituted derivatives of the BTBP (**L41** and **L44**) and BTPhen (**L42** and **L45**) ligands, respectively, exhibited very low solubilities in the standard solvent used for the extraction studies, 1-octanol. This was so drastic for the hydroxy-BTPhen **L45** that the extraction screening study was unable to be completed. The hydroxy-BTBP **L44**, ketone-BTBP **L41** and ketone-BTPhen **L42** ligands were tested at concentrations <10 mM as a result of their poor solubility. The limited solubility seen with the BTPhens in particular, correlates to the calculated Fsp^3 values obtained. These values were 0.41 and 0.47 for the ketone-BTPhen **L42** and hydroxyl-BTPhen **L45** respectively, both equal to and lower than the corresponding benchmark ligand $CyMe_4$-BTPhen **1.17** and the lowest of all the functionalised $CyMe_4$-BTPhen ligands.

The ligand **L43** required the addition of *tert*-butyl benzene to ensure dissolution of the ligand with the concentration adjusted accordingly to maintain a concentration of 0.01 M for the increased volume of diluent. After completing the extraction test with varying nitric acid concentrations for the standard duration of 1 hour, there was no observed precipitate in the sample, Figure 170.

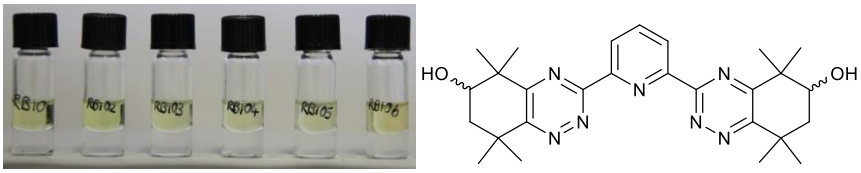

Figure 170: (a) Photographs of the sample tubes after the first screening test using **L43**, with increasing [HNO_3] from left to right; (b) molecular structure of **L43**.

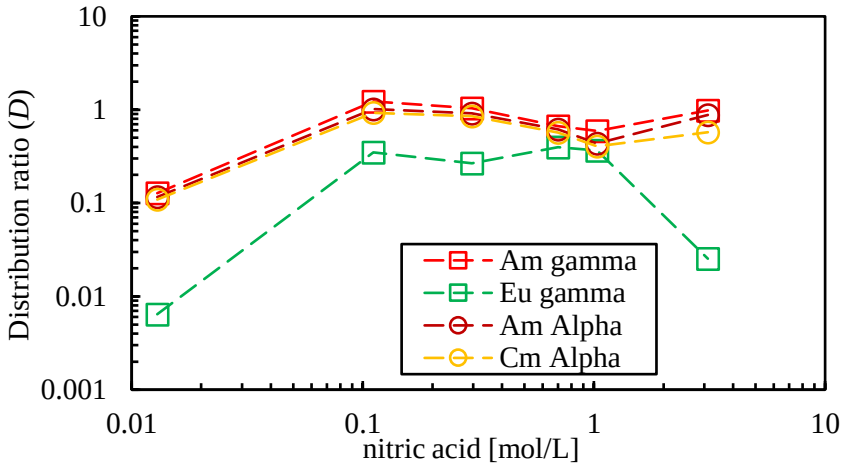

Figure 171: Distribution ratios for extraction of ^{152}Eu, ^{241}Am, ^{244}Cm by **L43** measured by α- and γ-spectroscopy as a function of the nitric acid concentration of the aqueous phase (1 hr, 22 °C at 2,200 rpm). Organic phase: 10 mM **L43** in 1-octanol/*tert*-butylbenzene (ratio: 7/1).

With increasing HNO_3 concentration, the distribution ratios rise gradually before levelling off for Am and Cm, Figure 171. It is known that Ln(III) complexes of bis-triazine ligands are thermodynamically less stable than those of An(III) complexes and may aid in explaining the drop in *D* ratios for Eu(III). This decrease in the D_{Eu} may result from an increased competition between ligand protonation and ligand complexation, with the Eu-ligand complexes less likely to form at this concentration. Such phenomenon have been observed previously in theoretical and experimental investigations with ligands containing the 1,2,4-triazine rings.[169] It can be assumed that this effect would similarly be observed in this ligand due to its similarity. The maximum SF obtained for this ligand is 38.78, considerably lower than the $CyMe_4$-BTP, which has a SF of 5000, Section 1.5.2.

The extraction study with **L44** was completed at a concentration lower than 0.1 M in 1-octanol as a result of its low solubility. The addition of *tert*-butyl benzene had little effect on aiding the dissolution of the ligand and it was decided to screen the ligand at the lower concentration with efforts made to avoid the precipitated ligand. After contact with the HNO_3 aqueous phase for 1 hour there was precipitate observed at the interface and throughout the (organic phase) for RBR-131, at the lowest HNO_3 concentration, Figure 172. This precipitation is deemed to be the insoluble material transferred from the prepared organic phase when preparing the extraction. At

higher HNO_3 concentrations we see minimal to no precipitation after phase contact suggesting the acidic aqueous phase somehow aids in dissolution of the ligand sample. As a result of the solubility issue, and hence lower concentration of the ligand in the organic phase, lower *D* ratios were expected.

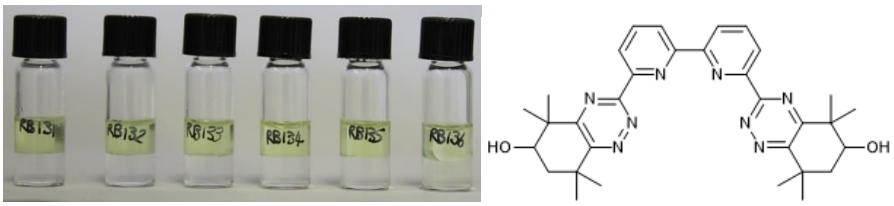

Figure 172: (a) Photographs of the sample tubes after the first screening test using **L44**, with increasing [HNO_3] from left to right; (b) molecular structure of **L44**.

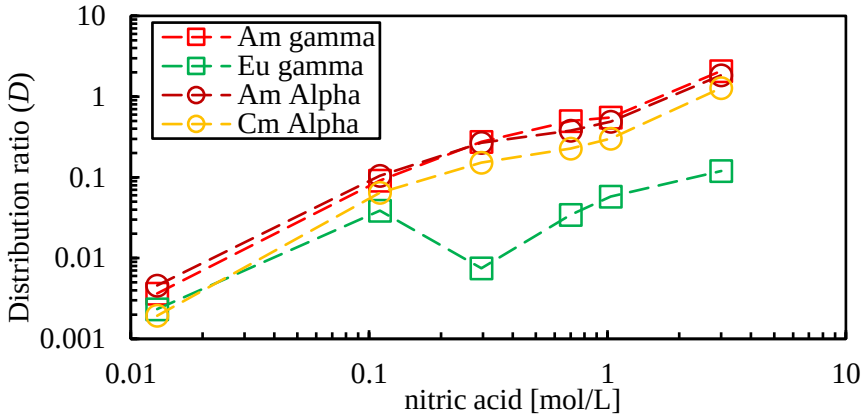

Figure 173: Distribution ratios for extraction of ^{152}Eu, ^{241}Am, ^{244}Cm by **L44** measured by α- and γ- spectroscopy as a function of the nitric acid concentration of the aqueous phase (1hr, 22 °C at 2,200 rpm). Organic phase: <10 mM **L44** in 1-octanol/*tert*-butylbenzene (ratio: 7:1)

There is a gradual increase in the *D* ratio for both An(III); Am(III) and Cm(III) as a function of the HNO_3 concentration, Figure 173. Interestingly, for Eu(III) there is a drop in the *D* ratio at 0.296 M HNO_3 before it gradually increases again thereafter. This results in an increase in the $SF_{Am/Eu}$ to 36.83 where previously it had been minimal at the lowest HNO_3 concentrations, at 2.36. Further research into increasing the HNO_3 concentration beyond 3 M may be necessary to see if the *D* ratio continues to increase to values above 1, otherwise this ligand would be unsuitable for the reprocessing industry. Additional studies could be completed in the future using this ligand and a phase transfer agent, as was carried out with $CyMe_4$-BTBP **1.09**, to see how this impacts on the extraction performance.

The introduction of the ketone group in ligand **L40** has a slightly negative impact on the *D* ratios for Am(III) and Cm(III) when compared to the hydroxyl-BTP **L43**, especially at the lower HNO_3 concentrations, Figure 174. The $SF_{Am/Eu}$ is consistently above 60 from the concentration of 0.01 M. Although there is a general increase in *D* ratios as the HNO_3 concentration increases this reaches a maximum of 0.9 at 1 M HNO_3, which would be unsuitable for the reprocessing industry. The slight drop in the *D* value for all radioisotopes at 3 M HNO_3 is likely to be a result of the precipitate that was observed at the interface during this particular screening test.

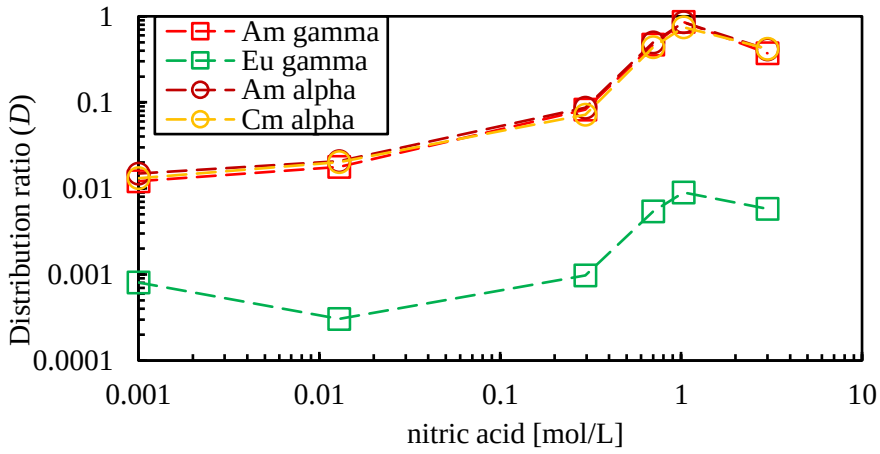

Figure 174: Distribution ratios for extraction of ^{152}Eu, ^{241}Am, ^{244}Cm by **L40** measured by α- and γ- spectroscopy as a function of the nitric acid concentration of the aqueous phase (1hr, 22 °C at 2,200 rpm). Organic phase: 10 mM **L40** in 1-octanol.

A parallel observation was made for **L41** in comparison to **L44**, in which the ligand didn't fully dissolve in the diluent. Based upon the calculated parameters for these ligands, in which the log *P* and Fsp^3 were low, a reduced solubility in 1-octanol was predicted. Again, at the lowest nitric acid concentration there was significant precipitation observed, but this disappears with increased HNO_3 concentrations, Figure 175. Interestingly, upon contact with the 3 M HNO_3 aqueous phase, a change in colour of the organic phase and some leaching of colour into the aqueous phase was observed. Although the exact reason for this is unclear, it could be a result of dissolution of the protonated ligand into the aqueous phase at higher HNO_3 concentrations due to the fact the ligand is less lipophilic than $CyMe_4$-BTBP **1.09**. There is an increase in the *D* ratios of all radioisotopes from 0.1 M to 1.0 M HNO_3 concentrations, Figure 176. When in contact with the 3 M HNO_3

aqueous phase, there is a decrease in the observed *D* ratios, which may coincide with the observed leaching of colour, and most likely dissolution of the ligand **L41**, into the aqueous phase. The $SF_{Am/Eu}$ reaches a maximum of 145 observed at 0.1 M HNO_3. At the required conditions for the SANEX process (3-6 M HNO_3), the $SF_{Am/Eu}$ falls to 96. Despite this, as the *D* ratio for Am(III) and Cm(III) remain below 1 across all concentrations it would be an unsuitable ligand choice for the reprocessing industry, as an increased number of extraction steps would be required to extract all the An(III) when compared to a ligand with greater *D* ratios.

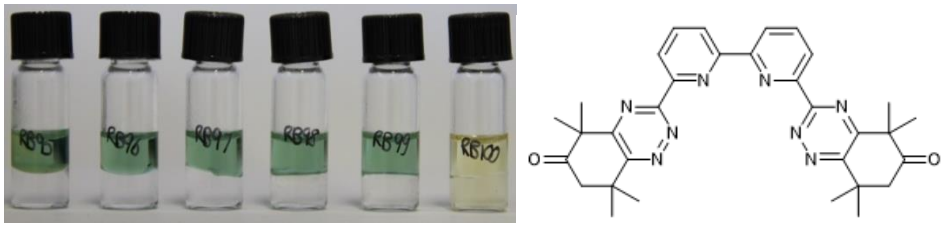

Figure 175: (a) Photographs of the sample tubes after the first screening test using **L41**, with increasing [HNO_3] from left to right; (b) molecular structure of **L41**.

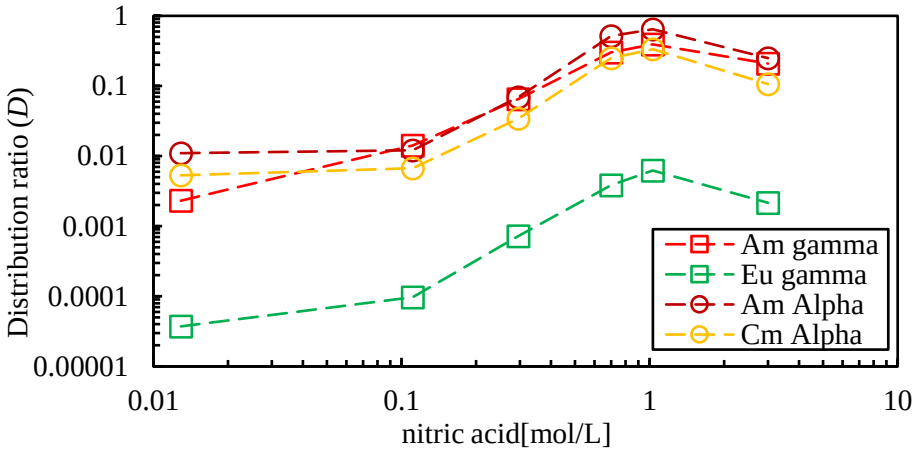

Figure 176: Distribution ratios for extraction of ^{152}Eu, ^{241}Am, ^{244}Cm by **L41** measured by α- and γ- spectroscopy as a function of the nitric acid concentration of the aqueous phase (1hr, 22 °C at 2,200 rpm). Organic phase: 10 mM **L41** in 1-octanol.

The methylated ligand **L48** was tested for its extraction properties following previous procedures. There was no observed precipitate formation for the methoxy-BTPhen ligand **L48** across all HNO_3 concentrations, Figure 177. There was a notable colour change of the organic phase when the screening test was completed at 3 M HNO_3, which correlates to a decrease in the *D* ratio for all radioisotopes. This could be due to ligand protonation at the higher acidity, which would

compete with metal ion complexation. Unfortunately, ligand kinetic studies were unable to be completed with this ligand due to time constraints during the research visits.

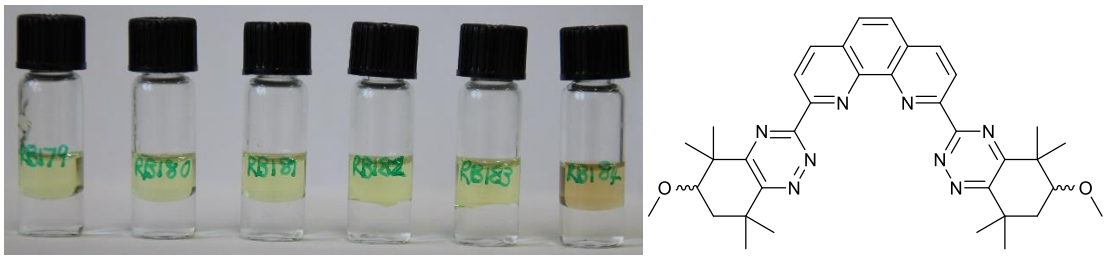

Figure 177: (a) Photographs of the sample tubes after the first screening test using **L48**, with increasing [HNO_3] from left to right; (b) molecular structure of **L48**.

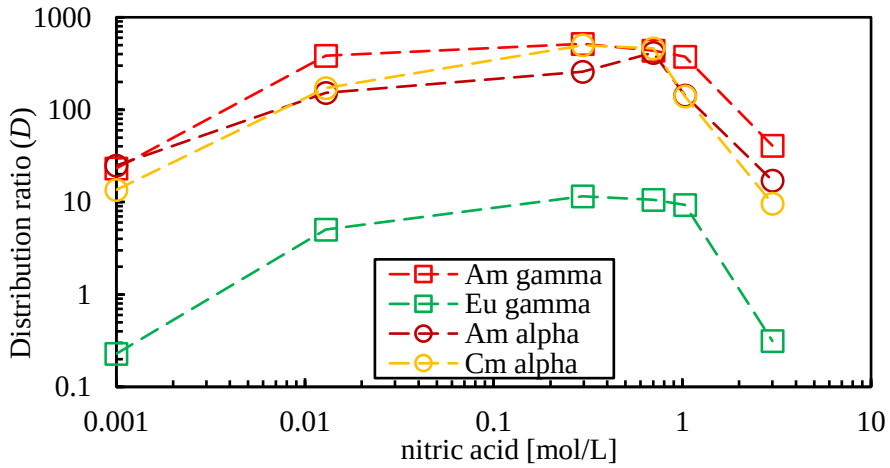

Figure 178: Distribution ratios for extraction of ^{152}Eu, ^{241}Am, ^{244}Cm by **L48** measured by α- and γ- spectroscopy as a function of the nitric acid concentration of the aqueous phase (1hr, 22 °C at 2,200 rpm). Organic phase: 10 mM **L48** in 1-octanol.

Across all HNO_3 concentrations the *D* ratios for both Am(III) and Cm(III) by ligand **L48** were above 10. The maximum *D* ratio obtained for Am(III) was over 500 (from γ-spectroscopy) at 0.7 M HNO_3, Figure 178. Thus, a very efficient extraction of Am(III) and Cm(III) was observed by ligand **L48**. There is a slight disparity between the results obtained for α- and γ-spectroscopy as a result of some solid deposits upon the α-plates, which can have a negative impact upon the results obtained. However the *D* ratio for Am(III), as obtained via α-spectroscopy, is still over 400 at the same HNO_3 concentration. Alongside this, the relatively high *D* ratios observed for Am(III) and Cm(III) at 0.001 M HNO_3 may result in non-optimum performance during the back extraction (stripping) stages of a future process, where the metal is back-extracted removed from

the loaded organic phase into dilute HNO_3 so the organic phase/ligand can be recycled. This is typically completed at low HNO_3 concentrations where ideally the *D* ratios for Am(III) and Cm(III) are below 1. The $SF_{Am/Eu}$ averages at 40 across the HNO_3 concentrations, with a maximum value over 100 being obtained at 0.001 M HNO_3 and 3.0 M HNO_3. Thus, the extraction of Am(III) and Cm(III) by this ligand is highly efficient and reasonably selective, though the Am(III)/Eu(III) selectivity is not as high as that observed previously for $CyMe_4$-BTPhen **1.17**.[95]

4.6. Conclusion

The addition of the hydroxyl group to the benchmark $CyMe_4$-ligands doesn't appear to improve the solubility of the ligands within required diluents, up until the extreme case where we were unable to test **L45** as a result of its insolubility. A similar observation was made for the ketone-derived ligands (**L40**, **L41** and **L42**). This poor solubility also resulted in difficulty during synthesis and analysis meaning it could result in drastic issues during industry implementation where precipitation must be avoided at all costs due to the complexity of monitoring the system. Although this effect is reduced for the BTBP and then again in the BTP, there is still a solubility issue for the **L44**. These results correlate to the low Fsp^3 values for these ligands and confirm the methodology. Those ligands with the greatest Fsp^3 values, 0.59 and 0.53 for **L43** and **L48**, respectively showed no precipitate once in the diluent used for the screening test.

The introduction of the additional HBD/HBA functional groups in the hydroxyl-derived ligands and ketone-derived ligands appears to negatively impact the extraction capabilities of these ligands. This is most likely as a consequence of their reduced solubility in the utilised diluent. The methoxy-BTPhen **L48** in contrast shows excellent extraction properties up until a HNO_3 concentration of 1 M.

Overall, these ligands offer mixed results in which the addition of HBD/HBA functional groups appears to have hindered their extraction capabilities rather than enhanced as previously expected, which may be a consequence of the groups used. Further studies would be necessary with this ligand in particular, specifically a study on its extraction kinetics as well as considering using longer alkyl chains when forming the ether.

Chapter 5

Conclusions and Future Work

5. Conclusions and Further Work

5.1. Future Work

The use of novel, modified bis-triazine ligands should be subject to more, detailed examination in future. A greater range of modified camphor-BTP, camphor-BTBP and especially camphor-BTPhen ligands should be synthesised and screened for selective actinide extraction. Similarly, the synthesis and screening of a greater range of modified $CyMe_4$-ligands (BTP, BTBP and especially BTPhen) is also warranted. This will not only identify the best functional groups that confer the optimum extraction properties to each family of ligands, but will also allow the novel ligand design approach discussed herein to be fully validated for a much greater range of ligands.

In order to establish more definite solubility values for those ligands with promising applications, a more robust method for testing solubility would need to be applied. Due to the limited quantities of some of the samples obtained, a different volume of 1-octanol was added to each vial. A more precise method may be to see how much of each ligand dissolves in a fixed volume (eg: 1 mL) of 1-octanol, to determine the saturation point. The results obtained could provide additional evidence for the positive correlation observed between the Fsp^3 values of the ligands and the solubility results obtained.

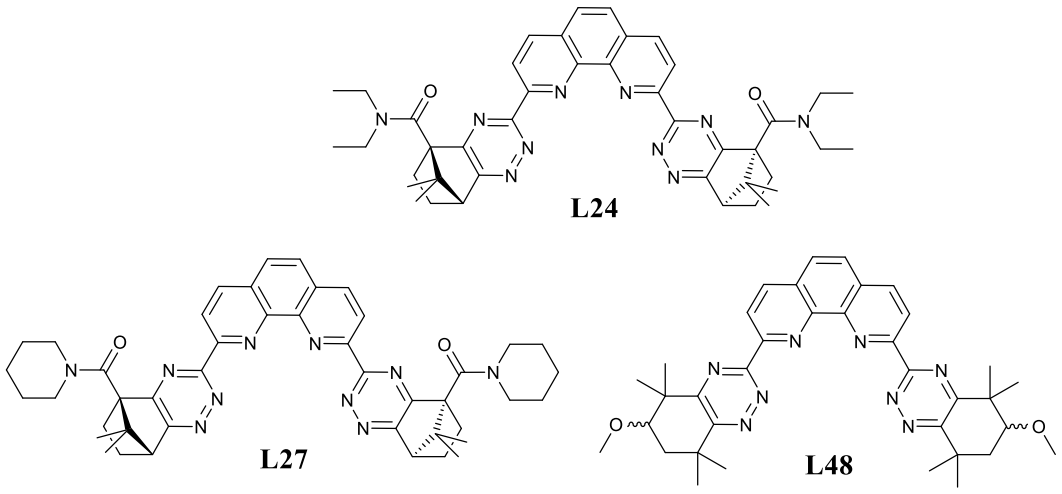

Figure 179: Structures of the most prominent ligands for future development.

In terms of those ligands which showed promise for their development for a future industrial process, in particular **L24**, **L27** and **L48**, further studies will need to be completed, Figure 179.

Studying the extraction of Am(III) and Cm(III) in the presence of all the trivalent lanthanides as well as some interfering fission and corrosion products would determine the likely applicability of the ligands for further process development (eg: towards being implemented in a laboratory-scale 'hot-test' using genuine spent fuel solutions). Studying the stabilities of the ligands towards radiolysis will establish the likely lifetime of the ligand when used under real process conditions, i.e. how many times the ligand can be recycled for continuous use before it degrades. Extraction kinetics studies on **L27** will allow a comparison between this and the diethylamine-derived BTPhen ligand **L24**, to determine which shows the greatest improvement when compared to the benchmark ligand $CyMe_4$-BTBP **1.09**. The effects of different solvents will need to be explored to determine their impact on the distribution ratios and separation factors. It has previously been shown that the diluent can have a drastic impact not only on ligand solubility but also on the distribution ratios of individual isotopes, as in the case of camphor-BTP **1.31** when dissolved in 1-octanol or a kerosene/1-octanol mixture.

In further developments, it would be interesting to explore in more depth exactly how and why these ligands complex and extract trivalent actinides at the molecular level. For example, it would be useful to experimentally determine the pKa values of the novel ligands. This would give an understanding of how easily these ligands are protonated when in contact with the nitric acid aqueous phase. In addition, measurement of the stability constants of the lanthanide and actinide complexes (e.g. by UV-vis spectrophotometry or time-resolved laser-induced fluorescence spectroscopy) would be useful to determine the different thermodynamic stabilities of the formed metal complexes, which has previously been shown to correlate with actinide/lanthanide extraction selectivity. Together with further studies aimed at probing the stoichiometries of the formed complexes (eg: by NMR titrations, ESI-MS, X-ray crystallography), this would help to rationalise some of the observed solvent extraction results, particularly when poor metal extraction is observed.

5.2. Conclusions

Within the discussed work, the main aims and objectives were to improve both the solubility and rates of extraction for the currently available benchmark ligands $CyMe_4$-BTBP **1.09** and $CyMe_4$-

BTPhen **1.17**. A variety of novel bis-1,2,4-triazine ligands were successfully synthesised via three different approaches that involved introducing an amine bridge into the BTP ligand structure, functionalising the camphor group in the camphorquinone-derived ligands and synthesising a range of ligands via functionalised $CyMe_4$-diketone derivatives.

The Pd(0)-catalysed Buchwald Hartwig reaction allowed the synthesis of a variety of ligands containing one or two amine (NH) bridges. The introduction of these bridges resulted in all ligands showing poor extraction properties, despite these ligands showing improved solubilities in 1-octanol. It has been determined, through X-ray crystallography and computational studies that the likely reason for their poor extraction capability results from the ligands existing only in the *trans-trans* conformation, instead of the complexing *cis-cis* conformation. Introduction of alkyl chains onto the amine nitrogens had no impact on their ability to extract trivalent actinides or lanthanides, but did improve ligand solubilities in all cases.

The functionalisation of the camphorquinone group with amide moieties resulted in a general improvement in ligand solubility when compared to the benchmark ligand **1.09**. In particular the diethylamine-derived BTPhen **L24** and piperidine-derived BTPhen **L27** showed high distribution ratios for Am(III) and Cm(III) and a high separation factor for Am(III) over Eu(III) ($SF_{Am/Eu}$). The extraction kinetics for **L24** showed a significant improvement in comparison to the benchmark ligand **1.09**. Further solvent extraction studies on **L27** will allow the direct comparison with **L24**. Further studies on both ligands can build upon these positive results to pave the way for possible future industrial use.

The functionalisation of the $CyMe_4$-diketone group via alternative synthesis, to introduce alcohol, ether and ketone moieties, had mixed results. There was a comparable, or in the case of the functionalised novel $CyMe_4$-BTPhen ligands **L42** and **L45**, decreased solubility in comparison to the benchmark ligand **1.17**. The introduction of the methoxy group in **L48** resulted in improved solubility and promising solvent extraction results, suggesting that further *O*-alkyl derivatives with longer alkyl groups could be explored to further improve the ligand solubility in the required diluents.

In terms of the ligand design approach, there was a correlation between the Fsp^3 value and the ligand solubility in 1-octanol suggesting that this parameter can be utilised to give an early prediction of ligand solubility. The introduction of hydrogen bond donor (HBD) and hydrogen bond acceptor (HBA) functional groups, in particular with the camphor-derived ligands, gave promising results. In introducing these HBD/HBA groups, care must be executed to ensure that the calculated log *P* value isn't so drastically reduced as to result in ligands that are so polar that they partition into the aqueous phase. Some ligands, in particular those ligands containing the morpholine group, saw significant issues with precipitation when in contact with the nitric acid aqueous phase in comparison to the piperidine-derived BTPhen ligand **L27**. The presence of the oxygen atom in the morpholine ring, in place of an sp^3 carbon atom in the piperidine ring, clearly has a noteworthy effect on the ligand solubility during extraction experiments.

Overall, a variety of novel ligands have been synthesised with mixed results in terms of their extraction properties. It is determined that introducing flexibility in the ligands, as is observed through the addition of an amine (NH) between the 1,2,4-tiazine and pyridine group, has a significant impact on their ability to extract the An(III) from the Ln(III). The functionalisation of the camphor group with an amide results in ligands, in particular the BTPhens **L24** and **L27** show improvements when compared to the benchmark ligand **1.09**. Functionalisation of the $CyMe_4$-diketone **1.09** resulted in only one ligand observing promising extraction results and this approach may require further investigations. The innovative ligand design approach reported herein has been shown to be reasonably robust in predicting the ligand solubility in the required diluent and could be used in future developments in this area. Improvement of extraction kinetics will require further evaluation on the most promising ligands discussed in this thesis, but has the potential for application based upon initial results for **L24**.

Chapter 6

Methodology

6. Methodology

All NMR titrations, solubility studies and extraction experiments were completed by myself, unless otherwise stated.

6.1. General procedure for NMR titrations

Stock solutions of the ligands at a concentration of 0.1 M were prepared in deuterated chloroform of methanol, dependent upon ligand solubility. A 0.5 mL sample of this stock solution was taken for each NMR titration. Stock solutions at a concentration of 0.01 M of the respective nitrate lanthanide salt; $La(NO_3)_3$, $Y(NO_3)_3$, or $Lu(NO_3)_3$, and transition metal salts; $AgNO_3$ or $NiNO_3$. These stock solutions are prepared in the same deuterated solvent as the ligand stock solution they are to be titrated with. One equivalent of the lanthanide or transition metal stock solution, equal to 200 μL was added individually to the ligand stock solution up to a maximum of 1.2 equivalents, equal to 2.4 mL. A ^{1}H NMR spectra was obtained for each equivalent of stock solution added and overlaid. All NMR spectra were recorded on a 400 MHz spectrometer at room temperature.

6.2. General procedure for solubility studies

The solubility measurements were carried out at Northumbria University. A small sample of each individual ligand was weighed. This was dosed with 1-octanol dropwise and the sample sonicated, this addition was continued until complete dissolution of the ligand. At this point the mass was again taken to determine the amount of 1-octanol added. The solubility was calculated by taking the mass (g) of ligand dissolved in 1 L of 1-octanol and dividing by the molecular weight of each molecule. The sample was then left overnight to ensure complete dissolution.

6.3. Experimental details for actinide extraction experiments

All extraction experiments and α- and γ-analytical measurements were performed at the Forschungzentrum Jülich, Germany by myself enabled through the aid of a Mobility Grant awarded by the Royal Society of Chemistry. Nitric acid solutions were supplied by Merck AG. The radiotracers ^{241}Am, ^{244}Cm and ^{152}Eu were purchased from Isotopendienst M. Blaseg GmbH, Waldburg, Germany; Oak Ridge National Laboratory, Oak Ridge, TN, USA and Eckert & Ziegler

Nuclitec GmbH, Braunschweig, Germany. Lanthanide salts were obtained from a variety of commercial sources and used as received.

Extraction experiments were carried out using equal volumes of 500 µL of each phase; aqueous and organic. The aqueous phase was composed of a nitric acid solution (0.001 – 3 M) and 10µL of the aqueous tracer. The nitric acid solution contained all lanthanides except promethium in a concentration of 10^{-5} mol L^{-1} for each lanthanide used. The aqueous tracer contained 278 kBq mL^{-1} of ^{152}Eu, 155 kBq mL^{-1} of ^{241}Am and 151 kBq mL^{-1} of ^{244}Cm. The organic and aqueous solutions were prepared by dissolving weighed quantities of the desired substance in the desired solvent. For aqueous dilutions, demineralised water (18.2 MΩcm) was used. Nitric acid solutions were prepared by dilution from a 65% nitric acid solution EMSURE® for analysis. The organic solutions were prepared in a 0.01 M solution in 3.5 ml of 1-octanol. Where necessary *tert*-butyl benzene was added to aid in dissolution of the ligand.

The shaking experiments were carried out in a temperature-controlled aluminium block (22 °C) using an IKA Vibrax VXR shaking device at a speed of 2,200 rpm, for the required time period. Afterwards, centrifugation was applied to maintain a complete separation of the phases and they were subsequently separated using pipettes. Gamma measurements of ^{152}Eu (122 keV) and ^{241}Am (60 keV) were carried out using a Eurisys EGC35-195-R germanium coaxial N-type detector. Alpha measurements were carried out for ^{241}Am (5,486 keV) and ^{244}Cm (5,805 keV) using an Ortec Octête-pc eight-chamber alpha measurements system, equipped with Passivated Implanted Planar Silicon (PIPS) detectors. Sample preparation was done by homogenizing the 10 µL alpha-spectroscopy sample in 100 µL of a mixture of Zapon varnish and acetone (1:100 v/v). This mixture was distributed over a stainless steel plate obtained from Berthold, Bad Wildbad, Germany. The sample was dried under a heating lamp and annealed into the stainless steel plate by a gas-flame burner.

For stable elements, inductively coupled plasma mass spectrometry (ICP-MS) was applied using a Perkin Elmer SCIEX Elan 6100 DRC. Aqueous samples were measured after dilution in 1% v/v nitric acid solution without further treatment. Organic samples were measured directly in a tenside

matrix (Triton-X-100) in 1% v/v nitric acid after dilution. The distribution ratios *D* were calculated as the quotient of the concentration or activity of the metal ion in the organic phase over the concentration of activity of the metal ion in the aqueous phase (D = [M](org)/[M](aq)). The separation between two metal ions is expressed using the separation factor, being the quotient of the distribution ratios of the two metal ions ($SF = D_{M1} / D_{M2}$). The uncertainties of the data achieved from the method described above is <5% for $0.01 < D < 100$. Below and above these limits, the uncertainties are lower than 20% for all data shown.

6.4. Experimental details for fission/corrosion product extraction

The composition of the synthetic PUREX raffinate solution used is shown in X. It was prepared by a specific strategy for the dissolution of the reagents, which is mainly based on the use of metal nitrate salts. It corresponds to a PUREX raffinate with a volume of 5000 L/t UO_2 fuel with an initial ^{235}U enrichment of 3.5% and thermal burn-up of 33,000 MWd/tHM after 3 years of cooling. The relatively high concentrations of sodium (Na) and iron (Fe) in the raffinate are due to purification steps for the U/Pu product produced by the PUREX process and solvent clean-up steps.[170]

Table 23: Composition of the synthetic PUREX raffinate solution (HAR).

Element	Concentration [mg/L]*	Element	Concentration [mg/L]	Element	Concentration [mg/L]
Y	78	Ba	247	Rb	67
La	209	Cd	19	Rh	77
Ce	480	Cr	80	Ru	368
Pr	195	Cs	449	Sb	4
Nd	716	Cu	20	Se	24
Sm	146	Fe	1979	Sn	11
Eu	40	Mo	642	Sr	156
Gd	46	Na	2000	Te	109
Ag	9	Ni	41	Zr	698
Al	2	Pd	102		
HNO_3	3.1 mol/L				

*or as shown

6.5. Computational Studies

The computational studies were completed at Northumbria University by Dr Mark Sims. All density functional theory calculations were performed using the Gaussian 09 Software Package (Revision C.01), and all calculaions were carried out on molecules in the gas phase. The relaxed potential energy scans were carried out using the B3LYP functionl and the 6-31G(d) basis set, providing an acceptable compromise between accuracy and speed for the large number of calculations that were performed. The final optimisations were carried out using the B3LYP functional and the 6-311+G(d,p) basis set. The absence of negative frequencies was checked to confirm that the minimum energy structures had been obtained.

Chapter 7

Experimental

7. Experimental

Solvents were purchased from Fisher Scientific, Sigma Aldrich and Alfa Aesar at reagent or HPLC grade and used as received. Dichloromethane (DCM), chloroform ($CHCl_3$), toluene and acetonitrile (MeCN) were dried over molecular sieves (4 Å) for a minimum of two days. Ethyl acetate (EtOAc) was stored over calcium hydride and distilled before use. Ether refers to the use of diethyl ether and was dried over sodium wire overnight where required.

Reagents were used as purchased from Sigma Aldrich, Fluorochem, Alfra Aesar, and Acros Organics.

Column chromatography was performed using Fisher Scientific silica gel Å (35-70 μL) or Fluorochem silica gel Å (40-63 μL).

NMR spectra were recorded using a JEOL ELS400 Delta 400 MHz spectrometer in deuterated chloroform, unless otherwise stated. The chemical shifts (δ) were reported in parts per million (ppm) downfield from a tetramethylsilane standard and coupling constants (*J*) are recorded in Hertz (Hz). NMR assignments were verified by appropriate experiments including; ^{13}C-DEPT and ^{1}H-^{1}H COSY. The multiplicities are denoted as follows: singlet (s), doublet (d), triplet (t), quartet (q), quintet (qu), sextet (se), septet (sp), multiplet (m), double doublet (dd), double triplet (dt), triple doublet (td), triple triplet (tt), double double doublet (ddd), broad (br).

Mass spectrometry was completed at the EPSRC National Mass Spectrometry Service Centre at Swansea University using spectrometers including a Thermo Scientific LTQ Orbitrap XL Mass Spectrometer. Low resolution electrospray (ESI) was the ionisation technique generally employed.

Melting points were obtained on a SRS DigiMelt MPA160 with an upper limit of 260 ºC.

Note: All experimental procedures follow the order as presented in the thesis, with the exception of the final ligands synthesised. The final ligands are grouped together at the end of the experimental section, in the order they appear in the thesis.

2.2.3: 1,6-Diethyl 2,2,5,5-tetramethylhexanedioate[95]

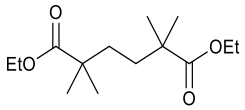

Anhydrous diethyl ether (100 ml) was placed in oven-dried 250 ml 3-necked flask and sealed under a N_2 atmosphere. Diisopropylamine (8.4 ml, 59.00 mmol) was added via syringe and the solution cooled to -20 °C using a acetone/liquid N_2 bath. Upon cooling *n*-BuLi (1.6 M, 34.0 ml, 54.00 mmol), was added dropwise via syringe and the solution stirred at -20 °C for 1 hour. Ethyl isobutyrate (7.4 ml, 54.00 mmol) was then added dropwise via syringe over 10 minutes and the solution allowed to warm to room temperature. The solution was stirred at room temperature for 1 hour before ethylene glycol bis-*p*-toluenesulfonate (10.00 g, 27.00 mmol) was added in small aliquots over a period of 15 minutes. This was heated under reflux for 24 hour before been allowed to cool. The white solid was filtered and washed with diethyl ether (60 ml) and DCM (100 ml) and the filtrate quenched with saturated aq. ammonium chloride (60 ml). The phases were mixed and separated and the aq. phase extracted with diethyl ether (3 x 20 ml). The combined organic extracts were washed with H_2O (30 ml) and dried ($MgSO_4$). The solvent was removed under reduced pressure to leave the crude product as a yellow liquid (8.75 g). The product was purified by vacuum distillation to afford the product as a colourless liquid (4.75 g, 68%). Bp = 72 – 80 °C at 0.1 mbar.

^{1}H-NMR δ_H (399.8 MHz): 4.06 (4H, q, *J* = 6.87 Hz, 2 x C*H*$_2$CH$_3$), 1.39 (4H, s, 3-C*H*$_2$ and 4-C*H*$_2$) 1.19 (6H, t, *J* = 6.87 Hz, 2 x CH$_2$C*H*$_3$), 1.10 (12H, s, 2 x 2-C*H*$_3$, 2 x 5-C*H*$_3$);

^{13}C-NMR (100.5 MHz): 177.7 (1-*C*O and 6-*C*O), 60.2 (2 x O*C*H$_2$CH$_3$), 41.9 (2-*C* and 5-*C*), 35.5 (3-*C*H$_2$ and 4-*C*H$_2$), 25.1 (2 x 2-*C*H$_3$ and 2 x 5-*C*H$_3$), 14.2 (2 x CH$_2$*C*H$_3$) ppm.

NMR data was consistent with literature values.

2.2.4: 1,2-Bis(trimethylsilyloxy)-3,3,6,6-tetramethylcyclohex-1-ene[95]

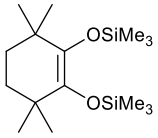

Dry toluene (50 ml) was placed in an oven fried flask and sealed under N_2 before adding the sodium metal (1.15 g, 49.60 mmol). The flask was heated under reflux (150 °C) until the sodium had melted. 1,6-Diethyl 2,2,5,5-tetramethylhexanedioate **2.2.3** (2.24 g, 9.90 mmol) and the chlorotrimethylsilane (6.3 ml) were subsequently added. The mixture was refluxed for 3 days before been allowed to cool to room temperature. The mixture was filtered carefully through a Büchner funnel and the sodium metal quenched slowly with EtOH. The solid residue was washed with toluene (30 ml) and THF (20 ml). The filtrate was evaporated under reduced pressure to give an orange oil, which was taken straight to the next step (1.77 g, 70% crude).

^{1}H-NMR δ_H (399.8 MHz): 1.33 (4H, s, 4-C*H*$_2$ and 5-C*H*$_2$), 0.92 (12H, s, 2 x 3-C*H*$_3$ and 2 x 6-C*H*$_3$), 0.09 (18H, s, 2 x OSi(C*H*$_3$)$_3$);

^{13}C-NMR (100.5 MHz): 140.9 (1-*C* and 2-*C*), 37.7 (4-*C*H$_2$ and 5-*C*H$_2$), 29.6 (3-*C* and 6-*C*), 27.83 (2 x 3-*C*H$_3$ and 2 x 6-*C*H$_3$), 3.6 (2 x OSi(*C*H$_3$)$_3$) ppm.

NMR data was consistent with literature values.

2.2.5: 3,3,6,6-Tetramethylcyclohexane-1,2-dione[95]

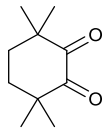

1,2-Bis(trimethylsilyloxy)-3,3,6,6-tetramethylcyclohex-1-ene **2.2.4** (1.77 g, 7.00 mmol) was dissolved in DCM (20 ml) in a 100 ml flask. Bromine (0.3 ml, 7.00 mmol) was added slowly dropwise over 5 minutes. Stir at room temperature for 1 hour then dilute the solution with DCM (20 ml). The solution was washed with H_2O (4 x 10 ml) and saturated aq. sodium sulphite (2 x 15 ml) and dried ($MgSO_4$). The solvent was removed under reduced pressure to leave an orange oil. The product was purified by column chromatography (silica gel: 2:1 hexane:EtOAc) to leave the product as a dark orange oil, which crystallised when left (0.47 g, 41%).

^{1}H-NMR δ_H (399.8 MHz): 1.88 (4H, s, 4-C*H*$_2$ and 5-C*H*$_2$), 1.15 (12H, s, 2 x 3-C*H*$_3$ and 2 x 6-C*H*$_3$) ppm.

NMR data was consistent with literature values.

2.2.11: 5,6-Diethyl-1,2,4-triazin-3-amine[171]

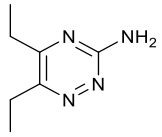

Aminoguanidine bicarbonate (3.1 g, 22.00 mmol) was suspended in H_2O (40 ml) and hexane-3,4-dione (2.8 ml, 22.00 mmol) was added slowly. The reaction mixture was stirred at room temperature overnight before being heated to 100 °C for 5 hours. The solution was cooled to room temperature and the solid filtered and washed with H_2O (20 ml) to collect the product as a yellow solid (2.65 g, 79%).

^{1}H-NMR δ_H (399.8 MHz): 5.26 (2H, s, br, N*H*$_2$), 2.86 (2H, q, *J* = 7.79, 7.33 Hz, C*H*$_2$), 2.69 (2H, q, *J* = 7.79, 7.33 Hz, C*H*$_2$), 1.32 (3H, t, *J* = 7.79, 7.33 Hz, C*H*$_3$), 1.27 (3H, t, *J* = 7.79, 7.33 Hz, C*H*$_3$);

^{13}C-NMR (100.5 MHz): 163.2 (Ar*C*), 161.8 (Ar*C*), 152.8 (Ar*C*), 26.8 (*C*H$_2$), 25.0 (*C*H$_2$), 13.0 (*C*H$_3$), 11.2 (*C*H$_3$) ppm.

LRMS (ESI +ve) *m/z:* 153.13; calculated for $[C_7H_{12}N_4+H]^+$: 153.11

NMR data was consistent with literature values.

2.2.12: 5,5,8,8-Tetramethyl-5,6,7,8-tetrahydro-1,2,4-benzotriazin-3-amine

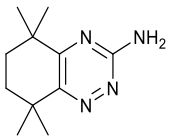

A suspension of 3,3,6,6-tetramethylcyclohexane-1,2-dione **2.2.5** (0.52 g, 3.00 mmol) and aminoguanidine bicarbonate (0.41 g, 2.50 mmol) in EtOH(50 ml) was refluxed for 24 hour. The solvent was removed under reduced pressure and the resulting orange residue was recrystallized from methanol. Filtration left an off-white solid as the product (0.27 g, 53%).

^{1}H-NMR δ_H (399.8 MHz): 4.99 (2H, s, br, N*H*$_2$), 1.74 (4H, s, 2 x C*H*$_2$), 1.38 (6H, s, 2 x C*H*$_3$), 1.27 (6H, s, 2 x C*H*$_3$);

^{13}C-NMR (100.5 MHz): 165.4 (Ar*C*), 161.3 (Ar*C*), 155.5 (Ar*C*), 36.8 (*C*), 35.5 (*C*), 34.0 (*C*H$_2$), 33.3 (*C*H$_2$), 29.8 (2 x *C*H$_3$), 29.0 (2 x *C*H$_3$) ppm.

LRMS (ESI +ve) m/z 207.17; *calculated for* $[C_{11}H_{18}N_4 + H]^+$ 207.16

2.2.13: 5,5,7,7-Tetramethyl-6,7-dihydro-5*H*-cyclopenta[e][1,2,4]triazin-3-amine

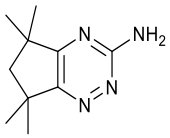

A suspension of 3,3,5,5-tetramethylcyclopentane-1,2-dione **2.2.7** (0.21 g, 1.30 mmol) and aminoguanidine bicarbonate (0.17 g, 1.20 mmol) were suspended in the diketone (30 ml) and refluxed overnight. The mixture was concentrated under reduced pressure to leave a yellow solid (218 mg, 93%).

m.p: 222.1-223.3 °C

^{1}H-NMR δ_H **(399.8 MHz):** 5.70 (2H, s, br, N*H*$_2$), 1.93 (2H, s, 6-C*H*$_2$), 1.41 (6H, s, 2 x C*H*$_3$), 1.31 (6H, s, 2 x C*H*$_3$);

^{13}C-NMR (100.5 MHz): 171.8 (Ar*C*), 163.0 (Ar*C*), 160.0 (Ar*C*), 53.3 (6-*C*H$_2$), 40.6 (*C*), 39.5 (*C*), 29.9 (2 x *C*H$_3$), 28.8 (2 x *C*H$_3$) ppm.

HRMS m/z: 193.1445. C*alculated for* $[C_{10}H_{16}N_4 + H]^+$: 193.1448

2.2.14 (1*R*,8*S*)-8,11,11-Trimethyl-3,4,6-triazatricyclo[6.2.1.0^{2,7}]undeca-2,4,6-trien-5-amine[172]

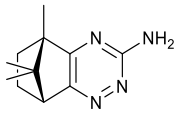

A suspension of (1*S*)-(+)-camphorquinone (1.05 g, 6.00 mmol) and aminoguanidine bicarbonate (0.68 g, 5.00 mmol) in EtOH (50 ml) was heated under reflux (120 °C) for 24 hour. The solvent was removed under reduced pressure and the resulting residue was recrystallized from hot methanol. Filtration left the product as an off-white solid (0.97 g, 95%).

m.p: 260.1-261.5 °C

^{1}H-NMR δ_H **(399.8 MHz):** 5.16 (2H, s, br, N*H*$_2$), 3.06 (1H, d, *J* = 4.12 Hz, 1-C*H*), 2.20 (1H, tt, *J* = 10.99, 4.12 Hz, C*H*$_{exo}$), 1.96 (1H, td, *J* = 10.99, 3.66 Hz, C*H*$_{exo}$), 1.41 – 1.28 (2H, m, 2 x C*H*$_{endo}$), 1.24 (3H, s, C*H*$_3$), 1.05 (3H, s, C*H*$_3$), 0.65 (3H, s, C*H*$_3$);

^{13}C-NMR (100.5 MHz): 172.2 (Ar*C*), 161.71 (Ar*C*), 158.5 (Ar*C*), 54.5 (*C*), 53.9 (*C*), 50.4 (1-*C*H), 31.5 (*C*H_2), 24.7 (*C*H_2), 20.1 (*C*H_3), 18.3 (*C*H_3), 9.1 (*C*H_3) ppm.

LRMS (ESI -ve) *m/z* 204.73; *calculated for* [$C_{11}H_{16}N_4$]: 204.14

NMR data was consistent with literature values.

(E)-1-[Amino(methylsulfanyl)methylidiene]hydrazine-1-ium iodide[173]

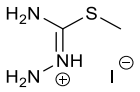

A solution of thiosemicarbazide (5.09 g, 55.00 mmol) in EtOH (50 ml) was cooled to 0 °C before iodomethane (4.40 ml, 66.00 mmol) was slowly added dropwise. The mixture was refluxed at 80 °C overnight before cooling to room temperature. The precipitate that formed was filtered and washed with petroleum ether (50 ml). The solvent removed under reduced pressure to leave the product as a pale solid (11.96 g, 93%).

^{1}H-NMR δ_H (399.8 MHz, DMSO-D6): 10.51 (1H, s, br, N*H*), 9.07 (2H, s, br, NH_2), 5.19 (2H, s, br, NH_2), 3.31 (3H, s, SCH_3) ppm.

NMR data was consistent with literature values.

2.2.19: 5,6-Diethyl-3-(methylsulfanyl)-1,2,4-triazine

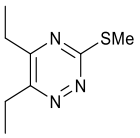

Methylthiosemicarbazide hydrogen iodide (0.42 g, 1.70 mmol) was dissolved in a solution of EtOH and H_2O (20 ml, 4:1 ratio). This solution was added dropwise, over 5 minutes, to a solution of hexane-3,4-dione (0.21 ml, 1.70 mmol) and sodium bicarbonate (0.15 g, 1.90 mmol) in EtOH and H_2O (20 ml, 4:1). The mixture was stirred at room temperature overnight, then under reflux for 5 hour. The mixture was allowed to cool to room temperature and evaporated to dryness. The residue was diluted with H_2O (30 ml) and extracted with DCM (4 x 10 ml). The combined organic layers were dried ($MgSO_4$) and the solvent removed under reduced pressure to leave the product as a yellow liquid (0.30 g, 97%).

^{1}H-NMR δ_H (399.8 MHz): 2.94 (2H, q, *J* = 7.79, 7.33 Hz, C*H*$_2$), 2.78 (2H, q, *J* = 7.79, 7.33 Hz, C*H*$_2$), 2.66 (3H, s, SC*H*$_3$), 1.38 (3H, t, *J* = 7.33 Hz, C*H*$_3$), 1.32 (3H, t, *J* = 7.33 Hz, C*H*$_3$);

^{13}C-NMR (100.5 MHz): 170.8 (Ar*C*), 161.9 (Ar*C*), 156.9 (Ar*C*), 26.9 (*C*H$_2$), 25.3 (*C*H$_2$), 13.9 (S*C*H$_3$), 12.2 (*C*H$_3$), 11.0 (*C*H$_3$) ppm.

2.2.25: 1λ^5,5λ^5-diazatetracyclo[7.6.2.0^5,^{17}.0^{12},^{16}]heptadeca-1(15),5,7,9,11,13,16-heptaene-1,5-bis(ylium) dibromide[174]

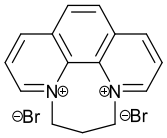

A mixture of 1,10-phenanthroline (1.07 g, 5.55 mmol) and 1,3-dibromoproane (2.51 ml, 24.42 mmol) were dissolved in nitrobenzene (25 ml). The reaction mixture was then stirred at 120 °C for 24 hour. Upon completion the precipitate was collected via filtration and washed with toluene. The resulting solid was recrystallized from a solution of EtOH/H$_2$O (5:1, 20 ml) to give the yellow solid (1.42 g, 67%).

^{1}H-NMR δ_H (399.8 MHz, DMSO D6): 9.84 (2H, d, *J* = 5.50 Hz, Ar*H*), 9.51 (2H, d, *J* = 8.24 Hz, Ar*H*), 8.69 (2H, s, Ar*H*), 8.68-8.66 (2H, m, Ar*H*), 5.12 (4H, t, *J* = 6.87 Hz, 2 x C*H*$_2$), 3.22 (2H, qu, 6.87 Hz, CH$_2$);

^{13}C-NMR (100.5 MHz, DMSO D6): 151.9 (Ar*C*H), 146.8 (Ar*C*H), 134.0 (Ar*C*), 133.8 (Ar*C*), 130.1 (Ar*C*H), 127.7 (Ar*C*H), 60.2 (2 x *C*H$_2$), 55.5 (*C*H$_2$), ppm.

NMR data was consistent with literature values.

2.2.26: *N, N'*-Propane-1,10-phenanthroline-3,9-dione[174]

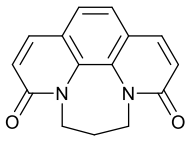

Method A:

A solution of potassium ferricyanide (1.55 g, 4.71 mmol) and sodium hydroxide (0.71 g, 17.68 mmol) in H$_2$O (5 ml) was cooled too under 5 °C and stirred for 15 minutes. A solution of **2.2.25**

(0.21 g, 0.52 mmol) in water (10 ml) was added and the mixture was stirred for 1 hour below 5 °C before being stirred at room temperature for 2 hour. The resulting solution was neutralised by the dropwise addition of concentrated hydrochloric acid and then extracted with chloroform (3 x 20 ml), dried ($MgSO_4$) and the solvent removed under reduced pressure. Purification was achieved by column chromatography (silica gel, DCM:MeOH, 60-30:1) to yield the product as a dark brown solid (13.8 mg, 11%).

Method B:[138]

A suspension of **2.2.25** (3.04 g, 7.97 mmol) in *tert*-butanol (80 ml) was refluxed at 40 °C for 21 hours. Potassium *tert*-butoxide (3.58 g, 31.87 mmol) was added in small portions slowly and refluxed for 24 hours. Upon completion the solution was allowed to cool to room temperature before the precipitate was filtered. The filtrant was dissolved in H_2O (10 ml) and extracted with DCM (4 x 10 ml), dried ($MgSO_4$). The solvent was evaporated to leave the product as a brown solid (1.20 g, 69%).

^{1}H-NMR δ_H (399.8 MHz): 7.72 (2H, d, *J* = 9.62 Hz, 2 x ArC*H*), 7.37 (2H, s, 5-ArC*H*, 6-ArC*H*), 6.81 (2H, d, *J* = 9.62 Hz, ArC*H*), 4.32 (4H, br, s, 2 x CH_2), 2.44 (2H, qu, *J* = 6.87, 6.41 Hz, CH_2); **^{13}C-NMR (100.5 MHz)**: 162.7 (2 x CO), 138.8 (2 x ArCH), 132.1 (2 x ArC), 123.1 (2 x ArCH), 122.8 (2 x ArCH), 122.7 (ArC), 45.7 (2 x *C*H_2), 25.8 (*C*H_2) ppm.

LRMS (ESI +ve) m/z 253.16; *calculated for* $[C_{15}H_{12}N_2O_2 + H]^+$: 253.09

NMR data was consistent with literature values.

2.2.27: 2,9-Dichloro-1,10-phenanthroline[138]

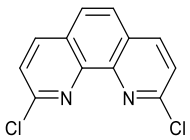

A mixture of **2.2.26** (0.22 g, 0.87 mmol), phosphorous pentachloride (0.42 g, 1.84 mmol) and phosphorus oxychloride (15 ml) were refluxed for 18 hour under N_2. Excess phosphorus oxychloride was removed under reduced pressure and ice H_2O (30 ml) was added. The solution was basified with aq. ammonia (2 M) to give a pale brown precipitate which was filtered and dried under vacuum (0.17 g, 78%).

^{1}H-NMR δ_H (399.8 MHz): 8.22 (2H, d, *J* = 8.70 Hz, ArC*H*) 7.84 (2H, s, 5-ArC*H*, 6-ArC*H*) 7.66 (2H, d, *J* = 8.24 Hz, ArC*H*);

^{13}C-NMR (100.5 MHz): 152.0 (2 x Ar*C*), 144.9 (2 x Ar*C*), 138.8 (2 x Ar*C*H), 127.7 (2 x Ar*C*), 126.2 (Ar*C*H), 124.9 (Ar*C*H) ppm.

LRMS (ESI +ve) *m/z* 250.11; *calculated for* [$C_{12}H_6Cl_2N_2$ + H]: 250.99

NMR data was consistent with literature values.

2.2.28: 2,9-Dibromo-1,10-phenanthroline[175]

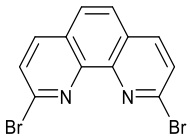

2.2.27 (0.49 g, 1.95 mmol) was suspended in phosphorus tribromide (3 ml) and placed under N_2. The mixture was heated at 170 °C for 17 hour before cooling to room temperature, then further to 0 °C. The mixture was quenched by the slow addition of cold water and neutralised with saturated aq. $NaHCO_3$. The solid that precipitated was collected by filtration, washed with H_2O (20 ml) and left to dry overnight to leave an off white solid (0.35 g, 53 %).

^{1}H-NMR δ_H (399.8 MHz): 8.10 (2H, d, *J* = 8.24 Hz, ArC*H*, ArC*H*) 7.83 (2H, s, 5-ArC*H*, 6-ArC*H*) 7.80 (2H, d, *J* = 8.24 Hz, Ar-C*H*);

^{13}C-NMR (100.5 MHz): 145.5 (ArC), 143.1 (ArC), 138.2 (ArCH), 128.5 (ArCH), 127.9 (ArC), 126.5 (ArCH) ppm.

LRMS (ESI +ve) *m/z:* 339.03 *calculated for* [$C_{29}H_{37}N_9$ + H]$^+$: 339.89

NMR data was consistent with literature values.

2.3.2: 6-Bromopyridine-2-carbohydrazonamide[142]

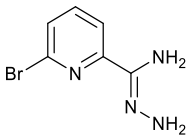

6-Bromopyridine-2-carbonitrile (0.40 g, 2.19 mmol) was suspended in EtOH (25 ml) and cooled to 0°C. Hydrazine hydrate (50-60%, 5 ml) was added slowly and then stirred at 0°C for 1 hour.

Mixture allowed to warm to room temperature and refluxed at 40 °C overnight. The solution was allowed to cool and the solid was filtered and washed with minimal hexane. The product was a white fluffy solid (414 mg, 88%).

^{1}H-NMR δ_H (399.8 MHz): 7.97 (1H, d, *J* = 7.79 Hz, ArC*H*), 7.55 (1H, t, *J* = 7.79 Hz, 4-ArC*H*), 7.45 (1H, d, *J* = 7.79 Hz, ArC*H*), 5.13 (2H, s, br, NH_2), 4.64 (2H, s, br, NH_2);

^{13}C-NMR (100.5 MHz): 153.8 (*C*), 142.0 (*C*), 140.1 (*C*), 139.9 (Ar*C*H), 127.3 (Ar*C*H), 118.9 (Ar*C*H) ppm.

NMR data was consistent with literature values.

2.3.3: 2-Bromo-6-(5,5,7,7-tetramethyl-5H, 6H, 7H-cyclopenta[e] [1,2,4] triazin-3-yl)pyridine

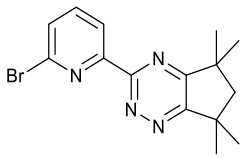

3,3,5,5-Tetramehtylcyclopentane-1,2-dione **2.2.7** (158 mg, 1.02 mmol) and 6-bromopyridine-2-carbohydrazonamide **2.3.2** (200 mg, 0.93 mmol) was suspended in AcOH (5 ml) and refluxed over the weekend. The solution was cooled and the AcOH removed under reduced pressure. Purification was achieved through column chromatography (silica gel; DCM 100%, with increasing MeOH fraction) to yield the project as a yellow solid (172 mg, 56%).

m.p: 90.1-92.4 °C

^{1}H-NMR δ_H (399.8 MHz): 8.47 (1H, d, *J* = 7.79 Hz, ArC*H*), 7.76 (1H, t, *J* = 7.79 Hz, 4-ArC*H*), 7.64 (1H, d, *J* = 7.79 Hz, ArC*H*), 2.06 (2H, s, 6-CH_2), 1.52 (6H, s, 2 x CH_3), 1.46 (6H, s, 2 x CH_3);

^{13}C-NMR (100.5 MHz): 171.0 (Ar*C*), 167.9 (Ar*C*), 161.7 (Ar*C*), 154.9 (Ar*C*), 142.7 (Ar*C*), 139.1 (Ar*C*H), 129.7 (Ar*C*H), 122.8 (Ar*C*H), 52.9 (6-*C*H_2), 41.3 (*C*), 40.4 (*C*), 29.7 (2 x *C*H_3), 29.0 (2 x *C*H_3) ppm.

HRMS (ESI +ve) m/z 333.0712; *calculated for* $[C_{15}H_{17}BrN_4 + H]^+$: 333.0709

2.3.4: 2-Bromo-6-{(1*R*,8*S*)-8,11,11-trimethyl-3,4,6-triazatricyclo[6.2.1.0^{2,7}]undeca-2,4,6-trien-5-yl}pyridine

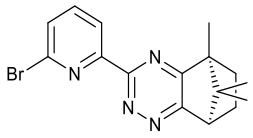

(1*S*)-(+)-Camphorquinone (0.43 g, 2.78 mmol) and 6-bromopyridine-2-carbohydrazonamide **2.3.2** (0.47 g, 2.19 mmol) was suspended in AcOH (5 ml) and refluxed overnight. The solution was cooled and the AcOH removed under reduced pressure. The product was purified by column chromatography (silica gel; DCM 100%, with increasing EtOAc fraction). Product was a yellow solid (0.67 g, 88%).

m.p: 156.7-157.5 °C

^{1}H-NMR δ_H (399.8 MHz): 8.49 (1H, d, *J* = 7.33 Hz, ArC*H*), 7.73 (1H, t, *J* = 7.79 Hz, 4-ArC*H*), 7.63 (1H, d, *J* = 7.79 Hz, ArC*H*), 4.58 (1H, d, *J* = 4.58 Hz, 1-C*H*), 2.39 – 2.30 (1H, s, CH_{exo}), 2.11 – 2.03 (1H, s, CH_{exo}), 1.44 (3H, s, CH_3), 1.43 – 1.39 (2H, m, 2 x CH_{endo}) 1.12 (3H, s, CH_3), 0.64 (3H, s, CH_3);

^{13}C-NMR (100.5 MHz): 171.3 (Ar*C*), 165.6 (Ar*C*), 160.6 (Ar*C*), 154.9 (Ar*C*), 142.6 (Ar*C*), 139.2 (Ar*C*H), 129.7 (Ar*C*H), 122.8 (Ar*C*H), 55.6 (*C*), 54.5 (*C*), 51.1 (1-*C*H), 31.1 (CH_2), 24.2 (CH_2), 20.1 (CH_3), 18.3 (CH_3), 9.3 (CH_3) ppm.

HRMS (ESI +ve) m/z: 345.0711; *calculated for* $[C_{16}H_{17}BrN_4 + H]^+$: 345.0709

3.2.2: Pyridine-2,6-bisamidrazone [176]

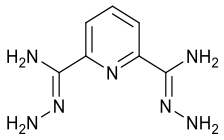

Pyridine-2,6-dicarbonitrile (1.00 g, 7.74 mmol) was dissolved in hydrazine monohydrate (50-60%, 10 ml) and EtOH (10 ml) added. The mixture was stirred for 5.5 hour and the white precipitate was filtered and washed with EtOH (15 ml). The solid was recrystallized in water and filtered to leave a white fluffy solid as the product (0.96 g, 64%).

^{1}H-NMR δ_H (399.8 MHz, DMSO-D6): 7.80 (2H, d, *J* = 7.79 Hz, 2 x ArC*H*), 7.66 (1H, d, *J* = 7.33 Hz, ArC*H*), 7.64 (1H, d, 7.33 Hz, ArC*H*), 6.06 (4H, s, br, NH_2), 5.26 (4H, s, br, NH_2);

^{13}C-NMR (100.5 MHz, DMSO-D6): 151.8 (*C*), 145.0 (*C*), 137.5 (Ar*C*H), 119.4 (2 x Ar*C*H) ppm.

NMR data consistant with literature values.

3.2.7: 1,10-phenanthroline-2,9-dicarbaldehyde [95]

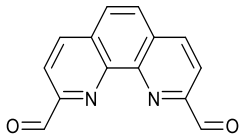

Selenium dioxide (2.28 g, 20.52 mmol) was dissolved in 1,4-dioxane (80 ml) and water (3 ml) and heated to reflux. Neocuproine (2.02 g, 9.68 mmol) was dissolved in 1,4-dioxane (60 ml) and added dropwise slowly over 30 minutes. The solution was refluxed for 30 minutes before the reaction mixture was filtered whilst hot. The filtrate was allowed to cool to room temperature, then further to 0 °C and the precipitated solid was filtered and washed with dioxane (15 ml). The solid was triturated with chloroform (100 ml) and filtered. The filtrate was evaporated to afford the dialdehyde as a pale brown solid (0.76 g). The remaining filtrant was triturated with chloroform (50 ml) and filtered then washed with chloroform (20 ml). The filtrate was evaporated to afford the dialdehyde as a pale brown solid (0.72 g). Further trituration of the filtrant yielded a further (0.60 g) of the dialdehyde; total yield (2.08 g, 91%).

^{1}H-NMR δ_H (399.8 MHz): 10.61 (2H, s, C*H*O), 8.56 (2H, d, *J* = 8Hz, ArC*H*), 8.44 (2H, d, *J* = 8Hz, Ar-C*H*), 8.10 (2H, s, ArC*H*);

^{13}C-NMR (100.5 MHz): 193.4 (2 x *C*HO), 152.7 (2 x Ar*C*), 146.0 (2 x Ar*C*), 138.0 (2 x Ar*C*H), 131.6 (2 x Ar*C*), 129.1 (2 x Ar*C*H), 120.5 (2 x Ar*C*H) ppm.

NMR data was consistent with literature values.

3.2.9: 1,10-Phenanthroline-2,9-dicarbonitrile[95]

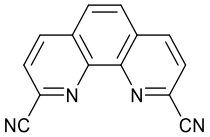

Method A:

To a suspension of dialdehyde **3.2.7** (1.25 g, 5.31 mmol), in dry acetonitrile (100 ml) was added hydroxylamine hydrochloric acid (0.76 g, 11.68 mmol) and triethylamine (5 ml). The mixture was heated under reflux for 4 hours and then allowed to cool to room temperature. Subsequently *p*-toluenesulfonyl chloride (3.61 g, 17.53 mmol) and 1,8-diazabicyclo[5.4.0]undec-7-ene (2.45 ml, 15.93 mmol) were added and the mixture heated under reflux for 21 hour. The reaction mixture was filtered whilst hot and washed with hot acetonitrile (10 ml). The filtrate was evaporated to afford a brown semi-solid which was triturated with MeOH (35 ml). The solid was filtered and washed with MeOH (30 ml) and Et_2O (20 ml) to afford the dinitrile **3.2.9** as a light brown solid (0.66 g, 54%).

^{1}H-NMR δ_H (399.8 MHz): 8.48 (2H, d, *J* = 8.24 Hz, ArC*H*), 8.08 (2H, d, *J* = 8.24 Hz, ArC*H*), 8.02 (2H, s, ArC*H*);

Method B:[148]

1,10-Phenanthroline-2,9-dicarboxamide **3.2.13** (1.39 g, 5.22 mmol) was dissolved in phosphorus oxychloride (10 ml) and refluxed for 20 hour. Solution cooled to room temperature and poured onto ice-water (100 ml) with external cooling. The slurry was diluted with water (100 ml) and the resulting precipitate was filtered and washed with water (2 x 60 ml) and diethyl ether (2 x 60 ml). The resulting brown solid was left to dry overnight (0.51 g, 43%).

^{1}H-NMR δ_H (399.8 MHz, DMSO-D6): 8.85 (2H, d, *J* = 8.24 Hz, ArC*H*), 8.43 (2H, d, *J* = 8.24 Hz, ArC*H*), 8.28 (2H, s, ArC*H*) ppm.

NMR data was consistent with literature values.

3.2.11: 2,9-bis(trichloromethyl)-1,10-phenanthroline[105]

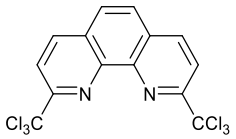

A stirred solution of 2,9-dimethyl-1,10-phenanthroline (2.06 g, 9.60 mmol), *N*-chlorosuccinimide (9.23 g, 69.14 mmol) and azobisisobutyronitrile (AIBN) (8.00 mg, 0.05 mmol) were refluxed for 18 hour. The resulting mixture was washed with a 1 M solution of NaOH (6 x 90 ml) and a saturated solution of K_2CO_3 (2 x 90 ml), dried over $MgSO_4$ and evaporated under reduced pressure to afford a yellow crystalline solid (3.72 g, 93%).

^{1}H-NMR δ_H (399.8 MHz): 8.45 (2H, d, *J* = 8.47 Hz, 4-ArC*H* and 7-ArC*H*), 8.33 (2H, d, *J* = 8.47 Hz, 3-ArC*H* and 8-ArC*H*), 7.98 (2H, s, 5-ArC*H* and 6-ArC*H*);

^{13}C-NMR (100.5 MHz): 158.0 (*C*Cl_3), 143.2 (Ar*C*), 138.2 (4-Ar*C*H and 7-ArCH), 129.2 (Ar*C*), 127.6 (5-Ar*C*H and 6-Ar*C*H), 120.5 (3-Ar*C*H and 8-Ar*C*H) ppm.

NMR data was consistent with literature values.

3.2.12: dimethyl 1,10-phenanthroline-2,9-dicarboxylate[105]

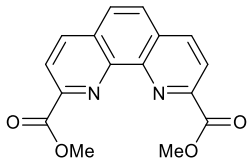

A suspension of **3.2.11** (2.00 g, 4.82 mmol) in H_2SO_4 (3 ml) was heated at 95 °C for 4 hr. The resulting solution was cooled to room temperature and CH_3OH (2.3 ml) was added dropwise. The mixture was heated at reflux for a further 1.5 hr before being allowed to cool. This was then neutralised by addition of a saturated solution of $NaHCO_3$ (30 ml). The resulting precipitate was filtered and washed with H_2O (3 x 25 ml) and diethyl ether (6 x 25 ml) and allowed to dry to leave a light tan solid (1.01 g, 70%).

^{1}H-NMR δ_H (399.8 MHz): 8.75 (2H, d, *J* = 8.24 Hz, ArC*H* and ArC*H*), 8.43 (2H, d, *J* = 8.24 Hz, ArC*H* and ArC*H*), 8.23 (2H, s, ArC*H* and ArC*H*), 4.03 (6, s, 2 x OCH_3);

^{13}C-NMR (100.5 MHz): 166.0 (2 x Ar*C*O), 148.2 (2 x Ar*C*), 145.6 (2 x Ar*C*), 138.6 (2 x Ar*C*H), 131.1 (2 x Ar*C*), 129.1 (2 x Ar*C*H), 124.3 (2 x Ar*C*H), 53.3 (2 x O*C*H_3) ppm.

NMR data was consistent with literature values.

3.2.13: 1,10-phenanthroline-2,9-dicarboxamide [105]

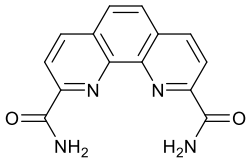

A suspension of **3.2.12** (1.01 g, 3.40 mmol) and NH_4Cl (76 mg, 1.41 mmol) in concentrated NH_4OH (30 ml) was stirred at room temperature for 24 hour. The resulting precipitate was filtered and washed with H_2O (2 x 40 ml) and diethyl ether (2 x 40 ml). This was left to dry overnight to yield the diamide as a beige solid (0.79 g, 87 %).

^{1}H-NMR δ_H (399.8 MHz, DMSO-D6): 8.98 (2H, s, br, N*H*$_2$), 8.72 (2H, d, *J* = 8.24 Hz, 2 x ArC*H*), 8.47 (2H, d, *J* = 8.24 Hz, 2 x ArC*H*), 8.17 (2H, s, 2 x ArC*H*), 7.90 (2H, s, br, N*H*$_2$);

^{13}C-NMR (100.5 MHz, DMSO-D6): 166.6 (2 x ArCO), 150.5 (2 x ArC), 144.5 (2 x ArC), 138.5 (2 x Ar*C*H), 130.7 (2 x ArC), 128.4 (2 x Ar*C*H), 121.6 (2 x Ar*C*H) ppm.

NMR data was consistent with literature values.

3.2.10: 1,10-Phenanthroline-2,9-dicarbohydrazonamide[95]

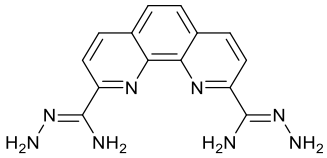

To a suspension of dinitrile **3.2.9** (0.66 g , 2.88 mmol) in EtOH (40 ml) was added hydrazine hydrate (50-60%, 20 ml). The suspension was stirred at room temperature for 3 days then at 40 °C for 4 hour. The solid was filtered and washed with H_2O (20 ml) and allowed to dry in air overnight to afford the product as a pale yellow solid (0.75 g, 88%).

^{1}H-NMR δ_H (399.8MHz, DMSO-D6): 8.38 (2H, d, *J* = 8.70 Hz, ArC*H*), 8.28 (2H, d, *J* = 8.70 Hz, ArC*H*), 7.95 (2H, s, ArC*H*), 6.14 (2H, s, br, N*H*$_2$), 5.67 (2H, s, br, N*H*$_2$);

NMR data was consistent with literature values.

General synthesis of ketopinic acid-amide derivatives.

Method A:[149]

(1S)-ketopinic acid (0.10 g, 0.55 mmol), *N*-(3-dimethylaminopropyl)-*N*'-ethylcarbodiimide hydrochloride (0.13 g, 0.66 mmol), 4-(dimethylamino)pyridine (0.08 g, 0.66 mmol) were dissolved in DCM (10 ml) and mixture stirred for 30 minutes. Morpholine (0.05 ml, 0.55 mmol) was subsequently added and the mixture stirred at room temperature for 24 hour. H_2O (5 ml) was added and the resulting layers separated. The aqueous layer was extracted with DCM (20 ml) and the combined organic layers were washed with aq. hydrochloric acid (2 x 10 ml), H_2O (10 ml), aq. NaOH (2 x 10 ml), H_2O (10 ml), brine (10 ml) and dried ($MgSO_4$). The solvent was removed under reduced pressure to leave the product.

Method B:[151]

(1S)-ketopinic acid (0.10 g, 0.55 mmol) and thionyl chloride (1.0 ml) were added to a 50 ml flask and refluxed for 2 hour. The remaining $SOCl_2$ was removed under reduced pressure. The acyl chloride was dissolved in DCM (2 ml) and added to a mixture of trimethylamine (0.2 ml, 0.83 mmol) and morpholine (0.1 ml, 0.83 mmol) in DCM (2 ml) at 0 °C. The mixture was stirred at 0 °C for 10 minutes then at room temperature for 18 hour. H_2O (10 ml) added and the aqueous layer was separated and washed with DCM (3 x 10 ml). The combined organic layers were washed with brine (10 ml), dried (Na_2SO_4) and the solvent removed under reduced pressure to leave the product.

3.3.1: 7,7-Dimethyl-1-(morpholine-4-carbonyl)bicyclo[2.2.1]heptan-2-one[151]

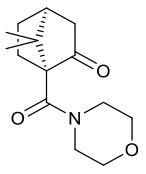

Yield (Method A): 27 mg, 19%.

Yield (Method B): 120 mg, 86% as a white solid.

^{1}H-NMR δ_H (399.8 MHz): 3.78 – 3.65 (8H, m, 4 x C*H*$_2$), 3.58 – 3.30 (2H, m, CH_2), 2.52 (1H, ddd, *J* = 18.78, 5.04, 2.75 Hz, C*H*), 2.27 (1H, td, *J* = 12.82, 3.21 Hz, C*H*), 2.15 – 2.06 (1H, m,

C*H*), 2.04 – 1.98 (2H, m, 2 x C*H*), 1.91 (1H, d, *J* = 18.78 Hz, C*H*), 1.46 (1H, ddd, *J* = 9.16, 6.87, 3.21 Hz, C*H*), 1.23 (3H, s, CH_3), 1.21 (3H, s, CH_3);

^{13}C-NMR (100.5 MHz): 212.6 (2-*C*O), 167.7 (*C*O), 67.3 (1-*C*), 67.1 (4 x *C*H_2), 50.6 (7-*C*), 43.7 (*C*H_2), 43.1 (4-*C*H), 27.2 (*C*H_2), 27.1 (*C*H_2), 21.3 (*C*H_3), 21.0 (*C*H_3) ppm.

NMR data was consistent with literature values.

3.3.2: 7,7-Dimethyl-1-(piperidine-1-carbonyl)bicyclo[2.2.1]heptan-2-one[151]

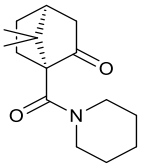

Yield (Method A): 71 mg, 52%.

Yield (Method B): 735 mg, 90%.

^{1}H-NMR δ_H (399.8 MHz): 3.56 – 3.35 (4H, m, br CH_2), 2.50 (1H, ddd, *J* = 18.32, 4.58, 2.75 Hz, 4-C*H*), 2.24 – 2.17 (1H, m, C*H*), 2.04 – 1.94 (2H, m, 2 x C*H*), 1.90 (1H, t, *J* = 4.58 Hz, C*H*), 1.83 (1H, d, *J* = 18.32 Hz, C*H*), 1.56 – 1.46 (6H, m, br, 3 x CH_2), 1.41 – 1.38 (1H, m, C*H*), 1.14 (3H, s, CH_3), 1.12 (3H, s, CH_3);

^{13}C-NMR (100.5 MHz): 211.4 (2-*C*O), 166.3 (*C*O), 66.4 (1-*C*), 49.6 (*C*), 42.7 (2 x *C*H_2), 42.1 (4-*C*H), 26.5 (*C*H_2), 26.1 (CH_2), 25.3 (3 x *C*H_2), 23.6 (*C*H_2), 20.3 (*C*H_3), 20.1 (*C*H_3) ppm.

NMR data was consistent with literature values.

3.3.3: *N,N*-Dimethyl-7,7-dimethyl-2-oxobicyclo[2.2.1]heptane-1-carboxamide[177]

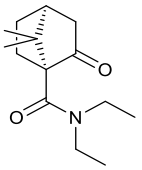

Yield (Method A): 54 mg, 42%;

Yield (Method B): 665 mg, 84%, as a beige solid.

^{1}H-NMR δ_H (399.8 MHz): 3.58 – 3.41 (2H, m, CH_2), 3.16 (2H, sp, *J* = 7.33, 6.87 Hz, CH_2), 2.50 (1H, ddd, *J* = 18.32, 5.04, 3.21 Hz, C*H*), 2.27 (1H, dd, *J* = 11.91, 4.12 Hz, C*H*), 2.09 (1H, tq, *J* = 11.91, 7.33, 2.75 Hz, C*H*), 2.02 – 1.95 (2H, m, 2 x C*H*), 1.91 (1H, d, *J* = 18.32 Hz, C*H*), 1.45

(1H, ddd, *J* = 11.91, 4.12, 3.21 Hz, C*H*), 1.22 (3H, s, CH_3), 1.21 (3H, s, CH_3), 1.13 (3H, t, *J* = 7.33. 6.87 Hz, CH_3);

^{13}C-NMR (100.5 MHz): 212.7 (*C*O), 168.2 (*C*O), 67.6 (*C*), 50.7 (*C*), 43.9 (*C*H_2), 43.2 (*C*H), 41.8 (*C*H_2), 40.3 (*C*H_2), 27.7 (*C*H_2), 27.1 (*C*H_2), 21.6 (*C*H_3), 20.9 *(C*H_3), 14.3 (*C*H_3), 12.8 (*C*H_3) ppm.

NMR data was consistent with literature values.

3.3.4: 7,7-dimethyl-2-oxo-N-(propan-2-yl)bicyclo[2.2.1]heptane-1-carboxamide[178]

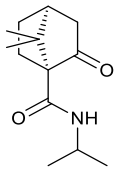

Yield (Method B): 434 mg, 97%, as a light yellow oil.

^{1}H-NMR δ_H (399.8 MHz): 7.42 (1H, s, br, N*H*), 4.12 (1H, se, *J* = 6.87, 6.41 Hz, NC*H*), 2.58-2.47 (2H, m, 2 x C*H*), 2.19-2.10 (1H, m, C*H*), 2.09-2.05 (1H, m, C*H*), 1.97 (1H, d, *J* = 18.32 Hz, C*H*), 1.61-1.54 (1H, m, C*H*), 1.42 (1H, ddd. *J* = 6.62, 6.41, 3.66, C*H*), 1.25 (3H, s, CH_3), 1.19 (3H, d, *J* = 6.41, CH_3), 1.16 (3H, d, *J* = 6.41, CH_3), 0.97 (3H, s, CH_3);

^{13}C-NMR (100.5 MHz): 217.7 (*C*O), 168.0 (*C*O), 64.5 (*C*), 50.2 (*C*), 43.9 (*C*H_2), 43.2 (*C*H), 40.8 (N*C*H), 28.2 (*C*H_2), 27.8 (*C*H_2), 23.1 (*C*H_3), 22.5 (*C*H_3), 21.2 (*C*H_3), 20.4 (*C*H_3) ppm.

NMR data was consistent with literature values.

3.3.5: *N*,7,7-trimethyl-2-oxobicyclo[2.2.1]heptane-1-carboxamide[179]

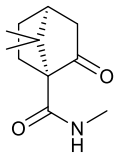

Yield (Method B): 523 mg, 81%, as a clear oil.

^{1}H-NMR δ_H (399.8 MHz): 7.52 (1H, s, br, NH_2), 2.77 (3H, d, *J* = 4.58 Hz, CH_3), 2.49 – 2.41 (2H, m, 2 x C*H*), 2.12 – 2.04 (1H, m, C*H*), 2.01 (1H, t, *J* = 4.58, 4.12 Hz, C*H*), 1.90 (1H, d, *J* = 18.32, C*H*), 1.55 – 1.48 (1H, m, C*H*), 1.39 – 1.33 (1H, m, C*H*), 1.19 (3H, s, CH_3), 0.90 (3H, s, CH_3);

^{13}C-NMR (100.5 MHz): 217.5 (*C*O), 169.7 (*C*ON), 64.6 (*C*), 50.1 *(C*), 43.7 (*C*H_2), 43.2 (*C*H), 28.4 (*C*H_2), 27.7 (*C*H_2), 25.7 (*C*H_3), 21.0 (*C*H_3), 20.4 (*C*H_3) ppm.

NMR data was consistent with literature values.

3.3.6: *N*-hexyl-7,7-dimethyl-2-oxobicyclo[2.2.1]heptane-1-carboxamide[180]

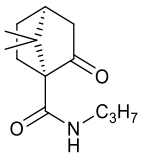

Yield (Method B): 434 mg, 88%, as a clear oil.

^{1}H-NMR δ_H (399.8 MHz): 7.63 (1H, s, br, NH), 3.35 – 3.18 (2H, m, NCH_2), 2.59 – 2.48 (2H, m, CH_2), 2.15 (1H, tq, *J* = 12.14, 4.12, 3.66 Hz, CH), 2.08 (1H, t, *J* = 4.12 Hz, C*H*), 1.98 (1H, d, *J* = 18.78 Hz, C*H*), 1.63 – 1.51 (3H, m, 1 x CH, 1 x CH_2), 1.43 (1H, td, *J* = 4.12, 3.66 Hz, C*H*), 1.26 (3H, s, CH_3), 0.98 (3H, s, CH_3), 0.93 (3H, t, *J* = 7.33 Hz, CH_3);

^{13}C-NMR (100.5 MHz): 217.9 (*C*O), 169.1 (N*C*O), 64.6 (*C*), 50.2 (*C*), 43.9 (*C*H_2), 43.2 (*C*H), 40.6 (*C*H_2), 28.4 (*C*H_2), 27.8 (*C*H_2), 22.9 (*C*H_2), 21.1 (*C*H_3), 20.5 (*C*H_3), 11.5 (*C*H_3) ppm.

NMR data was consistent with literature values.

3.3.7: *N*-hexyl-7,7-dimethylbicyclo[2.2.1]heptane-1-carboxamide

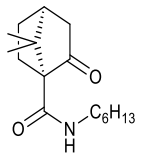

Yield (Method B): 695 mg, 80%, as a clear oil.

^{1}H-NMR δ_H (399.8 MHz): 7.62 (1H, s, br, N*H*), 3.36 – 3.21 (2H, m, NCH_2), 2.58 – 2.48 (2H, m, CH_2), 2.15 (1H, tq, *J* = 11.91, 4.12, 3.66 Hz, C*H*), 2.08 (1H, t, *J* = 4.58/4.12 Hz, C*H*), 1.98 (1H, d, *J* = 18.78 Hz, C*H*), 1.63 – 1.40 (4H, m, 1 x C*H*, 1 x CH_2), 1.35 – 1.28 (6H, td, *J* = 4.12, 3.66 Hz, C*H*), 1.26 (3H, s, CH_3), 0.97 (3H, s, CH_3), 0.88 (3H, t, *J* = 6.41 Hz, CH_3);

^{13}C-NMR (100.5 MHz): 217.8 (*C*O), 169.0 (N*C*O), 64.6 (*C*), 50.1 (*C*), 43.9 (*C*H_2), 43.2 (*C*H), 38.9 (*C*H_2), 31.5 (*C*H_2), 29.5 (*C*H_2), 28.4 (*C*H_2), 27.8 (*C*H_2), 26.6 (*C*H_2), 22.6 (*C*H_2), 21.1 (*C*H_3), 20.4 (*C*H_3), 14.1 (*C*H_3) ppm.

3.3.9: 7,7-dimethyl-2,3-dioxobicyclo[2.2.1]heptane-1-carboxylic acid[152]

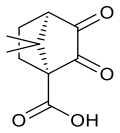

Method A:

(S)-(+)-ketopinic acid (0.80 g, 4.40 mmol) and SeO_2 (1 eq., 0.50 g, 4.40 mmol) were refluxed in acetic acid. A further 0.2 eq. of SeO_2 were added and the reaction monitored via TLC to monitor completion of the reaction. The reaction mixture was filtered through celite and washed with EtOAc before the solvent was removed under reduced pressure. The viscous yellow oil was dissolved in DCM and diluted with hexane. The solid was filtered and washed with hexane.

Method B:

(*S*)-(+)-Ketopinic acid (0.50 g, 2.74 mmol) was suspended in AcOH (5 ml) and the solution heated to 90 °C. A solution of bromine (0.20 ml, 3.26 mmol) in AcOH (3 ml) was added slowly over 20 minutes. Upon addition the solution was maintained at 90 °C for a further 2 hours, before cooling to room temperature and stirring for a further 20 hours. Upon completion the mixture was added dropwise to an ice cooled solution of water with stirring. The resulting precipitate was filtered and washed with water. The solid was left to dry overnight to leave the crude solid (0.52 g). The crude solid (1.98 mmol) was suspended in DMSO (20 ml) and sodium iodide (0.31 g, 1.98 mmol) added. The mixture was heated to 150 °C and air was pumped through the reaction mixture for 7 hours. Upon completion the solution was cooled and water (60 ml) subsequently added followed by sodium thiosulfate (0.20 g). The mixture was extracted with EtOAc (2 x 20 ml), the organic phases washed with water (5 x 10 ml) and dried (Na_2SO_4). The solvent was removed under reduced pressure.

Method A: **Yield**: 0.15 g, 70%, as a yellow solid.

Method B: **Yield**: 0.08 g, 20%, as a pale yellow solid.

^{1}H-NMR δ_H (399.8 MHz): 2.72 (1H, d, *J* = 5.04 Hz, 4-C*H*), 2.42 (1H, td, *J* = 12.82, 4.58 Hz, C*H*), 2.28 (1H, tt, *J* = 5.04, 4.58 Hz, C*H*), 2.03 (1H, tt, *J* = 5.04, 4.58 Hz, C*H*), 1.71 (1H, ddd, *J* = 5.04, 4.58 Hz, C*H*), 1.25 (3H, s, CH_3), 1.25 (3H, s, CH_3);

^{13}C-NMR (100.5 MHz): 201.0 (*C*O), 199.5 (*C*O), 172.6 (*C*O), 67.3 (*C*), 58.0 (4-*C*H), 44.8 (*C*), 26.6 (*C*H_2), 22.1 (*C*H_3), 21.4 (*C*H_2), 18.4 (*C*H_3) ppm.

NMR data was consistent with literature values.

3.3.8: 7,7-Dimethyl-1-(morpholine-4-carbonyl)bicyclo[2.2.1]heptane-2,3-dione

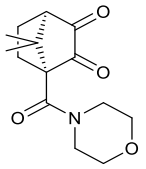

Yield: 480 mg, 58%, as a yellow solid.

^{1}H-NMR δ_H (399.8 MHz): 3.81 - 3.44 (8H, m, 4 x C*H*$_2$), 2.59 (1H, d, *J* = 5.04 Hz, C*H*), 2.46 (1H, td, *J* = 12.82, 4.58, 4.12 Hz, C*H*), 2.30 (1H, tt, *J* = 13.28, 5.04 Hz, C*H*), 2.17 (1H, ddd, *J* = 9.16, 4.58, 4.12 Hz, C*H*), 1.75 (1H, ddd, *J* = 9.16, 4.58, 4.12 Hz, C*H*), 1.37 (3H, s, C*H*$_3$), 1.28 (3H, s, C*H*$_3$);

^{13}C-NMR (100.5 MHz): 200.1 (*C*O), 198.0 (*C*O), 165.3 (*C*O), 67.0 (4 x *C*H_2), 57.7 (*C*H), 45.8 (*C*), 27.3 (*C*H_2), 22.7 (*C*H_2), 22.3 (*C*H_3), 19.3 (*C*H_3) ppm.

HRMS (ESI +ve) m/z: 266.1389; *calculated for* $[C_{14}H_{19}NO_4 + H]^+$ 266.1387

3.3.10: *N*,*N*-Diethyl-7,7-dimethyl-2,3-dioxobicyclo[2.2.1]heptane-1-carboxamide

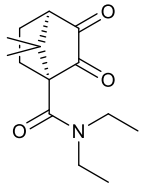

Yield: 340 mg, 67%, yellow solid.

m.p: 144.0-145.5 °C

^{1}H-NMR δ_H (399.8 MHz): 3.55 (1H, qu, *J* = 14.65, 7.33, 6.87 Hz, C*H*), 3.36 (1H, qu, *J* = 14.65, 7.33, 6.87 Hz, C*H*) 3.23 (2H, qu, *J* = 14.20, 7.33, 6.87 Hz, 2 x NC*H*), 2.56 (1H, d, *J* = 5.04 Hz, C*H*), 2.46 (1H, td, *J* = 13.28, 4.58, 4.12 Hz, C*H*), 2.29 (1H, tt, *J* = 13.74, 5.04 4.58 Hz, C*H*), 2.14 (1H, ddd, *J* = 9.16, 4.58 Hz, C*H*), 1.74 (1H, ddd, *J* = 5.04, 4.58, 4.12 Hz, C*H*), 1.34 (3H, s, C*H*$_3$), 1.29 (3H, s, C*H*$_3$), 1.18 (6H, sp, *J* = 7.33, 6.87, 6.41 Hz, 2 x C*H*$_3$);

^{13}C-NMR (100.5 MHz): 200.7 (*C*O), 198.2 (*C*O), 165.7 (*C*O), 67.5 (*C*), 57.7 (*C*H), 45.9 (*C*), 41.9 (N*C*H$_2$), 40.5 (N*C*H$_2$), 27.8 (*C*H$_2$), 22.7 (*C*H$_2$), 22.5 (*C*H$_3$), 19.2 (*C*H$_3$), 14.4 (*C*H$_3$), 12.7 (*C*H$_3$) ppm.

3.3.11: 7,7-dimethyl-1-(piperidine-1-carbonyl)bicyclo[2.2.1]heptane-2,3-dione

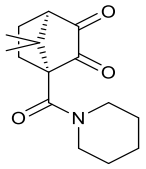

Yield: 500 mg, 70% as a yellow solid.

^{1}H-NMR δ_H (399.8 MHz): 3.57 – 3.37 (4H, m, 2 x C*H*$_2$), 2.55 (1H, d, J = 5.04 Hz, 4-C*H*), 2.46 (1H, ddd, J = 4.61, 4.58 Hz, C*H*), 2.32 – 2.13 (2H, m, 2 x C*H*), 2.05 – 1.95 (1H, m, C*H*) 1.76 – 1.60 (6H, m, 3 x C*H*$_2$), 1.34 (3H, s, C*H*$_3$), 1.26 (3H, ,s, C*H*$_3$);

^{13}C-NMR (100.5 MHz): 200.7 (2-*C*O), 198.1 (3-*C*O), 165.0 (N*C*O), 65.9 (1-*C*), 57.8 (4-*C*H), 45.8 (7-*C*), 27.6 (*C*H$_2$), 24.5 (*C*H$_2$), 22.4 (*C*H$_3$), 19.5 (*C*H$_3$) ppm.

3.3.12: *N*,7,7-trimethyl-2,3-dioxobicyclo[2.2.1]heptane-1-carboxamide

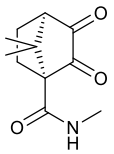

Yield: 176 mg, 33% as a solid.

^{1}H-NMR δ_H (399.8 MHz): 7.20 (1H, s, br, N*H*), 2.90 (3H, d, *J* = 4.58 Hz, NC*H*$_3$), 2.75 (1H, td, *J* = 4.58, 4.12 Hz, C*H*), 2.67 (1H, d, *J* = 5.04 Hz, 4-C*H*), 2.36 (1H, tt, *J* = 5.04, 4.58 Hz, C*H*), 1.82 (1H, ddd, *J* = 5.04, 4.58, 4.12 Hz, C*H*), 1.72 (1H, ddd, *J* = 4.58, 4.12 Hz, C*H*), 1.37 (3H, s, C*H*$_3$), 1.05 (3H, s, C*H*$_3$);

^{13}C-NMR (100.5 MHz): 201.9 (CO), 200.1 (CO), 167.2 (CO), 65.3 (C), 58.0 (CH), 45.6 (C), 28.5 (CH$_2$), 26.1 (CH$_3$), 22.8 (CH$_2$), 22.1 (CH$_3$), 19.4 (CH$_3$) ppm.

3.3.13: 7,7-dimethyl-2,3-dioxo-N-propylbicyclo[2.2.1]heptane-1-carboxamide

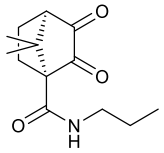

Yield (Method B): 200 mg, 45 %, as a yellow oil.

^{1}H-NMR δ_H (399.8 MHz): 7.22 (1H, s, br, N*H*), 3.33-3.18 (2H, m, CH_2), 2.73 (1H, td, *J* = 5.04, 4.58, 4.12 Hz, 4-C*H*), 2.64 (1H, d, *J* = 5.04 Hz, C*H*), 2.34 (1H, tt, *J* = 5.04, 4.58 Hz, C*H*), 1.79 (1H, ddd, *J* = 4.58, 4.12 Hz, C*H*), 1.70 (1H, ddd, *J* = 4.58, 4.12 Hz, C*H*), 1.60 – 1.50 (5H, m, CH_2 and CH_3), 1.33 (3H, s, CH_3), 1.03 (3H, s, CH_3);

^{13}C-NMR (100.5 MHz): 202.0 (*C*O), 200.1 (*C*O), 166.6 (N*C*O), 65.4 (*C*), 58.1 (*C*H), 45.6 (*C*), 43.9 (*C*H_2), 41.1 (*C*H_2), 28.4 (*C*H_2), 22.9 (*C*H_2), 22.2 (*C*H_3), 19.5 (*C*H_3), 11.50 (*C*H_3) ppm.

3.3.14: 7,7-dimethyl-2,3-dioxo-N-(propan-2-yl)bicyclo[2.2.1]heptane-1-carboxamide

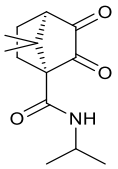

Yield (Method B): 320 mg, 42%, as a pale yellow solid.

^{1}H-NMR δ_H (399.8 MHz): 6.96 (1H, s, br, NH), 4.10 (1H, sep, J = 6.41 Hz, CH), 2.71 (1H, td, J = 4.58, 4.12 Hz, CH), 2.62 (1H, d, J = 5.04 Hz, 4-CH), 2.31 (1H, tt, J = 5.04, 4.58 Hz, CH), 1.77 (1H, ddd, J = 4.58, 4.12 Hz, CH), 1.67 (1H, ddd, J = 4.58, 4.12 Hz, CH), 1.31 (3H, s, CH_3), 1.19 (3H, d, J = 6.41 Hz, CH_3), 1.15 (3H, d, J= 6.41 Hz, CH_3), 1.01 (3H, s, CH_3);

^{13}C-NMR (100.5 MHz): 201.8 (CO), 200.1 (CO), 165.5 (NCO), 65.2 (C), 58.0 (CH), 45.5 (C), 41.3 (CH), 28.2 (CH_2), 27.7 (CH_2), 22.9 (CH_3), 22.7 (CH_3), 22.0 (CH_3), 19.3 (CH_3) ppm.

4.2.2: 2,2,5,5-Tetramethylcyclohexane-1,3-dione[159]

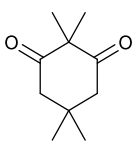

Dimedone (5.00 g, 35.67 mmol) was dissolved in a mixture of EtOH/H_2O (1:1, 100 ml), potassium carbonate (9.88 g, 71.34 mmol) was added and the mixture cooled to 0 °C. Iodomethane (6.0 ml, 90.95 mmol) was slowly added and the reaction mixture was stirred at 70 °C for 6 hour. The mixture was cooled to room temperature and water added to quench the reaction. The precipitate was filtered, dissolved in DCM and dried ($MgSO_4$) to leave the product as a white solid (4.25 g, 71%).

^{1}H-NMR δ_H (399.8 MHz): 1.61 (4H, s, 2 x C*H*$_2$), 1.30 (6H, s, 2 x C*H*$_3$), 0.99 (6H, s, 2 x C*H*$_3$);

^{13}C-NMR (100.5 MHz): 210.5 (*C*O), 60.5 (*C*-5), 51.1 (2 x *C*H_2), 30.7 (2-*C*), 28.5 (2 x *C*H_3), 22.2 (2 x *C*H_3) ppm.

LRMS (ESI -ve) m/z; 167.82; *calculated for* $[C_{10}H_{15}O_2 - H]^-$: 167.11

NMR data was consistent with literature values.

4.2.3: 3,3,6,6-Tetramethylcyclohexane-1,2,4-trione[160]

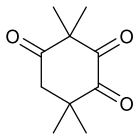

2,2,5,5-Tetramethylcyclohexane-1,3-dione **4.2.2** (1.04 g, 5.94 mmol) and selenium dioxide (1.34 g, 11.89 mmol, eq) were refluxed in 1,4-dioxane (35 ml) for 24 hour. The selenium metal was filtered off through celite and this was washed with EtOAc. The product was purified through column chromatography (silica gel: EtOAc:Hexane, 1:4) to yield the product as an off white solid (0.31 g, 29%).

^{1}H-NMR δ_H (399.8 MHz): 2.89 (2H, s, 5-C*H*$_2$), 1.37 (6H, s, 2 x C*H*$_3$), 1.21 (6H, s, 2 x C*H*$_3$);

^{13}C-NMR (100.5 MHz): 205.5 (*C*O), 202.3 (*C*O), 200.7 (*C*O), 63.2 (3-*C*), 49.9 (5-*C*H_2), 42.8 (6-*C*), 23.5 (2 x C*H*$_3$), 21.1 (2 x C*H*$_3$) ppm.

LRMS (ESI) *m/z*; 182.0949 *calculated for* $[C_{10}H_{14}O_3]$: 182.0943

NMR data was consistant with literature values.

4.2.5: *N,N*-Dimethylcarbamoylmethyltriphenylphosphonium [161]

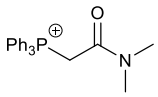

A solution of triphenylphosphine (0.45 g, 1.65 mmol) and 2-chloro-*N,N*-dimethylacetamide (0.18 ml, 1.65 mmol) were suspended in chloroform (10 ml) and refluxed for 3.5 hours. The solution was concentrated under reduced pressure and ether added to the residue and left to stir until a white solid precipitated. The precipitate was subsequently filtered to leave the product as a white solid (0.59 g, 99%).

^{1}H-NMR δ_H (399.8 MHz): 7.94 (3H, d, *J* = 13.28 Hz, 3 x ArC*H*), 7.92 (3H, d, *J* = 13.28 Hz, 3 x ArC*H*), 7.73 (3H, m, 3 x ArC*H*), 7.63 (6H, m, 6 x ArC*H*), 5.77 (2H, d, *J* = 12.82 Hz, CH_2), 3.48 (3H, s, CH_3), 2.87 (3H, s, CH_3);

^{13}C-NMR (100.5 MHz): 164.0 (*C*O), 134.3 ($^{2}J_{CP}$ = 2.88 Hz, 3 x Ar*C*H), 134.00 ($^{3}J_{CP}$ = 9.58 Hz, Ar*C*H), 129.9 ($^{4}J_{CP}$ = 12.46 Hz, Ar*C*H), 120.2 (*C*), 119.3 (*C*), 39.4 (N*C*H$_3$), 35.8 (N*C*H$_3$), 34.4 (CH$_2$);

^{13}P{^{1}H}-NMR δ_P (162 MHz): 22.20 ppm.

NMR data was consistent with literature values.

4.2.6: *N,N*-Dimethyl-2-(triphenyl-phosphanylidene)acetamide [161]

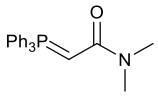

Sodium hydride (0.21 g, 8.69 mmol) was suspended in anhydrous DCM (10 ml) and a solution of *N,N*-dimethylcarbamoylmethyltriphenylphosphonium **4.2.5** (0.61 g, 1.74 mmol) in anhydrous DCM (10 ml) was added slowly under N_2 and stirred for 40 minutes. The solution was filtered through celite and concentrated to give a pale yellow semi-solid to which hexane (10 ml) was added. The resulting off-white solid was filtered to give the product (0.35 g, 58%).

^{1}H-NMR δ_H (399.8 MHz): 7.69 (6H, d, *J* = 7.79 Hz, ArC*H*), 7.66 (6H, d, *J* = 7.33 Hz, ArC*H*), 5.52 – 7.47 (6H, m, ArC*H*), 7.44-7.43 (12H, m, ArC*H*), 2.95 (7H, s, PCH and 2 x NCH_3);

^{13}C-NMR (100.5 MHz): 133.1 ($^{2}J_{CP}$ = 9.58 Hz, 6 x Ar*C*H), 131.4 (3 x Ar*C*H), 129.8 (Ar*C*), 128.5 ($^{2}J_{CP}$ = 11.50 Hz, 6 x Ar*C*H), 36.8 (P*C*H and 2 x N*C*H$_3$);

$^{13}P\{^{1}H\}$-NMR δ_P (162 MHz): 29.90 ppm.

NMR data was consistent with literature values.

4.2.10: diethyl [2-(dimethylcarbamoyl)acetyl]phosphonite[162]

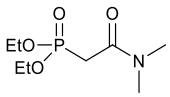

A mixture of 2-chloro-*N*,*N*-dimethylacetamide (1.0 ml, 9.72 mmol) and triethyl phosphite (1.7 ml, 9.72 mmol) were stirred at 180°C for 16 hour before cooling to room temperature. Excess triethyl phosphite was removed by vacuum distillation to leave the product as a pale oil (1.75 g, 80%).

^{1}H-NMR δ_H (399.8 MHz): 4.18 (4H, m, OCH_2), 3.13 (3H, s, NCH_3), 3.04 (2H, d, J = 21.98 Hz, PCH_2), 2.98 (3H, s, NCH_3), 1.35 (6H, t, ^{1}J = 7.33, 6.87 Hz, ^{2}J = 14.20 Hz, CH_3CH$_2$O);

^{13}C-NMR (100.5 MHz): 164.8 ($^{2}J_{CP}$ = 5.75 Hz, *C*O), 62.61 ($^{2}J_{CP}$ = 6.71 Hz, 2 x *C*H$_2$CH$_3$), 38.6 (NCH$_3$), 35.8 (NCH$_3$), 32.7 (COCH$_2$), 16.4 ($^{3}J_{CP}$ = 5.75 Hz, 2 x *C*H$_3$);

^{13}P{^{1}H}-NMR δ_P (162 MHz): 22.25 ppm.

NMR data was consistent with literature values.

4.2.12: 3-Methylene-2,2,5,5-tetramethylcyclohexan-1-one[181]

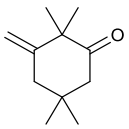

Methyltriphenylphosphonium bromide (5.16 g, 14.40 mmol) was suspended in dry diethyl ether (30 ml) and placed under N_2. *t*-BuOK (1.65 g, 14.40 mmol) was added and stirred at room temperature for 2 hours to leave a yellow solution. 2,2,5,5-Tetramethylcyclohexane-1,3-dione **4.2.2** (1.21 g, 7.20 mmol) was suspended in dry diethyl ether (20 ml) and the Wittig reagent was added dropwise over 10 minutes. The solution was stirred at 40 °C for 24 hours and monitored via TLC. The solution was allowed to cool, the precipitate filtered and the solvent removed under reduced pressure. The sample was triturated with hexane and the white solid, phosphorus oxide,

was filtered. The product was purified by column chromatography (silica gel: hexane:EtOAc, 5:1) to leave the product as a clear oil (0.37 g, 31%).

^{1}H-NMR δ_H (399.8 MHz): 4.89 (1H, s, C=C*H*), 4.79 (1H, s, C=C*H*), 2.37 (2H, s, CH_2), 2.34 (2H, s, CH_2), 1.26 (6H, s, 2 x CH_3), 0.90 (6H, s, 2 x CH_3);

^{13}C-NMR (100.5 MHz): 213.9 (1-*C*O), 151.3 (*C*=CH_2), 110.4 (C=*C*H_2), 51.3 (*C*H_2), 45.9 (*C*H_2), 27.0 (2 x CH_3), 24.4 (2 x CH_3) ppm.

NMR data was consistent with literature values.

4.2.16: 3-(Hexylamino)-2,2,5,5-tetramethylcyclohexan-1-one

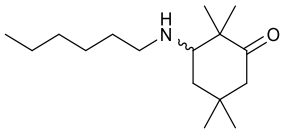

Sodium triacetoxyborohydride (0.55 g, 2.50 mmol) was dissolved in anhy. THF (15 ml). 2,2,5,5-Tetramethylcyclohexane-1,3-dione (0.20 g, 1.20 mmol) dissolved in anhy. THF (5 ml) and hexylamine (0.20 ml, 1.40 mmol) were added slowly. The reaction mixture was stirred at room temperature for 24hours. Upon completion the reaction was quenched by the slow addition of water and then extracted with chloroform (3 x 10 ml) and dried ($MgSO_4$). The solvent was removed under reduced pressure and residue purified by column chromatography (silica gel: 100 % DCM) to leave the product as a clear oil (50 mg, 17 %).

^{1}H-NMR δ_H (399.8 MHz): 5.72 (1H, s, br, N*H*), 3.73 (1H, dd, *J* = 5.95, 4.58 Hz, 3-C*H*NH), 3.23 (2H, q, *J* = 6.87, 6.41 Hz, CH_2CH_2NH), 2.50 (1H, d, *J* = 13.74 Hz, CH_{exo}), 1.98 (1H, dd, *J* = 13.74, 1.37 Hz, CH_{endo}), 1.80-1.78 (2H, m, CH_2), 1.44 (2H, qu, *J* = 7.33, 6.87 Hz, CH_2), 1.35-1.26 (6H, m, 2 x CH_2, CH_3), 1.15 (3H, s, CH_3), 1.11 (3H, s, CH_3), 1.08 (3H, s, CH_3), 0.88 (3H, t, *J* = 6.41 Hz, CH_2CH_3), 0.87 (3H, s, CH_3);

^{13}C-NMR (100.5 MHz): 214.6 (*C*O), 73.9 (3-*C*H), 50.6 (2-*C*), 50.2 (*C*H_2), 43.1 (*C*H_2), 39.7 (*C*H_2), 31.9 (*C*H_3), 31.8 (5-*C*), 31.5 (*C*H_2), 29.5 (*C*H_2), 26.7 (*C*H_3), 26.6 (*C*H_2), 22.6 (*C*H_2), 21.2 (*C*H_3), 18.7 (*C*H_3), 14.0 (*C*H_3) ppm.

LRMS (ESI +ve) m/z 207.17; *calculated for* $[C_{11}H_{18}N_4 + H]^+$ 207.16

4.2.22: 3-Hydroxy-2,2,5,5-tetramethylcyclohexan-1-one[182]

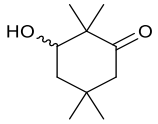

2,2,5,5-Tetramethylcyclohexane-1,3-dione **4.2.2** (3.65 g, 21.68 mmol) was dissolved in MeOH (45 ml). A solution of sodium borohydride (0.21 g, 5.56 mmol, 0.25 eq) in H_2O (20ml) was added dropwise over 15 minutes. The reaction mixture was stirred for 20 minutes and monitored via TLC using vanillin. Upon completion the solution was diluted with a sat. ammonium chloride solution (20 ml) and extracted with EtOAc (5 x 20 ml). The organic layers were collected and washed with sat. brine solution (30 ml) then dried (Na_2SO_4). The solvent was removed under reduced pressure to leave a pale oil which was purified by column chromatography (silica gel: EtOAc:Hexane, 1:4) to yield the product as a white solid (2.09 g, 57%).

^{1}H-NMR δ_H (399.8 MHz): 3.73 (1H, t, *J* = 6.87 Hz, C*H*OH), 2.50 (1H, d, *J* = 13.74 Hz, CH_{exo}), 1.96 (1H, dd, *J* = 13.74, 1.83 Hz, CH_{endo}), 1.91 (1H, s, br, O*H*), 1.80-1.77 (2H, m, CH_2), 1.14 (3H, s, CH_3), 1.11 (3H, s, CH_3), 1.08 (3H, s, CH_3), 0.87 (3H, s, CH_3);

^{13}C-NMR (100.5 MHz): 214.49 (*C*O), 74.01 (*C*HOH), 50.54 (*C*-3), 50.19 (*C*H_2), 43.04 (*C*H_2), 31.89 (*C*H_3), 31.86 (*C*-5), 26.74 (*C*H_3), 21.292 (*C*H_3), 18.63 (*C*H_3) ppm.

LRMS (ESI +ve) *m/z* 170.87; *calculated for* [$C_{10}H_{18}O_2$]: 170.13

NMR data was consistent with literature values.

4.2.23: 4-Hydroxy-3,3,6,6-tetramethylcyclohexane-1,2-dione

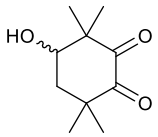

3-Hydroxy-2,2,5,5-tetramethylcyclohexan-1-one **4.2.22** (0.15 g, 0.88 mmol) was suspended in 1,4-dioxane (10 ml). Selenium dioxide (0.30 g, 2.64 mmol) was added and the mixture refluxed for 5.5 hours. Upon completion, diethyl ether (10ml) was added and the solution washed with brine (3x 10 ml), dried ($NaSO_4$) and the solvent removed under reduced pressure. The product was purified by column chromatography (silica gel: EtOAc : hexane, 1:4) to yield the product as a yellow oil (70 mg, 41%).

^{1}H-NMR δ_H (399.8 MHz): 4.03 (1H, q, *J* = 4.58. 4.12 Hz, 4-C*H*OH), 2.12-2.00 (3H, m, 5-C*H*$_2$ and O*H*), 1.25 (3H, s, C*H*$_3$), 1.23 (3H, s, C*H*$_3$), 1.15 (3H, s, C*H*$_3$), 1.12 (3H, s, C*H*$_3$);

^{13}C-NMR (100.5 MHz): 206.4 (*C*O), 205.33 (*C*O), 72.5 (4-*C*HOH), 53.9 (3-*C*), 44.9 (6-*C*), 42.3 (5-*C*H$_2$), 24.6 (*C*H$_3$), 24.1 (*C*H$_3$), 20.5 (*C*H$_3$), 16.4 (*C*H$_3$) ppm.

4.2.25: 3-methoxy-2,2,5,5-tetramethylcyclohexan-1-one

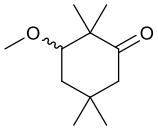

Sodium hydride (0.18 g, 7.56 mmol) was suspended in anhy. THF (10 ml) and placed under N_2. 3-Hydroxy ketone **4.2.22** (0.86 g, 5.04 mmol) in anhy. THF (6 ml) was added slowly and the mixture stirred at room temperature for 30 minutes. Iodomethane (1.3 ml, 20.15 mmol) was added and the mixture refluxed at 40 °C for 20 hours. Further iodomethane (0.5 ml) was added and the mixture stirred for 3 hours. The reaction was quenched with H_2O (15 ml), extracted with EtOAc (3 x 15 ml). The combined organic phases were washed with brine (15 ml) and dried ($MgSO_4$). The product was purified by column chromatography (silica gel: 5:1 hexane:EtOAc) to leave a clear oil (0.75 g, 82%).

^{1}H-NMR δ_H (399.8 MHz): 3.38 (3H, s, OCH_3), 3.13 (1H, dd, *J* = 11.45, 4.58, 4.12 Hz, 3-CH), 2.47 (1H, d, *J* = 13.74 Hz, CH_{exo}), 2.03 (1H, dd, *J* = 13.74, 2.29 Hz, CH_{endo}), 1.86 (1H, ddd, *J* = 6.87, 4.58, 4.12, 2.29 Hz, CH_{exo}), 1.65 (1H, t, *J* = 13.28 Hz, CH_{endo}), 1.14 (3H, s, CH_3), 1.09 (3H, s, CH_3), 1.07 (3H, s, CH_3), 0.86 (3H, s, CH_3);

^{13}C-NMR (100.5 MHz): 214.3 (1-CO), 83.6 (OCH_3), 58.1 (3-CH), 50.5 (CH_2), 50.4 (C), 38.6 (CH_2), 31.9 (CH_3), 31.7 (C), 26.9 (CH_3), 21.5 (CH_3), 19.5 (CH_3) ppm.

HRMS (ESI +ve) m/z; 184.1459 *calculated for* [$C_{11}H_{20}O_2$]: 184.1463

4.2.26: 4-methoxy-3,3,6,6-tetramethylcyclohexane-1,2-dione

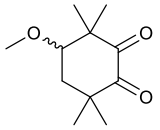

The starting methoxy-ketone **4.2.25** (0.75 g, 4.12 mmol) was dissolved in 1,4-dioxane (15 ml) and SeO_2 (0.91 g, 8.23 mmol) was added. The mixture was refluxed for 72 hours before cooling to room temperature. The resulting selenium metal was filtered through celite and washed with EtOAc. The solution was concentrated under reduced pressure to leave the product as an orange oil (0.70 g, 86%).

^{1}H-NMR δ_H (399.8 MHz): 3.41 (3H, s, C*H*$_3$), 3.39 (1H, t, *J* = 4.12 Hz, C*H*), 2.09 (1H, dd, *J* = 4.12 Hz, C*H*), 2.00 (1H, dd, *J* = 7.79 Hz, C*H*), 1.24 (3H, s, C*H*$_3$), 1.20 (3H, s, C*H*$_3$), 1.15 (3H, s, C*H*$_3$), 1.12 (3H, s, C*H*$_3$);

^{13}C-NMR (100.5 MHz): 206.4 (CO), 204.7 (CO), 82.5 (CH), 58.0 (CH_3), 53.8 (C), 45.1 (C), 37.5 (CH_2), 24.9 (*C*H_3), 24.4 (*C*H_3), 21.0 (*C*H_3), 17.6 (*C*H_3) ppm.

HRMS (ESI +ve) m/z; 199.1328 *calculated for* $[C_{11}H_{18}O_3+H]^+$: 199.1329

4.2.27: *N,N*-Dimethyl-2-[(2,2,5,5-tetramethyl-3-oxocyclohexyl)oxy]acetamide

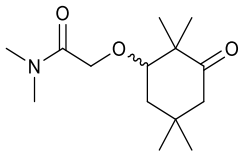

Sodium hydride (0.08 g, 3.50 mmol) was suspended in anhy. DMF (10 ml). A solution of 4-hydroxy-3,3,6,6-tetramethylcyclohexane-1,2-dione **4.2.22** (0.05 g, 0.30 mmol) in anhy. DMF (5 ml) was added slowly and the solution stirred for 30 minutes. 2-Chloro-*N,N*-dimethylacetamide (0.3 ml, 3.00 mmol) was added and the reaction mixture stirred at room temperature overnight. The reaction was quenched with sat. aq. NH_4Cl solution and extracted with EtOAc (3 x 10 ml). The combined organic layers were washed with H_2O (3 x 10 ml) and brine (2 x 10 ml) and then dried ($MgSO_4$). The solvent and remaining 2-chloro-*N,N*-dimethylacetamide were removed under reduced pressure to leave the product as a dark oil (48 mg, 58%). This was taken straight forward for the next step.

^{1}H-NMR δ_H (399.8 MHz): 4.18 (2H, q, *J* = 13.74, 13.28, 12.82 Hz, C*H*$_2$CO), 3.40 (1H, dd, *J* = 6.41, 4.58 Hz, C*H*), 3.07 (3H, s, NC*H*$_3$), 2.96 (3H, s, NC*H*$_3$), 2.47 (1H, d, *J* = 13.74 Hz, C*H*), 2.05 (1H, d, *J* = 13.74 Hz, C*H*), 1.93 (1H, dd, *J* = 13.28, 4.58 Hz, C*H*), 1.74 (1H, t, *J* = 12.36, 11.91 Hz, C*H*), 1.16 (3H, s, C*H*$_3$), 1.12 (3H, s, C*H*$_3$), 1.08 (3H, s, C*H*$_3$), 0.86 (3H, s, C*H*$_3$) ppm.

4.2.28: *N,N*-Dimethyl-2-[(2,2,5,5-tetramethyl-3,4-dioxocyclohexyl)oxy]acetamide

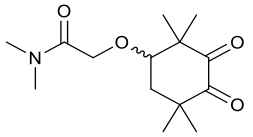

N,N-Dimethyl-2-[(2,2,5,5-tetramethyl-3-oxocyclohexyl)oxy]acetamide **4.2.27** (1.02 g, 4.00 mmol) was suspended in 1,4-dioxane (25 ml) and SeO_2 (0.68 g, 6.02 mmol) was subsequently added. The mixture was allowed to reflux for 18 hours before cooling to room temperature. The mixture was filtered through celite to remove the precipitated selenium metal and washed with EtOAc. The mixture was concentrated and purified by column chromatography (silica gel: DCM 100%, with increasing EtOAc fraction) to leave the product as a yellow oil (480 mg, 44%).

^{1}H-NMR δ_H (399.8 MHz): 4.26 (2H, d, *J* = 3.21 Hz, C*H*$_2$), 3.73 (1H, dd, *J* = 4.12 Hz, C*H*), 3.06 (3H, s, C*H*$_3$), 2.97 (3H, s, C*H*$_3$), 2.22 – 2.06 (2H, m, C*H*$_2$), 1.23 (3H, s, C*H*$_3$), 1.22 (3H, s, C*H*$_3$), 1.15 (3H, s, C*H*$_3$), 1.14 (3H, s, C*H*$_3$);

^{13}C-NMR (100.5 MHz): 206.1 (*C*O), 204.5 (*C*O), 169.1 (*C*ON), 81.4 (*C*H), 69.6 (*C*H$_2$), 53.80 (*C*), 44.9 (*C*), 38.0 (*C*H$_2$), 36.8 (*C*H$_3$), 35.5 (*C*H$_3$), 25.0 (*C*H$_3$), 24.2 (*C*H$_3$), 21.0 (*C*H$_3$), 17.6 (*C*H$_3$) ppm.

HRMS (ESI +ve) *m/z* 270.1702; *calculated for* [$C_{14}H_{23}NO_4$ + H]: 270.1700

4.2.29: 3-(2-Methoxyethoxy)-2,2,5,5-tetramethylcyclohexan-1-one

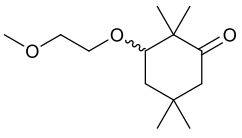

Sodium hydride (0.18 g, 4.63 mmol) was suspended in anhy THF (10 ml) and a solution of 4-hydroxy-3,3,6,6-tetramethylcyclohexane-1,2-dione (0.23 g, 1.32 mmol) was added at room temperature. The reaction mixture was stirred for 30 minutes before been cooled to 0°C.

Potassium iodide (0.80 g, 5.28 mmol) and 1-bromo-2-methoxyethane (0.50 ml, 5.28 mmol) were added slowly and the reaction refluxed for 24 hour. The reaction was quenched through the addition of water. The product was extracted with EtOAc (5 x 15 ml), the combined organics were washed with brine (50 ml) and dried ($MgSO_4$). The solvent was removed under reduced pressure to leave an orange residue. This was purified by column chromatography (silica gel: hexane:EtOAc, 2:1) to yield the product as a clear oil (50 mg, 16%).

^{1}H-NMR δ_H (399.8 MHz): 3.76-3.70 (1H, m, CH), 3.56-3.50 (3H, m, OC*H*$_2$C*H*O), 3.39 (3H, s, OCH_3), 3.29 (1H, dd, *J* = 10.99, 4.58 Hz, OC*H*), 2.47 (1H, d, *J* = 13.74 Hz, C*H*$_{exo}$), 2.03 (1H, dd, *J* = 13.74, 2.29 Hz, C*H*$_{endo}$), 1.86-1.84 (1H, m, C*H*$_{exo}$), 1.74 (1H, q, *J* = 12.82, 10.99, C*H*$_{endo}$), 1.15 (3H, s, C*H*$_3$), 1.10 (3H, s, C*H*$_3$), 1.08 (3H, s, C*H*$_3$), 0.86 (3H, s, C*H*$_3$);

^{13}C-NMR (100.5 MHz): 214.4 (*C*O), 82.4 (O*C*H), 72.3 (O*C*H$_2$), 69.9 (O*C*H$_2$), 59.1 (O*C*H$_3$), 50.5 (*C*), 50.4 (*C*H$_2$), 39.5 (*C*H$_2$CO), 31.8 (*C*), 31.7 (*C*H$_3$), 26.9 (*C*H$_3$), 21.5 (*C*H$_3$), 19.6 (*C*H$_3$) ppm.

4.2.30: 4-(2-Methoxyethoxy)-3,3,6,6-tetramethylcyclohexane-1,2-dione

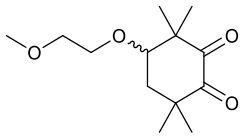

3-(2-Methoxyethoxy)-2,2,5,5-tetramethylcyclohexan-1-one **4.2.29** (0.05 g, 0.21 mmol) was suspended in 1,4-dioxane (10 ml) and selenium dioxide (0.07 g, 0.63 mmol) was added. The mixture was refluxed for 2 days and the selenium dioxide was filtered through silica. The product was extracted with ether (3 x 10 ml), and the combined organics were washed with H_2O (10 ml) and brine (10 ml) and dried (Na_2SO_4). The solvent was removed under reduced pressure to leave the product as a pale yellow oil (30 mg, 51%).

^{1}H-NMR δ_H (399.8 MHz): 3.78-3.73 (1H, m, OC*H*), 3.61-3.52 (3H, m, OC*H*$_2$C*H*O), 3.38 (3H, s, C*H*$_3$), 2.12 – 2.00 (2H, m, C*H*$_2$), 1.24 (3H, s, C*H*$_3$), 1.21 (3H, s, C*H*$_3$), 1.14 (3H, s, C*H*$_3$), 1.13 (3H, s, C*H*$_3$);

^{13}C-NMR (100.5 MHz): 206.4 (*C*O), 204.8 (*C*O), 81.3 (*C*H), 72.3 (*C*H$_2$), 70.0 (*C*H$_2$), 59.1 (*C*H$_3$), 53.9 (*C*), 45.0 (*C*), 38.5 (*C*H$_2$), 24.9 (*C*H$_3$), 24.3 (*C*H$_3$), 20.9 (*C*H$_3$), 17.6 (*C*H$_3$) ppm.

HRMS *m/z;* 243.1593; *calculated for* [$C_{13}H_{22}O_4$]: 243.1591

General Buchwald Hartwig Cross Coupling Synthesis

Xantphos (0.42 g, 0.73 mmol) was suspended in 1,4-dioxane (20 ml) and degassed with N_2 for 10 minutes. To this was added $Pd_2(DBA)_3$ (0.22 g, 0.24 mmol) and the mixture was stirred for a further 10 minutes. 5,5,8,8-Tetramethyl-5,6,7,8-tetrahydro-1,2,4-benzotriazin-3-amine **2.2.12** (0.95 g, 4.90 mmol), 2,6-dibromopyridine (0.59 g, 2.45 mmol) and caesium carbonate (3.32 g, 9.80 mmol) were subsequently added and the reaction mixture was refluxed for 24 hours under N_2. The resulting solution was filtered and the solid was washed with EtOAc and the solution was concentrated to leave an orange solid. Purification was achieved via column chromatography (silica gel: EtOAc/Hexane: 2:1).

L1: 2-*N*,6-*N*-Bis(5,6-diethyl-1,2,4-triazin-3-yl)pyridine-2,6-diamine

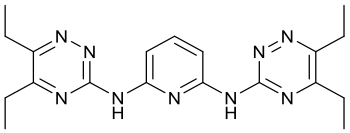

Yield: 53 mg, 26% as a yellow solid.

m.p: 263.1-264.5 °C

^{1}H-NMR δ_H (399.8MHz): 9.27 (2H, s, 2 x N*H*), 8.07 (2H, d, *J* = 8.24 Hz, 2 x Ar*H*), 7.74 (1H, t, *J* = 8.24, 7.33 Hz, Ar*H*), 2.91 (4H, q, *J* = 7.33 Hz, 2 x C*H*$_2$), 2.78 (4H, q, *J* = 7.33 Hz, 2 x C*H*$_2$), 1.36 (6H, t, *J* = 7.79 Hz, 2 x C*H*$_3$), 1.31 (6H, t, *J* = 7.79 Hz, 2 x C*H*$_3$);

^{13}C-NMR (100.5 MHz): 162.8 (2 x Ar*C*), 158.4 (2 x Ar*C*), 154.2 (2 x Ar*C*), 150.8 (2 x Ar*C*), 140.2 (Ar*C*H), 107.0 (2 x *C*H), 26.8 (2 x *C*H$_2$), 25.1 (2 x *C*H$_2$), 12.5 (2 x *C*H$_3$), 10.8 (2 x *C*H$_3$) ppm.

LRMS (ESI +ve) *m/z:* 380.26 *calculated for* $[C_{19}H_{25}N_9 + H]^+$: 380.23

HRMS (ESI +ve) *m/z*: 380.2302 *calculated for* $[C_{19}H_{25}N_9 + H]^+$: 380.2306

L3: N2-{8,11,11-Trimethyl-3,4,6-triazatricyclo[6.2.1.0^{2,7}]undeca-2(7),3,5-trien-5-yl}-N6-{8,11,11-trimethyl-3,4,6-triazatricyclo[6.2.1.0^{2,7}]undeca-2,4,6-trien-5-yl}pyridine-2,6-diamine

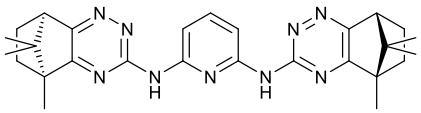

Yield: 0.96 g, 81% as a pale yellow solid.

m.p: 251.3-252.1 °C

^{1}H-NMR δ_H (399.8MHz): 8.54 (2H, s, br, 2 x N*H*), 8.10 (2H, d, *J* = 8.24 Hz, 2 x ArC*H*), 7.74 (1H, t, *J* = 8.24 Hz, ArC*H*), 3.10 (2H, d, *J* = 4.12 Hz, 2 x C*H*), 2.21 (2H, m, 2 x CH_{exo}), 1.98 (2H, m, 2 x CH_{exo}), 1.38 (4H, m, 4 x CH_{endo}), 1.25 (6H, s, 2 x CH_3), 1.05 (6H, s, 2 x CH_3), 0.65 (6H, s, 2 x CH_3);

^{13}C-NMR (100.5 MHz): 171.7 (Ar*C*), 162.5 (Ar*C*), 159.7 (Ar*C*), 158.4 (Ar*C*), 151.0 (Ar*C*), 140.2 (Ar*C*H), 107.4 (2 x Ar*C*H), 60.4 (*C*), 54..8 (*C*), 54.1 (*C*), 53.5 (*C*), 50.6 (*C*), 36.5 (*C*), 31.4 (2 x *C*H_2), 23.9 (2 x *C*H_2), 19.4 (2 x *C*H_3), 17.6 (2 x *C*H_3), 8.4 (2 x *C*H_3) ppm.

LRMS (ESI +ve) *m/z:* 484.36; *calculated for* $[C_{27}H_{33}N_9 + H]^+$: 484.29

HRMS (ESI +ve) *m/z*: 484.2923 *calculated for* $[C_{27}H_{33}N_9 + H]^+$: 484.2932

L4: N2,N6-Bis(5,5,8,8-tetramethyl-5,6,7,8-tetrahydro-1,2,4-benzotriazin-3-yl)pyridine-2,6-diamine

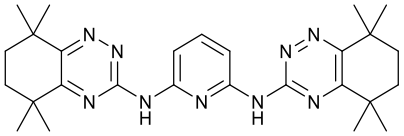

Yield: 26 mg, 22% as a pale yellow solid.

m.p: 184.8-186.2 °C

^{1}H-NMR δ_H (399.8 MHz): 8.35 (2H, s, br, 2 x N*H*), 8.06 (2H, d, *J* = 8.24 Hz, 2 x ArC*H*), 7.74 (1H, t, *J* = 8.24, 7.79 Hz, ArC*H*), 1.80 (8H, s, 4 x CH_2), 1.43 (12, s, 4 x CH_3), 1.34 (12, s, 4 x CH_3);

^{13}C-NMR (100.5 MHz): 164.9 (Ar*C*), 158.1 (Ar*C*), 156.9 (Ar*C*), 150.8 (Ar*C*), 140.2 (Ar*C*H), 106.6 (2 x Ar*C*H), 37.1 (*C*), 35.8 (*C*), 34.0 (*C*H_2), 33.2 (*C*H_2), 29.8 (*C*H_3), 29.2 (*C*H_3) ppm.

LRMS (ESI +ve) *m/z:* 487.59 *calculated for* $[C_{27}H_{37}N_9]$: 487.32

HRMS *m/z*: 488.3231 *calculated for* $[C_{27}H_{37}N_9 + H]^+$: 488.3245

L5: N2,N6-bis({5,5,7,7-tetramethyl-5H,6H,7H-cyclopenta[e][1,2,4]triazin-3-yl})pyridine-2,6-diamine

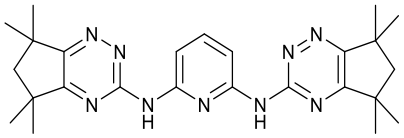

Yield: 285 mg, 95% as a pale yellow solid.

m.p: 159.9-161.5 °C

^{1}H-NMR δ_H (399.8 MHz): 8.35 (2H, s, br, 2 x N*H*), 8.13 (2H, d, *J* = 8.24 Hz, 2 x ArC*H*), 7.75 (1H, t, *J* = 8.24, 7.79 Hz, 4-ArC*H*), 1.98 (4H, s, 2 x 6-CH_2), 1.46 (12H, s, 4 x CH_3), 1.36 (12H, s, 4 x CH_3);

^{13}C-NMR (100.5 MHz): 171.3 (Ar*C*), 161.6 (Ar*C*), 159.5 (Ar*C*), 150.7 (Ar*C*), 140.3 (4-Ar*C*H), 107.0 (2 x Ar*C*H), 53.1 (6-*C*H_2), 40.7 (*C*), 39.7 (*C*), 29.8 (4 x *C*H_3), 28.8 (4 x *C*H_3) ppm.

HRMS m/z: 460.2926 calculated for $[C_{25}H_{33}N_9 + H]^+$: 460.2932

L6: N2-{8,11,11-Trimethyl-3,4,6-triazatricyclo[6.2.1.0^{2},^{7}]undeca-2(7),3,5-trien-5-yl}B-N6-{8,11,11-trimethyl-3,4,6-triazatricyclo[6.2.1.0^{2},^{7}]undeca-2,4,6-trien-5-yl}pyrazine-2,6-diamine

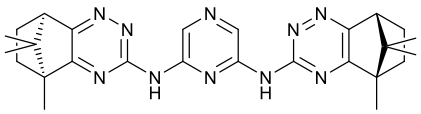

Yield: 236 mg, 56% as an orange solid.

m.p: 184.9-186.8 °C

^{1}H-NMR δ_H (399.8 MHz): 10.02 (2H, s, br, N*H*), 9.40 (2H, s, ArC*H*), 3.15 (2H, d, *J* = 3.66 Hz, C*H*), 2.29 – 2.24 (2H, m, 2 x CH_{exo}), 2.02 – 1.97 (2H, m, 2 x CH_{exo}), 1.43 – 1.42 (4H, m, 4 x CH_{endo}), 1.28 (6H, s, 2 x CH_3), 1.08 (6H, s, 2 x CH_3), 0.67 (6H, s, 2 x CH_3);

^{13}C-NMR (100.5 MHz): 172.0 (Ar*C*), 160.4 (Ar*C*), 158.2 (Ar*C*), 147.0 (Ar*C*), 129.8 (Ar*C*), 55.0 (*C*), 54.3 (*C*), 50.6 (*C*H), 31.3 (*C*H_2), 24.5 (*C*H_2), 20.1 (*C*H_3), 18.3 (*C*H_3), 9.1 (*C*H_3) ppm.

HRMS (ESI +ve) m/z: 485.2871.

L7: N2,N6-bis(5,6-dimethyl-1,2,4-triazin-3-yl)pyridine-2,6-diamine

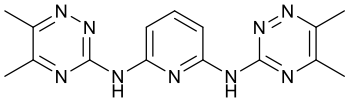

Yield: 217 mg, 53% as an orange solid.

m.p: 241.1-242.4 °C

^{1}H-NMR δ_H (399.8MHz): 8.50 (2H, s, br, 2 x N*H*), 8.06 (2H, d, *J* = 8.24 Hz, 2 x ArC*H*), 7.75 (1H, t, *J* = 8.24 Hz, ArC*H*), 2.60 (6H, s, 2 x CH_3), 2.48 (6H, s, 2 x CH_3);

^{13}C-NMR (100.5 MHz): 159.5 (2 x Ar*C*), 158.4 (2 x Ar*C*), 150.7 (2 x Ar*C*), 150.6 (2 x Ar*C*), 140.3 (Ar*C*H), 107.0 (2 x Ar*C*H), 21.8 (2 x *C*H_3), 18.9 (2 x *C*H_3) ppm.

HRMS (ESI +ve) *m/z*: 324.1674 *calculated for* $[C_{15}H_{17}N_9 + H]^+$: 324.1680

L8: N6-{8,11-dimethyl-3,4,6-triazatricyclo[6.2.1.0^{2,7}]undeca-2(7),3,5-trien-5-yl}-N6'-{8,11,11-trimethyl-3,4,6-triazatricyclo[6.2.1.0^{2,7}]undeca-2,4,6-trien-5-yl}-[2,2'-bipyridine]-6,6'-diamine

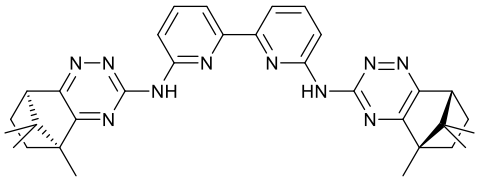

Yield: 118 mg, 67% as an orange solid.

m.p: 260+ °C

^{1}H-NMR δ_H (399.8 MHz): 7.71 (2H, t, *J* = 7.79 Hz, 2 x ArC*H*-4), 7.43 (2H, d, *J* = 7.79, ArCH and ArC*H*), 7.40 (2H, d, *J* = 7.79, ArC*H* and ArC*H*), 2.81 (2H, d, *J* = 3.66 Hz, 2 x C*H*), 2.34 – 2.20 (2H, m, 2 x CH_{exo}), 2.03 – 1.97 (2H, m, 2 x CH_{exo}), 1.57 – 1.44 (2H, m, 4 x CH_{endo}), 1.32 (6H, s, 2 x CH_3), 1.07 (6H, s, 2 x CH_3), 0.76 (6H, s, 2 x CH_3);

^{13}C-NMR (100.5 MHz): 172.1 (2 x Ar*C*), 154.5 (2 x Ar*C*), 154.0 (2 x Ar*C*), 153.6 (2 x Ar*C*), 152.2 (2 x Ar*C*), 136.7 (2 x Ar*C*H), 125.0 (2 x Ar*C*H), 112.3 (2 x Ar*C*H), 54.1 (2 x *C*), 53.6 (2 x *C*), 50.3 (2 x *C*H), 31.5 (2 x *C*H_2), 24.9 (2 x *C*H_2), 20.6 (2 x *C*H_3), 18.3 (2 x *C*H_3), 9.2 (2 x *C*H_3) ppm.

HRMS (ESI +ve) *m/z*: 561.3209 calculated for $[C_{32}H_{36}N_{10} + H]^+$: 561.3203

L14: N,6-Bis({5,5,7,7-tetramethyl-5H,6H,7H-cyclopenta[e][1,2,4]triazin-3-yl})pyridin-2-amine

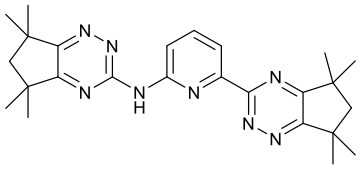

Yield: 106 mg, 80% as a yellow solid.

m.p: 130.9-131.8 °C

^{1}H-NMR δ_H (399.8 MHz): 8.73 (1H, d, *J* = 8.24 Hz, ArC*H*), 8.64 (1H, s, br, N*H*), 8.24 (1H, d, *J* = 7.79 Hz, ArC*H*), 7.92 (1H, t, *J* = 8.24, 7.79 Hz, ArC*H*), 2.05 (2H, s, CH_2), 1.98 (2H, s, CH_2), 1.52 (6H, s, CH_3), 1.46 (6H, s, CH_3), 1.45 (6H, s, CH_3), 1.34 (6H, s, CH_3);

^{13}C-NMR (100.5 MHz): 171.5 (Ar*C*), 170.7 (Ar*C*), 167.5 (Ar*C*), 162.4 (Ar*C*), 161.8 (Ar*C*), 159.3 (Ar*C*), 152.6 (Ar*C*), 151.8 (Ar*C*), 139.1 (Ar*C*H), 118.1 (Ar*C*H), 114.7 (Ar*C*H), 53.0 (*C*H_2), 52.9 (*C*H_2), 41.2 (*C*), 40.7 (*C*), 40.3 (*C*), 39.7 (*C*), 29.8 (*C*H_3), 29.7 (*C*H_3), 29.0 (*C*H_3), 28.7 (*C*H_3) ppm.

HRMS (ESI +ve) *m/z*: 445.2813 *calculated for* $[C_{25}H_{32}N_8 + H]^+$: 445.2823

L15: 8,11,11-Trimethyl-N-(6-{5,5,7,7-tetramethyl-5H,6H,7H-cyclopenta[e][1,2,4]triazin-3-yl}pyridin-2-yl)-3,4,6-triazatricyclo[6.2.1.0^{2},^{7}]undeca-2(7),3,5-trien-5-amine

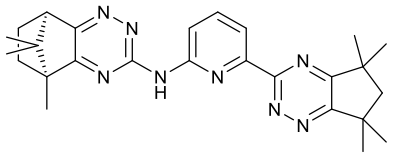

Yield: 103 mg, 50% as a yellow solid.

m.p: 139.4-141.0 °C

^{1}H-NMR δ_H (399.8 MHz): 9.10 (1H, s, br, N*H*), 8.77 (1H, d, *J* = 8.24 Hz, ArC*H*), 8.26 (1H, d, *J* = 7.79 Hz, ArC*H*), 7.95 (1H, t, *J* = 8.24, 7.79 Hz, ArC*H*), 4.12 (1H, d, *J* = 4.12 Hz, C*H*), 2.26 – 2.19 (1H, m, CH_{exo}), 2.01 (1H, s, CH_2), 2.00 – 1.94 (1H, m, CH_{exo}), 1.50 (3H, s, CH_3), 1.49 (3H, s, CH_3), 1.41 (3H, s, CH_3), 1.40 (3H, s, CH_3), 1.38 – 1.32 (2H, m, CH_{endo}), 1.19 (3H, s, CH_3), 1.05 (3H, s, CH_3), 0.61 (3H, s, CH_3);

^{13}C-NMR (100.5 MHz): 171.7 (Ar*C*), 170.6 (Ar*C*), 167.4 (Ar*C*), 162.4 (Ar*C*), 159.8 (Ar*C*), 158.1 (Ar*C*), 152.8 (Ar*C*), 151.6 (Ar*C*), 139.2 (Ar*C*H), 117.9 (Ar*C*H), 114.9 (Ar*C*H), 54.6 (*C*), 54.0 (*C*), 52.9 (*C*H$_2$), 50.5 (*C*H), 41.2 (*C*), 40.3 (*C*), 31.3 (*C*H$_2$), 29.7 (2 x *C*H$_3$), 29.0 (*C*H$_3$), 29.9 (*C*H$_3$), 24.5 (*C*H$_2$), 20.1 (*C*H$_3$), 18.2 (*C*H$_3$), 9.0 (*C*H$_3$) ppm.

HRMS (ESI +ve) *m/z*: 457.2816 *calculated for* [$C_{26}H_{32}N_8$ + H]$^+$: 457.2823

L16: 8,11,11-trimethyl-N-(6-{8,11,11-trimethyl-3,4,6-triazatricyclo[6.2.1.0^{2},^{7}]undeca-2,4,6-trien-5-yl}pyridin-2-yl)-3,4,6-triazatricyclo[6.2.1.0^{2},^{7}]undeca-2(7),3,5-trien-5-amine

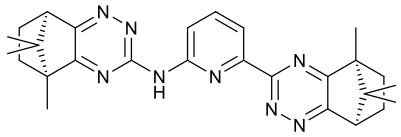

Yield: 54 mg, 27% as a yellow solid.

m.p: 237.8-239.4 °C

^{1}H-NMR δ_H (399.8 MHz): 8.72 (1H, d, *J* = 8.24 Hz, ArC*H*), 8.46 (1H, s, br, N*H*), 8.23 (1H, d, *J* = 7.33 Hz, ArC*H*), 7.93 (1H, t, *J* = 8.24, 7.33 Hz, ArC*H*), 3.29 (1H, d, *J* = 4.58 Hz, C*H*), 3.12 (1H, d, *J* = 4.12 Hz, C*H*), 2.36 – 2.22 (2H, m, 2 x CH_{exo}), 2.10 – 1.98 (2H, m, 2 x CH_{exo}), 1.43 (3H, s, C*H*$_3$) 1.43 – 1.38 (4H, m, 4 x CH_{endo}), 1.28 (3H, s, C*H*$_3$), 1.12 (3H, s, C*H*$_3$), 1.08 (3H, s, C*H*$_3$), 0.66 (3H, s, C*H*$_3$), 0.65 (3H, s, C*H*$_3$);

^{13}C-NMR (100.5 MHz): 170.9 (2 x Ar*C*), 165.3 (2 x Ar*C*), 161.2 (Ar*C*), 160.0 (Ar*C*), 158.1 (Ar*C*), 152.7 (Ar*C*), 139.2 (Ar*C*H), 117.9 (Ar*C*H), 114.9 (Ar*C*H), 55.5 (*C*), 54.7 (*C*), 54.4 (*C*), 54.1 (*C*), 51.1 (*C*H), 50.5 (*C*H), 31.4 (*C*H$_2$), 31.1 (*C*H$_2$), 24.5 (*C*H$_2$), 24.3 (*C*H$_2$), 20.1 (*C*H$_3$), 18.3 (*C*H$_3$), 18.3 (*C*H$_3$), 9.2 (*C*H$_3$), 9.0 (*C*H$_3$) ppm.

HRMS (ESI +ve) *m/z*: 469.2815 *calculated for* [$C_{27}H_{32}N_8$ + H]$^+$: 469.2823

L17: *N*-{5,5,7,7-tetramethyl-5H,6H,7H-cyclopenta[e][1,2,4]triazin-3-yl}-6-{8,11,11-trimethyl-3,4,6-triazatricyclo[6.2.1.0^{2,7}]undeca-2,4,6-trien-5-yl}pyridin-2-amine

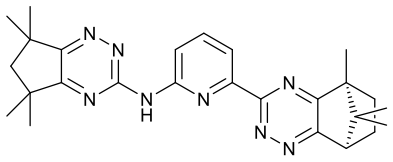

Yield: 105 mg, 36% as a yellow solid.

m.p: 229.8-230.4 °C

^{1}H-NMR δ_H (399.8 MHz): 8.74 (1H, d, *J* = 8.24 Hz, ArC*H*), 8.69 (1H, s, br, N*H*), 8.25 (1H, d, *J* = 7.79 Hz, ArC*H*), 7.93 (1H, t, *J* = 8.24, 7.79 Hz, ArC*H*), 3.29 (1H, *J* = 4.12 Hz, C*H*), 2.33 (1H, *J* = 4.58, 4.12, 3.66 Hz, CH_{exo}), 2.09 – 2.05 (1H, m, CH_{exo}), 1.98 (2H, s, CH_2), 1.46 (6H, s, 2 x CH_3), 1.42 (3H, s, CH_3), 1.42 – 1.40 (2H, m, 2 x CH_{endo}), 1.34 (6H, s, 2 x CH_3), 1.11 (3H, s, CH_3), 0.63 (3H, s, CH_3);

^{13}C-NMR (100.5 MHz): 171.4 (Ar*C*), 170.9 (Ar*C*), 165.2 (Ar*C*), 161.8 (Ar*C*), 161.3 (Ar*C*), 159.4 (Ar*C*), 152.6 (Ar*C*), 151.9 (Ar*C*), 139.1 (Ar*C*H), 118.0 (Ar*C*H), 114.7 (Ar*C*H), 55.5 (*C*), 54.4 (*C*), 53.0 (*C*H_2), 51.1 (*C*H), 40.7 (*C*), 39.7 (*C*), 31.11 (*C*H_2), 29.8 (*C*H_3), 28.8 (*C*H_3), 24.3 (*C*H_2), 20.1 (*C*H_3), 18.3 (*C*H_3), 9.24 (*C*H_3) ppm.

HRMS (ESI +ve) *m/z*: 457.2817 *calculated for* $[C_{26}H_{32}N_8 + H]^+$: 457.2823

<u>General alkylation of Buchwald Hartwig ligands</u>

L3 (0.49 g, 1.13 mmol) in anhy THF (10 ml) and added to a suspension of sodium hydride (0.05 g, 2.25 mmol, 2 eq.) in anhy THF (15 ml) with ice cooling under N_2. This was stirred at room temperature for 30 minutes before warming to 40°C for a following 30 minutes. The reaction mixture was allowed to cool to room temperature then iodomethane (0.8 ml, 11.26 mmol) was added. The reaction mixture was stirred at room temperature for 1 hour, then at reflux overnight. Upon completion the reaction was quenched with NH_4Cl (15 ml) and extracted with EtOAc (5 x 15 ml), dried ($MgSO_4$) and the solvent removed under reduced pressure. The product was purified by column chromatography (silica gel: 100% DCM, with increasing EtOAc) to elute firstly the unsymmetrical product followed by the symmetrical product.

L10: N2,N6-Dimethyl-N2-{8,11,11-trimethyl-3,4,6-triazatricyclo[6.2.1.0^{2},^{7}]undeca-2(7),3,5-trien-5-yl}-N6-{8,11,11-trimethyl-3,4,6-triazatricyclo[6.2.1.0^{2},^{7}]undeca-2,4,6-trien-5-yl}pyridine-2,6-diamine

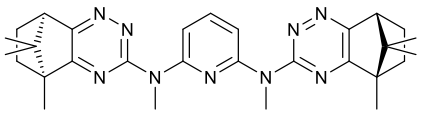

Yield: 135 mg, 23% as an orange solid.

^{1}H-NMR δ_H (399.8 MHz): 7.79 (1H, t, *J* = 8.24 Hz, ArC*H*), 7.23 (2H, d, *J* = 8.24 Hz, 2 x ArC*H*), 3.90 (3H, s, NCH_3), 2.90 (2H, d, *J* = 4.12 Hz, C*H*), 2.28 (2H, td, *J* = 9.62, 4.12, 3.66 Hz, 2 x CH_{exo}), 2.11-2.04 (2H, m, 2 x CH_{exo}), 1.56 (4H, q, *J* = 9.62 Hz, 4 x CH_{endo}), 1.21 (3H, s, CH_3), 1.10 (3H, s, CH_3), 0.81 (3H, s, CH_3);

^{13}C-NMR (100.5 MHz): 178.0 (2 x Ar*C*), 154.4 (2 x Ar*C*), 152.3 (2 x Ar*C*), 151.8 (2 x Ar*C*), 141.1 (Ar*C*H), 110.4 (2 x Ar*C*H), 55.0 (2 x *C*), 53.2 (2 x *C*), 49.7 (2 x *C*H_3), 43.8 (2 x *C*H), 31.5 (2 x *C*H_2), 24.6 (2 x *C*H_2), 20.6 (2 x *C*H_3), 18.0 (2 x *C*H_3), 9.1 (2 x *C*H_3) ppm.

LRMS (ESI +ve) *m/z:* 526.46 *calculated for* $[C_{29}H_{37}N_9 + CH_3]^+$: 526.34

HRMS (ESI +ve) *m/z*: 512.3245 *calculated for* $[C_{29}H_{37}N_9 + H]^+$: 512.3245

L11: N2-Methyl-N6-{8,11,11-trimethyl-3,4,6-triazatricyclo[6.2.1.0^{2},^{7}]undeca-2(7),3,5-trien-5-yl}-N2-{8,11,11-trimethyl-3,4,6-triazatricyclo[6.2.1.0^{2},^{7}]undeca-2,4,6-trien-5-yl}pyridine-2,6-diamine

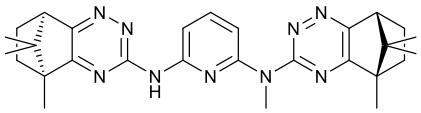

Yield: 71 mg, 12% as an orange solid.

^{1}H-NMR δ_H (399.8 MHz): 8.10 (1H, d, *J* = 7.79 Hz, ArC*H*), 7.63 (1H, t, *J* = 8.24, 7.79 Hz, ArC*H*) 6.76 (1H, d, *J* = 7.79 Hz, ArC*H*), 3.74 (3H, s, NCH_3), 3.11 (1H, d, *J* = 4.12 Hz, C*H*), 2.72 (1H, d, *J* = 4.12 Hz, C*H*), 2.27–2.13 (2H, m, 2 x CH_{exo}), 2.04–1.87 (2H, m, 2 x CH_{exo}), 1.46 (2H, td, *J* = 7.79, 3.21 Hz, 2 x CH_{endo}), 1.38 (2H, td, *J* = 7.79, 6.87, 3.21 Hz, 2 x CH_{endo}), 1.28 (3H, s, -CH_3), 1.07 (3H, s, -CH_3), 1.06 (3H, s, -CH_3), 1.02 (3H, s, -CH_3), 0.78 (3H, s, -CH_3), 0.66 (3H, s, -CH_3);

^{13}C-NMR (100.5 MHz): 175.6 (Ar*C*), 171.6 (Ar*C*), 159.5 (Ar*C*), 158.4 (Ar*C*), 151.0 (Ar*C*), 150.2 (Ar*C*), 148.8 (Ar*C*), 139.3 (Ar*C*), 111.7 (2 x Ar*C*H), 106.2 (Ar*C*H), 54.7 (*C*), 54.3 (*C*), 54.1 (*C*), 52.0 (*C*), 50.5 (*C*H), 49.5 (*C*H), 41.6 (CH_3), 31.5 (CH_2), 31.4 (CH_2), 24.9 (CH_2), 24.6 (CH_2), 20.4 (CH_3), 20.1 (CH_3), 18.3 (CH_3), 17.9 (CH_3), 9.1 (CH_3), 9.0 (CH_3) ppm.

LRMS (ESI +ve) *m/z:* 498.35 *calculated for* $[C_{28}H_{35}N_9 + H]^+$: 498.30

HRMS (ESI +ve) *m/z*: 498.3079 *calculated for* $[C_{28}H_{35}N_9 + H]^+$: 498.3088

L12: N2,N6-Dibutyl-N2-{8,11,11-trimethyl-3,4,6-triazatricyclo[6.2.1.0^{2},^{7}]undeca-2(7),3,5-trien-5-yl}-N6-{8,11,11-trimethyl-3,4,6-triazatricyclo[6.2.1.0^{2},^{7}]undeca-2,4,6-trien-5-yl}pyridine-2,6-diamine

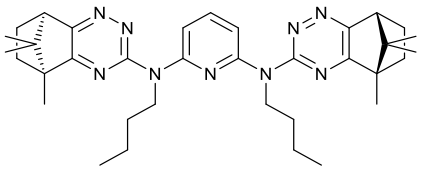

Yield: 100 mg, 13% as an orange solid.

m.p: 99.8-101.2 °C

^{1}H-NMR δ_H (399.8 MHz): 7.82 (1H, t, *J* = 8.24 Hz, ArC*H*), 7.19 (2H, d, *J* = 8.24 Hz, ArC*H*), 4.24-4.17 (4H, m, 2 x NCH_2), 2.90 (2H, d, *J* = 4.12 Hz, 2 x C*H*), 2.33-2.25 (2H, m, 2 x CH_{exo}), 2.11-2.07 (2H, 2 x CH_{exo}), 1.87 (4H, qu, *J* = 7.79, 7.33 Hz, 2 x CH_2), 1.56 (4H, m, 2 x CH_2), 1.42 (4H, qu, *J* = 7.79, 7.33 Hz, 4 x CH_{endo}), 1.21 (3H, s, CH_3), 1.10 (3H, s, CH_3), 1.00 (6H, t, *J* = 7.33 Hz, 2 x CH_3) 0.80 (3H, s, CH_3);

^{13}C-NMR (100.5 MHz): 177.6 (Ar*C*), 154.1 (Ar*C*), 152.4 (Ar*C*), 151.7 (Ar*C*), 141.6 (Ar*C*H), 110.6 (Ar*C*H), 55.3 (CH_2), 55.0 (*C*), 53.2 (*C*), 49.8 (*C*H), 31.4 (CH_2), 30.2 (CH_2), 29.8 (CH_2), 29.7 (*C*), 24.5 (CH_2), 20.5 (CH_3), 17.9 (CH_3), 14.0 (CH_3), 9.2 (CH_3) ppm.

HRMS (ESI +ve) *m/z*: 596.4178 *calculated for* $[C_{35}H_{49}N_9 + H]^+$: 596.4184

L13: N2-Butyl-N6-{8,11,11-trimethyl-3,4,6-triazatricyclo[6.2.1.0^{2,7}]undeca-2(7),3,5-trien-5-yl}-N2-{8,11,11-trimethyl-3,4,6-triazatricyclo[6.2.1.0^{2,7}]undeca-2,4,6-trien-5-yl}pyridine-2,6-diamine

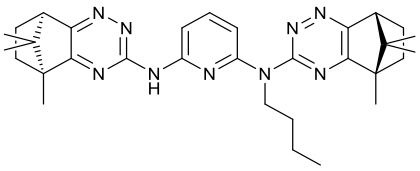

Yield: 0.11 g, 16% as an orange solid.

^{1}H-NMR δ_H (399.8 MHz): 8.11 (1H, d, J = 8.24 Hz, ArC*H*), 7.77 (1H, s, br, ArC*H*), 6.91 (1H, s, br, ArC*H*), 4.20 (2H, s, br, NCH_2), 3.10 (1H, d, *J* = 4.12 Hz, C*H*), 2.82 (1H, s, br, C*H*), 2.30-2.19 (2H, m, 2 x CH_{exo}), 2.03-1.95 (2H, m, 2 x CH_{exo}), 1.87 (2H, qu, *J* = 7.79, 7.33 Hz, CH_2), 1.51-1.36 (6H, m, 1 x CH_2, 2 x CH_{endo}), 1.32 (3H, s, CH_3), 1.09 (3H, s, CH_3), 1.06 (3H, s, CH_3), 1.04 (3H, s, CH_3), 0.98 (3H, t, *J* = 7.79, 7.33 Hz, CH_3), 0.77 (3H, s, CH_3), 0.66 (3H, s, CH_3);

^{13}C-NMR (100.5 MHz): 158.4 (2 x Ar*C*), 112.1 (2 x Ar*C*H), 106.3 (Ar*C*H), 54.8 (*C*), 54.7 (*C*), 54.4 (*C*H_2), 50.6 (*C*H), 49.7 (*C*H), 31.3 (*C*H_2), 31.2 (*C*H_2), 29.5 (*C*H_2), 24.7(*C*H_2), 24.5 (*C*H_2), 20.4 (*C*H_3), 20.2 (*C*H_3), 19.9 (*C*H_2), 18.2 (*C*H_3), 17.9 (*C*H_3), 13.8 (*C*H_3), 9.1 (*C*H_3), 9.0 (*C*H_3) ppm. (NB: sample wasn't concentrated enough to obtain full ^{13}C NMR spectrum.)

HRMS (ESI +ve) *m/z*: 540.3552 *calculated for* $[C_{31}H_{41}N_9 + H]^+$: 540.3558

N,8,11,11-tetramethyl-N-[6-(1,1,3,3-tetramethyl-2,3-dihydro-1H-inden-5-yl)pyridin-2-yl]-

L18: 3,4,6-triazatricyclo[6.2.1.0^{2,7}]undeca-2(7),3,5-trien-5-amine

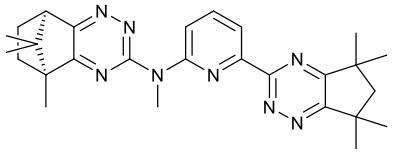

Yield: 0.11 g, 15% as an orange solid.

^{1}H-NMR δ_H (399.8 MHz): 8.21 (1H, d, *J* = 7.79 Hz, ArC*H*), 7.91 (1H, d, *J* = 8.24 Hz, ArC*H*), 7.81 (1H, t, *J* = 8.24, 7.79 Hz, ArC*H*), 3.94 (3H, s, NCH_3), 3.11 (1H, d, *J* = 4.12 Hz, C*H*), 2.27 – 2.18 (1H, m, CH_{exo}), 1.99 (1H, td, *J* = 9.62, 4.12 Hz, CH_{exo}), 1.53 (6H, s, 2 x CH_3), 1.46 (6H, s, 2 x CH_3), 1.41 – 1.30 (2H, m, 2 x CH_{endo}), 1.22 (3H, s, CH_3), 1.06 (3H, s, CH_3), 0.66 (3H, s, CH_3);

^{13}C-NMR (100.5 MHz): 170.6 (Ar*C*), 167.2 (Ar*C*), 162.7 (Ar*C*), 160.7 (Ar*C*), 159.3 (Ar*C*), 156.0 (Ar*C*), 151.7 (Ar*C*), 137.1 (Ar*C*H), 121.0 (Ar*C*H), 119.1 (Ar*C*H), 54.7 (*C*), 54.0 (*C*), 52.9 (*C*H$_2$), 50.5 (*C*H), 41.1 (*C*), 40.2 (*C*), 35.6 (*C*H$_3$), 31.4 (*C*H$_2$), 29.6 (2 x *C*H$_3$), 29.0 (2 x *C*H$_3$), 24.6 (*C*H$_2$), 20.0 (*C*H$_3$), 18.3 (*C*H$_3$), 9.0 (*C*H$_3$) ppm.

General synthesis of the camphor-derived ligands:

The 7,7-dimethyl-1-(morpholine-4-carbonyl)bicycle[2.2.1]heptane-2,3-dione **3.3.8** (0.20 g, 0.75 mmol) and pyridine-2,6-bisamidrazone (0.11 g, 0.55 mmol) were refluxed in acetic acid overnight. The acetic acid was removed under reduced pressure and the ligand recrystallized.

L28: 8,11,11-trimethyl-5-(6'-{8,11,11-trimethyl-3,4,6-triazatricyclo[6.2.1.0^{2},^{7}]undeca-2,4,6-trien-5-yl}-[2,2'-bipyridin]-6-yl)-3,4,6-triazatricyclo[6.2.1.0^{2},^{7}]undeca-2(7),3,5-triene

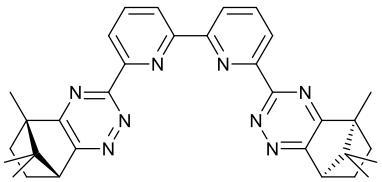

Yield: 203 mg, 53% as a pale yellow solid.

m.p: 176.3-178.0 °C

^{1}H-NMR δ_H (399.8 MHz): 8.93 (2H, d, *J* = 7.79 Hz, 2 x ArC*H*), 8.60 (2H, d, *J* = 7.79 Hz, 2 x ArC*H*), 8.08 (2H, t, *J* = 7.79 Hz, 2 x ArC*H*), 3.32 (2H, d, *J* = 4.12 Hz, 2 x C*H*), 2.39 – 2.32 (2H, m, 2 x C*H*$_{exo}$), 2.14 – 2.08 (2H, m, 2 x C*H*$_{exo}$), 1.52 – 1.41 (4H, m, 4 x C*H*$_{endo}$), 1.49 (6H, s, 2 x C*H*$_3$), 1.15 (6H, s, 2 x C*H*$_3$), 0.69 (6H, s, 2 x C*H*$_3$);

^{13}C-NMR (100.5 MHz): 171.1 (2 x Ar*C*), 165.3 (2 x Ar*C*), 161.7 (2 x Ar*C*), 156.1 (2 x Ar*C*), 153.0 (2 x Ar*C*), 138.0 (2 x Ar*C*H), 124.3 (2 x Ar*C*H), 123.1 (2 x Ar*C*H), 55.6 (2 x *C*), 54.5 (2 x *C*), 51.2 (2 x *C*H), 31.1 (2 x *C*H$_2$), 24.3 (2 x *C*H$_2$), 20.2 (2 x *C*H$_3$), 18.4 (2 x *C*H$_3$), 9.3 (2 x *C*H$_3$) ppm.

HRMS (ESI +ve) *m/z:* 531.2972 *calculated for* [$C_{32}H_{34}N_8$ + H]$^+$: 531.2979

L29: 2-{8,11,11-trimethyl-3,4,6-triazatricyclo[6.2.1.0^{2,7}]undeca-2(7),3,5-trien-5-yl}-9-{8,11,11-trimethyl-3,4,6-triazatricyclo[6.2.1.0^{2,7}]undeca-2,4,6-trien-5-yl}-1,10-phenanthroline

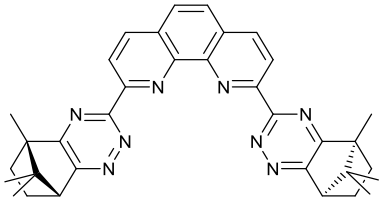

Yield: 111 mg, 59% as a pale yellow solid.

^{1}H-NMR δ_H (399.8 MHz): 8.87 (2H, d, *J* = 8.24 Hz, 2 x ArC*H*), 8.45 (2H, d, *J* = 8.24 Hz, 2 x ArC*H*), 7.94 (2H, s, 2 x ArC*H*), 3.31 (2H, d, *J* = 4.12 Hz, 2 x C*H*), 2.12 (2H, m, 2 x CH_{exo}), 2.12 (2H, td, *J* = 9.62, 3.66 Hz, 2 x CH_{exo}), 1.60 (6H, s, 2 x CH_3), 1.54 (2H, m, 2 x CH_{endo}), 1.45 (2H, m, 2 x CH_{endo}), 1.15 (6H, s, 2 x CH_3), 0.70 (6H, s, 2 x CH_3);

^{13}C-NMR (100.5 MHz): 171.4 (2 x Ar*C*), 165.5 (2 x Ar*C*), 161.8 (2 x Ar*C*), 153.7 (2 x Ar*C*), 146.2 (2 x Ar*C*), 137.3 (2 x Ar*C*H), 129.7 (2 x Ar*C*), 127.6 (2 x Ar*C*H), 123.3 (2 x Ar*C*H), 55.6 (2 x *C*), 54.7 (2 x *C*), 51.2 (2 x *C*H), 31.1 (2 x *C*H_2), 24.3 (2 x *C*H_2), 20.3 (2 x *C*H_3), 18.4 (2 x *C*H_3), 9.6 (2 x *C*H_3) ppm.

HRMS (ESI +ve) *m/z:* 555.2971 *calculated for* $[C_{34}H_{34}N_8 + H]^+$: 555.2979

L19: (1R,8R)-5-{6-[(1R,8R)-11,11-Dimethyl-8-(morpholine-4-carbonyl)-3,4,6-triazatricyclo[6.2.1.0^{2,7}]undeca-2,4,6-trien-5-yl]pyridin-2-yl}.-11,11-dimethyl-8-(morpholine-4-carbonyl)-3,4,6-triazatricyclo[6.2.1.0^{2,7}]undeca-2(7),3,5-triene

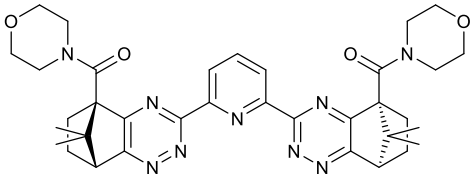

Yield: 130 mg, 60% as a beige solid.

m.p: 201.9-202.9 °C

^{1}H-NMR δ_H (399.8 MHz): 8.54 (2H, d, *J* = 7.79 Hz, 2 x ArC*H*), 8.12 (1H, t, *J* = 8.24, 7.79 Hz, ArC*H*), 4.13-3.39 (8H, m, 4 x CH_2), 3.28 (2H, d, *J* = 4.12 Hz, 2 x C*H*), 2.68 (2H, td, *J* = 10.99,

3.66 Hz, 2 x C*H*), 2.55-2.56 (2H, m, 2 x C*H*), 1.92-1.86 (2H, m, 2 x C*H*), 1.57-1.50 (2H, m, 2 x C*H*), 1.43 (6H, s, 2 x CH_3), 0.99 (6H, s, 2 x CH_3);

^{13}C-NMR (100.5 MHz): 166.8 (2 x Ar*C*), 166.6 (2 x Ar*C*O), 165.1 (2 x Ar*C*), 161.1 (2 x Ar*C*) 154.0 (2 x Ar*C*), 138.1 (Ar*C*H), 124.9 (2 x Ar*C*H), 67.2 (4 x *C*H_2), 62.2 (2 x *C*), 60.2 (2 x *C*), 51.4 (2 x *C*H), 28.7 (2 x *C*H_2), 24.5 (2 x *C*H_2), 21.5 (2 x *C*H_3), 20.5 (2 x *C*H_3) ppm.

HRMS (ESI +ve) *m/z:* 652.3351 *calculated for* $[C_{35}H_{41}N_9O_4+H]^+$: 652.3354

L20: (1R,8R)-5-{6'-[(1R,8R)-11,11-Dimethyl-8-(morpholine-4-carbonyl)-3,4,6-triazatricyclo[6.2.1.0^{2,7}]undeca-2,4,6-trien-5-yl]-[2,2'-bipyridin]-6-yl}-11,11-dimethyl-8-(morpholine-4-carbonyl)-3,4,6-triazatricyclo[6.2.1.0^{2,7}]undeca-2(7),3,5-triene

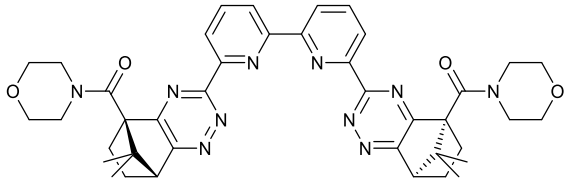

Yield: 184 mg, 70% as a pale yellow solid.

m.p: 231.7-232.3 °C

^{1}H-NMR δ_H (399.8 MHz): 8.83 (2H, d, *J* = 7.79 Hz, 2 x ArC*H*), 8.56 (2H, d, *J* = 7.79 Hz, 2 x ArC*H*), 8.07 (2H, t, *J* = 7.79 Hz, 2 x ArC*H*), 4.17 – 3.52 (16H, m, 8 x CH_2), 3.28 (2H, d, *J* = 4.12 Hz, 2 x C*H*), 2.74 – 2.67 (2H, m, 2 x C*H*), 2.56 - 2.47 (2H, m, 2 x C*H*), 1.96 - 1.89 (2H, m, 2 x C*H*), 1.57 (2H, td, *J* = 3.66 Hz, 2 x C*H*), 1.43 (6H, s, CH_3), 1.01 (6H, s, CH_3);

^{13}C-NMR (100.5 MHz): 167.0 (2 x *C*), 166.9 (2 x *C*), 165.0 (2 x *C*), 161.4 (2 x *C*O), 156.3 (2 x *C*), 152.9 (2 x *C*), 138.0 (2 x ArCH), 124.4 (2 x Ar*C*H), 123.2 (2 x Ar*C*H), 67.2 (8 x *C*H_2), 62.4 (2 x *C*), 60.2 (2 x *C*), 51.4 (2 x *C*H), 28.9 (2 x *C*H_2), 24.5 (2 x *C*H_2), 21.7 (2 x *C*H_3), 20.5 (2 x *C*H_3) ppm.

HRMS (ESI +ve) *m/z:* 729.3612 *calculated for* $[C_{40}H_{44}N_{10}O_4 + H]^+$: 729.3620

L21: 2-[(1R,8R)-11,11-Dimethyl-8-(morpholine-4-carbonyl)-3,4,6-triazatricyclo[6.2.1.0^{2},^{7}]undeca-2(7),3,5-trien-5-yl]-9-[(1R,8R)-11,11-dimethyl-8-(morpholine-4-carbonyl)-3,4,6-triazatricyclo[6.2.1.0^{2},^{7}]undeca-2,4,6-trien-5-yl]-1,10-phenanthroline

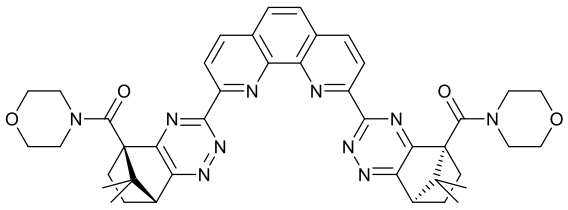

Yield: 180 g, 86% as a dark beige solid.

m.p: 255.0-255.6 °C (viscous)

^{1}H-NMR δ_H (399.8 MHz): 8.56 (2H, d, *J* = 8.24 Hz, 2 x ArC*H*), 8.50 (2H, d, *J* = 8.24 Hz, 2 x ArC*H*), 7.98 (2H, s, 2 x ArC*H*), 4.1–3.4 (16H, m, 8 x CH_2), 3.29 (2H, d, *J* = 4.12 Hz, 2 x C*H*), 2.70 (2H, td, *J* = 4.12, 3.66 Hz, 2 x C*H*), 2.53-2.46 (2H, m, 2 x C*H*), 2.05-1.94 (2H, m, 2 x C*H*), 1.59-1.50 (2H, m, 2 x C*H*), 1.43 (6H, s, CH_3), 1.03 (6H, s, CH_3);

^{13}C-NMR (100.5 MHz): 166.8 (2 x *C*), 166.7 (2 x *C*), 164.9 (2 x *C*), 161.9 (2 x *C*O), 153.8 (2 x *C*), 146.4 (2 x *C*), 137.4 (2 x ArCH), 129.6 (2 x *C*), 127.6 (2 x Ar*C*H), 123.1 (2 x Ar*C*H), 67.2 (8 x *C*H_2), 62.4 (2 x *C*), 60.2 (2 x *C*), 51.4 (2 x *C*H), 28.9 (2 x *C*H_2), 24.3 (2 x *C*H_2), 21.6 (2 x *C*H_3), 20.5 (2 x *C*H_3) ppm.

HRMS (ESI +ve) *m/z:* 753.3614 *calculated for* $[C_{42}H_{44}N_{10}O_4+H]^+$: 753.3620

L22: (1R,8R)-5-{6-[(1R,8R)-8-(Diethylcarbamoyl)-11,11-dimethyl-3,4,6-triazatricyclo[6.2.1.0^{2},^{7}]undeca-2,4,6-trien-5-yl]pyridin-2-yl}.-N,N-diethyl-11,11-dimethyl-3,4,6-triazatricyclo[6.2.1.0^{2},^{7}]undeca-2(7),3,5-triene-8-carboxamide

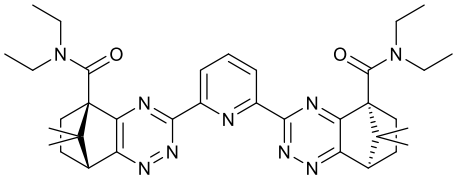

Yield: 28 mg, 20% as a pale beige solid.

m.p: 212.9-214.0 °C

^{1}H-NMR δ_H (399.8 MHz): 8.48 (2H, d, *J* = 7.79 Hz, 2 x ArC*H*), 8.07 (1H, t, *J* = 7.79 Hz, ArC*H*), 3.75 (2H, q, *J* = 7.79, 6.87 Hz, NCH_2), 3.65 (2H, q, *J* = 6.87 Hz, NCH_2), 3.48 (2H, q, *J* = 7.33, 6.87 Hz, NCH_2), 3.39 (2H, q, *J* = 6.87 Hz, NCH_2), 3.25 (2H, d, *J* = 4.12 Hz, 2 x C*H*), 2.70 (2H, td, *J* = 6.87, 4.12 Hz, 2 x C*H*), 2.51-2.43 (2H, m, 2 x C*H*), 1.86 (2H, ddd, *J* = 12.82, 7.79, 3.66 Hz, 2 x C*H*), 1.52 (2H, ddd, *J* = 12.82, 7.33, 3.66 Hz, 2 x C*H*), 1.39 (3H, s, CH_3), 1.27 (3H, dt, *J* = 6.87, 5.04 Hz, 2 x NCH$_2$CH_3), 0.98 (3H, s, CH_3);

^{13}C-NMR (100.5 MHz): 167.4 (2 x Ar*C*) 167.0 (2 x *C*O), 165.2 (2 x ArC), 161.1 (2 x ArC), 154.3 (2 x ArC), 138.0 (Ar*C*H) 124.8 (2 x Ar*C*H), 62.6 (2 x *C*), 60.2 (2 x *C*), 51.4 (2 x *C*H), 42.7 (2 x *C*H$_2$), 40.5 (2 x *C*H$_2$), 29.3 (2 x *C*H$_2$), 24.3 (2 x *C*H$_2$), 21.8 (2 x *C*H$_3$), 20.3 (2 x *C*H$_3$), 14.7 (2 x *C*H$_3$), 12.9 (2 x *C*H$_3$) ppm.

HRMS (ESI +ve) *m/z:* found 624.3762; *calculated for* [$C_{35}H_{45}N_9O_2$ + H]$^+$: 624.3769

L23: (1R,8R)-5-{6'-[(1R,8R)-8-(Diethylcarbamoyl)-11,11-dimethyl-3,4,6-triazatricyclo[6.2.1.0^{2},^{7}]undeca-2,4,6-trien-5-yl]-[2,2'-bipyridin]-6-yl-N,N-diethyl-11,11-dimethyl-3,4,6-triazatricyclo[6.2.1.0^{2},^{7}]undeca-2(7),3,5-triene-8-carboxamide

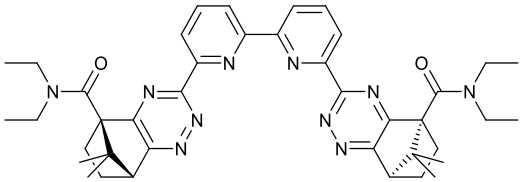

Yield: 19 mg, 15% as a pale yellow solid.

^{1}H-NMR δ_H (399.8 MHz): 8.88 (2H, d, *J* = 7.33 Hz, 2 x ArC*H*), 8.51 (2H, d, *J* = 8.24 Hz, 2 x ArC*H*), 8.03 (2H, t, *J* = 8.24, 7.33 Hz, 2 x ArC*H*), 3.89-3.76 (4H, m, 2 x NCH_2), 3.36-3.28 (4H, m, 2 x NH_2), 3.25 (2H, d, *J* = 4.12 Hz, 2 x C*H*), 2.74 – 2.67 (2H, m, 2 x C*H*), 2,53-2.46 (2H, m, 2 x C*H*), 1.89 (2H, ddd, *J* = 12.36, 7.79, 4.12, Hz, 2 x C*H*), 1.56 (2H, ddd, *J* = 12.36, 7.79, 4.12 Hz, 2 x C*H*), 1.41 (6H, s, 2 x CH_3), 1.32-1.25 (12H, m, 4 x CH_3), 1.02 (6H, s, 2 x CH_3);

^{13}C-NMR (100.5 MHz): 167.1 (Ar*C*), 165.2 (Ar*C*), 161.2 (Ar*C*), 156.1 (Ar*C*), 152.8 (Ar*C*), 137.8 (Ar*C*H), 124.0 (Ar*C*H), 122.9 (Ar*C*H), 62.6 (*C*), 60.2 (*C*), 51.4 (*C*H), 42.5 (*C*H$_2$), 40.3 (*C*H$_2$), 29.3 (*C*H$_2$), 24.4 (*C*H$_2$), 21.9 (2 x *C*H$_3$), 20.3 (2 x *C*H$_3$), 14.6 (2 x *C*H$_3$), 12.8 (2 x *C*H$_3$) ppm.

HRMS (ESI +ve) *m/z:* 701.4028; *calculated for* [$C_{40}H_{48}N_{10}O_2$ + H]$^+$: 701.4034

L24: (1R,8R)-5-{9-[(1R,8R)-8-(Diethylcarbamoyl)-11,11-dimethyl-3,4,6-triazatricyclo[6.2.1.0^{2},^{7}]undeca-2,4,6-trien-5-yl]-1,10-phenanthrolin-2-yl}

v-N,N-diethyl-11,11-dimethyl-3,4,6-triazatricyclo[6.2.1.0^{2},^{7}]undeca-2(7),3,5-triene-8-carboxamide

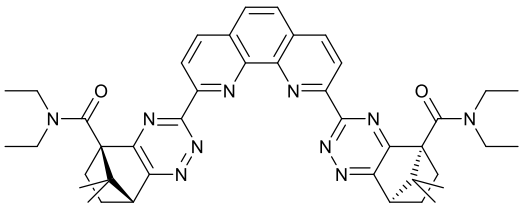

Yield: 83 mg, 21% as a beige solid.

m.p: 195.2-195.8 °C

^{1}H-NMR δ_H (399.8 MHz): 8.69 (2H, d, *J* = 8.70 Hz, 2 x ArC*H*), 8.46 (2H, d, *J* = 8.70 Hz, 2 x ArC*H*), 7.95 (2H, s, 2 x ArC*H*), 3.98-3.92 (2H, m, NCH_2), 3.76-3.70 (2H, m, NCH_2), 3.66-3.61 (2H, m, NCH_2), 3.48-3.43 (2H, m, NCH_2), 3.24 (2H, d, *J* = 4.12 Hz, 2 x C*H*), 2.70 (2H, ddd, *J* = 9.16, 8.70, 3.66 Hz, 2 x C*H*), 2.53-2.45 (2H, m, 2 x C*H*), 1.95-1.88 (2H, m, 2 x C*H*), 1.56 (2H, ddd, *J* = 9.16, 8.70, 3.66 Hz, 2 x C*H*), 1.42 (6H, s, 2 x CH_3), 1.30 (6H, t, *J* = 7.33 Hz, 2 x NCH$_2$CH_3), 1.25 (6H, t, *J* = 7.33 Hz, 2 x NCH$_2$CH_3), 1.01 (6H, s, 2 x CH_3);

^{13}C-NMR (100.5 MHz): 167.0 (2 x *C*O), 165.3 (4 x Ar*C*), 161.3 (2 x Ar*C*), 153.5 (2 x Ar*C*), 146.5 (2 x Ar*C*), 137.3 (2 x Ar*C*H), 129.7 (2 x Ar*C*), 127.6 (2 x Ar*C*H), 122.9 (2 x Ar*C*H), 62.7 (2 x *C*), 60.3 (2 x *C*), 51.4 (2 x *C*H), 43.0 (2 x *C*H$_2$), 40.9 (2 x *C*H$_2$), 29.3 (2 x *C*H$_2$), 24.3 (2 x *C*H$_2$), 21.8 (2 x *C*H$_3$), 20.3 (2 x *C*H$_3$), 15.3 (2 x *C*H$_3$), 13.1 (2 x *C*H$_3$) ppm.

HRMS (ESI +ve) *m/z:* 725.4028 *calculated for* [$C_{42}H_{48}N_{10}O_2$ + H]$^{+}$: 725.4034

L25: 5-{6-[11,11-dimethyl-1-(methylcarbamoyl)-3,4,6-triazatricyclo[6.2.1.0^{2},^{7}]undeca-2,4,6-trien-5-yl]pyridin-2-yl}-N,11,11-trimethyl-3,4,6-triazatricyclo[6.2.1.0^{2},^{7}]undeca-2(7),3,5-triene-1-carboxamide

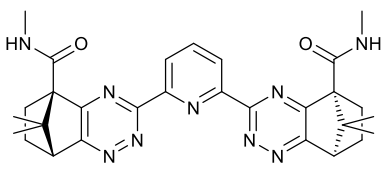

Yield: 82 mg, 42% as a pale yellow solid.

^{1}H-NMR δ_H (399.8 MHz): 9.75 (2H, s, br, 2 x N*H*), 8.08 (2H, d, *J* = 7.79 Hz, 2 x ArC*H*), 7.76 (1H, t, *J* = 7.79 Hz, ArC*H*), 3.10 (2H, d, *J* = 4.12 Hz, 2 x C*H*), 2.25 - 2.17 (2H, m, 2 x C*H*), 1.99 – 1.94 (2H, m, 2 x C*H*), 1.45 – 1.37 (4H, m, 4 x C*H*), 1.23 (6H, s, 2 x CH_3), 1.05 (6H, s, 2 x CH_3), 0.65 (6H, s, 2 x CH_3);

^{13}C-NMR (100.5 MHz): 171.6 (Ar*C*O), 159.6 (Ar*C*), 158.5 (Ar*C*), 151.1 (Ar*C*), 140.0 (Ar*C*H), 107.7 (Ar*C*H), 54.7 (*C*), 54.1 (*C*), 50.6 (*C*H), 31.3 (*C*H_2), 24.6 (*C*H_2), 20.1 (*C*H_3), 18.3 (*C*H_3), 9.1 (*C*H_3) ppm.

L26: (1R,8R)-5-{6'-[(1R,8R)-11,11-Dimethyl-8-(methylcarbamoyl)-3,4,6-triazatricyclo[6.2.1.0^{2},^{7}]undeca-2,4,6-trien-5-yl]-[2,2'-bipyridin]-6-yl}-N,11,11-trimethyl-3,4,6-triazatricyclo[6.2.1.0^{2},^{7}]undeca-2(7),3,5-triene-8-carboxamide

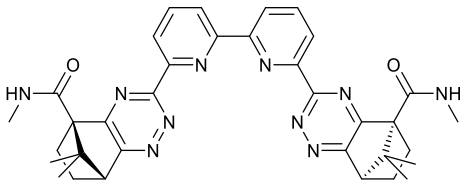

Yield: 125 mg, 56% as a pale yellow solid.

m.p: 260+ °C

^{1}H-NMR δ_H (399.8 MHz): 8.86 (2H, d, *J* = 7.79 Hz, 2 x ArC*H*), 8.67 (2H, d, *J* = 7.79 Hz, 2 x ArC*H*), 8.11 (2H, t, *J* = 7.79 Hz, 2 x ArC*H*), 3.11 (6H, d, *J* = 4.58 Hz, 2 x NCH_3), 2.93 (2H, td, *J* = 9.62, 3.66 Hz, 2 x C*H*), 2.62 – 2.55 (2H, m, 2 x C*H*), 1.63 (2H, td, *J* = 9.62, 3.66 Hz, 2 x C*H*), 1.56 – 1.52 (2H, m, 2 x C*H*), 1.50 (6H, s, CH_3), 0.80 (6H, s, CH_3);

^{13}C-NMR (100.5 MHz): 169.2 (2 x *C*O), 167.1 (Ar*C*), 165.5 (Ar*C*), 138.2 (2 x Ar*C*H), 136.4 (ArC), 124.2 (2 x Ar*C*H), 122.9 (2 x Ar*C*H), 61.2 (2 x *C*), 59.2 (2 x *C*), 51.8 (2 x *C*H), 29.8 (2 x *C*H_2), 26.8 (2 x *C*H), 25.2 (2 x *C*H_2), 20.8 (2 x *C*H_3), 20.4 (2 x *C*H_3), 20.3 (2 x *C*H_3) ppm.

HRMS (ESI +ve) *m/z:* 617.3089 *calculated for* $[C_{44}H_{48}N_{10}O_2 + H]^+$: 617.3095

L27: 2-[(1R,8R)-11,11-Dimethyl-8-(piperidine-1-carbonyl)-3,4,6-triazatricyclo[6.2.1.0^{2,7}]undeca-2(7),3,5-trien-5-yl]-9-[(1R,8R)-11,11-dimethyl-8-(piperidine-1-carbonyl)-3,4,6-triazatricyclo[6.2.1.0^{2,7}]undeca-2,4,6-trien-5-yl]-1,10-phenanthroline

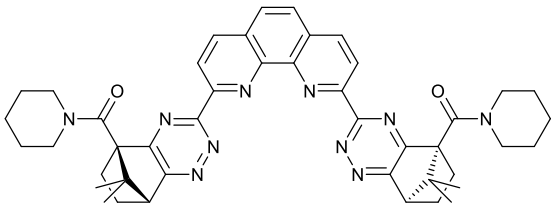

Yield: 98 mg, 12% as a pale yellow solid.

m.p: 240.4-241.6 °C

^{1}H-NMR δ_H (399.8 MHz): 8.68 (2H, d, *J* = 8.24 Hz, 2 x ArC*H*), 8.48 (2H, d, *J* = 8.70 Hz, 2 x ArC*H*), 7.97 (2H, s, 2 x ArC*H*), 3.88 – 3.55 (8H, m, 4 x CH_2), 3.24 (2H, d, *J* = 4.12 Hz, 2 x C*H*), 2.72 (2H, td, *J* = 4.12, 3.66 Hz, 2 x CH_{exo}), 2.53 – 2.46 (2H, m, 2 x CH_{exo}), 1.95 (2H, ddd, *J* = 4.12, 3.66 Hz, 2 x CH_{endo}), 1.67 (12H, s, br, 6 x CH_2), 1.57 – 1.50 (2H, m, 2 x CH_{endo}), 1.43 (6H, s, 2 x CH_3), 0.99 (6H, s, 2 x CH_3);

^{13}C-NMR (100.5 MHz): 166.9 (*C*O), 166.2 (Ar*C*), 164.9 (Ar*C*), 162.1 (Ar*C*), 154.1 (Ar*C*), 146.7 (Ar*C*), 137.0 (Ar*C*H), 129.4 (Ar*C*), 127.5 (Ar*C*H), 123.3 (Ar*C*H), 62.7 (*C*), 60.1 (*C*), 51.5 (*C*H), 29.3 (*C*H_2), 27.2 (*C*H_2), 26.0 (*C*H_2) 24.5 (*C*H_2), 24.4 (*C*H_2), 21.7 (*C*H_3), 20.7 (*C*H_3) ppm.

HRMS (ESI +ve) *m/z:* 749.4028 *calculated for* $[C_{44}H_{48}N_{10}O_2 + H]^+$: 749.4034

L40: 5,5,8,8-tetramethyl-3-[6-(5,5,8,8-tetramethyl-6-oxo-5,6,7,8-tetrahydro-1,2,4-benzotriazin-3-yl)pyridin-2-yl]-5,6,7,8-tetrahydro-1,2,4-benzotriazin-6-one

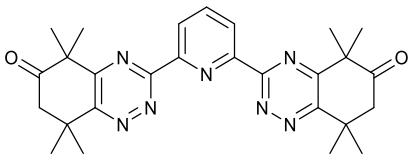

Yield: 41 mg, 21% as a yellow solid.

m.p: 224.4-225.0 °C

^{1}H-NMR δ_H (399.8 MHz): 8.73 (2H, d, *J* = 7.79 Hz, 2 x Ar*C*H), 8.17 (1H, t, *J* = 7.79 Hz, Ar*C*H), 2.85 (4H, s, 2 x *C*H_2), 1.65 (12H, s, 4 x *C*H_3), 1.56 (12H, s, 4 x *C*H_3);

^{13}C-NMR (100.5 MHz): 209.4 (2 x *C*O), 162.7 (2 x Ar*C*), 162.1 (2 x Ar*C*), 161.2 (2 x Ar*C*), 153.7 (2 x Ar*C*), 138.3 (Ar*C*H), 125.4 (2 x Ar*C*H), 50.7 (2 x *C*), 50.6 (2 x *C*H_2), 37.9 (2 x *C*), 28.6 (4 x *C*H_3), 26.0 (4 x *C*H_3) ppm.

HRMS (ESI +ve) *m/z:* 486.2601 *calculated for* $[C_{27}H_{31}N_7O_2 + H]^+$: 486.2612

L41: 5,5,8,8-Tetramethyl-3-[6'-(5,5,8,8-tetramethyl-6-oxo-5,6,7,8-tetrahydro-1,2,4-benzotriazin-3-yl)-[2,2'-bipyridin]-6-yl]-5,6,7,8-tetrahydro-1,2,4-benzotriazin-6-one

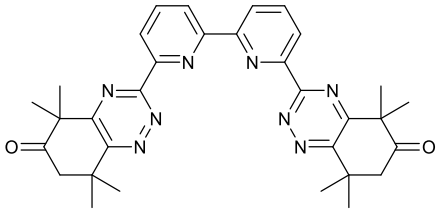

Yield: 119 mg, 58% as a pale green solid.

m.p: 260+ °C

^{1}H-NMR δ_H (399.8 MHz): 8.98 (2H, d, *J* = 7.79 Hz, ArC*H*), 8.58 (2H, d, *J* = 7.79 Hz, ArC*H*), 8.10 (2H, t, *J* = 7.79 Hz, ArC*H*), 2.87 (4H, s, 2 x CH_2), 1.66 (12H, s, 2 x CH_3), 1.58 (12H, s, 2 x CH_3);

^{13}C-NMR (100.5 MHz): 209.6 (*C*O), 162.4 (Ar*C*), 162.1 (Ar*C*), 161.0 (Ar*C*), 156.1 (Ar*C*), 152.2 (Ar*C*), 138.1 (Ar*C*H), 124.2 (Ar*C*H), 123.3 (Ar*C*H), 50.6 (2 x *C*H_2), 37.9 (2 x *C*), 28.6 (4 x *C*H_3), 26.1 (4 x *C*H_3) ppm.

HRMS (ESI +ve) *m/z:* 563.2869 *calculated for* $[C_{32}H_{34}N_8O_2 + H]^+$: 563.2877

L42: 5,5,8,8-tetramethyl-3-[9-(5,5,8,8-tetramethyl-6-oxo-5,6,7,8-tetrahydro-1,2,4-benzotriazin-3-yl)-1,10-phenanthrolin-2-yl]-5,6,7,8-tetrahydro-1,2,4-benzotriazin-6-one

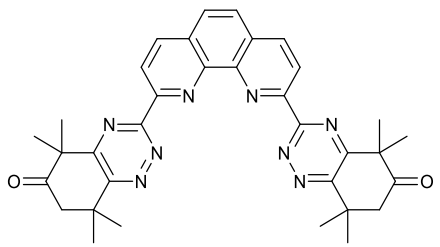

Yield: 28 mg, 12% as a yellow solid.

^{1}H-NMR δ_H (399.8 MHz): 8.95 (2H, d, *J* = 8.24 Hz, 2 x ArC*H*), 8.54 (2H, d, *J* = 8.24 Hz, 2 x ArC*H*), 8.00 (2H, s, 2 x ArC*H*), 2.87 (4H, s, 2 x CH_2), 1.76 (12H, s, 4 x CH_3), 1.58 (12H, s, 4 x CH_3);

^{13}C-NMR (100.5 MHz): 209.6 (*C*O), 163.1 (Ar*C*), 162.5 (Ar*C*), 161.3 (Ar*C*), 153.3 (Ar*C*), 146.5 (Ar*C*), 137.7 (Ar*C*H), 130.1 (Ar*C*), 127.9 (Ar*C*H), 123.7 (Ar*C*H), 51.0 (*C*H), 50.5 (*C*H_2), 38.0 (*C*H), 28.6 (*C*H_3), 26.0 (*C*H_3) ppm.

Further analysis was unable to be completed as a result of a lost sample.

L43: 3-[6-(6-Hydroxy-5,5,8,8-tetramethyl-5,6,7,8-tetrahydro-1,2,4-benzotriazin-3-yl)pyridin-2-yl]-5,5,8,8-tetramethyl-5,6,7,8-tetrahydro-1,2,4-benzotriazin-6-ol

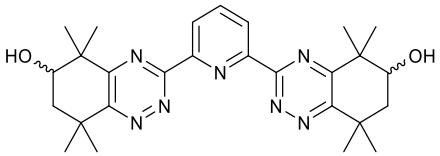

Yield: 104 mg, 39%

^{1}H-NMR δ_H (399.8 MHz): 8.68 (2H, d, *J* = 7.79 Hz, 2 x ArC*H*), 8.12 (1H, t, *J* = 7.79 Hz, ArC*H*), 4.04 (2H, dd, *J* = 5.95, 4.12 Hz, 2 x 6-C*H*), 2.12 – 2.00 (4H, m, 2 x 7-CH_2), 1.61 (6H, s, 2 x CH_3), 1.58 (6H, s, 2 x CH_3), 1.45 (6H, s, 2 x CH_3), 1.38 (6H, s, 2 x CH_3);

^{13}C-NMR (100.5 MHz): 164.0 (2 x Ar*C*), 162.1 (2 x Ar*C*), 160.9 (2 x Ar*C*), 153.7 (2 x Ar*C*), 138.4 (2 x Ar*C*H), 125.3 (Ar*C*H), 71.3 (2 x 6-*C*H), 60.4 (2 x *C*), 41.2 (2 x 7-*C*H_2), 36.9 (2 x *C*), 31.0 (2 x *C*H_3), 29.8 (2 x *C*H_3), 25.7 (2 x *C*H_3), 22.9 (2 x *C*H_3) ppm.

HRMS (ESI +ve) *m/z*: 490.2913 *calculated for* $[C_{27}H_{35}N_7 + H]^+$: 490.2925

L44: 3-[6'-(6-Hydroxy-5,5,8,8-tetramethyl-5,6,7,8-tetrahydro-1,2,4-benzotriazin-3-yl)-[2,2'-bipyridin]-6-yl]-5,5,8,8-tetramethyl-5,6,7,8-tetrahydro-1,2,4-benzotriazin-6-ol

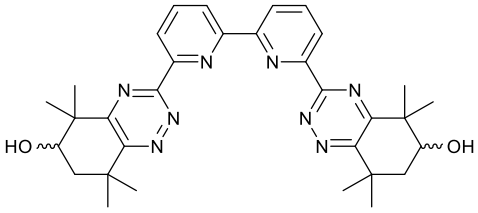

4-Hydroxy-3,3,6,6-tetramethylcyclohexane-1,2-dione (0.15 g, 0.83 mmol) were suspended in EtOH (20 ml) and the bis-amidrazone (0.11 g, 0.40 mmol) was added. The mixture was refluxed for 40 hours before been allowed to cool to room temperature. The solvent was removed under reduced pressure and DCM added. The solid was filtered and triturated in DCM and the solid filtered to leave the product as a pale yellow solid (40 mg, 15%).

m.p: 260+ °C

^{1}H-NMR δ_H (399.8 MHz, DMSO D6): 8.97 (2H, d, *J* = 7.79 Hz, ArC*H*), 8.56 (2H, d, *J* = 7.79 Hz, ArC*H*), 8.06 (2H, t, *J* = 7.79 Hz, ArC*H*), 4.06 (2H, dd, *J* = 10.07, 4.58 Hz, C*H*), 2.12-2.02 (4H, m, CH_2), 1.67 (3H, s, CH_3), 1.60 (3H, s, CH_3), 1.48 (3H, s, CH_3), 1.42 (3H, s, CH_3);

^{13}C-NMR (100.5 MHz): 163.4 (2 x Ar*C*), 161.6 (2 x Ar*C*), 161.2 (2 x Ar*C*) 156.1 (2 x Ar*C*), 152.6 (2 x Ar*C*), 138.0 (2 x Ar*C*H), 124.0 (2 x Ar*C*H), 123.0 (2 x Ar*C*H), 71.7 (2 x *C*H), 41.1 (2 x *C*H_2), 36.9 (2 x *C*), 31.5 (2 x *C*), 31.2 (2 x *C*H_3), 29.9 (2 x *C*H_3), 25. 7 (2 x *C*H_3), 22.8 (2 x *C*H_3) ppm.

HRMS (ESI +ve) *m/z*: 567.3189 *calculated for* $[C_{32}H_{38}N_8O_2 + H]^+$: 567.3190

L45: 3-[9-(6-Hydroxy-5,5,8,8-tetramethyl-5,6,7,8-tetrahydro-1,2,4-benzotriazin-3-yl)-1,10-phenanthrolin-2-yl]-5,5,8,8-tetramethyl-5,6,7,8-tetrahydro-1,2,4-benzotriazin-6-ol

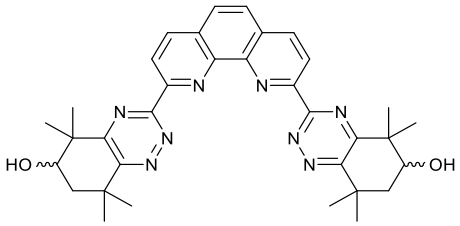

The BTPhen amidrazone **3.2.10** (0.20 g, 0.66 mmol) and 4-hydroxy-3,3,6,6-tetramethylcyclohexane-1,2-dione (0.22 g, 1.32 mmol) were suspended in EtOH (40 ml) and refluxed at 120 °C for 2 days. Upon completion the reaction was allowed to cool. The solid that precipitated was filtered and washed with DCM (10 ml) and EtOH (10 ml). The solid was triturated with DCM and filtered again to give the product as a yellow solid (90 mg, 23%).

m.p: 260+ °C

^{1}H-NMR δ_H (399.8 MHz, DMSO D6): 8.79 (2H, d, *J* = 8.70 Hz, 2 x ArC*H*), 8.72 (2H, d, *J* = 8.24 Hz, 2 x ArC*H*), 8.22 (2H, s, 2 x ArC*H*), 3.93-3.90 (2H, m, 2 x C*H*), 2.02-1.92 (4H, m, 2 x CH_2), 1.57 (3H, s, 2 x CH_3), 1.54 (3H, s, 2 x CH_3), 1.44 (3H, s, 2 x CH_3), 1.33 (3H, s, 2 x CH_3) ppm.

Due to limited solubility of this sample, a ^{13}C NMR spectra could not be obtained.

HRMS (ESI +ve) *m/z*: 591.3179 *calculated for* $[C_{32}H_{38}N_8O_2 + H]^+$: 591.3190

L48: 2,9-bis(6-methoxy-5,5,8,8-tetramethyl-5,6,7,8-tetrahydro-1,2,4-benzotriazin-3-yl)-1,10-phenanthroline

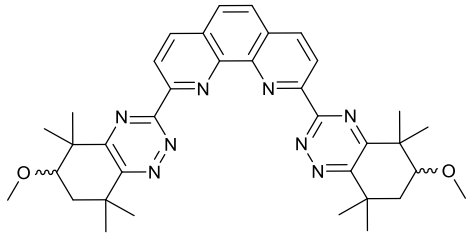

Yield: 20 mg, 24% as a pale yellow solid.

m.p: 248.9-249.8 ℃

^{1}H-NMR δ_H (399.8 MHz): 8.90 (2H, m, overlapping signals, 2 x ArC*H*), 8.48 (2H, d, *J* = 8.24 Hz, 2 x ArC*H*), 7.95 (2H, s, 2 x ArC*H*), 3.50 (6H, s, 2 x OCH_3), 3.46 (2H, dd, *J* = 10.53, 3.66 Hz, 2 x C*H*), 3.30 (2H, s, br, disappears on D_2O shake, H_2O), 2.16 – 2.10 (2H, m, CH_2), 1.99 (2H, td, *J* = 10.53, 3.66 Hz, CH_2), 1.69 (3H, s, CH_3), 1.66 (6H, s, 2 x CH_3), 1.62 (3H, s, CH_3), 1.59 (3H, s, CH_3) 1.54 (3H, s, CH_3), 1.48 (3H, s, CH_3), 1.44 (3H, s, CH_3);

^{13}C-NMR (100.5 MHz): 164.2 (2 x Ar*C*), 162.1 (2 x Ar*C*), 161.9 (2 x Ar*C*), 153.9 (2 x Ar*C*), 146.6 (Ar*C*), 137.3 (2 x Ar*C*H), 129.8 (2 x Ar*C*), 127.61 (2 x Ar*C*H), 123.5 (2 x Ar*C*H), 81.2 (2 x *C*H), 57.6 (2 x O*C*H$_3$), 43.1 (*C*), 42.2 (*C*), 37.0 (*C*), 36.6 (*C*H$_2$), 36.5 (*C*H$_2$), 35.9 (*C*), 31.5 (*C*H$_3$), 31.0 (*C*H$_3$), 30.8 (*C*H$_3$), 30.3 (*C*H$_3$), 26.5 (*C*H$_3$), 25.9 (*C*H$_3$), 23.6 (*C*H$_3$), 23.1 (*C*H$_3$) ppm.

HRMS (ESI +ve) *m/z:* 619.3501 *calculated for* $[C_{36}H_{42}N_8O_2 + H]^+$: 619.3503

Chapter 8

Appendix

8. Appendix

8.1. NMR titration studies

The data below covers all ^{1}H NMR titrations covered during this thesis, as discussed. It includes the data of the relative integrations for each ligand titration. With the exception of the ligands that observed no movement of the ^{1}H NMR signals.

Table 24: ^{1}H NMR titration of **L19** with $La(NO_3)_3$.

Metal:ligand ratio	Relative integrations (from ^{1}H NMR spectra)			
	Free ligand (x)	**1:1 Complex (y)**	**1:2 complex (z)**	x + y + z
0.0	1.00	0.00	0.00	1
0.1	1.00	0.00	0.00	1
0.2	1.00	0.00	0.00	1
0.3	0.00	0.00	1.00	1
0.4	0.00	0.00	1.00	1
0.5	0.00	0.00	1.00	1
0.6	0.00	0.00	1.00	1
0.7	0.00	0.00	1.00	1
0.8	0.00	0.00	1.00	1
0.9	0.00	0.00	1.00	1
1.0	0.00	0.00	1.00	1
1.1	0.00	0.00	1.00	1
1.2	0.00	0.00	1.00	1

Table 25: ^{1}H NMR titration of **L19** with $Y(NO_3)_3$

Metal:ligand ratio	Relative integrations (from ^{1}H NMR spectra)			
	Free ligand (x)	**1:1 Complex (y)**	**1:2 complex (z)**	x + y + z
0.0	1.00	0.00	0.00	1
0.1	0.66	0.00	0.34	1
0.2	0.00	0.16	0.84	1
0.3	0.00	0.40	0.60	1
0.4	0.00	0.58	0.42	1
0.5	0.00	0.73	0.27	1
0.6	0.00	1.00	0.20	1
0.7	0.00	1.00	0.15	1
0.8	0.00	1.00	0.00	1
0.9	0.00	1.00	0.00	1
1.0	0.00	1.00	0.00	1
1.1	0.00	1.00	0.00	1
1.2	0.00	1.00	0.00	1

Table 26: ^{1}H NMR titration of **L24** with $La(NO_3)_3$

Metal:ligand ratio	Relative integrations (from ^{1}H NMR spectra)			
	Free ligand (x)	**1:1 Complex (y)**	**1:2 complex (z)**	x + y + z
0.0	1.00	0.00	0.00	1
0.1	0.83	0.00	0.17	1
0.2	0.55	0.00	0.45	1
0.3	0.00	0.00	1.00	1
0.4	0.00	0.00	1.00	1
0.5	0.00	0.15	0.85	1
0.6	0.00	0.33	0.67	1
0.7	0.00	0.56	0.44	1
0.8	0.00	0.87	0.13	1
0.9	0.00	1.00	0.00	1
1.0	0.00	1.00	0.00	1
1.1	0.00	1.00	0.00	1
1.2	0.00	1.00	0.00	1

Table 27: ^{1}H NMR titration of **L24** with $Lu(NO_3)_3$

Metal:ligand ratio	Relative integrations (from ^{1}H NMR spectra)			
	Free ligand (x)	**1:1 Complex (y)**	**1:2 complex (z)**	x + y + z
0.0	1.00	0.00	0.00	1
0.1	0.90	0.00	0.10	1
0.2	0.79	0.00	0.21	1
0.3	0.50	0.00	0.50	1
0.4	0.00	0.12	0.88	1
0.5	0.00	0.18	0.82	1
0.6	0.00	0.27	0.73	1
0.7	0.00	0.32	0.68	1
0.8	0.00	0.32	0.68	1
0.9	0.00	0.39	0.61	1
1.0	0.00	0.41	0.59	1
1.1	0.00	0.43	0.57	1
1.2	0.00	0.46	0.54	1

Table 28: ^{1}H NMR titration of **L24** with $Y(NO_3)_3$

Metal:ligand ratio	Relative integrations (from ^{1}H NMR spectra)			
	Free ligand (x)	**1:1 Complex (y)**	**1:2 complex (z)**	x + y + z
0.0	1.00	0.00	0.00	1
0.1	0.78	0.00	0.22	1
0.2	0.43	0.00	0.57	1
0.3	0.15	0.00	0.85	1
0.4	0.00	0.00	1.00	1
0.5	0.00	0.00	1.00	1
0.6	0.00	0.53	0.47	1
0.7	0.00	0.60	0.40	1
0.8	0.00	0.69	0.31	1
0.9	0.00	0.72	0.28	1
1.0	0.00	0.75	0.25	1
1.1	0.00	0.75	0.25	1
1.2	0.00	0.78	0.22	1

Table 29: ^{1}H NMR titration of **L22** with $La(NO_3)_3$

Metal:ligand ratio	Relative integrations (from ^{1}H NMR spectra)			
	Free ligand (x)	**1:1 Complex (y)**	**1:2 complex (z)**	x + y + z
0.0	1.00	0.00	0.00	1
0.1	1.00	0.00	0.00	1
0.2	1.00	0.00	0.00	1
0.3	0.87	0.00	0.13	1
0.4	0.83	0.00	0.17	1
0.5	0.52	0.00	0.48	1
0.6	0.00	0.00	1.00	1
0.7	0.00	0.00	1.00	1
0.8	0.00	0.00	1.00	1
0.9	0.00	0.00	1.00	1
1.0	0.00	0.00	1.00	1
1.1	0.00	0.00	1.00	1
1.2	0.00	0.00	1.00	1

Table 30: ^{1}H NMR titration of **L27** with $La(NO_3)_3$

Metal:ligand ratio	Relative integrations (from ^{1}H NMR spectra)			
	Free ligand (x)	**1:1 Complex (y)**	**1:2 complex (z)**	x + y + z
0.0	1.00	0.00	0.00	1
0.1	0.92	0.00	0.08	1
0.2	0.67	0.00	0.33	1
0.3	0.52	0.00	0.48	1
0.4	0.22	0.00	0.78	1
0.5	0.00	0.10	0.90	1
0.6	0.00	0.24	0.76	1
0.7	0.00	0.36	0.64	1
0.8	0.00	0.56	0.44	1
0.9	0.00	0.69	0.31	1
1.0	0.00	0.74	0.26	1
1.1	0.00	0.75	0.25	1
1.2	0.00	0.78	0.22	1

Table 31: ^{1}H NMR titration of **L44** with $La(NO_3)_3$

Metal:ligand ratio	Relative integrations (from ^{1}H NMR spectra)			
	Free ligand (x)	**1:1 Complex (y)**	**1:2 complex (z)**	x + y + z
0.0	1.00	0.00	0.00	1
0.1	0.79	0.00	0.21	1
0.2	0.56	0.00	0.44	1
0.3	0.26	0.00	0.74	1
0.4	0.07	0.00	0.93	1
0.5	0.00	0.00	1.00	1
0.6	0.00	0.00	1.00	1
0.7	0.00	0.00	1.00	1
0.8	0.00	0.00	1.00	1
0.9	0.00	0.00	1.00	1
1.0	0.00	0.00	1.00	1
1.1	0.00	0.00	1.00	1
1.2	0.00	0.00	1.00	1

Table 32: ^{1}H NMR titration of **L44** with $Y(NO_3)_3$

Metal:ligand ratio	Relative integrations (from ^{1}H NMR spectra)			
	Free ligand (x)	**1:1 Complex (y)**	**1:2 complex (z)**	x + y + z
0.0	1.00	0.00	0.00	1
0.1	1.00	0.00	0.00	1
0.2	0.75	0.00	0.25	1
0.3	0.55	0.00	0.45	1
0.4	0.36	0.00	0.64	1
0.5	0.19	0.00	0.81	1
0.6	0.08	0.00	0.92	1
0.7	0.00	0.00	1.00	1
0.8	0.00	0.00	1.00	1
0.9	0.00	0.00	1.00	1
1.0	0.00	0.00	1.00	1
1.1	0.00	0.00	1.00	1
1.2	0.00	0.00	1.00	1

8.2. Solvent extraction studies

The data below corresponds to the extraction studies as a function of the nitric acid concentration. The extraction of the radionuclides Am(III), Cm(III) and Eu(III) into 1-octanol are represented by their individual *D* ratios (D_{Am}, D_{Cm} and D_{Eu}) and $SF_{Am/Eu}$, for the separation of Am(III) and Eu(III). The D_{Am} and D_{Eu} represent the values received from gamma-spectroscopy and D_{Cm} from alpha spectroscopy.

8.2.1. Data for 3-amino-1,2,4-triazine ligands

Table 33: Extraction of Am(III), Cm(III) and Eu(IIII) by **L3**.

[HNO_3] concentration (mol/L)	$\boldsymbol{D_{Am}}$	$\boldsymbol{D_{Cm}}$	$\boldsymbol{D_{Eu}}$	$\boldsymbol{SF_{Am/Eu}}$
0.013	0.001	0.00	0.001	1.03
0.111	0.006	0.00	0.005	1.10
0.296	0.006	0.00	0.005	1.11
0.700	0.001	0.00	0.001	1.19
1.031	0.003	0.00	0.002	1.32
3.110	0.003	0.00	0.002	1.75

Table 34: Extraction of Am(III), Cm(III) and Eu(IIII) by **L4.**

[HNO_3] concentration (mol/L)	D_{Am}	D_{Cm}	D_{Eu}	$SF_{Am/Eu}$
0.013	0.000	0.00	0.000	2.82
0.111	0.000	0.00	0.000	1.22
0.296	0.000	0.00	0.000	0.31
0.700	0.000	0.00	0.000	0.30
1.031	0.000	0.00	0.001	0.48
3.110	0.001	0.00	0.000	1.88

Table 35: Extraction of Am(III), Cm(III) and Eu(IIII) by **L6.**

[HNO_3] concentration (mol/L)	D_{Am}	D_{Cm}	D_{Eu}	$SF_{Am/Eu}$
0.013	0.000	0.00	0.000	1.18
0.111	0.000	0.00	0.000	2.56
0.296	0.000	0.00	0.000	2.37
0.700	0.000	0.00	0.000	1.95
1.031	0.000	0.00	0.000	2.32
3.110	0.002	0.00	0.001	1.44

Table 36: Extraction of Am(III), Cm(III) and Eu(IIII) by **L8**

[HNO_3] concentration (mol/L)	D_{Am}	D_{Cm}	D_{Eu}	$SF_{Am/Eu}$
0.013	0.009	0.001	0.003	3.13
0.111	0.008	0.001	0.003	2.56
0.296	0.026	0.001	0.005	5.62
0.700	0.010	0.001	0.058	0.17
1.031	0.019	0.001	0.002	10.64
3.110	0.022	0.002	0.016	1.39

Table 37: Extraction of Am(III), Cm(III) and Eu(IIII) by **L10**. (a) This result is an outlier as a result of the Eu gamma measurement.

[HNO_3] concentration (mol/L)	D_{Am}	D_{Cm}	D_{Eu}	$SF_{Am/Eu}$
0.013	0.000	0.01	0.000	1.83
0.111	0.002	0.00	0.001	1.31
0.296	0.000	000	0.000	127.60 [a]
0.700	0.000	0.00	0.000	0.48
1.031	0.010	0.00	0.009	1.10
3.110	0.001	0.00	0.001	1.15

Table 38: Extraction of Am(III), Cm(III) and Eu(IIII) by **L11**.

[HNO_3] concentration (mol/L)	D_{Am}	D_{Cm}	D_{Eu}	$SF_{Am/Eu}$
0.013	0.001	0.00	0.000	3.04
0.111	0.000	0.00	0.000	0.36
0.296	0.000	0.00	0.001	0.32
0.700	0.000	0.00	0.000	0.72
1.031	0.000	0.00	0.000	1.96
3.110	0.001	0.00	0.001	0.71

Table 39: Extraction of Am(III), Cm(III) and Eu(IIII) by **L12**.

[HNO_3] concentration (mol/L)	D_{Am}	D_{Cm}	D_{Eu}	$SF_{Am/Eu}$
0.013	0.001	0.00	0.002	0.46
0.111	0.004	0.02	0.003	1.52
0.296	0.002	0.00	0.020	0.10
0.700	0.003	0.01	0.002	1.26
1.031	0.001	0.00	0.002	0.50
3.110	0.002	0.00	0.003	0.67

Table 40: Extraction of Am(III), Cm(III) and Eu(IIII) by **L13**.

[HNO_3] concentration (mol/L)	D_{Am}	D_{Cm}	D_{Eu}	$SF_{Am/Eu}$
0.013	0.001	0.00	0.002	0.32
0.111	0.002	0.00	0.002	0.79
0.296	0.001	0.01	0.002	0.34
0.700	0.005	0.00	0.003	1.33
1.031	0.002	0.00	0.002	0.93
3.110	0.002	0.00	0.003	0.68

Table 41: Extraction of Am(III), Cm(III) and Eu(IIII) by **L14**.

[HNO_3] concentration (mol/L)	D_{Am}	D_{Cm}	D_{Eu}	$SF_{Am/Eu}$
0.013	0.001	0.00	0.003	0.30
0.111	0.001	0.00	0.003	0.28
0.296	0.001	0.00	0.003	0.34
0.700	0.001	0.00	0.002	0.45
1.031	0.001	0.00	0.002	0.53
3.110	0.002	0.00	0.003	0.75

Table 42: Extraction of Am(III), Cm(III) and Eu(IIII) by **L15**.

[HNO_3] concentration (mol/L)	D_{Am}	D_{Cm}	D_{Eu}	$SF_{Am/Eu}$
0.013	0.000	0.00	0.000	0.36
0.111	0.000	0.00	0.000	0.37
0.296	0.000	0.00	0.000	0.51
0.700	0.000	0.00	0.000	0.65
1.031	0.000	0.00	0.000	0.26
3.110	0.001	0.00	0.001	0.56

Table 43: Extraction of Am(III), Cm(III) and Eu(IIII) by **L17**.

[HNO_3] concentration (mol/L)	D_{Am}	D_{Cm}	D_{Eu}	$SF_{Am/Eu}$
0.013	0.001	0.00	0.001	0.54
0.111	0.001	0.00	0.001	0.77
0.296	0.001	0.00	0.002	0.39
0.700	0.001	0.00	0.002	0.46
1.031	0.001	0.00	0.001	0.79
3.110	0.001	0.00	0.002	0.67

8.2.2. Data for modified camphor ligands

Table 44: Extraction of Am(III), Cm(III) and Eu(IIII) by **L19**.

[HNO_3] concentration (mol/L)	D_{Am}	D_{Cm}	D_{Eu}	$SF_{Am/Eu}$
0.013	0.100	0.22	0.002	51.21
0.111	3.335	3.53	0.105	31.88
0.296	3.407	2.74	0.653	5.22
0.700	1.880	1.71	0.618	3.04
1.031	1.315	1.03	0.360	3.65
3.110	0.692	0.52	0.201	3.45

Table 45: Extraction of Am(III), Cm(III) and Eu(IIII) by **L20**.

[HNO_3] concentration (mol/L)	D_{Am}	D_{Cm}	D_{Eu}	$SF_{Am/Eu}$
0.013	0.003	0.00	0.003	1.03
0.111	0.015	0.01	0.004	4.12
0.296	0.033	0.04	0.010	3.25
0.700	0.037	0.04	0.023	1.63
1.031	0.039	0.04	0.022	1.77
3.110	0.035	0.02	0.004	8.18

Table 46: Extraction of Am(III), Cm(III) and Eu(IIII) by **L21**. Note: D_{Cm} were unable to be obtained due to solid deposits on the α-discs.

[HNO_3] concentration (mol/L)	D_{Am}	D_{Cm}	D_{Eu}	$SF_{Am/Eu}$
0.013	0.013	-	0.111	0.11
0.111	0.030	-	0.045	0.67
0.296	0.064	-	0.090	0.71
0.700	0.084	-	0.100	0.84
1.031	0.080	-	0.087	0.92
3.110	0.187	-	0.037	5.09

Table 47: Extraction of Am(III), Cm(III) and Eu(IIII) by **L22**.

[HNO_3] concentration (mol/L)	D_{Am}	D_{Cm}	D_{Eu}	$SF_{Am/Eu}$
0.013	0.740	0.719	0.014	53.52
0.111	31.861	22.369	0.023	149.55
0.296	220.718	410.487	2.776	79.50
0.700	184.676	298.822	2.563	72.05
1.031	117.327	196.846	1.601	73.30
3.110	1.889	3.205	0.024	78.29

Table 48: Extraction of Am(III), Cm(III) and Eu(IIII) by **L23**.

[HNO_3] concentration (mol/L)	D_{Am}	D_{Cm}	D_{Eu}	$SF_{Am/Eu}$
0.013	0.010	0.005	0.003	3.21
0.111	0.099	0.040	0.003	28.74
0.296	0.787	0.300	0.006	123.17
0.700	3.292	1.342	0.026	124.43
1.031	4.678	2.076	0.039	120.63
3.110	1.310	0.552	0.013	102.55

Table 49: Extraction of Am(III), Cm(III) and Eu(IIII) by **L24**.

[HNO_3] concentration (mol/L)	D_{Am}	D_{Cm}	D_{Eu}	$SF_{Am/Eu}$
0.013	0.959	0.92	0.116	8.28
0.111	11.383	12.66	1.418	8.03
0.296	28.434	18.99	2.757	10.31
0.700	35.562	29.56	2.205	16.13
1.031	41.751	31.12	1.736	24.05
3.110	70.031	44.39	0.627	111.77

Table 50: Extraction of Am(III), Cm(III) and Eu(IIII) by **L25**.

[HNO_3] concentration (mol/L)	D_{Am}	D_{Cm}	D_{Eu}	$SF_{Am/Eu}$
0.013	0.001	0.00	0.001	0.65
0.111	0.005	0.01	0.002	2.00
0.296	0.022	0.02	0.002	11.19
0.700	0.030	0.03	0.003	11.08
1.031	0.055	0.03	0.005	12.05
3.110	0.011	0.01	0.003	4.09

Table 51: Extraction of Am(III), Cm(III) and Eu(IIII) by **L26**.

[HNO_3] concentration (mol/L)	D_{Am}	D_{Cm}	D_{Eu}	$SF_{Am/Eu}$
0.013	0.002	0.001	0.003	0.88
0.111	0.005	0.004	0.003	2.01
0.296	0.013	0.010	0.004	3.27
0.700	0.028	0.020	0.007	4.29
1.031	0.035	0.022	0.008	4.17
3.110	0.049	0.032	0.006	8.69

Table 52: Extraction of Am(III), Cm(III) and Eu(IIII) by **L27**.

[HNO_3] concentration (mol/L)	D_{Am}	D_{Cm}	D_{Eu}	$SF_{Am/Eu}$
0.013	2.001	1.16	0.175	11.43
0.111	18.906	9.05	0.449	42.08
0.296	44.248	24.36	0.866	21.12
0.700	54.881	14.82	0.746	73.59
1.031	55.202	16.78	0.587	94.05
3.110	42.983	16.59	0.186	230.87

Table 53: Extraction of Am(III), Cm(III) and Eu(IIII) by **L28**.

[HNO_3] concentration (mol/L)	D_{Am}	D_{Cm}	D_{Eu}	$SF_{Am/Eu}$
0.013	0.018	0.010	0.003	5.77
0.111	0.170	0.057	0.003	48.96
0.296	0.841	0.312	0.007	128.49
0.700	3.063	1.102	0.020	153.36
1.031	7.708	1.752	0.058	133.42
3.110	0.110	0.067	0.005	22.04

Table 54: Extraction of Am(III), Cm(III) and Eu(IIII) by **L29**.

[HNO_3] concentration (mol/L)	D_{Am}	D_{Cm}	D_{Eu}	$SF_{Am/Eu}$
0.013	2.190	0.833	0.017	129.66
0.111	15.014	4.923	0.067	223.31
0.296	40.393	7.699	0.153	264.62
0.700	46.972	12.179	0.178	264.43
1.031	25.110	12.116	0.238	105.50
3.110	7.912	2.664	0.037	211.06

8.2.3. Data for modified $CyMe_4$-ligands

Table 55: Extraction of Am(III), Cm(III) and Eu(IIII) by **L40**.

[HNO_3] concentration (mol/L)	D_{Am}	D_{Cm}	D_{Eu}	$SF_{Am/Eu}$
0.013	0.012	0.013	0.001	15.05
0.111	0.018	0.020	0.000	58.46
0.296	0.083	0.087	0.001	84.61
0.700	0.468	0.499	0.005	86.14
1.031	0.859	0.851	0.009	95.58
3.000	0.371	0.411	0.006	63.84

Table 56: Extraction of Am(III), Cm(III) and Eu(IIII) by **L41**.

[HNO_3] concentration (mol/L)	D_{Am}	D_{Cm}	D_{Eu}	$SF_{Am/Eu}$
0.013	0.002	0.005	0.000	61.99
0.111	0.014	0.007	0.000	145.69
0.296	0.065	0.034	0.001	89.88
0.700	0.301	0.249	0.004	78.44
1.031	0.392	0.334	0.006	62.93
3.110	0.209	0.106	0.002	96.69

Table 57: Extraction of Am(III), Cm(III) and Eu(IIII) by **L43**.

[HNO_3] concentration (mol/L)	D_{Am}	D_{Cm}	D_{Eu}	$SF_{Am/Eu}$
0.013	0.128	0.11	0.006	19.82
0.111	1.226	0.93	0.348	3.52
0.296	1.038	0.85	0.267	3.89
0.700	0.669	0.57	0.397	1.69
1.031	0.591	0.41	0.365	1.62
3.110	0.984	0.57	0.025	38.78

Table 58: Extraction of Am(III), Cm(III) and Eu(IIII) by **L44**.

[HNO_3] concentration (mol/L)	D_{Am}	D_{Cm}	D_{Eu}	$SF_{Am/Eu}$
0.013	0.004	0.002	0.002	1.56
0.111	0.091	0.064	0.039	2.36
0.296	0.276	0.153	0.008	36.83
0.700	0.499	0.228	0.034	14.49
1.031	0.550	0.301	0.058	9.47
3.110	2.084	1.281	0.120	17.37

Table 59: Extraction of Am(III), Cm(III) and Eu(IIII) by **L48**.

[HNO_3] concentration (mol/L)	D_{Am}	D_{Cm}	D_{Eu}	$SF_{Am/Eu}$
0.013	23.173	13.606	0.228	101.54
0.111	384.945	171.851	5.039	76.39
0.296	515.981	497.934	11.542	44.68
0.700	436.918	461.780	10.591	41.25
1.031	374.838	139.553	9.326	40.19
3.110	40.788	9.610	0.314	129.73

8.3. Extraction kinetics studies

Below is the data for extraction studies of those ligands that exhibited some extraction at varying contact times, HNO_3 concentration remains constant in each study.

Table 60: Extraction of Am(III), Cm(III) and Eu(III) by **L24** at 0.296 mol/L HNO_3 with Ln-all^{-5} mol/L

Contact time (min)	D_{Am}	D_{Cm}	D_{Eu}	$SF_{Am/Eu}$
5	23.972	22.244	2.888	8.302
10	25.141	23.713	3.039	8.274
20	26.549	24.316	2.982	8.903
30	24.647	24.863	3.013	8.180
45	25.818	19.631	3.048	8.471
60	25.438	24.423	3.051	8.336

Table 61: Extraction of Am(III), Cm(III) and Eu(III) by **L19** at 0.296 mol/L HNO_3 with Ln-all^{-5} mol/L

Contact time (min)	D_{Am}	D_{Cm}	D_{Eu}	$SF_{Am/Eu}$
5	2.426	2.061	0.727	3.337
10	2.611	2.336	0.847	3.083
20	2.456	2.464	0.769	3.194
30	2.415	2.326	0.778	3.104
45	2.557	2.359	0.783	3.264
60	2.585	2.545	0.777	3.326

[1] T. R. Society, in *The Royal Society Science Policy Centre report 10/11*, The Royal Society, London, **2011**.
[2] G. H. Marcus, *Progress in Nuclear Energy* **2008**, *50*, 92-96.
[3] P. Beck, *Prospects and strategies for nuclear power: Global boom or dangerous diversion?*, Earthscan, **1994**; B. K. Sovacool, *Contesting the future of nuclear power: a critical global assessment of atomic energy*, World Scientific, **2011**.
[4] W. N. Association, World Nuclear Association, **2017**.
[5] I. A. E. Agency, *Vol. GC(59)/1*, **2015**.
[6] Fusion for Energy, fusionforenergy.europa.eu, **2015**; W. N. Association, (Ed.: W. N. Association), World Nuclear Association, www.world-nuclear.org, **2018**; A. Shah, greenworldinvestor.com, **2011**.
[7] N. E. Agency, (Ed.: OECD), **2010**.
[8] J. M. McKibben, *Radiochimica Acta* **1984**, *36*, 3-16.
[9] H. H. Dam, D. N. Reinhoudt, W. Verboom, *Chemical Society Reviews* **2007**, *36*, 367-377.
[10] http://www.acsept.org/; S. Bourg, C. Hill, C. Caravaca, C. Rhodes, C. Ekberg, R. Taylor, A. Geist, G. Modolo, L. Cassayre, R. Malmbeck, M. Harrison, G. de Angelis, A. Espartero, S. Bouvet, N. Ouvrier, *Nuclear Engineering and Design* **2011**, *241*, 3427-3435.
[11] http://www.sacsess.eu/.
[12] http://www.geniors.eu/.
[13] S. Andersson, C. Ekberg, J. Liljenzin, M. Nilsson, G. Skarnemark, Annual Report R-04-22, Swedish Nuclear Fuel and Waste Management Co., Stockholm, Sweden, **2004**.
[14] J. Mathur, M. Murali, K. Nash, *Solvent Extraction and Ion Exchange* **2001**, *19*, 357-390.
[15] M. Salvatores, G. Palmiotti, *Progress in Particle and Nuclear Physics* **2011**, *66*, 144-166.
[16] K. A. Gschneidner, L. Eyring, G. H. Lander, *Handbook on the physics and chemistry of rare earths*, *Vol. 32*, Elsevier, **2002**.
[17] R. G. Pearson, *Journal of the American Chemical Society* **1963**, *85*, 3533-3539.
[18] A. G. Maddock, *Inorganica Chimica Acta* **1987**, *139*, 7-12.
[19] https://www-nds.iaea.org/sgnucdat/a2.htm.
[20] M. Altmaier, X. Gaona, T. Fanghänel, *Chemical Reviews* **2013**, *113*, 901-943.
[21] C. Adam, P. Kaden, B. B. Beele, U. Müllich, S. Trumm, A. Geist, P. J. Panak, M. A. Denecke, *Dalton Transactions* **2013**, *42*, 14068-14074.
[22] S. Y. Ning, X. P. Wang, Q. Zou, W. Q. Shi, F. D. Tang, L. F. He, Y. Z. Wei, *Scientific Reports* **2017**, *7*, 14679.
[23] M. F. S. J. D. Law, Idaho National Laboratory, Idaho, **2010**.
[24] C. Madic, B. Boullis, P. Baron, F. Testard, M. Hudson, J.-O. Liljenzin, B. Christiansen, M. Ferrando, A. Facchini, A. Geist, *Journal of Alloys and Compounds* **2007**, *444*, 23-27.
[25] Z. Anyun, H. Jingxin, Z. Xianye, W. Fangding, *Solvent Extraction and Ion Exchange* **2001**, *19*, 965-979.
[26] G. Modolo, H. Asp, C. Schreinemachers, H. Vijgen, *Solvent Extraction and Ion Exchange* **2007**, *25*, 703-721.
[27] L. Berthon, J. Morel, N. Zorz, C. Nicol, H. Virelizier, C. Madic, *Separation Science and Technology* **2001**, *36*, 709-728.
[28] D. Serrano-Purroy, P. Baron, B. Christiansen, R. Malmbeck, C. Sorel, J.-P. Glatz, *Radiochimica Acta* **2005**, *93*, 351-355.
[29] G. Modolo, H. Asp, H. Vijgen, R. Malmbeck, D. Magnusson, C. Sorel, *Solvent Extraction and Ion Exchange* **2008**, *26*, 62-76.
[30] D. Magnusson, B. Christiansen, J. P. Glatz, R. Malmbeck, G. Modolo, D. Serrano-Purroy, C. Sorel, *Solvent Extraction and Ion Exchange* **2009**, *27*, 26-35.
[31] C. Madic, M. J. Hudson, J.-O. Liljenzin, J.-P. Glatz, R. Nannicini, A. Facchini, Z. Kolarik, R. Odoj, *Progress in Nuclear Energy* **2002**, *40*, 523-526.
[32] D. M. Whittaker, T. L. Griffiths, M. Helliwell, A. N. Swinburne, L. S. Natrajan, F. W. Lewis, L. M. Harwood, S. A. Parry, C. A. Sharrad, *Inorganic Chemistry* **2013**, *52*, 3429-3444.
[33] A. Geist, C. Hill, G. Modolo, M. R. S. J. Foreman, M. Weigl, K. Gompper, M. J. Hudson, *Solvent Extraction and Ion Exchange* **2006**, *24*, 463-483.

[34] D. Magnusson, B. Christiansen, M. R. S. Foreman, A. Geist, J. P. Glatz, R. Malmbeck, G. Modolo, D. Serrano-Purroy, C. Sorel, *Solvent Extraction and Ion Exchange* **2009**, *27*, 97-106.
[35] K. Bell, C. Carpentier, M. Carrott, A. Geist, C. Gregson, X. Hérès, D. Magnusson, R. Malmbeck, F. McLachlan, G. Modolo, U. Müllich, M. Sypula, R. Taylor, A. Wilden, *Procedia Chemistry* **2012**, *7*, 392-397.
[36] R. Taylor, M. Carrott, H. Galan, A. Geist, X. Hères, C. Maher, C. Mason, R. Malmbeck, M. Miguirditchian, G. Modolo, *Procedia Chemistry* **2016**, *21*, 524-529.
[37] E. Aneheim, C. Ekberg, A. Fermvik, M. R. S. J. Foreman, T. Retegan, G. Skarnemark, *Solvent Extraction and Ion Exchange* **2010**, *28*, 437-458.
[38] M. C. R. Malmbeck, B. Christiansen, A. Geist, X. Heres, D. Magnusson, G. Modolo, C. Sorel, R. Taylor, A. Wilden., *Sustainable Nuclear Energy Conference*, Manchester, UK, **2014**.
[39] S. A. Ansari, P. Pathak, P. K. Mohapatra, V. K. Manchanda, *Chemical Reviews* **2012**, *112*, 1751-1772.
[40] J. Brown, F. McLachlan, M. Sarsfield, R. Taylor, G. Modolo, A. Wilden, *Solvent Extraction and Ion Exchange* **2012**, *30*, 127-141.
[41] A. Geist, U. Müllich, D. Magnusson, P. Kaden, G. Modolo, A. Wilden, T. Zevaco, *Solvent Extraction and Ion Exchange* **2012**, *30*, 433-444.
[42] M. Carrott, K. Bell, J. Brown, A. Geist, C. Gregson, X. Hères, C. Maher, R. Malmbeck, C. Mason, G. Modolo, *Solvent Extraction and Ion Exchange* **2014**, *32*, 447-467.
[43] a) M. J. Carrot, C. R. Gregson, R. J. Taylor, *Solvent Extraction and Ion Exchange* **2013**, *31*, 463-482; b) J. E. Birkett, M. J. Carrott, O. D. Fox, C. J. Jones, C. J. Maher, C. V. Roube, R. J. Taylor, D. A. Woodhead, *Journal of Nuclear Science and Technology* **2007**, *44*, 337-343.
[44] N. E. Agency, in *Eleventh Information Exchange Meeting*, Nuclear Energy Agency, San Francisco, California, USA, **2012**.
[45] E. Aneheim, C. Ekberg, A. Fermvik, M. R. S. J. Foreman, B. Grűner, Z. Hájková, M. Kvičalová, *Solvent Extraction and Ion Exchange* **2011**, *29*, 157-175.
[46] E. Löfström-Engdahl, E. Aneheim, C. Ekberg, M. Foreman, G. Skarnemark, *Solvent Extraction and Ion Exchange* **2013**, *31*, 604-616.
[47] M. Miguirditchian, C. Sorel, B. Cames, I. Bisel, P. Baron, D. Espinoux, J. N. Calor, C. Viallesoubranne, B. Lorrain, M. Masson, *HA demonstration in the Atalante facility of the Ganex 1st cycle for the selective extraction uranium from HLW*, **2009**.
[48] E. Aneheim, C. Ekberg, M. R. Foreman, E. Löfström-Engdahl, N. Mabile, *Separation Science and Technology* **2012**, *47*, 663-669.
[49] E. Aneheim, B. Grüner, C. Ekberg, M. R. S. Foreman, Z. Hájková, E. Löfström-Engdahl, M. G. Drew, M. J. Hudson, *Polyhedron* **2013**, *50*, 154-163.
[50] M. Sypula, A. Wilden, C. Schreinemachers, R. Malmbeck, A. Geist, R. Taylor, G. Modolo, *Solvent Extraction and Ion Exchange* **2012**, *30*, 748-764.
[51] E. Aneheim, C. Ekberg, M. R. StJ. Foreman, *Solvent Extraction and Ion Exchange* **2013**, *31*, 237-252.
[52] A. Wilden, C. Schreinemachers, M. Sypula, G. Modolo, *Solvent Extraction and Ion Exchange* **2011**, *29*, 190-212.
[53] D. Magnusson, A. Geist, A. Wilden, G. Modolo, *Solvent Extraction and Ion Exchange* **2013**, *31*, 1-11.
[54] S. Lange, A. Wilden, G. Modolo, F. Sadowski, M. Gerdes, D. Bosbach, *Solvent Extraction and Ion Exchange* **2017**, *35*, 161-173.
[55] K. L. Nash, *Solvent Extraction and Ion Exchange* **2015**, *33*, 1-55.
[56] a) T. S. Grimes, R. D. Tillotson, L. R. Martin, *Solvent Extraction and Ion Exchange* **2014**, *32*, 378-390; b) J. L. Lapka, K. L. Nash, *Solvent Extraction and Ion Exchange* **2015**, *33*, 346-361.
[57] C. Wagner, U. Müllich, A. Geist, P. J. Panak, *Solvent Extraction and Ion Exchange* **2016**, *34*, 103-113.
[58] A. Leoncini, J. Huskens, W. Verboom, *Chemical Society Reviews* **2017**.
[59] M. J. Hudson, F. W. Lewis, L. M. Harwood, *Strategies and Tactics in Org. Synth.* **2013**, *9*, 177-202.

[60] M. G. Drew, P. B. Iveson, M. J. Hudson, J. O. Liljenzin, L. Spjuth, P.-Y. Cordier, Å. Enarsson, C. Hill, C. Madic, *Journal of the Chemical Society, Dalton Transactions* **2000**, 821-830.
[61] a) M. Trumm, C. Wagner, B. Schimmelpfennig, A. Geist, P. Panak, *Dalton Transactions* **2016**, *45*, 12308-12311; b) C. M. Ruff, U. Müllich, A. Geist, P. J. Panak, *Dalton Transactions* **2012**, *41*, 14594-14602; c) F. W. Lewis, L. M. Harwood, M. J. Hudson, A. Geist, V. N. Kozhevnikov, P. Distler, J. John, *Chemical Science* **2015**, *6*, 4812-4821; d) C. Wagner, U. Müllich, A. Geist, P. J. Panak, *Dalton Transactions* **2015**, *44*, 17143-17151.
[62] M. L. Neidig, D. L. Clark, R. L. Martin, *Coordination Chemistry Reviews* **2013**, *257*, 394-406.
[63] P. B. Iveson, C. Rivière, D. Guillaneux, M. Nierlich, P. Thuéry, M. Ephritikhine, C. Madic, *Chemical Communications* **2001**, 1512-1513.
[64] J. C. Berthet, C. Rivière, Y. Miquel, M. Nierlich, C. Madic, M. Ephritikhine, *European Journal of Inorganic Chemistry* **2002**, *2002*, 1439-1446.
[65] M. Kaneko, S. Miyashita, S. Nakashima, *Inorganic Chemistry* **2015**, *54*, 7103-7109.
[66] I. Hagström, L. Spjuth, Å. Enarsson, J. O. Liljenzin, M. Skålberg, M. J. Hudson, P. B. Iveson, C. Madic, P. Y. Cordier, C. Hill, N. Francois, *Solvent Extraction and Ion Exchange* **1999**, *17*, 221-242.
[67] N. Boubals, M. G. B. Drew, C. Hill, M. J. Hudson, P. B. Iveson, C. Madic, M. L. Russell, T. G. A. Youngs, *Journal of the Chemical Society, Dalton Transactions* **2002**, 55-62
[68] F. W. Lewis, M. J. Hudson, L. M. Harwood, *Synlett* **2011**, *2011*, 2609-2632.
[69] P. Cordier, C. Hill, P. Baron, C. Madic, M. Hudson, J. Liljenzin, *Journal of Alloys and Compounds* **1998**, *271*, 738-741.
[70] a) M. G. B. Drew, C. Hill, M. J. Hudson, P. B. Iveson, C. Madic, L. Vaillant, T. G. A. Youngs, *New Journal of Chemistry* **2004**, *28*, 462-470; b0 S. Andersson, C. Ekberg, M. R. S. Foreman, M. J. Hudson, J. O. Liljenzin, M. Nilsson, G. Skarnemark, K. Spahiu, *Solvent Extraction and Ion Exchange* **2003**, *21*, 621-636.
[71] S. Andersson, C. Ekberg, J.-O. Liljenzin, M. Nilsson, G. Skarnemark, *Radiochimica Acta* **2004**, *92*, 863-867.
[72] M. J. Hudson, M. G. B. Drew, M. R. S. Foreman, C. Hill, N. Huet, C. Madic, T. G. A. Youngs, *Dalton Transactions* **2003**, 1675-1685.
[73] M. J. Hudson, M. G. Drew, M. R. S. Foreman, C. Hill, N. Huet, C. Madic, T. G. Youngs, *Dalton Transactions* **2003**, 1675-1685.
[74] a) Z. Kolarik, U. Mullich, F. Gassner, *Solvent Extraction and Ion Exchange* **1999**, *17*, 1155-1170; b) Z. Kolarik, U. Müllich, F. Gassner, *Solvent Extraction and Ion Exchange* **1999**, *17*, 23-32.
[75] a) S. Colette, B. Amekraz, C. Madic, L. Berthon, G. Cote, C. Moulin, *Inorganic chemistry* **2002**, *41*, 7031-7041; b) S. Colette, B. Amekraz, C. Madic, L. Berthon, G. Cote, C. Moulin, *Inorganic chemistry* **2003**, *42*, 2215-2226; c) S. Colette, B. Amekraz, C. Madic, L. Berthon, G. Cote, C. Moulin, *Inorganic chemistry* **2004**, *43*, 6745-6751; d) N. L. Banik, M. A. Denecke, A. Geist, G. Modolo, P. J. Panak, J. Rothe, *Inorganic Chemistry Communications* **2013**, *29*, 172-174.
[76] A. Bremer, U. Müllich, A. Geist, P. J. Panak, *New Journal of Chemistry* **2015**, *39*, 1330-1338.
[77] S. Trumm, G. Wipff, A. Geist, P. J. Panak, T. Fanghänel, *Radiochimica Acta* **2011**, *99*, 13-16.
[78] C. Hill, D. Guillaneux, L. Berthon, C. Madic, *Journal of Nuclear Science and Technology* **2002**, *39*, 309-312.
[79] C. Hill, L. Berthon, D. Guillaneux, J. Dancausse, C. Madic, CEA-Marcoule/DEN, **2004**.
[80] M. J. Hudson, C. E. Boucher, D. Braekers, J. F. Desreux, M. G. B. Drew, M. R. S. J. Foreman, L. M. Harwood, C. Hill, C. Madic, F. Marken, T. G. A. Youngs, *New Journal of Chemistry* **2006**, *30*, 1171-1183.
[81] E. Buncel, I.-H. Um, *Tetrahedron* **2004**, *60*, 7801-7825.
[82] S. Trumm, A. Geist, P. J. Panak, T. Fanghänel, *Solvent Extraction and Ion Exchange* **2011**, *29*, 213-229.

[83] M. R. S. J. Foreman, M. J. Hudson, A. Geist, C. Madic, M. Weigl, *Solvent Extraction and Ion Exchange* **2005**, *23*, 645-662.
[84] M. Nilsson, S. Andersson, F. Drouet, C. Ekberg, M. Foreman, M. Hudson, J. O. Liljenzin, D. Magnusson, G. Skarnemark, *Solvent Extraction and Ion Exchange* **2006**, *24*, 299-318.
[85] A. Geist, C. Hill, G. Modolo, M. R. S. J. Foreman, M. Weigl, K. Gompper, M. J. Hudson, *Solvent Extraction and Ion Exchange* **2006**, *24*, 463-483.
[86] M. R. S. Foreman, M. J. Hudson, M. G. B. Drew, C. Hill, C. Madic, *Dalton Transactions* **2006**, 1645-1653.
[87] C. Ekberg, E. Aneheim, A. Fermvik, M. Foreman, E. Löfström-Engdahl, T. Retegan, I. Spendlikova, *Journal of Chemical & Engineering Data* **2010**, *55*, 5133-5137.
[88] A. Afsar, P. Distler, L. M. Harwood, J. John, J. Westwood, *The Journal of Organic Chemistry* **2016**.
[89] F. W. Lewis, L. M. Harwood, M. J. Hudson, P. Distler, J. John, K. Stamberg, A. Núñez, H. Galán, A. G. Espartero, *European Journal of Organic Chemistry* **2012**, *2012*, 1509-1519.
[90] C. Ekberg, E. Löfström-Engdahl, E. Aneheim, M. R. S. Foreman, A. Geist, D. Lundberg, M. Denecke, I. Persson, *Dalton Transactions* **2015**, *44*, 18395-18402.
[91] E. Löfström-Engdahl, E. Aneheim, C. Ekberg, M. Foreman, J. Halleröd, G. Skarnemark, *The Journal of Chemical Thermodynamics* **2014**, *76*, 64-69.
[92] A. Bhattacharyya, M. Mohapatra, P. K. Mohapatra, T. Gadly, S. K. Ghosh, D. Manna, T. K. Ghanty, N. Rawat, B. S. Tomar, *European Journal of Inorganic Chemistry* **2017**, *2017*, 820-828.
[93] S. Trumm, G. Lieser, M. R. Foreman, P. J. Panak, A. Geist, T. Fanghänel, *Dalton Transactions* **2010**, *39*, 923-929.
[94] a) A. Bremer, D. M. Whittaker, C. A. Sharrad, A. Geist, P. J. Panak, *Dalton Transactions* **2014**, *43*, 2684-2694; b) M. Steppert, I. Císařová, T. Fanghänel, A. Geist, P. Lindqvist-Reis, P. Panak, P. Štěpnička, S. Trumm, C. Walther, *Inorganic Chemistry* **2012**, *51*, 591-600.
[95] F. W. Lewis, L. M. Harwood, M. J. Hudson, M. G. Drew, J. F. Desreux, G. Vidick, N. Bouslimani, G. Modolo, A. Wilden, M. Sypula, *Journal of the American Chemical Society* **2011**, *133*, 13093-13102.
[96] F. W. Lewis, L. M. Harwood, M. J. Hudson, M. G. B. Drew, V. Hubscher-Bruder, V. Videva, F. Arnaud-Neu, K. Stamberg, S. Vyas, *Inorganic Chemistry* **2013**, *52*, 4993-5005.
[97] F. W. Lewis, L. M. Harwood, M. J. Hudson, M. G. Drew, A. Wilden, M. Sypula, G. Modolo, T.-H. Vu, J.-P. Simonin, G. Vidick, *Procedia Chemistry* **2012**, *7*, 231-238.
[98] H. Wu, Q.-Y. Wu, C.-Z. Wang, J.-H. Lan, Z.-R. Liu, Z.-F. Chai, W.-Q. Shi, *Dalton Transactions* **2016**, *45*, 8107-8117.
[99] A. Afsar, L. M. Harwood, M. J. Hudson, P. Distler, J. John, *Chemical Communications* **2014**, *50*, 15082-15085.
[100] R. A. Wigeland, T. H. Bauer, T. H. Fanning, E. E. Morris, *Nuclear Technology* **2006**, *154*, 95-106.
[101] A. A. James Westwood, Laurence M. Harwood, Michael J. Hudson, Jan John, Petr Distler., *Heterocycles* **2015**, *93*, 453-464.
[102] D. M. Laventine, A. Afsar, M. J. Hudson, L. M. Harwood, *Heterocycles* **2012**.
[103] A. Afsar, D. M. Laventine, L. M. Harwood, M. J. Hudson, A. Geist, *Chemical Communications* **2013**, *49*, 8534-8536.
[104] A. Afsar, L. M. Harwood, M. J. Hudson, J. Westwood, A. Geist, *Chemical Communications* **2015**, *51*, 5860-5863.
[105] A. C. Edwards, C. Wagner, A. Geist, N. A. Burton, C. A. Sharrad, R. W. Adams, R. G. Pritchard, P. J. Panak, R. C. Whitehead, L. M. Harwood, *Dalton Transactions* **2016**, *45*, 18102-18112.
[106] A. C. Edwards, C. Wagner, A. Geist, N. A. Burton, C. A. Sharrad, R. W. Adams, R. Pritchard, P. J. Panak, R. Whitehead, L. Harwood, *Dalton Transactions* **2016**.
[107] M. A. Higginson, N. D. Kyle, O. J. Marsden, P. Thompson, F. R. Livens, S. L. Heath, *Dalton Transactions* **2015**, *44*, 16547-16552.

[108] P. Distler, J. Kondé, J. John, Z. Hájková, J. Švehla, B. Grüner, *Nukleonika* **2015**, *60*, 885-891.
[109] H. Schmidt, A. Wilden, G. Modolo, D. Bosbach, B. Santiago-Schübel, M. Hupert, J. Švehla, B. Grüner, C. Ekberg, *Procedia Chemistry* **2016**, *21*, 32-37.
[110] J. Kondé, P. Distler, J. John, J. Švehla, B. Grüner, Z. Bělčická, *Procedia Chemistry* **2016**, *21*, 174-181.
[111] C. A. Lipinski, F. Lombardo, B. W. Dominy, P. J. Feeney, *Advanced Drug Delivery Reviews* **1997**, *23*, 3-25.
[112] C. A. Lipinski, *Drug Discovery Today: Technologies* **2004**, *1*, 337-341.
[113] C. A. Lipinski, F. Lombardo, B. W. Dominy, P. J. Feeney, *Advanced Drug Delivery Reviews* **2001**, *46*, 3-26.
[114] F. Lovering, J. Bikker, C. Humblet, *Journal of Medicinal Chemistry* **2009**, *52*, 6752-6756.
[115] a) A. S. Guram, S. L. Buchwald, *Journal of the American Chemical Society* **1994**, *116*, 7901-7902; b) A. S. Guram, R. A. Rennels, S. L. Buchwald, *Angewandte Chemie International Edition in English* **1995**, *34*, 1348-1350; c) J. Louie, J. F. Hartwig, *Tetrahedron Letters* **1995**, *36*, 3609-3612; d) J. F. Hartwig, *Accounts of Chemical Research* **1998**, *31*, 852-860.
[116] C. Sambiagio, S. P. Marsden, A. J. Blacker, P. C. McGowan, *Chemical Society Reviews* **2014**, *43*, 3525-3550.
[117] a) C. L. McMullin, B. Rühle, M. Besora, A. G. Orpen, J. N. Harvey, N. Fey, *Journal of Molecular Catalysis A: Chemical* **2010**, *324*, 48-55; b) T.R. Cundari, J. Deng, *Journal of Physical Organic Chemistry* **2005**, *18*, 417-425.
[118] K. W. Anderson, R. E. Tundel, T. Ikawa, R. A. Altman, S. L. Buchwald, *Angewandte Chemie International Edition* **2006**, *45*, 6523-6527.
[119] Q. Shen, T. Ogata, J. F. Hartwig, *Journal of the American Chemical Society* **2008**, *130*, 6586-6596.
[120] M. R. Biscoe, T. E. Barder, S. L. Buchwald, *Angewandte Chemie International Edition* **2007**, *46*, 7232-7235.
[121] a) I. C. F. R. Ferreira, M.-J. R. P. Queiroz, G. Kirsch, *Tetrahedron* **2003**, *59*, 975-981; b) D. S. Surry, S. L. Buchwald, *Angewandte Chemie International Edition* **2008**, *47*, 6338-6361.
[122] J. J. Low, W. A. Goddard, *Journal of the American Chemical Society* **1986**, *108*, 6115-6128.
[123] M. S. S. Palanki, H. Akiyama, P. Campochiaro, J. Cao, C. P. Chow, L. Dellamary, J. Doukas, R. Fine, C. Gritzen, J. D. Hood, S. Hu, S. Kachi, X. Kang, B. Klebansky, A. Kousba, D. Lohse, C. C. Mak, M. Martin, A. McPherson, V. P. Pathak, J. Renick, R. Soll, N. Umeda, S. Yee, K. Yokoi, B. Zeng, H. Zhu, G. Noronha, *Journal of Medicinal Chemistry* **2008**, *51*, 1546-1559.
[124] E. Garnier, J. Audoux, E. Pasquinet, F. Suzenet, D. Poullain, B. Lebret, G. Guillaumet, *The Journal of Organic Chemistry* **2004**, *69*, 7809-7815.
[125] a) B. C. Hamann, J. F. Hartwig, *Journal of the American Chemical Society* **1998**, *120*, 3694-3703; b) T. E. Barder, S. L. Buchwald, *Journal of the American Chemical Society* **2007**, *129*, 12003-12010.
[126] A. A. Ruch, S. Handa, F. Kong, V. N. Nesterov, D. R. Pahls, T. R. Cundari, L. M. Slaughter, *Organic & Biomolecular Chemistry* **2016**, *14*, 8123-8140.
[127] C. Amatore, A. Jutand, *Coordination Chemistry Reviews* **1998**, *178-180*, 511-528.
[128] N. C. Bruno, M. T. Tudge, S. L. Buchwald, *Chemical Science* **2013**, *4*, 916-920.
[129] a) G. Noronha, K. Barrett, A. Boccia, T. Brodhag, J. Cao, C. P. Chow, E. Dneprovskaia, J. Doukas, R. Fine, X. Gong, *Bioorganic & Medicinal Chemistry Letters* **2007**, *17*, 602-608; b) M. S. Palanki, H. Akiyama, P. Campochiaro, J. Cao, C. P. Chow, L. Dellamary, J. Doukas, R. Fine, C. Gritzen, J. D. Hood, *Journal of Medicinal Chemistry* **2008**, *51*, 1546-1559.
[130] S. Tai, E. J. Dover, S. V. Marchi, J. D. Carrick, *The Journal of Organic Chemistry* **2015**, *80*, 6275-6282.
[131] B. J. Mincher, G. Modolo, S. P. Mezyk, *Solvent Extraction and Ion Exchange* **2010**, *28*, 415-436.

[132] K. N. Tevepaugh, J. D. Carrick, S. Tai, J. G. Coonce, L. H. Delmau, D. D. Ensor, *Solvent Extraction and Ion Exchange* **2016**, *34*, 13-25.
[133] L. M. Klingensmith, E. R. Strieter, T. E. Barder, S. L. Buchwald, *Organometallics* **2006**, *25*, 82-91.
[134] S. Shekhar, J. F. Hartwig, *Journal of the American Chemical Society* **2004**, *126*, 13016-13027.
[135] Y. Sunesson, E. Limé, S. O. Nilsson Lill, R. E. Meadows, P.-O. Norrby, *The Journal of Organic Chemistry* **2014**, *79*, 11961-11969.
[136] a) L. Pellegatti, E. Vedrenne, J.-M. Leger, C. Jarry, S. Routier, *Synlett* **2009**, *2009*, 2137-2142; b) L. Pellegatti, E. Vedrenne, J.-M. Leger, C. Jarry, S. Routier, *Tetrahedron* **2010**, *66*, 4383-4389.
[137] J. F. Hartwig, *Inorganic Chemistry* **2007**, *46*, 1936-1947.
[138] H. C. Guo, R. H. Zheng, H. J. Jiang, *Organic Preparations and Procedures International* **2012**, *44*, 392-396.
[139] a) R. K. Gujadhur, C. G. Bates, D. Venkataraman, *Organic Letters* **2001**, *3*, 4315-4317; b) A. Bencini, V. Lippolis, *Coordination Chemistry Reviews* **2010**, *254*, 2096-2180; c) P. G. Sammes, G. Yahioglu, *Chemical Society Reviews* **1994**, *23*, 327-334.
[140] A. Kiyomori, J.-F. Marcoux, S. L. Buchwald, *Tetrahedron Letters* **1999**, *40*, 2657-2660.
[141] J. W. Cleveland, J. D. Carrick, *European Journal of Organic Chemistry* **2017**, *2017*, 3318-3327.
[142] A. L. Chin, J. D. Carrick, *The Journal of Organic Chemistry* **2016**, *81*, 1106-1115.
[143] F. W. Lewis, L. M. Harwood, M. J. Hudson, U. Müllich, A. Geist, *Chemical Communications* **2015**, *51*, 9189-9192.
[144] M. Weigl, A. Geist, U. Müllich, K. Gompper, *Solvent Extraction and Ion Exchange* **2006**, *24*, 845-860.
[145] a) Y. B. Zhongqiang Zhou, *Heteroatom Chemistry* **2008**, *19*, 682-687; b) L. H. K. Paul D. Bartlett, *Organic Syntheses* **1965**, *45*, 689; c) A. Piątek, C. Chapuis, *Tetrahedron Letters* **2013**, *54*, 4247-4249.
[146] T. Ishizuka, L. E. Sinks, K. Song, S.-T. Hung, A. Nayak, K. Clays, M. J. Therien, *Journal of the American Chemical Society* **2011**, *133*, 2884-2896.
[147] G. R. Pabst, O. C. Pfüller, J. Sauer, *Tetrahedron* **1999**, *55*, 5047-5066.
[148] A. Afsar, J. Cowell, P. Distler, L. M. Harwood, J. John, J. Westwood, *Synlett* **2017**, *28*, 2795-2799.
[149] T. de las Casas Engel, B. Lora Maroto, S. de la Moya Cerero, *European Journal of Organic Chemistry* **2010**, *2010*, 1717-1727.
[150] C. A. G. N. Montalbetti, V. Falque, *Tetrahedron* **2005**, *61*, 10827-10852.
[151] H.-L. Wu, P.-Y. Wu, Y.-N. Cheng, B.-J. Uang, *Tetrahedron* **2016**, *72*, 2656-2665.
[152] A. García Martínez, E. Teso Vilar, A. García Fraile, P. Martínez-Ruiz, *Tetrahedron: Asymmetry* **2005**, *16*, 2329-2332.
[153] a) T. Połoński, *Journal of the Chemical Society, Perkin Transactions 1* **1983**, 305-309; b) T. Połoński, *Journal of the Chemical Society, Chemical Communications* **1982**, 208-209.
[154] L. Xu, A. Zhang, Y. Lu, H. Yang, Z. Liu, *RSC Advances* **2016**, *6*, 99859-99866.
[155] K. Hattori, T. Yoshida, K.-i. Rikuta, T. Miyakoshi, *Chemistry letters* **1994**, *23*, 1885-1888.
[156] J. Kannappan, A. V. Bedekar, *Journal of Chemical Research* **2012**, *36*.
[157] P. D. B. L. H. Knox, J. D. Roberts, *Organic Synthesis* **1965**, *45*, 55.
[158] T. Retegan, M. Drew, C. Ekberg, E. L. Engdahl, M. J. Hudson, A. Fermvik, M. R. Foreman, G. Modolo, A. Geist, *Solvent extraction and ion exchange* **2014**, *32*, 720-736.
[159] D. W. Theobald, *Tetrahedron* **1978**, *34*, 1567-1569.
[160] Y. Gaoni, E. Wenkert, *The Journal of Organic Chemistry* **1966**, *31*, 3809-3814.
[161] J. Vicente, M.-T. Chicote, M.-C. Lagunas, P. G. Jones, *Journal of the Chemical Society, Dalton Transactions* **1991**, 2579-2583.
[162] J. Petrova, S. Momchilova, E. T. K. Haupt, J. Kopf, G. Eggers, *Phosphorus, Sulfur, and Silicon and the Related Elements* **2002**, *177*, 1337-1347.
[163] L. Fitjer, U. Quabeck, *Synthetic Communications* **1985**, *15*, 855-864.

[164] M. E. Flanagan, T. A. Blumenkopf, W. H. Brissette, M. F. Brown, J. M. Casavant, C. Shang-Poa, J. L. Doty, E. A. Elliott, M. B. Fisher, M. Hines, *Journal of Medicinal Chemistry* **2010**, *53*, 8468-8484.
[165] A. F. Abdel-Magid, K. G. Carson, B. D. Harris, C. A. Maryanoff, R. D. Shah, *The Journal of Organic Chemistry* **1996**, *61*, 3849-3862.
[166] D. J. Strub, L. Balcerzak, M. Niewiadomska, J. Kula, M. Sikora, J. Gibka, S. Lochyński, *Tetrahedron: Asymmetry* **2014**, *25*, 1038-1045.
[167] A. W. Marsman, C. A. van Walree, R. W. Havenith, L. W. Jenneskens, M. Lutz, A. L. Spek, E. T. Lutz, J. H. van der Maas, *Journal of the Chemical Society, Perkin Transactions 2* **2000**, 501-510.
[168] K. Ohgane, F. Karaki, T. Noguchi-Yachide, K. Dodo, Y. Hashimoto, *Bioorganic & Medicinal Chemistry Letters* **2014**, *24*, 3480-3485.
[169] M. A. Denecke, A. Rossberg, P. J. Panak, M. Weigl, B. Schimmelpfennig, A. Geist, *Inorganic Chemistry* **2005**, *44*, 8418-8425.
[170] a) L. Cecille, D. Landat, F. Mannone, Radiochemical and Radioanalytical Letters **1977**, *31*, 19-28; bL. Cecille, M. Le Stang, F. Mannone, *Radiochemical and Radioanalytical Letters* **1977**, *31*, 29-37.
[171] D. N. Kamber, Y. Liang, R. J. Blizzard, F. Liu, R. A. Mehl, K. N. Houk, J. A. Prescher, *Journal of the American Chemical Society* **2015**, *137*, 8388-8391.
[172] S.-I. Nagai, T. Ueda, M. Takamura, A. Nagatsu, N. Murakami, J. Sakakibara, *Journal of Heterocyclic Chemistry* **1998**, *35*, 293-296.
[173] E. C. Taylor, J. E. Macor, *The Journal of Organic Chemistry* **1987**, *52*, 4280-4287.
[174] M. G. Schwab, M. Takase, A. Mavrinsky, W. Pisula, X. Feng, J. A. Gámez, W. Thiel, K. S. Mali, S. de Feyter, K. Müllen, *Chemistry – A European Journal* **2015**, *21*, 8426-8434.
[175] T. Ishi-i, R. Hirashima, N. Tsutsumi, S. Amemori, S. Matsuki, Y. Teshima, R. Kuwahara, S. Mataka, *The Journal of Organic Chemistry* **2010**, *75*, 6858-6868.
[176] F. H. Case, *Journal of Heterocyclic Chemistry* **1971**, *8*, 1043-1046.
[177] P. Schenone, A. Tasca, G. Bignardi, L. Mosti, *European Journal of Medicinal Chemistry* **1975**, *10*, 412-417.
[178] G. Cabella, G. Jommi, R. Pagliarin, G. Sello, M. Sisti, *Tetrahedron* **1995**, *51*, 1817-1826.
[179] X. Li, R. Lou, C.-H. Yeung, A. S. C. Chan, W. K. Wong, *Tetrahedron: Asymmetry* **2000**, *11*, 2077-2082.
[180] T. Mino, S. Hata, K. Ohtaka, M. Sakamoto, T. Fujita, *Tetrahedron Letters* **2001**, *42*, 4837-4839.
[181] K. G. Hancock, R. O. Grider, *Journal of the American Chemical Society* **1974**, *96*, 1158-1168.
[182] P. Brownbridge, P. K. G. Hodgson, R. Shepherd, S. Warren, *Journal of the Chemical Society, Perkin Transactions 1* **1976**, 2024-2034.